

THE UNIVERSITY OF HULL

**The Characterization of Surface Waves
on Low-Observable Structures**

being a Thesis submitted for the Degree of

Master of Science

in the University of Hull

by

Serge Yves Marcel Roland Stroobandt, Ing. (Oostende (B), Hon.)

August 1997

Abstract

Edge diffracted waves resulting from surface discontinuities contribute significantly to the radar cross section of an object. Although this problem could be alleviated by altering the shape of the edge discontinuity, this is not always possible due to other mission requirements.

The back-scatter from edge diffracted waves may also be reduced by converting the incoming radar waves into surface waves whose intensity is significantly reduced before reaching the surface discontinuity. This can be achieved by employing isotropic surface wave absorbing materials backed by a metal surface. However, for plane surface waves, the effectiveness of these materials is shown to be strongly polarization dependent.

This work suggests a new strategy which involves replacing the scattering surface by an electromagnetic soft surface. This would result in a complete elimination of the edge diffracted waves in the radar direction, independently of radar polarization.

Furthermore, a new measuring apparatus based on a partially filled rectangular waveguide has been developed for determining the attenuation constant and phase constant of plane surface waves propagating along metal-backed surface wave absorbing materials. Measurements are presented which validate this new measuring method.

Keywords: RCS Management, Surface Waves, Radar Absorbing Materials, Electromagnetic Measurements

Contents

Abstract	II
Acknowledgements	V
1 Introduction	1
1.1 Stealth Design	1
1.2 Reducing the RCS Contribution of Edge Diffracted Waves	10
1.3 Outline of this Text	13
1.4 Conclusions	14
1.5 References	14
2 Hertz Potentials	15
2.1 Introduction	15
2.2 Hertz's Wave Equation for Source Free Homogeneous Linear Isotropic Media	17
2.3 Hertz's Wave Equation in Orthogonal Curvilinear Coordinate Systems with Two Arbitrary Scale Factors	18
2.4 Hertz's Wave Equation in a Cartesian Coordinate System	19
2.5 Hertz's Wave Equation for a 2D-Uniform Guiding Structure	20
2.6 Hertz's Wave Equation in a Circular Cylindrical Coordinate System	22
2.7 Conclusions	25
2.8 References	25
3 Plane Surface Waves Along Plane Layers of Isotropic Media	26
3.1 Definition	26
3.2 Plane Surface Waves and the Brewster Angle Phenomenon	27
3.3 Plane Surface Waves, Total Reflection and Leaky Waves	28
3.4 Plane Surface Waves along a Coated, Electric Perfectly Conducting Plane	30
3.5 Plane Surface Waves along a Planar Three-Layer Structure	79
3.6 Plane Surface Waves along the Plane Interface of Two Half Spaces	91
3.7 Appendix A: The Phase Velocity of an Inhomogeneous Wave in a Loss Free Medium	95
3.8 Appendix B: Proof of $-j\sqrt{x} = \sqrt{-x}$	96
3.9 Conclusions	97
3.10 References	98
4 Axial Surface Waves in Isotropic Media	99
4.1 Definition	99
4.2 Axial Surface Waves along a Coated, Electric Perfectly Conducting Cylinder	100
4.3 Field Distribution of Axial Surface Waves along a Coated, Electric Perfectly Conducting Cylinder	105
4.4 Conclusions	107
4.5 References	107

5 RCS Management of Edge Diffracted Waves	108
5.1 Introduction	108
5.2 Converting the Incident Space Wave into Attenuated Surface Waves	109
5.3 Soft Surfaces	111
5.4 The Practical Realization of a Soft Surface	113
5.5 Conclusions	119
5.6 References	120
6 Surface Wave Absorber Measurements	121
6.1 Introduction	121
6.2 A Historical Overview of Surface Wave Measurement Techniques	122
6.3 A Plane Surface Wave Simulator Cell Based on a Partially Filled Rectangular Waveguide	126
6.4 Conclusions	158
6.5 References	158
7 Conclusions	159

Acknowledgements

First of all I would like to thank Dr Peter Lederer of the Defence Evaluation and Research Agency (DERA) Malvern for his interest in this work and financial sponsoring.

I am also very grateful for the enormous amount of support received from my supervisor Dr Francis C. Smith. Not only was he always prepared to discuss my work and willing to help, he also closely monitored my progress, asked questions when needed, stimulated research and inspired. I could not have wished for a better supervisor.

My stay in Hull would not have been as pleasurable and unforgettable as it was without the help from the friendly staff at the university - a special 'thank you' also to Mr John Hodgson of the workshop -, the company of my colleagues Lindsey, Margarita, Dinah, Ali, Marcus, Russell, João, Jean and Ricardo and all the other new friends I made in Hull.

This work would also not have been possible without the love and care of my parents, who supported me both mentally and financially. Finally, I also would like to thank my family, friends and current employers for showing their patience and living with me while I was writing up this thesis.

1 Introduction

1.1 Stealth Design

1.1.1 What is Stealth Design?

The purpose of designing an object in stealth technology is to reduce the likelihood of betraying its presence and to minimize the probability of its detection when active search and tracking techniques are employed [1]. For an object to be “stealth”, it needs to have a low optical visibility in addition to being low-observable in the infrared spectrum and at all radar frequency bands. Also, the emission of acoustic noise should be low.

The theory and techniques presented in this text relate only to the behaviour of objects illuminated by electromagnetic waves at radar frequencies. Although the popular image of stealth is the realisation of “invisible” targets, the practical aim is to achieve “low observability” for certain aspect angles [2].

Stealth technology is generally associated with aircraft (Fig. 1.1), however this technology also receives increasingly more attention in ship designs. This is clearly demonstrated by the well-known French marine frigate “La Fayette” and United States “Arsenal” and “Sea Shadow”. The Sea Shadow (Fig. 1.2) has the ability to navigate on the information received from a tactical data link solely, thus eliminating the need for a large number of windows and onboard sensors [3]. The scarcity of external features further reduces the radar cross section of the vessel. UK’s plans to build stealth ships are also taking shape in the form of the “Sea Wraith” and “Project Cougar” [4].



Figure 1.1: The F-117A stealth fighter plane; its “faceted” shape, internal weapon bays and location of jet inlets are characteristic for many stealth aircraft designs. Note also that the jet intakes are located on top of the wings. Inset: The wings are indented at the rear end and the usual 90° dihedral corner reflectors at the tail have been eliminated.

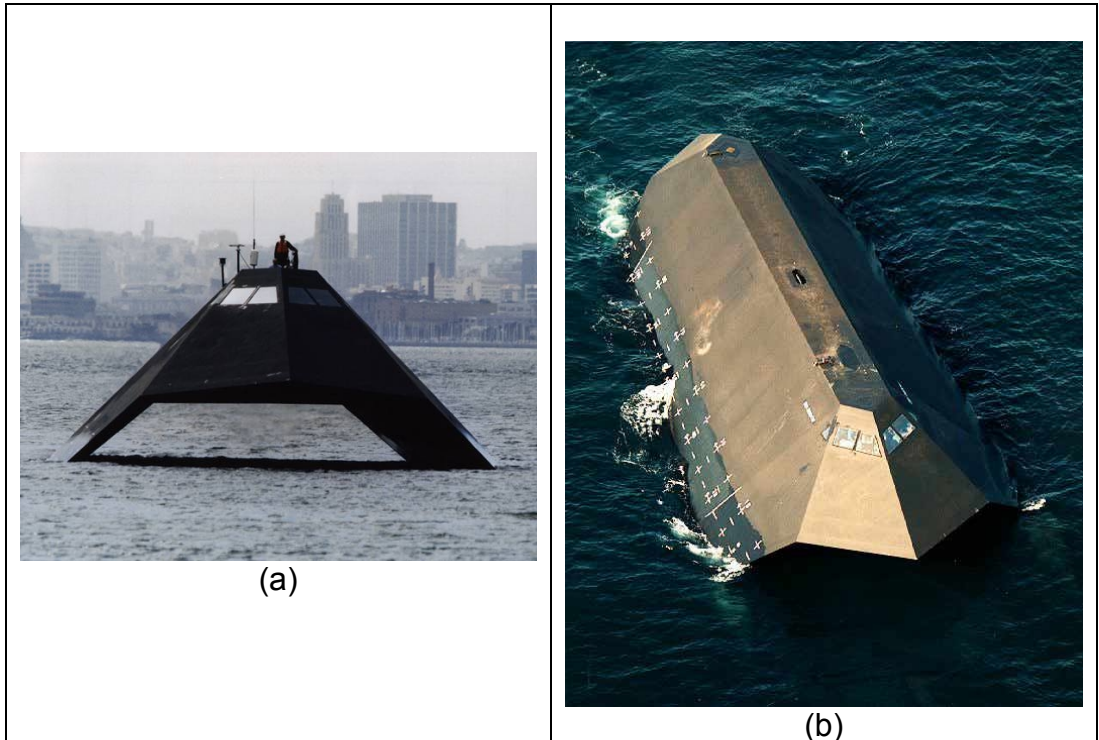


Figure 1.2a: The United States "Sea Shadow"

Figure 1.2b: The number of discontinuities in the hull have been reduced to an absolute minimum; only two hatches for the crew and one air inlet on the roof of the vehicle.

Some of the stealth techniques employed in military designs also have civilian applications. The "invisible" struts and masts described in [5] and [6] are an excellent example of this. In these references is explained how a ship-borne radar will suffer less from blockage and unwanted echoes when the masts in its immediate vicinity are treated with an electromagnetic hard surface. (See also Chapter 5 in this text.)

1.1.2 What is the Radar Cross Section (RCS) of an Object?

The *radar cross section (RCS)* of an object is defined as the projected area of an equivalent perfect reflector with uniform properties in all directions (i.e. a sphere) and which will return the same amount of power per unit solid angle (steradian) as the object [1]. The datum reference for RCS is often taken as a sphere of 1m^2 echoing area, that is a sphere with diameter

$$D = \sqrt{\frac{4}{\pi}} \approx 1.1284\text{m}.$$

A more mathematical definition of RCS is [2]

$$\sigma = \lim_{R \rightarrow +\infty} 4\pi R^2 \frac{\bar{E}_s \cdot \bar{E}_s^*}{\bar{E}_i \cdot \bar{E}_i^*}$$

where σ is the RCS and \bar{E}_i and \bar{E}_s are the phasor representations of the incident and scattered electric field intensities, respectively. The superscript * denotes the complex conjugate. σ has the units of area and is usually expressed in square meters.

The RCS of some common perfectly conducting scatterers can easily be calculated from geometrical optics ($\sigma = \pi\rho_1\rho_2$ where ρ_1 and ρ_2 are the radii of curvature) and have been tabulated (see for example [2]).

For most objects, radar cross section is a three-dimensional map of scattering contributions located on the object and which vary as a function of frequency, aspect angles (azimuth ϕ and elevation θ) and polarization [7]. The *scattering matrix* describes the scattering behaviour of the target as a function of polarization, as it contains four RCS values (VV, VH, HV and HH; the first letter denotes the transmission polarization, the second letter is the polarization at receive) from which the RCS can be derived at any polarization:

$$\sigma(f, \theta, \phi) = \begin{bmatrix} \sigma_{VV}(f, \theta, \phi) & \sigma_{VH}(f, \theta, \phi) \\ \sigma_{HV}(f, \theta, \phi) & \sigma_{HH}(f, \theta, \phi) \end{bmatrix}.$$

Radar cross section is the only factor in the radar equation that is within control of the stealth design engineer, hence its importance:

$$P_r = \frac{P_t G_t}{4\pi R^2} \cdot \frac{\sigma}{4\pi R^2} \cdot A_r \quad (1)$$

where

P_r is the received power,

P_t is the transmitted power,

G_t is the antenna gain on transmit,

R is the distance between the target and the radar (i.e. the range),

σ is the radar cross section and

A_r is the effective antenna aperture on receive.

Of course, active electronic countermeasures (ECM) can further reduce the probability of radar detection. However, ECM is not regarded as a stealth technique.

1.1.3 Why Reduce RCS?

There are several reasons for reducing the RCS of any target [7]:

- Prevent, or at least delay or deteriorate enemy radar detection,
- Force the enemy radar to increase its transmitting power, thus increasing its detection range and vulnerability,
- Prevent correct target classification through the analysis of “hot spots”,
- Induce the enemy to underestimate target dimensions,
- Reduce the jamming power necessary to protect the target,
- Increase the effectiveness of chaff,
- Simplify the construction and deployment of decoys.

In conclusion, all the above considerations have the common purpose of increasing target survivability. However, as has been mentioned previously, RCS reducing techniques can also be employed to prevent one’s own radar from receiving unwanted echoes from nearby “friendly” objects.

Quite often the direction of radiation will result in head-on illumination of the target [1]. As can be deduced from the table below ([1], [2] and [8]), the aim is to make a fighter plane’s head-on RCS approach that of a bird. However it is obvious that consideration must also be given to other aspects, including those from below or to one side when ground- or space- based radar is the threat. In this context it should also be noted that a different approach is likely to be necessary when the threat is a bi-static, as opposed to a mono-static radar [1].

Table 1.1: Typical head-on RCS values at microwave frequencies

Object	σ (m ²)
Pickup truck	200
Automobile	100
Jumbo jet airliner	100
B-52	100
Tank	50
Large bomber or commercial jet	40
Cabin cruiser boat	10
Large fighter aircraft	6
Small fighter aircraft or four-passenger jet	2
Adult male	1
Cruise missile	0.80
B-1B	0.75
Conventional winged missile	0.50
B-2	0.10
F-117A	0.025
Bird	0.010

1.1.4 Scattering Mechanisms

The electromagnetic waves that impinge upon the target are scattered by a variety of mechanisms [1]:

- *Specular*: Specular wave scattering is essentially a reflection of the incoming wave. The main contribution arises when the Poynting vector of the incoming wave vector is perpendicular to the local surface.
- *Diffraction*: Diffraction occurs when there is a discontinuity in the target geometry or a discontinuity in the electromagnetic material properties of the object.
- *Diffracted surface waves*: A surface wave (which belongs to the group of traveling waves; see also Section 3.4.8) may result when the incoming wave is more or less aligned along the length of a long thin coated body. The scattering arises when the surface wave encounters surface discontinuities, the end of the body or changes in the electromagnetic properties of the surface of the body. (See also Fig. 1.6.)
- *Radiation from creeping waves*: When the surface which supports a surface wave makes a gentle bend in the longitudinal plane of the surface wave, the surface wave will convert into an attenuated creeping wave that continues to follow the surface and space waves that radiate away from the surface, also called surface diffracted waves (Fig. 1.3) [9].

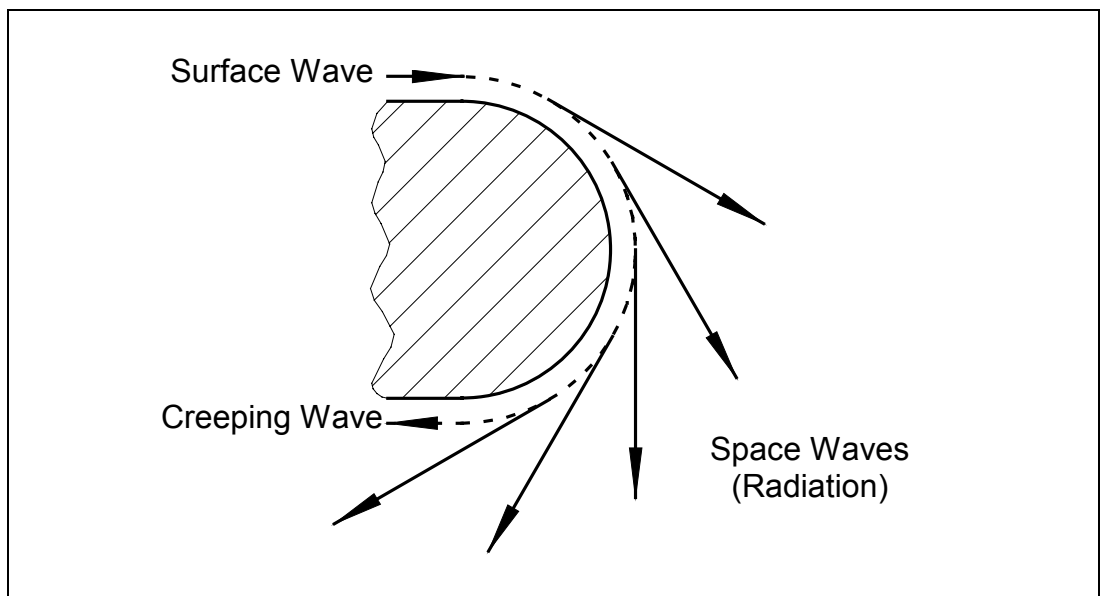


Figure 1.3: Radiation from creeping waves

All scattering mechanisms have one thing in common: the scattered waves are needed in addition to the incoming wave to satisfy the boundary conditions at the object.

The dependence of RCS upon wavelength can be categorized into three regimes (a is a major dimension of the target) [1]:

- The Rayleigh regime where $\lambda \geq 2\pi a$: In this regime σ varies smoothly with variation of λ . Moreover, $\sigma \sim V^2 \lambda^{-4}$ where V is the volume of the body,
- The resonant regime where rapid changes of σ are likely to occur,
- The optical regime where $\lambda \leq 2\pi a$: Here σ varies smoothly with λ and may tend to a definitive value for $\lambda \ll 2\pi a$.

1.1.5 Where to Reduce RCS

At radar frequencies of practical interest, the wavelength is often much smaller than the target's typical dimensions, and the electromagnetic scattering is practically a local phenomenon (i.e. optical regime). Besides particular resonance or multiple reflection effects, the scattering of each single reflecting element of a complex structure is not affected by the presence of the rest of the structure (except for masking effects) [7]. Hence, a radar echo can be seen as the superimposition of several echoes, each with a different amplitude and phase

$$\sigma = \sqrt{\sum_{n=1}^N (\sigma_n e^{j\varphi_n})^2} .$$

An average RCS value can be computed by assuming that phases are random uniform variables (this assumption is true for short wavelengths)

$$\sigma = \sum_{n=1}^N \sigma_n . \quad (2)$$

As can be seen from the radar equation (1), a reduction in σ by an order of magnitude only reduces the detection range by 44%. A very large reduction in σ is therefore essential to have a significant effect [1]. In view of (2), it is very important to work first on the main scattering contributions ("hot spots") of a target, because their reduction has the maximum effect on the overall RCS [7]. An overview of what contributes to the RCS of a typical fighter aircraft is given in Figure 1.5.

Only RCS contributions that can be accompanied by surface wave propagation (12 to 15 in Fig. 1.5) are dealt with in this text. These contributions are in general small compared with other contributions. However, in order to achieve RCS values that are as small as that of a bird, these smaller contributions need to be reduced as well. The methods and techniques presented in this text are intended to help achieve this. They are also helpful with the new, taxpayer-friendly trend of retrofitting or redesigning existing vehicles which were originally not designed in stealth technology.

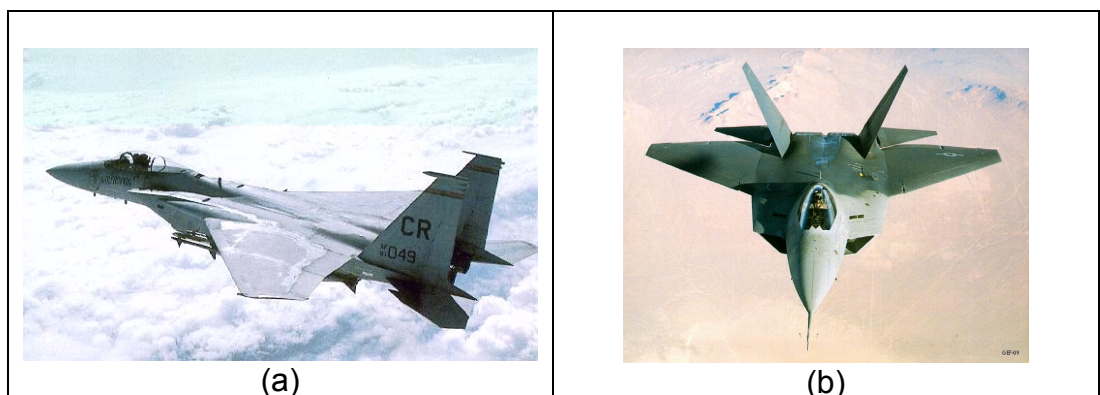


Figure 1.4a: The F-15, a conventional fighter plane

Figure 1.4b: The F-22, a stealth redesign of the F-15 with new low-observable jet intakes, shielded nozzles, cant rudders and internal weapon bays

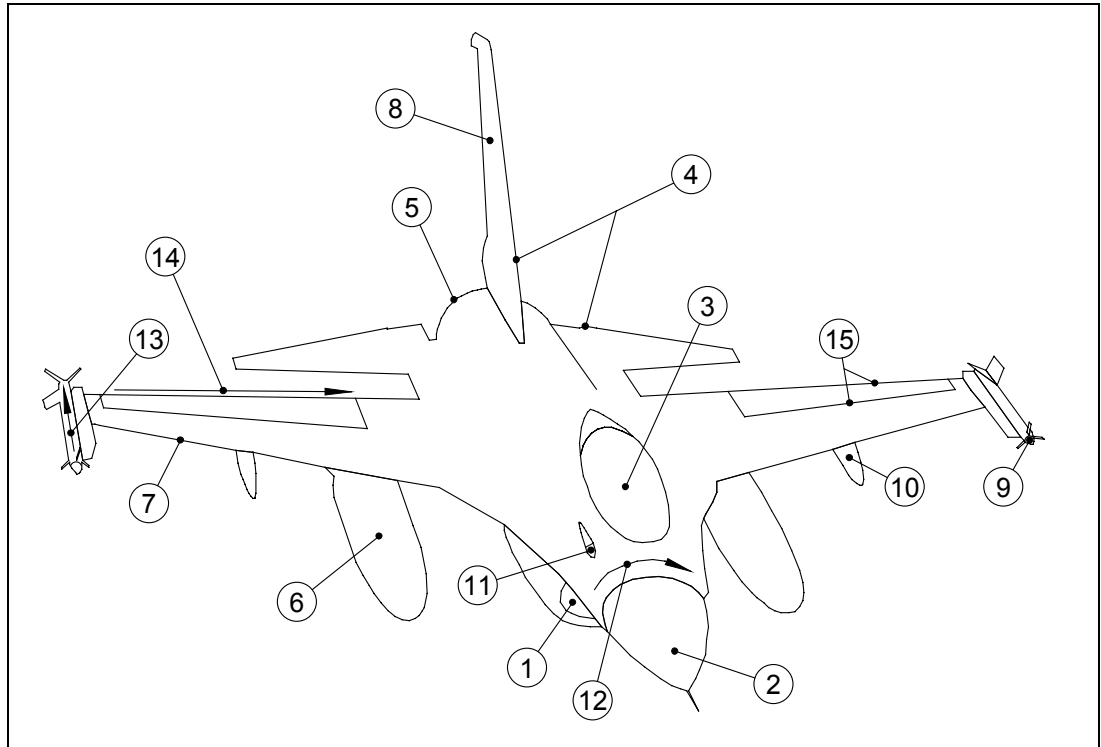


Figure 1.5: Contributions to the radar cross section of a fighter jet [1], [9]

Large scattering contributions (mainly due to reflection) are:

- 1) Air intake cavity (only for head-on illumination),
 - 2) Antenna behind radome, if transparent to illuminating radar,
 - 3) Canopy and cockpit cavity,
 - 4) Dihedral 90° corner reflector at tail junction (only for side illumination),
 - 5) Exhaust cavity (when viewed from rear (e.g. like in a missile attack)),
 - 6) Drop tank,
- Not shown: Glint from flat, slab sided fuselage (from normal to its side).

Scattering contributions that could be large, but not necessarily are:

- 7) Leading wing edge, especially if unswept,
 - 8) Glint from vertical and horizontal tails in isolation,
 - 9) Seeker,
- Not shown: Glint from propeller and rotor blades.

Smaller, but nevertheless significant scattering contributions are:

- 10) Weapon hard point,
 - 11) Gun muzzle and other local surface protuberances,
 - 12) Creeping wave along the fuselage,
 - 13) Axial surface wave along coated missile,
 - 14) Surface wave along trailing wing edge (only with side illumination) [10],
 - 15) Scattering at trailing wing edge and control surface gaps,
- Not shown: Scattering at edges of undercarriage fairing,
 Not shown: Local air intakes for cooling or air conditioning.

Contributions 12 to 15 can be accompanied by surface wave propagation effects if the surfaces are coated.

1.1.6 Techniques for Reducing RCS

There are essentially four techniques for reducing RCS:

- By shaping and masking,
- By treating the surface of the target with radar absorbing materials (RAM),
- By using local lumped impedances on the surface of the target,
- By employing electromagnetic soft or hard surfaces.

All four methods involve a change in the boundary conditions at the object: either a change in the location of the boundary or a change in the type of the boundary or both. The fourth technique is a relatively new technique [5] and [6]. Especially the potential benefits of electromagnetic soft boundaries for reducing RCS contributions from edge diffracted waves (13, 14 and 15 in Figure 1.5) are shown for the first time in this text (see Chapter 5).

Shaping and Masking

By using proper shapes, it is possible to reduce RCS for particular aspects, at the expense of other aspects, so that the target has minimum RCS in the most probable direction of radar illumination [7].

There are two distinctly different approaches to establishing the overall shape of a stealth object [1]:

- By adopting a compact, smooth blended external geometry. This technique is exemplified by the Northrop B-2 (Fig. 1.8 and 1.9),
- By employing a faceted configuration, using flat surfaces arranged to minimize normal reflections back toward the illuminating radar and, it is hoped, eliminate glint. The Lockheed-Martin F-117A (Fig. 1.1) is based on this design concept.

In this context it should also be noted that a flat plate focuses its back-scattering on a very narrow angular sector, with a high RCS value. A sphere, by contrast, has a low RCS value which is uniform at all angles. Thus, on a limited angular sector around the specular direction, spheres and cylinders give the lowest RCS values. If otherwise, RCS must be kept low on a wide angular sector, then it is better to use very narrow-beam shapes such as the flat plate, correctly aimed in order to avoid the specular flash [7].

The design of a stealth aircraft usually results in a flying-wing shape (Fig. 1.1 and 1.8). With such a shape, most contributions of Figure 1.5 are absent or significantly reduced. For more tips on designing stealth aircraft, refer to [1] and [7].

Radar Absorbing Materials

RAM may function in one of two distinctly different ways [1]:

- By admitting the signal and then attenuating its intensity. This type is particularly suited for use against a wide range of radar frequencies, and is sometimes referred to as broadband RAM. However, this type RAM has the disadvantage of being difficult to manufacture and is heavy and expensive [7]. Surface wave absorbing materials work in very much the same way but are polarization dependent,
- By generating internal reflections which interfere with the waves reflected from the outer surface. This type of RAM is called resonant RAM because it is only effective at a number of discrete frequencies.

Lumped Impedances

It is not inconceivable that for example the wings of an aircraft could be resonant at the low frequency of an over-the-horizon early warning radar. In such a case, the wings could be detuned and hence the RCS significantly reduced by inserting an inductance or capacitance at some point in the wings.

Electromagnetic Soft and Hard Surfaces

(See [5], [6] and Chapter 5 in this text for more information.)

1.2 Reducing the RCS Contribution of Edge Diffracted Waves

An illuminating radar beam parallel to an object's surface encountering a surface discontinuity generates edge diffracted waves in order to satisfy the boundary conditions at the discontinuity (Fig. 1.6).

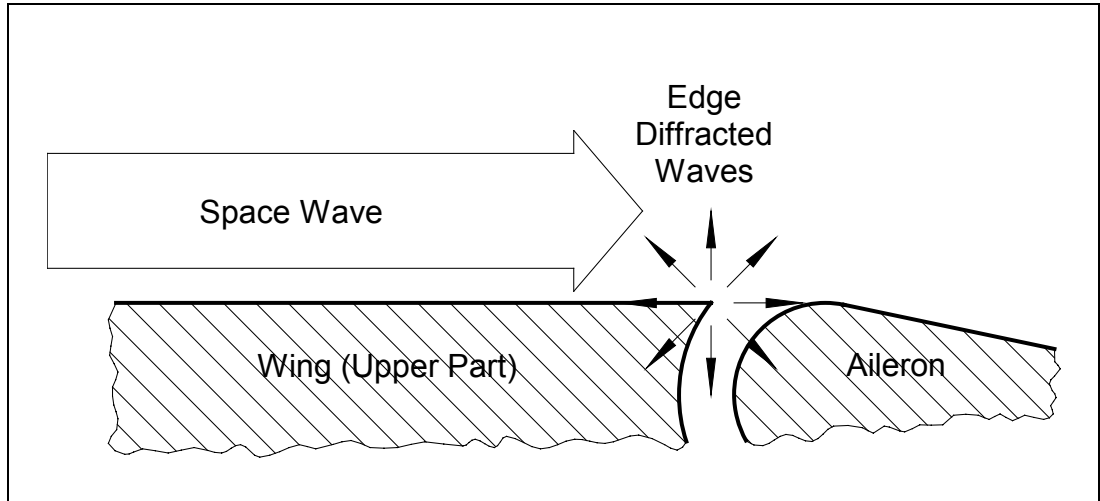


Figure 1.6: Edge diffracted waves at a surface discontinuity

The back-scattered edge diffracted waves are in phase if the discontinuity lies on a straight line perpendicular to the illumination direction (Fig. 1.7a). This leads to a strong RCS contribution [9].

For an ordinary aircraft the problem arises at the trailing edges of wings, at the gaps between wings and control surfaces (ailerons, flaps and rudders), at the edges of cargo doors, service hatches and undercarriage fairing and at the end of wing-mounted missiles (see Fig. 1.5).

There are three ways to overcome this problem:

- By indenting the edge discontinuity or
- By converting the illuminating space wave to surface waves whose intensity is significantly reduced before reaching the surface discontinuity. This can be achieved by employing isotropic surface wave absorbing materials backed by a metal surface,
- By replacing the surface by an electromagnetic soft surface.

The first method is depicted in Figure 1.7b where the approximate contour of a stealth air plane is shown (see also Fig. 1.8). Due to the indented shape of the rear edge, the edge diffracted waves going back to the radar are not in phase. Moreover, when this plane turns around its vertical axis (or the mono-static radar moves around this target), only two directions vulnerable for detection exist in a 180° sector [9]. This technique is however not particularly effective in the case of bi-static radars.

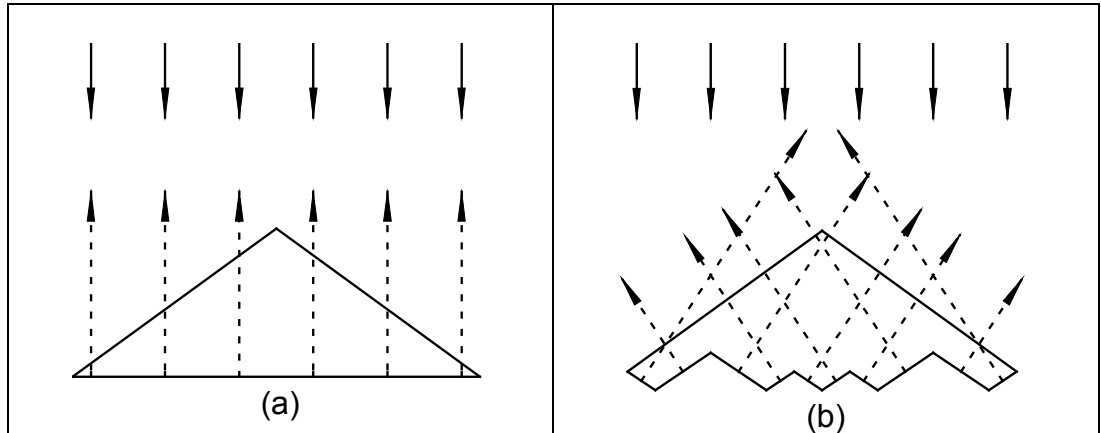


Figure 1.7a: Edge diffraction from the trailing edge of a straight wing
 Figure 1.7b: Edge diffraction from the trailing edge of an indented wing



Figure 1.8: The B-2 stealth bomber plane. A flying-wing design and an indented rear edge result in an extremely low RCS value.

Edge indentation can be found at many locations along the fuselage of a stealth aircraft, as is exemplified by Figures 1.8 to 1.12. However, it is not always possible to employ this technique due to aerodynamic requirements. This is especially true for the gaps between wings and control surfaces and for ordinary aircraft being retrofitted. In such cases, one has to resort to one of the other two methods which are discussed in Chapter 5.



Figure 1.9: The indented payload doors of a B-2



Figure 1.10: A close-up at the indented hatch of one of the F-117A's weapon bays



Figure 1.11: Indented surface discontinuities on the F-22's fuselage



Figure 1.12: The F-22 seen from aside.

1.3 Outline of this Text

Chapter 2 gives a review of Hertz potential theory. The convenience of expressing source free electromagnetic fields in terms of Hertz potentials is clearly demonstrated.

An unambiguous definition of plane surface waves is given in Chapter 3, followed by a rigorous investigation into the propagation mechanisms of plane surface waves along various planar and isotropic multi-layered surface wave absorber configurations. Dispersion equations are derived by treating these structures as boundary-value problems and solving them using Hertz potentials. Surface waves are compared with other kinds of traveling waves and the requirements for surface wave propagation are discussed. For a given isotropic layer structure, the propagation of plane surface waves is found to be strongly polarization dependent.

Axial surface waves are the type surface waves that can propagate along a coated metal cylinder (e.g. a missile (see Fig. 1.5)). They also very much resemble the waves that might propagate along the trailing edge of a wing (see also Fig. 1.5 and [10]). The dispersion equation of these axial surface waves is derived in Chapter 4.

Chapter 5 starts off by explaining the many restrictions of employing isotropic surface wave absorbing materials for reducing the back-scattering of edge diffracted waves. Once more is stressed that the effectiveness of isotropic surface wave absorbers strongly depends upon the polarization of the illuminating radar beam. An alternative technique which does not suffer from this problem is suggested for eliminating edge diffracted waves in the radar direction. This new technique consists in replacing the scattering surface by an electromagnetic soft surface. Ways to produce such a soft surface are also discussed.

Although soft boundaries form an electromagnetic superior solution for reducing the RCS resulting from edge diffracted waves, surface wave absorbers may still find many useful applications, even within RCS management. From this perspective it is obvious that there is a lot interest in determining the quality and efficacy of commercially available surface wave absorbers. Chapter 6 gives a brief historical overview of surface wave measurement techniques and their limitations. It appears that none of the existing techniques can be applied to measure the propagation characteristics of plane surface waves in a convenient way. However, this work resulted in the development of a new measuring apparatus, based on a partially filled rectangular waveguide, for determining the attenuation constant and phase constant of plane surface waves propagating along metal-backed surface wave absorbing materials. Measurements are presented which validate this new measuring method.

Finally, the conclusions of this work are drawn in Chapter 7 and suggestions are made for further work.

1.4 Conclusions

Edge diffracted waves resulting from surface discontinuities contribute significantly to the radar cross section of an object. Although this problem could be alleviated by indenting the edge discontinuity, this is not always possible due to other mission requirements.

However, the back-scatter from edge diffracted waves may also be reduced by converting the incoming radar waves into surface waves whose intensity is significantly reduced before reaching the surface discontinuity. This can be achieved by employing surface wave absorbing materials.

1.5 References

- [1] D. Howe, "Introduction to the basic technology of stealth aircraft: Part 2 - Illumination by the enemy (active considerations)," *Journal of Engineering for Gas Turbines and Power*, Vol. 113, January 1991, pp. 80-86
- [2] N. Williams, "Radar cross section: engineering for stealth," *Electronic Engineering*, February 1987, pp. 49-60
- [3] <http://www.atl.external.lmco.com/projects/solarwind/ni.3c.html>
- [4] A. Gilligan, "'Invisible' warships go all out for orders," *The Sunday Telegraph*, October 20, 1996, p. 11
- [5] P.-S. Kildal, *Research 1993-1995 at Antenna Group*, Department of Microwave Technology, Chalmers University of Technology, Gothenburg, Sweden, p. 15
- [6] P.-S. Kildal, A. A. Kishk and A. Tengs, "Reduction of forward scattering from cylindrical objects using hard surfaces," *IEEE Transactions on Antennas and Propagation*, Vol. 44, No. 11, November 1996, pp. 1509-1519
- [7] F. Bessi and F. Zaccà, "Introduction to 'stealth'," *Military Technology*, MILTECH, No. 5, 1989, pp. 68-78
- [8] J. A. Adam, "How to design an 'invisible' aircraft," *IEEE Spectrum*, April 1988, pp. 26-31
- [9] P. Y. Ufimtsev, "Comments on diffraction principles and limitations of RCS reduction techniques," *Proceedings of the IEEE*, Vol. 84, No. 12, December 1996, pp. 1828-1851
- [10] P. Diament, S. P. Schlesinger and A. Vigants, "A dielectric surface-wave structure: The V-line," *IRE Transactions on Microwave Theory Techniques*, Vol. MTT-9, p. 332, 1961

2 Hertz Potentials

2.1 Introduction

A general feature of classical electrodynamics is the fact that an electromagnetic field must be a solution of Maxwell's equations. Therefore many theoretical considerations on the structure of Maxwell's equations exist. The analysis of an electromagnetic field is often facilitated by the use of auxiliary functions known as potential functions (scalar, vectorial, tensorial) [1, p.23]. These are solutions of partial differential equations. The partial differential equations are such, that solving them for the potential functions is equivalent to the more tedious task of solving Maxwell's equations directly [2].

The most elegant approach to this is the field representation in terms of Green's tensors. However, this treatment has the fundamental disadvantage that tensor differential equations have to be solved. It is only for special kinds of media that Green's tensors can be reduced to scalar Green's functions [2].

It was shown by Hertz that an arbitrary electromagnetic field in a (source free) homogeneous linear isotropic medium can be defined in terms of a single vector potential $\vec{\Pi}$ [1, p.28]. *The Hertz vector potential* notation is an efficient mathematical formalism for solving electromagnetic problems. As will be shown, Hertz vector potential can be reduced to a set of two scalar potentials, which are solutions of Helmholtz's equations, for any orthogonal curvilinear coordinate system. These solutions are independent only in the case of an isotropic medium [2]. Note that at present the Hertz potential notation has been extended in order to take into account sources contained in the medium [1, pp. 30-32 & pp. 430-431]. However, this can not be done in a straightforward manner. The current and charge densities first need to be expressed in terms of *an electric polarization vector* \vec{P} using the formulas: $\vec{J} = \frac{\partial \vec{P}}{\partial t}$ and $\rho = -\vec{\nabla} \cdot \vec{P}$.

A lot of present day textbooks on the subject of electromagnetism rely heavily on *the magnetic vector potential* \vec{A} and *the scalar potential* ϕ , also often called the mixed potential method. The main advantage of this method is the fact that the two Helmholtz's equations that result from it (one vectorial and one scalar), directly take into account any current or charge sources lying in the medium. This is in contrast with the Hertz vector potential method where, as has been explained in the previous paragraph, the scalar potentials are more closely connected to the field intensities \vec{E} and \vec{H} .

The magnetic vector potential \vec{A} and the scalar potential ϕ are related to the Hertz vector potential as follows [1, pp. 28-29]: $\vec{A} = \mu\epsilon \frac{\partial \vec{\Pi}}{\partial t}$ and $\phi = -\vec{\nabla} \cdot \vec{\Pi}$, provided that \vec{A} is defined by $\vec{B} = \vec{\nabla} \times \vec{A}$ and not $\vec{H} = \vec{\nabla} \times \vec{A}$. (The latter definition is more common in East European countries.)

The big strength of the Hertz vector potential method lies with the fact that there is no need to check whether the solutions of the two scalar partial differential equations are solutions of the posed problem. This is clearly not the case with the mixed potential method [3, p. 679]. For problems situated in source free media, this property of the Hertz vector potential method far outweighs the advantages of any other method. This also explains why, in this text, the Hertz vector potential method is preferred over the mixed potential method.

In recent years, a lot of research effort went into the development of potential formulations for anisotropic, gyrotropic, chiral and spatially inhomogeneous media [2]. For a detailed discussion on scalar Hertz potentials for bigyrotropic media see [4].

2.2 Hertz's Wave Equation for Source Free Homogeneous Linear Isotropic Media

Assuming $e^{j\omega t}$ time dependence, *Hertz's wave equation* for a source free homogeneous linear isotropic medium, independent of the coordinate system, is [3, p. 729]

$$\nabla^2 \vec{\Pi} + k^2 \vec{\Pi} = 0 \quad (1)$$

where $\nabla^2 \vec{v} \equiv \vec{\nabla}(\vec{\nabla} \cdot \vec{v}) - \vec{\nabla} \times \vec{\nabla} \times \vec{v}$ (\vec{v} is any vector) [1, p. 25], [3, p. 95]

and $k^2 = -j\omega\mu(\sigma + j\omega\varepsilon) = \varepsilon\mu\omega^2 - j\omega\mu\sigma$.

(k is *the complex wave number* of the surrounding medium.)

Hertz's wave equation for source free homogeneous linear isotropic media (1) has two types of independent solutions: $\vec{\Pi}_e$ and $\vec{\Pi}_m$.

These result in independent sets of *E-type waves*

$$\vec{H} = (\sigma + j\omega\varepsilon)\vec{\nabla} \times \vec{\Pi}_e, \quad (2a)$$

$$\vec{E} = k^2 \vec{\Pi}_e + \vec{\nabla}(\vec{\nabla} \cdot \vec{\Pi}_e), \quad (2b)$$

and *H-type waves*, respectively [3, p. 729]

$$\vec{E} = -j\omega\mu \vec{\nabla} \times \vec{\Pi}_m, \quad (3a)$$

$$\vec{H} = k^2 \vec{\Pi}_m + \vec{\nabla}(\vec{\nabla} \cdot \vec{\Pi}_m). \quad (3b)$$

Note that throughout this text, permittivity ε will be treated as a complex quantity with two distinct loss contributions [5]

$$\varepsilon = \varepsilon' - j\varepsilon'' - j\frac{\sigma}{\omega}$$

where $-j\varepsilon''$ is the loss contribution due to molecular relaxation

and $-j\frac{\sigma}{\omega}$ is the conduction loss contribution. (The conductivity σ is measured at DC.)

However, in practice it is not always possible to make this distinction. This is often the case with metals and good dielectrics. In those cases all losses can be treated as though being entirely due to conduction or molecular relaxation, respectively.

Above relations follow from

$$\vec{\nabla} \times \vec{H} = j\omega\vec{D} + \vec{J} = j\omega(\varepsilon' - j\varepsilon'')\vec{E} + \sigma\vec{E}.$$

The loss tangent of a dielectric medium is defined by

$$\tan\delta \equiv \frac{\omega\varepsilon'' + \sigma}{\omega\varepsilon'}.$$

Permeability μ has only one loss contribution due to hysteresis: $\mu = \mu' - j\mu''$.

2.3 Hertz's Wave Equation in Orthogonal Curvilinear Coordinate Systems with Two Arbitrary Scale Factors

Consider a right-hand orthogonal curvilinear coordinate system with *curvilinear coordinates* (u_1, u_2, u_3) . Scale factor h_1 equals one and scale factors h_2 and h_3 can be chosen arbitrary.

(A detailed explanation of what curvilinear coordinates and scale factors are, can be found in [1, pp. 38-59] and [6, pp. 124-130], together with definitions of gradient, divergence, curl and Laplacian for such coordinate systems.)

Hertz's vector wave equation for source free homogeneous linear isotropic media (1) can be reduced to a scalar wave equation [3, pp. 729-730] by making use of the definitions given in [1, pp. 49-50]

$$\frac{\partial^2 \Pi}{\partial u_1^2} + \frac{1}{h_2 h_3} \frac{\partial}{\partial u_2} \left(\frac{h_3}{h_2} \frac{\partial \Pi}{\partial u_2} \right) + \frac{1}{h_2 h_3} \frac{\partial}{\partial u_3} \left(\frac{h_2}{h_3} \frac{\partial \Pi}{\partial u_3} \right) + k^2 \Pi = 0 \quad (4)$$

$$\text{with } \vec{\Pi} = \Pi(u_1, u_2, u_3) \vec{e}_1. \quad (5)$$

\vec{e}_1 is in the unit vector in the u_1 -direction.

The field components of the E-type waves are obtained by introducing (5) into (2a+b)

$$\begin{aligned} E_1 &= k^2 \Pi_e + \frac{\partial^2 \Pi_e}{\partial u_1^2}; \quad H_1 = 0, \\ E_2 &= \frac{1}{h_2} \frac{\partial^2 \Pi_e}{\partial u_1 \partial u_2}; \quad H_2 = \frac{(\sigma + j\omega\epsilon)}{h_3} \frac{\partial \Pi_e}{\partial u_3}, \\ E_3 &= \frac{1}{h_3} \frac{\partial^2 \Pi_e}{\partial u_1 \partial u_3}; \quad H_3 = -\frac{(\sigma + j\omega\epsilon)}{h_2} \frac{\partial \Pi_e}{\partial u_2}. \end{aligned} \quad (6)$$

The field components of the H-type waves are obtained by introducing (5) into (3a+b)

$$\begin{aligned} H_1 &= k^2 \Pi_m + \frac{\partial^2 \Pi_m}{\partial u_1^2}; \quad E_1 = 0, \\ H_2 &= \frac{1}{h_2} \frac{\partial^2 \Pi_m}{\partial u_1 \partial u_2}; \quad E_2 = -\frac{j\omega\mu}{h_3} \frac{\partial \Pi_m}{\partial u_3}, \\ H_3 &= \frac{1}{h_3} \frac{\partial^2 \Pi_m}{\partial u_1 \partial u_3}; \quad E_3 = \frac{j\omega\mu}{h_2} \frac{\partial \Pi_m}{\partial u_2}. \end{aligned} \quad (7)$$

As can be seen from (7) and (8), E-type waves have no H-component in the u_1 -direction, whereas H-type waves have no E-component in that direction. By choosing appropriate values for h_2 and h_3 , expressions for the field components in Cartesian, cylindrical (including parabolic and elliptic) and even spherical coordinate systems can be obtained.

The more general case with three arbitrary scale factors gives rise to an insoluble set of interdependent equations [1, pp. 50-51].

2.4 Hertz's Wave Equation in a Cartesian Coordinate System

The three scale factors h_1 , h_2 and h_3 all equal one in a right-hand Cartesian coordinate system (u_1, u_2, u_3) . Hence, Hertz's vector wave equation (4) simplifies to

$$\frac{\partial^2 \Pi}{\partial u_1^2} + \frac{\partial^2 \Pi}{\partial u_2^2} + \frac{\partial^2 \Pi}{\partial u_3^2} + k^2 \Pi = 0 \quad (8)$$

$$\text{with } \vec{\Pi} = \Pi(u_1, u_2, u_3) \vec{e}_1. \quad (9)$$

\vec{e}_1 is the unit vector in the u_1 -direction.

Therefore, the field components of the E-type waves are

$$\begin{aligned} E_1 &= k^2 \Pi_e + \frac{\partial^2 \Pi_e}{\partial u_1^2}; \quad H_1 = 0, \\ E_2 &= \frac{\partial^2 \Pi_e}{\partial u_1 \partial u_2}; \quad H_2 = (\sigma + j\omega\epsilon) \frac{\partial \Pi_e}{\partial u_3}, \\ E_3 &= \frac{\partial^2 \Pi_e}{\partial u_1 \partial u_3}; \quad H_3 = -(\sigma + j\omega\epsilon) \frac{\partial \Pi_e}{\partial u_2}. \end{aligned} \quad (10)$$

The field components of the H-type waves are

$$\begin{aligned} H_1 &= k^2 \Pi_m + \frac{\partial^2 \Pi_m}{\partial u_1^2}; \quad E_1 = 0, \\ H_2 &= \frac{\partial^2 \Pi_m}{\partial u_1 \partial u_2}; \quad E_2 = -j\omega\mu \frac{\partial \Pi_m}{\partial u_3}, \\ H_3 &= \frac{\partial^2 \Pi_m}{\partial u_1 \partial u_3}; \quad E_3 = j\omega\mu \frac{\partial \Pi_m}{\partial u_2}. \end{aligned} \quad (11)$$

2.5 Hertz's Wave Equation for a 2D-Uniform Guiding Structure

Propagation along a guiding structure occurs in one direction only. In this text, the x-axis is chosen to be parallel with the propagation direction. Therefore, the waves along a uniform guiding structure have only an $e^{j(\omega t - \beta_x x)}$ -dependence in that direction. This means that Hertz vector potentials for two-dimensional uniform guiding structures are of the form [3, p. 800]

$$\vec{\Pi} = F(y, z)e^{-j\beta_x x}\vec{e}_1$$

where \vec{e}_1 can be either in the x-, y- or z-direction

$$\text{and phase constant } \beta_x = \beta'_x - j\beta''_x = \frac{\gamma_x}{j}.$$

The propagation of electromagnetic waves is usually characterized in terms of the propagation constant $\gamma = \alpha + j\beta$, where α is called the attenuation constant.

The formulation for β used in this text, is consistent with the expression for γ , namely $\gamma = j(\beta' - j\beta'') = \beta'' + j\beta' \Rightarrow \beta'' \equiv \alpha$.

There exist a large number of 2D-uniform guiding structures, some of the best known examples are: the parallel wire line, coaxial cable, waveguide, strip line, microstrip line, slot line and the coplanar line.

Since $\frac{\partial^2 \Pi}{\partial x^2} = -\beta_x^2 \Pi$, Hertz's scalar wave equation (8) becomes

$$\frac{\partial^2 \Pi}{\partial y^2} + \frac{\partial^2 \Pi}{\partial z^2} + s^2 \Pi = 0 \quad (12)$$

$$\text{where } s^2 = k^2 - \beta_x^2 = \epsilon\mu\omega^2 - j\omega\mu\sigma - \beta_x^2. \quad (13)$$

Solutions to (12) can readily be found by separation of the variables. Namely, let $\Pi = Y(y)Z(z)e^{-j\beta_x x}$. (14)

Substituting (14) into (12) and dividing by (14) gives

$$\frac{1}{Y} \frac{d^2 Y}{dy^2} + \frac{1}{Z} \frac{d^2 Z}{dz^2} + s^2 = 0.$$

Since the last term in the above equation is independent of both y and z, the first two terms need to be this as well.

Therefore,

$$\frac{1}{Y} \frac{d^2 Y}{dy^2} = -s_y^2; \quad \frac{1}{Z} \frac{d^2 Z}{dz^2} = -s_z^2 \quad \text{and} \quad s_y^2 + s_z^2 = s^2. \quad (15)$$

The first two equations in (15) are linear homogeneous second order differential equations

$$\frac{d^2 Y}{dy^2} + s_y^2 Y = 0; \quad \frac{d^2 Z}{dz^2} + s_z^2 Z = 0.$$

Hence, suitable Hertz potential solutions for two-dimensional uniform guiding structures are of the form [6, p. 105]

$$\Pi = [c_1 e^{+js_y y} + c_2 e^{-js_y y}] \cdot [c_3 e^{+js_z z} + c_4 e^{-js_z z}] \cdot e^{-j\beta_x x}, \text{ or equally,}$$

$$\Pi = [c_5 \cos(s_y y) + c_6 \sin(s_y y)] \cdot [c_7 \cos(s_z z) + c_8 \sin(s_z z)] \cdot e^{-j\beta_x x}.$$

2.6 Hertz's Wave Equation in a Circular Cylindrical Coordinate System

In a cylindrical coordinate system, the scale factors are generally different from one, except for the scale factor associated with the symmetry axis, usually called the z-axis. In order to apply expression (4), the scale factor h_1 should equal one. Therefore, let $u_1 = z$.

The special case of a right-hand *circular* cylindrical coordinate system (r, ϕ, z) gives $u_1 = z$; $u_2 = r$ and $u_3 = \phi$. (16)

The differential line element $d\ell$ in a circular cylindrical coordinate system (r, ϕ, z) is [7]

$$d\ell = \sqrt{dr^2 + r^2d\phi^2 + dz^2}.$$

The scale factors are hence [6, p. 124]

$$h_1 = \left| \frac{\partial \ell}{\partial z} \right| = 1; \quad h_2 = \left| \frac{\partial \ell}{\partial r} \right| = 1 \quad \text{and} \quad h_3 = \left| \frac{\partial \ell}{\partial \phi} \right| = r. \quad (17)$$

Substitute (16) and (17) into (4) to get

$$\frac{\partial^2 \Pi}{\partial z^2} + \frac{1}{r} \frac{\partial}{\partial r} \left(r \frac{\partial \Pi}{\partial r} \right) + \frac{1}{r} \frac{\partial}{\partial \phi} \left(\frac{1}{r} \frac{\partial \Pi}{\partial \phi} \right) + k^2 \Pi = 0 \quad (18)$$

$$\text{with } \vec{\Pi} = \Pi(z, r, \phi) \vec{e}_z. \quad (19)$$

Propagation in cylindrical symmetric transmission lines occurs in one direction only, which is usually along the z-axis. This means that the expression for the Hertz vector potentials simplifies to

$$\vec{\Pi} = F(r, \phi) e^{-j\beta_z z} \vec{e}_z.$$

Since $\frac{\partial^2 \Pi}{\partial z^2} = -\beta_z^2 \Pi$, Hertz's scalar wave equation (18) becomes

$$\frac{1}{r} \frac{\partial}{\partial r} \left(r \frac{\partial \Pi}{\partial r} \right) + \frac{1}{r} \frac{\partial}{\partial \phi} \left(\frac{1}{r} \frac{\partial \Pi}{\partial \phi} \right) + s^2 \Pi = 0 \quad (20)$$

$$\text{where } s^2 = k^2 - \beta_z^2 = \epsilon \mu \omega^2 - j \omega \mu \sigma - \beta_z^2. \quad (21)$$

Solutions to (20) can readily be found by separation of the variables. Namely, let $\Pi = R(r)\Phi(\phi)e^{-j\beta_z z}$. (22)

Substituting (22) into (20) and dividing by (22) results in [3, p. 739]

$$\frac{1}{R} \left[\frac{1}{r} \frac{d}{dr} \left(r \frac{dR}{dr} \right) \right] + \frac{1}{\Phi} \left[\frac{1}{r} \frac{d}{d\phi} \left(\frac{1}{r} \frac{d\Phi}{d\phi} \right) \right] + s^2 = 0. \quad (23)$$

Multiplying (23) by r^2 gives

$$\frac{r}{R} \frac{d}{dr} \left(r \frac{dR}{dr} \right) + \frac{1}{\Phi} \frac{d^2 \Phi}{d\phi^2} + s^2 r^2 = 0. \quad (24)$$

Equation (24) can be separated using a separation constant n into

$$\frac{1}{\Phi} \frac{d^2 \Phi}{d\phi^2} = -n^2, \quad (25)$$

$$\frac{r}{R} \frac{d}{dr} \left(r \frac{dR}{dr} \right) + s_r^2 r^2 = n^2 \quad (26)$$

where $s_r^2 = s^2 = k^2 - \beta_z^2$.

Equation (25) is a linear homogeneous second order differential equation

$$\frac{d^2 \Phi}{d\phi^2} + n^2 \Phi = 0.$$

Solutions for Φ are of the form [6, p. 105]

$$\Phi = c_1 e^{+jn\phi} + c_2 e^{-jn\phi}, \text{ or equally,} \quad (27a)$$

$$\Phi = c_3 \cos(n\phi) + c_4 \sin(n\phi). \quad (27b)$$

Rewriting equation (26) results in an expression which can be recognized as Bessel's equation of order n [6, p. 106]

$$\frac{r}{R} \frac{d}{dr} \left(r \frac{dR}{dr} \right) + s_r^2 r^2 - n^2 = 0$$

$$\Rightarrow \frac{r}{R} \left(r \frac{d^2 R}{dr^2} + 1 \cdot \frac{dR}{dr} \right) + s_r^2 r^2 - n^2 = 0$$

$$\Rightarrow r^2 \frac{d^2 R}{dr^2} + r \frac{dR}{dr} + (s_r^2 r^2 - n^2) R = 0 \quad (28)$$

with $n \geq 0$.

Solutions to Bessel's equation of order n (28) are of the form [6, p. 106], [8, pp. 97-88]

$$R = c_5 J_n(s_r r) + c_6 Y_n(s_r r), \text{ or equally,} \quad (29a)$$

$$R = c_7 H_n^{(1)}(s_r r) + c_8 H_n^{(2)}(s_r r). \quad (29b)$$

These solutions are linearly independent only if n is a positive integer.

At this point, Hertz's scalar wave equation for circular cylindrical coordinate systems (20) is solved. It suffices to substitute any form of (27) and (29) into (22) to obtain the Hertz potential solutions.

Substituting (16) and (22) into (6) gives the field components of the E-type waves expressed in terms of a Hertz potential [3, p.740]

$$\begin{aligned}
 E_z &= s_r^2 \Pi_e; \quad H_z = 0, \\
 E_r &= -j\beta_z \frac{\partial \Pi_e}{\partial r}; \quad H_r = \frac{(\sigma + j\omega\epsilon)}{r} \frac{\partial \Pi_e}{\partial \phi}, \\
 E_\phi &= -j\frac{\beta_z}{r} \frac{\partial \Pi_e}{\partial \phi}; \quad H_\phi = -(\sigma + j\omega\epsilon) \frac{\partial \Pi_e}{\partial r}.
 \end{aligned} \tag{30}$$

Likewise, substitute (16) and (22) into (7) to obtain the field components of the H-type waves

$$\begin{aligned}
 H_z &= s_r^2 \Pi_m; \quad E_z = 0, \\
 H_r &= -j\beta_z \frac{\partial \Pi_m}{\partial r}; \quad E_r = -j\frac{\omega\mu}{r} \frac{\partial \Pi_m}{\partial \phi}, \\
 H_\phi &= -j\frac{\beta_z}{r} \frac{\partial \Pi_m}{\partial \phi}; \quad E_\phi = j\omega\mu \frac{\partial \Pi_m}{\partial r}.
 \end{aligned} \tag{31}$$

2.7 Conclusions

Chapter 2 gave a review of Hertz potential theory. The convenience of expressing source free electromagnetic fields in terms of Hertz potentials was clearly demonstrated. The theory is kept as general as possible, making it useful as a reference while solving many other electromagnetic problems.

2.8 References

- [1] J. A. Stratton, *Electromagnetic Theory*, McGraw-Hill, 1941
- [2] W. Weiglhofer, "Scalarisation of Maxwell's equations in general inhomogeneous bianisotropic media," *IEE Proceedings*, Vol. 134, Pt. H, No. 4, August 1987, pp. 357-360
- [3] K. Simonyi, *Theoretische Elektrotechnik*, Johann Ambrosius Barth, 10. Auflage, 1993, (in German)
- [4] W. Weiglhofer and W. Papousek, "Skalare Hertzsche Potentiale für anisotrope Medien," *Archiv für Elektronik und Übertragungstechnik*, Vol. 39, No. 6, Nov.-Dec. 1985, pp. 343-346, (in German)
- [5] R. E. Collin, *Foundations for Microwave Engineering*, McGraw-Hill, 2nd Ed., 1992, p. 26
- [6] M. R. Spiegel, *Mathematical Handbook of Formulas and Tables*, Schaum's Outline Series, McGraw-Hill, 1968
- [7] Joseph A. Edminister, *Electromagnetics*, Schaum's Outline Series, McGraw-Hill, 2nd Ed., 1993, p. 5
- [8] R. E. Collin, *Field Theory of Guided Waves*, IEEE Press, 2nd Ed., 1991

3 Plane Surface Waves along Plane Layers of Isotropic Media

3.1 Definition

A *plane surface wave* is defined as a plane wave that propagates along a plane interface of two different media without radiation [1, p.5].

Note that radiation in this context is construed as being energy converted from the surface wave field to some other field form.

Plane surface waves are inhomogeneous waves because the field is not constant along surfaces of constant phase. In fact, in the case of a surface wave the field decays exponentially over the wavefront with increase of distance from the surface.

There are E-type and H-type surface waves. The field of an E-type plane surface wave is depicted in Figure 3.1. For an H-type wave the E- and H-fields are interchanged and one of the fields is reversed in sign. Explicit equations for the fields of plane surface waves along various structures will be derived rigorously later in this chapter.

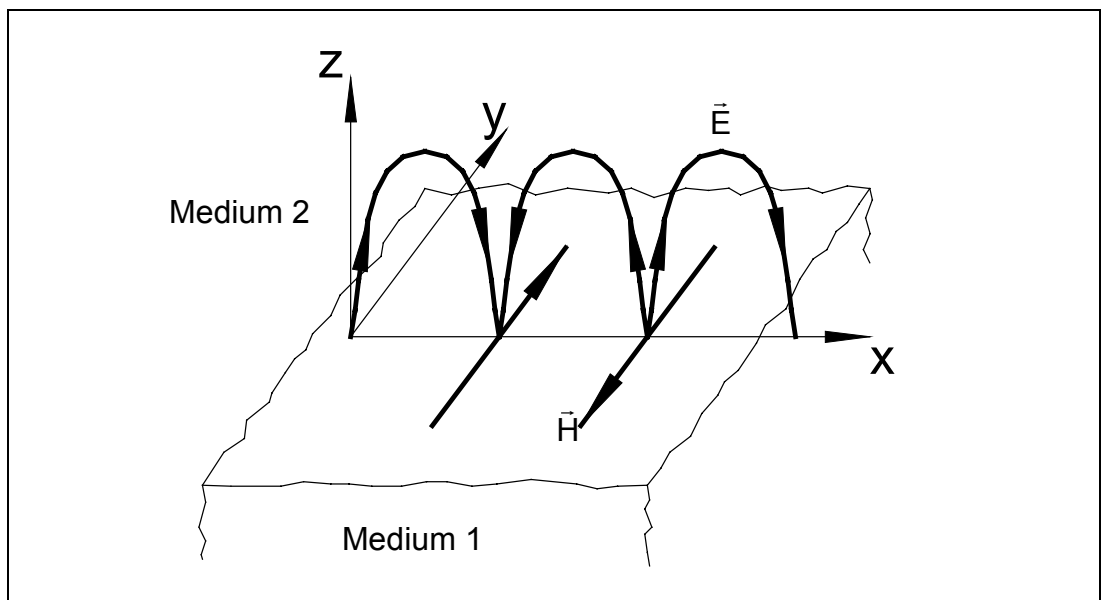


Figure 3.1: The field of an E-type plane surface wave

3.2 Plane Surface Waves and the Brewster Angle Phenomenon

There are many ways to explain the mechanism of surface waves. In the mid-fifties Barlow et al. introduced the concept of surface impedance for this purpose [1, pp. 15-17], [2], which will be explained in a later section. Earlier work by Zenneck (1907) associated plane surface waves with the Brewster angle phenomenon [1, pp. 29-33], [3, p. 697-701]. For this reason plane surface waves are sometimes also called *Zenneck waves*. Due to the many prevailing misconceptions, the relation between plane surface waves and the Brewster angle will receive some further attention here.

The Brewster angle is the angle of incidence at which a plane wave incident on a plane material interface is totally transmitted (i.e. without reflection) from one medium, called medium 2 here, into another medium, called medium 1. Both media are assumed to be half spaces. In lossless media, the Brewster angle phenomenon only occurs for perpendicular and parallel polarized incident plane waves. (The terms “perpendicular” and “parallel” refer to the orientation of the electric field intensity vector \vec{E}_i of the incident plane wave with respect to the plane of incidence.) The Brewster angle is different for the two types of polarization. From Fresnel’s equations [4], it can be shown that the Brewster angle for perpendicular polarized incident plane waves is

$$\theta_{B\perp} = a \sin \sqrt{\frac{1 - \frac{\epsilon_1 \mu_2}{\epsilon_2 \mu_1}}{1 - \left(\frac{\mu_2}{\mu_1}\right)^2}} \text{ and}$$

$$\theta_{B//} = a \sin \sqrt{\frac{1 - \frac{\epsilon_2 \mu_1}{\epsilon_1 \mu_2}}{1 - \left(\frac{\epsilon_2}{\epsilon_1}\right)^2}}$$

for parallel polarized incident plane waves.

Above equations result in a complex value for the Brewster angle:

- if, for perpendicular polarization, $\mu_2 > \mu_1$,
- or if, for parallel polarization, $\epsilon_2 > \epsilon_1$,
- or if at least one of the two media has losses.

The physical meaning of a *complex angle of incidence* is an inhomogeneous plane wave (which in fact very much resembles a surface wave) incident at that angle [1, p. 30], [3, p. 717], [5]. When the Brewster angle is complex, the angle for which the magnitude of the reflection coefficient is a minimum, is called *the pseudo-Brewster angle* [1, p. 31]. The Brewster angle is also sometimes called *the polarizing angle* since a wave with both perpendicular and parallel components and which is incident at the Brewster angle will produce a reflected wave with only a perpendicular or parallel component [6, p. 617]. To summarize, *the only connection between surface waves and the Brewster angle lies in the fact that the inhomogeneous wave required by a complex Brewster angle resembles a surface wave.*

3.3 Plane Surface Waves, Total Reflection and Leaky Waves

An idea of what the different fields along a material interface may look like, can be obtained by employing ray-optics theory once again. The existence of propagating plane surface waves along a coated perfectly conducting plane, for example, can be explained with the help of the total reflection phenomenon as shown in Figure 3.2.

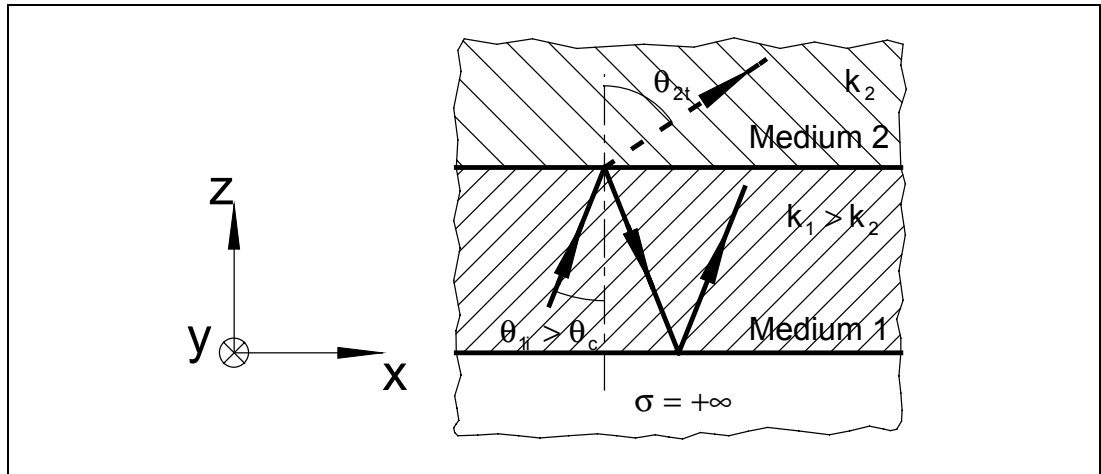


Figure 3.2: A ray-optics explanation for the propagation of plane surface waves along a coated perfectly conducting plane

Total reflection only occurs when a wave from medium 1 impinges upon medium 2 at an angle of incidence θ_{ii} equal to or exceeding *the critical angle* θ_c and then only if medium 1 is more “dense” than medium 2 ($k_1 > k_2$).

An expression for the critical angle as a function of k_1 and k_2 can be obtained as follows. The relation between the angles of reflection and refraction is given by Snell’s law $k_2 \cdot \sin(\theta_{2t}) = k_1 \cdot \sin(\theta_{ii})$

$$\Rightarrow \sin(\theta_{2t}) = \frac{k_1}{k_2} \sin(\theta_{ii}).$$

There will be no refracted wave if $\sin(\theta_{2t})$ is greater than one or equivalently, if $\sin(\theta_{ii}) > \frac{k_2}{k_1} = \sin(\theta_c)$.

$$\text{Hence, } \theta_c = \sin^{-1}\left(\frac{k_2}{k_1}\right).$$

As suggested in Figure 3.2, total reflection can be accompanied by a surface wave propagating in medium 1, parallel with the material interface. What is not shown, is the fact that a surface wave field most of the times also extends into medium 2. This will be proven in the next section. Note that a surface wave can exist along a coated perfectly conducting plane only if the coating (medium 1) is more dense than the upper half space (medium 2) ($k_1 > k_2$). If this is not the case or if the angle of incidence θ_{i1} is smaller than the critical angle θ_c , part of the wave in medium 1 will be transmitted into medium 2 with each partial reflection. Therefore, the field will quickly attenuate in the x-direction. The resulting inhomogeneous plane wave is called a *leaky wave* and propagates away from the interface (Fig. 3.3b).

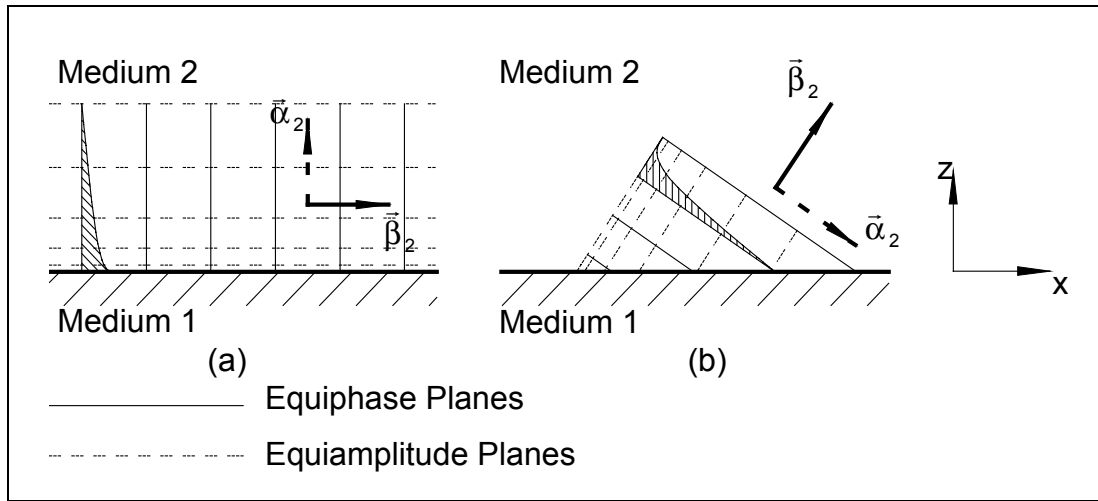


Figure 3.3: (a) A surface wave, (b) a leaky wave (Medium 2 is assumed to be loss free in this figure.)

Note that $\vec{\alpha}_2$ is perpendicular to $\vec{\beta}_2$ only if medium 2 is loss free ($\text{Im}(k_2) = 0$). This will be shown now.

$$k_2^2 = k_{2x}^2 + k_{2z}^2 = (\beta_{2x} - j\alpha_{2x})^2 + (\beta_{2z} - j\alpha_{2z})^2$$

$$\Rightarrow k_2^2 = \beta_{2x}^2 + \beta_{2z}^2 - (\alpha_{2x}^2 + \alpha_{2z}^2) - 2j(\alpha_{2x}\beta_{2x} + \alpha_{2z}\beta_{2z}).$$

$$\text{Only and only if } \text{Im}(k_2) = 0 \Rightarrow \alpha_{2x}\beta_{2x} + \alpha_{2z}\beta_{2z} = 0$$

$$\Rightarrow \vec{\alpha}_2 \cdot \vec{\beta}_2 = 0 \Rightarrow \vec{\alpha}_2 \perp \vec{\beta}_2.$$

For the sake of simplicity, $\vec{\alpha}_2$ will always be drawn for the case where medium 2 is loss free, i.e. perpendicular to $\vec{\beta}_2$. However, the theory developed in this text equally applies for lossy upper media.

Leaky waves violate the radiation condition since they only may exist if power is delivered to medium 1 from outside, in a direction towards the material interface with medium 2. This can be achieved by replacing the perfectly conducting plane in Figure 3.2 by the outer wall of a slotted waveguide. It also important to know that a leaky wave can not be excited by a plane wave incident from medium 2. In such a case, the result will be a standing wave in medium 2.

3.4 Plane Surface Waves along a Coated, Electric Perfectly Conducting Plane

3.4.1 Introduction

In the previous section the existence of surface waves was shown by making use of ray-optics theory, which is merely an approximate theoretical model. A rigorous approach consists of treating the layer structure as a boundary-value problem and solving it using Hertz potentials. A first analysis deals with the propagation of plane surface waves along the interface of a homogeneous linear isotropic half space with a homogeneous linear isotropic layer of finite height h that is supported by an electric perfectly conducting plane (Fig. 3.4). The solution of the more general three-layer structure with arbitrary material constants will be presented later in this chapter. The special case of an electric perfectly conducting substrate is presented first because it more readily provides the reader with a number of basic insights. It is important to note that the structures in the following sections can be solved both for forward propagating surface waves and leaky waves. For surface wave propagation it is necessary that $k_1 > k_2$. For leaky waves, k_1 may be smaller than k_2 . Leaky waves violate the radiation condition and are therefore of little practical interest to RCS management.

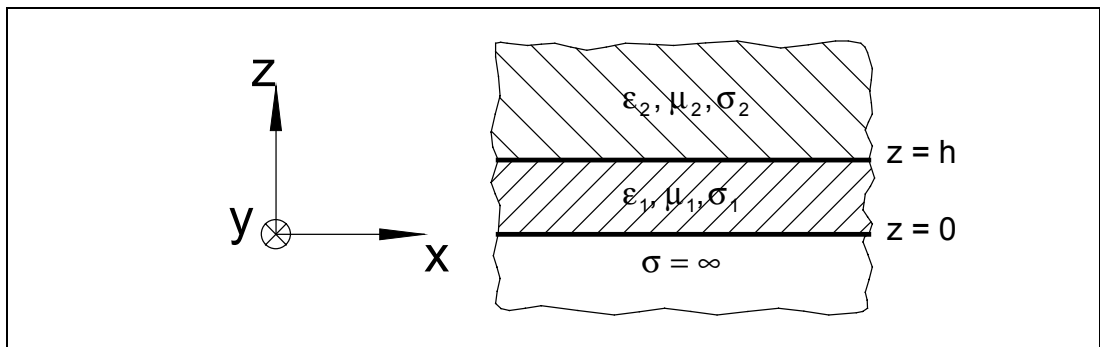


Figure 3.4: A coated, electric perfectly conducting plane; it is assumed that all media are homogeneous, linear and isotropic.

It is obvious that the Cartesian coordinate system (Section 2.4) is best suited for the analysis of plane waves. Assuming plane wave propagation in the x-direction, the structure of Figure 3.4 can be treated as a special case of a 2D-uniform guiding structure (see Section 2.5). Here however, none of the field components can have a y-dependence due to the fact that both media are infinite in the y-direction. Hence, the Hertz vector potential $\vec{\Pi}$ will have no y-dependence. Note that a field vector can still have components in the y-direction. For reasons that will be explained later, $\vec{\Pi}$ needs to be chosen in the z-direction.

A general expression for a Hertz vector potential having above-mentioned properties is

$$\vec{\Pi} = \Pi(z)e^{-j\beta x}\vec{e}_z. \quad (1)$$

In order to be able to apply (2.10) and (2.11), the relation between the curvilinear coordinates and the Cartesian coordinates must be as follows

$$u_1 = z; \quad u_2 = x \quad \text{and} \quad u_3 = y.$$

Substituting (1) into (2.10) results in general expressions for the field components of E-type waves within a medium

$$\begin{aligned} E_z &= k^2 \Pi_e + \frac{\partial^2 \Pi_e}{\partial z^2}; \quad H_z = 0, \\ E_x &= -j\beta_x \frac{\partial \Pi_e}{\partial z}; \quad H_x = (\sigma + j\omega\epsilon) \frac{\partial \Pi_e}{\partial y} = 0, \\ E_y &= \frac{\partial^2 \Pi_e}{\partial z \partial y} = 0; \quad H_y = j\beta_x (\sigma + j\omega\epsilon) \Pi_e. \end{aligned} \quad (2)$$

From (2) it can be seen that *E-type plane surface waves* are:

- 1) *longitudinal section magnetic* (LSM) waves; the magnetic field intensity \vec{H} has no component in the direction normal to the material interface ($H_z = 0$) and
- 2) *transversal magnetic* (TM) waves; the magnetic field intensity \vec{H} has no component in the propagation direction ($H_x = 0$).

Substituting (1) into (2.11) leads to general expressions for the field components of H-type waves within a medium

$$\begin{aligned} H_z &= k^2 \Pi_m + \frac{\partial^2 \Pi_m}{\partial z^2}; \quad E_z = 0, \\ H_x &= -j\beta_x \frac{\partial \Pi_m}{\partial z}; \quad E_x = -j\omega\mu \frac{\partial \Pi_m}{\partial y} = 0, \\ H_y &= \frac{\partial^2 \Pi_m}{\partial z \partial y} = 0; \quad E_y = \beta_x \omega\mu \Pi_m. \end{aligned} \quad (3)$$

It can be concluded from (3) that *H-type plane surface waves* are:

- 1) *longitudinal section electric* (LSE) waves; the electric field intensity \vec{E} has no component in the direction normal to the material interface ($E_z = 0$) and
- 2) *transversal electric* (TE) waves; the electric field intensity \vec{E} has no component in the propagation direction ($E_x = 0$).

3.4.2 E-Type Plane Surface Waves along a Coated, Electric Perfectly Conducting Plane

A suitable Hertz function for medium 1 that satisfies the boundary condition $E_x = 0$ at $z = 0$

$$\text{is } \Pi_1 = A_1 \cos(s_{z1}z) e^{-j\beta_x x}. \quad (4)$$

The factor $\cos(s_{z1}z)$ may be interpreted as a standing wave in the z -direction.

Introducing (4) into (2) results in

$$E_{z1} = A_1 (k_1^2 - s_{z1}^2) \cos(s_{z1}z) e^{-j\beta_x x}, \quad (5a)$$

$$E_{x1} = j\beta_x A_1 s_{z1} \sin(s_{z1}z) e^{-j\beta_x x}, \quad (5b)$$

$$E_{y1} = 0, \quad (5c)$$

$$H_{z1} = 0, \quad (5d)$$

$$H_{x1} = 0, \quad (5e)$$

$$H_{y1} = j\beta_x (\sigma_1 + j\omega\epsilon_1) A_1 \cos(s_{z1}z) e^{-j\beta_x x}. \quad (5f)$$

Recalling (2.13)

$$s_{z1}^2 = k_1^2 - \beta_x^2 \Rightarrow s_{z1} = +\sqrt{k_1^2 - \beta_x^2}. \quad (6)$$

It is only for a matter of convenience that s_{z1} is chosen to equal the positive square root. Choosing the negative square root would have no effect on the results.

A suitable Hertz function for medium 2 that satisfies the boundary condition $\vec{E} = \vec{H} = \vec{0}$ when $z \rightarrow +\infty$

$$\text{is } \Pi_2 = A_2 e^{-js_{z2}(z-h)} e^{-j\beta_x x}. \quad (7)$$

The factor $e^{-js_{z2}(z-h)}$ may be interpreted as a wave propagating in the positive z -direction with phase constant $s_{z2} = s'_{z2} - js''_{z2}$. Contrary to (6), the sign of s_{z2} is of importance here because s_{z2} belongs to the argument of an exponential function and therefore determines whether the solutions will be forward propagating surface waves or leaky waves. For surface waves, $s''_{z2} > 0 \Rightarrow \text{Im}(s_{z2}) < 0$, which corresponds to a decaying field in the positive z -direction. If on the other hand $\text{Im}(s_{z2}) > 0$, the wave is a leaky wave. In that case the radiation condition is violated because the field in medium 2 increases exponentially away from the interface.

The appropriate sign for s_{z2} can easily be found when both materials are lossless. k_2 and β_x are real numbers then. Moreover, all plane surface waves and leaky waves will be slow waves ($\beta_x > k_2$) as is the case for all inhomogeneous waves propagating in loss free media (see Appendix A).

For surface waves in loss free media, js_{z2} must be real and positive,

$$\text{hence } js_{z2} = +\sqrt{-s_{z2}^2} = +\sqrt{\beta_x^2 - k_2^2}$$

$$\Rightarrow s_{z2} = -j\sqrt{\beta_x^2 - k_2^2} = +\sqrt{k_2^2 - \beta_x^2} \quad (\text{see also Appendix B}),$$

whereas for leaky waves in loss free media

$$s_{z2} = -\sqrt{k_2^2 - \beta_x^2} \Rightarrow js_{z2} = -j\sqrt{k_2^2 - \beta_x^2} = -\sqrt{\beta_x^2 - k_2^2}.$$

However, things are more complicated when at least one of both media contains losses. Surface waves and leaky waves no longer need to be slow waves. The many possibilities for the value of s_{z2} will be discussed now for the case $k_2 = k_0$.

$$\text{Thus, } s_{z0}^2 = k_0^2 - \beta_x^2 = k_0^2 - (\beta'_x - j\beta''_x)^2 = k_0^2 - \beta_x'^2 + \beta_x''^2 + 2j\beta'_x\beta_x''$$

$$\Rightarrow \angle s_{z0}^2 = a \tan\left(\frac{2\beta'_x\beta_x''}{k_0^2 - \beta_x'^2 + \beta_x''^2}\right).$$

Finally, de Moivre's theorem gives

$$\angle s_{z0} = \frac{1}{2} a \tan\left(\frac{2\beta'_x\beta_x''}{k_0^2 - \beta_x'^2 + \beta_x''^2}\right) + p\pi$$

where p is either 0 or 1.

$$\text{Now, let } u = \left(\frac{2\beta'_x\beta_x''}{k_0^2 - \beta_x'^2 + \beta_x''^2}\right).$$

The four possibilities for the location of s_{z0} in the s_{z0} -plane (Fig. 3.5) are

$$u > 0, p = 0 \Rightarrow \angle s_{z0} \in \left]0, \frac{\pi}{4}\right[\Rightarrow \text{a leaky wave,}$$

$$u \geq 0, p = 1 \Rightarrow \angle s_{z0} \in \left[\pi, \frac{5\pi}{4}\right[\Rightarrow \text{a surface wave,}$$

$$u \leq 0, p = 0 \Rightarrow \angle s_{z0} \in \left]-\frac{\pi}{4}, 0\right] = \left]\frac{7\pi}{4}, 2\pi\right] \Rightarrow \text{a surface wave,}$$

$$u < 0, p = 1 \Rightarrow \angle s_{z0} \in \left]\frac{3\pi}{4}, \pi\right[\Rightarrow \text{a leaky wave.}$$

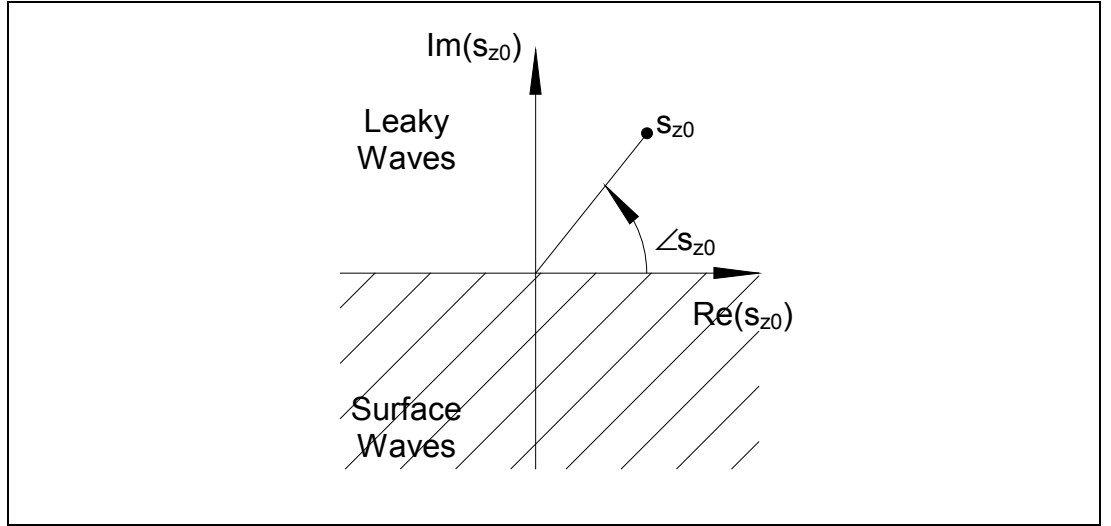


Figure 3.5: The complex s_{z0} -plane

Slow surface waves with moderate losses will most often fall into the third category. Equation (8a) gives rise to surface wave solutions as long as

$$u \leq 0 \Leftrightarrow k_0^2 - \beta_x'^2 + \beta_x''^2 \leq 0 \Leftrightarrow \beta_x''^2 \leq k_0^2 - \beta_x'^2$$

where k_0 , β_x' and β_x'' are all positive real numbers.

Even surface wave absorbers will almost always meet this requirement. This is shown by the numerical examples presented later in this chapter. However, to remain as general as possible, surface wave solutions are only obtained by letting $\text{Re}(js_{z2}) \geq 0$ or

$$js_{z2} = \text{sign}\left[\text{Re}\left(\sqrt{\beta_x^2 - k_2^2}\right)\right] \sqrt{\beta_x^2 - k_2^2}. \quad (8a)$$

To obtain leaky wave solutions, let

$$js_{z2} = -\text{sign}\left[\text{Re}\left(\sqrt{\beta_x^2 - k_2^2}\right)\right] \sqrt{\beta_x^2 - k_2^2}. \quad (8b)$$

Introducing (7) into (2) leads to

$$E_{z2} = A_2 (k_2^2 - s_{z2}^2) e^{-js_{z2}(z-h)} e^{-j\beta_x x}, \quad (9a)$$

$$E_{x2} = -\beta_x A_2 s_{z2} e^{-js_{z2}(z-h)} e^{-j\beta_x x}, \quad (9b)$$

$$E_{y2} = 0, \quad (9c)$$

$$H_{z2} = 0, \quad (9d)$$

$$H_{x2} = 0, \quad (9e)$$

$$H_{y2} = j\beta_x (\sigma_2 + j\omega\epsilon_2) A_2 e^{-js_{z2}(z-h)} e^{-j\beta_x x}. \quad (9f)$$

The tangential components of both \vec{E} and \vec{H} are continuous across the interface of two media and therefore

$$\begin{aligned} E_{x1} &= E_{x2} \text{ at } z = h \\ \Rightarrow A_1 s_{z1} \sin(s_{z1}h) &= jA_2 s_{z2}, \end{aligned} \quad (10)$$

$$\begin{aligned} \text{as well as } H_{y1} &= H_{y2} \text{ at } z = h \\ \Rightarrow (\sigma_1 + j\omega\epsilon_1)A_1 \cos(s_{z1}h) &= (\sigma_2 + j\omega\epsilon_2)A_2. \end{aligned} \quad (11)$$

Note that (10) and (11) would have resulted in a set of contradictory equations, if $\vec{\Pi}_{m,e}$ were chosen in any direction other than the z-direction.

Dividing (10) by (11) yields

$$\frac{s_{z1}}{\sigma_1 + j\omega\epsilon_1} \tan(s_{z1}h) = \frac{j s_{z2}}{\sigma_2 + j\omega\epsilon_2}. \quad (12)$$

Substituting (6) and (8a) into (12) results in the following expression for E-type surface waves

$$\frac{\sqrt{k_1^2 - \beta_x^2}}{\sigma_1 + j\omega\epsilon_1} \tan\left(h\sqrt{k_1^2 - \beta_x^2}\right) = \frac{\text{sign}\left[\text{Re}\left(\sqrt{\beta_x^2 - k_2^2}\right)\right]\sqrt{\beta_x^2 - k_2^2}}{\sigma_2 + j\omega\epsilon_2}. \quad (13)$$

This equation is transcendental and can therefore only be solved numerically for β_x . It is called a *dispersion equation* because it expresses the nonlinear frequency dependence of β_x . Both equation (12) and (13) are expressions for *the transverse resonance condition* which requires the same value for the longitudinal wave impedance looking straight down to the interface ($z = h$) (14) as for the longitudinal wave impedance looking straight up [7, p. 12-6]. Hence, there will be no reflection in the equivalent transmission line of the layer structure (Fig. 3.7).

Looking straight down from medium 2 to the interface, *the longitudinal surface impedance* is (for a definition see Section 5.3.2)

$$Z_{s\ell} = -\frac{E_\ell}{H_t} = -\frac{E_{x2}(z=h)}{H_{y2}(z=h)} = -\frac{j s_{z2}}{\sigma_2 + j\omega\epsilon_2} = j \frac{s_{z2}}{\omega\epsilon_2 - j\sigma_2}. \quad (14)$$

The minus sign in (14) originates from the fact that the Poynting vector $\vec{S} = \vec{E}_{x2} \times \vec{H}_{y2}$ is in the positive z-direction, whereas $Z_{s\ell}$ is the surface impedance at the interface, looking in the negative z-direction.

The value of the transversal surface impedance is undefined.

3.4.3 H-Type Plane Surface Waves along a Coated, Electric Perfectly Conducting Plane

A suitable Hertz function for medium 1 that satisfies the boundary condition $E_y = 0$ at $z = 0$

$$\text{is } \Pi_1 = A_1 \sin(s_{z1}z) e^{-j\beta_x x}. \quad (15)$$

The factor $\sin(s_{z1}z)$ may be interpreted as a standing wave in the z -direction.

Introducing (15) into (3) results in

$$H_{z1} = A_1 (k_1^2 - s_{z1}^2) \sin(s_{z1}z) e^{-j\beta_x x}, \quad (16a)$$

$$H_{x1} = -j\beta_x A_1 s_{z1} \cos(s_{z1}z) e^{-j\beta_x x}, \quad (16b)$$

$$H_{y1} = 0, \quad (16c)$$

$$E_{z1} = 0, \quad (16d)$$

$$E_{x1} = 0, \quad (16e)$$

$$E_{y1} = \beta_x \omega \mu_1 A_1 \sin(s_{z1}z) e^{-j\beta_x x}. \quad (16f)$$

Recalling (2.13)

$$s_{z1}^2 = k_1^2 - \beta_x^2 \Rightarrow s_{z1} = +\sqrt{k_1^2 - \beta_x^2}. \quad (17)$$

It is only for a matter of convenience that s_{z1} is chosen to equal the positive square root. Choosing the negative square root would have no effect on the results.

A suitable Hertz function for medium 2 that satisfies the boundary condition $\vec{E} = \vec{H} = \vec{0}$ when $z \rightarrow +\infty$

$$\text{is } \Pi_2 = A_2 e^{-js_{z2}(z-h)} e^{-j\beta_x x}. \quad (18)$$

For s_{z2} , the same reasoning applies as in the previous section.

Hence, surface wave solutions are obtained by letting $\text{Re}(js_{z2}) \geq 0$ or

$$js_{z2} = \text{sign} \left[\text{Re} \left(\sqrt{\beta_x^2 - k_2^2} \right) \right] \sqrt{\beta_x^2 - k_2^2}. \quad (19a)$$

To obtain leaky wave solutions, let

$$js_{z2} = -\text{sign} \left[\text{Re} \left(\sqrt{\beta_x^2 - k_2^2} \right) \right] \sqrt{\beta_x^2 - k_2^2}. \quad (19b)$$

Introducing (18) into (3) leads to

$$H_{z2} = A_2 (k_2^2 - s_{z2}^2) e^{-js_{z2}(z-h)} e^{-j\beta_x x}, \quad (20a)$$

$$H_{x2} = -\beta_x A_2 s_{z2} e^{-js_{z2}(z-h)} e^{-j\beta_x x}, \quad (20b)$$

$$H_{y2} = 0, \quad (20c)$$

$$E_{z2} = 0, \quad (20d)$$

$$E_{x2} = 0, \quad (20e)$$

$$E_{y2} = \beta_x \omega \mu_2 A_2 e^{-js_{z2}(z-h)} e^{-j\beta_x x}. \quad (20f)$$

The tangential components of both \vec{E} and \vec{H} are continuous across the interface of two media and therefore

$$H_{x1} = H_{x2} \text{ at } z = h$$

$$\Rightarrow A_1 s_{z1} \cos(s_{z1}h) = -jA_2 s_{z2}, \quad (21)$$

as well as $E_{y1} = E_{y2}$ at $z = h$

$$\Rightarrow \mu_1 A_1 \sin(s_{z1}h) = \mu_2 A_2. \quad (22)$$

Note that (22) and (21) would have resulted in a set of contradictory equations, if $\vec{\Pi}$ were chosen in any direction other than the z-direction.

Dividing (22) by (21) and multiplying both sides by $j\omega$ yields

$$\frac{j\omega\mu_1}{s_{z1}} \tan(s_{z1}h) = -\frac{j\omega\mu_2}{js_{z2}}. \quad (23)$$

Substituting (17) and (19a) into (23) results in the following expression for H-type surface waves

$$\frac{j\omega\mu_1}{\sqrt{k_1^2 - \beta_x^2}} \tan\left(h\sqrt{k_1^2 - \beta_x^2}\right) = -\frac{j\omega\mu_2}{\text{sign}\left[\text{Re}\left(\sqrt{\beta_x^2 - k_2^2}\right)\right]\sqrt{\beta_x^2 - k_2^2}}. \quad (24)$$

This dispersion equation is transcendental and can therefore only be solved numerically for β_x . Both equation (23) and (24) are expressions for the transverse resonance condition which requires the same value for the transversal wave impedance looking straight down to the interface ($z = h$) (25) as for the transversal wave impedance looking straight up [7, p. 12-6]. Hence, there will be no reflection in the equivalent transmission line of the layer (Fig. 3.7).

Looking straight down from medium 2 to the interface, *the transversal surface impedance* is (for a definition see Section 5.3.2)

$$Z_{st} = \frac{E_t}{H_\ell} = \frac{E_{y2}(z = h)}{H_{x2}(z = h)} = -\frac{\omega\mu_2}{s_{z2}} = -j\frac{\omega\mu_2}{js_{z2}}. \quad (25)$$

In (25), the Poynting vector $\vec{S} = \vec{E}_{y2} \times \vec{H}_{x2}$ is in the negative z-direction, the same direction used for determining Z_{st} . Hence, no change in sign is needed as in (14).

The value of the longitudinal surface impedance is undefined.

3.4.4 High-Frequency Solution for E-Type and H-Type Plane Surface Waves along a Coated, Electric Perfectly Conducting Plane

The transcendental equations (12) and (23) will now be solved in the limit case when the frequency $f \rightarrow +\infty$. The characteristics of a surface wave are primarily determined by the quantities β_x and js_{z2} , the phase constant in the propagation direction and the decay in the direction perpendicular to the material interface, respectively.

Applying (2.13) twice gives the relation between s_{z2} and s_{z1}

$$\begin{aligned} s_{z1}^2 - s_{z2}^2 &= k_1^2 - \beta_x^2 - k_2^2 + \beta_x^2 = k_1^2 - k_2^2 \\ \Rightarrow s_{z1}^2 &= k_1^2 - k_2^2 + s_{z2}^2. \end{aligned} \quad (27)$$

$s_{z1}h$ appears as the argument of a tangent function in the dispersion equation of both E-type as H-type surface waves. A tangent function takes on every positive value in the interval $[0, \pi/2[$ and every negative value in $]\pi/2, \pi]$. Consequently, the first root of dispersion equation (12), which corresponds to the fundamental E-type mode, occurs at $0 < s_{z1}h < \pi/2 \Rightarrow 0 < s_{z1} < \pi/2h$. Similarly, the first root of dispersion equation (23), which corresponds to the fundamental H-type mode, occurs at $\pi/2 < s_{z1}h < \pi \Rightarrow \pi/(2h) < s_{z1} < \pi/h$. So for both wave types, s_{z1} will always have a finite value.

By contrast, $k_1^2 - k_2^2$ will become infinite if $f \rightarrow +\infty$ because $k_1^2 - k_2^2 = (\epsilon_{r1}\mu_{r1} - \epsilon_{r2}\mu_{r2})\epsilon_0\mu_0\omega^2$.

Knowing the behaviour of s_{z1} and $k_1^2 - k_2^2$ for $f \rightarrow +\infty$, equation (27) must result in $s_{z2}^2 \rightarrow -\infty \Rightarrow js_{z2} \rightarrow +\infty$ for $f \rightarrow +\infty$. This means that the surface wave field will not extend outside the coating layer for extremely high frequencies. Optical dielectric waveguides work on this principle.

Also, $s_{z1}^2 \ll k_1^2$ for $f \rightarrow +\infty$, because, as was shown before, s_{z1} remains bounded for very high frequencies.

$$\text{Hence, } \beta_x^2 \Big|_{f \rightarrow +\infty} \equiv (k_1^2 - s_{z1}^2) \Big|_{f \rightarrow +\infty} = k_1^2 \Big|_{f \rightarrow +\infty}. \quad (28)$$

Thus at extremely high frequencies a surface wave behaves as a inhomogeneous plane wave propagating entirely in medium 1. In general, the wave will remain inhomogeneous because s_{z1} does not have to be zero in (5b) and (16b).

3.4.5 Low-Frequency Solution for E-Type Plane Surface Waves along Thin Coatings on a Plane PEC

When the frequency is very low, the wave number k_1 will be very small. Since $s_{z1} = \sqrt{k_1^2 - \beta_x^2}$, s_{z1} will also be very small. The tangent function in equation (12) can be approximated by its argument $s_{z1}h$ if also h is electrically small, but not necessarily zero.

If this is the case, the dispersion equation for E-type surface waves (12) reduces to

$$\frac{s_{z1}^2 h}{\sigma_1 + j\omega\epsilon_1} \Big|_{f \rightarrow 0} = \frac{j s_{z2}}{\sigma_2 + j\omega\epsilon_2} \Big|_{f \rightarrow 0}. \quad (29)$$

Raising the power of (29), substituting (27) and rewriting gives

$$\begin{aligned} h^2 (\sigma_2 + j\omega\epsilon_2)^2 s_{z1}^2 \Big|_{f \rightarrow 0} &= (\sigma_2 + j\omega\epsilon_2)^2 (k_1^2 - k_2^2 - s_{z1}^2) \Big|_{f \rightarrow 0} \\ \Rightarrow s_{z1}^2 \Big|_{f \rightarrow 0} &= \frac{(\sigma_1 + j\omega\epsilon_1)^2 (k_1^2 - k_2^2)}{(\sigma_1 + j\omega\epsilon_1)^2 + h^2 (\sigma_2 + j\omega\epsilon_2)^2} \Big|_{f \rightarrow 0}. \end{aligned} \quad (30)$$

Substitute (30) into (6) to get

$$\begin{aligned} \beta_x \Big|_{f \rightarrow 0} &= \sqrt{k_1^2 - \frac{(\sigma_1 + j\omega\epsilon_1)^2 (k_1^2 - k_2^2)}{(\sigma_1 + j\omega\epsilon_1)^2 + h^2 (\sigma_2 + j\omega\epsilon_2)^2}} \Big|_{f \rightarrow 0} \\ \Rightarrow \beta_x \Big|_{f \rightarrow 0} &= \sqrt{\frac{h^2 (\sigma_2 + j\omega\epsilon_2)^2 k_1^2 + (\sigma_1 + j\omega\epsilon_1)^2 k_2^2}{(\sigma_1 + j\omega\epsilon_1)^2 + h^2 (\sigma_2 + j\omega\epsilon_2)^2}} \Big|_{f \rightarrow 0} \end{aligned} \quad (31)$$

Moreover, if the coating is extremely thin ($h \rightarrow 0$), (31) simplifies to

$$\beta_x \Big|_{\substack{f \rightarrow 0 \\ h \rightarrow 0}} = k_2 \Big|_{f \rightarrow 0} \quad (32)$$

and $j s_{z2} \rightarrow 0$.

This means that at very low frequencies and when the coating is extremely thin, the propagating wave will no longer be an inhomogeneous plane surface wave but a homogeneous plane TEM-wave propagating entirely in medium 2. The wave will be homogeneous in this limit case because along a perfect electric conductor (PEC), the tangential components of an E-field are always zero.

A similar solution for H-type surface-waves along an electrically thin coating on a perfectly plane conductor does not exist. An explanation for this will be given in the next section.

3.4.6 Some Properties of Plane Surface Waves along a Coated, Electric Perfectly Conducting Plane

An important feature of surface waves is the fact that the type of surface wave that will propagate along a coated structure, is entirely determined by the surface impedance at the material interface of the structure.

For E-type surface waves, the expression found for the longitudinal surface impedance was (14)

$$Z_{s\ell} = j \frac{j s_{z2}}{\omega \epsilon_2 - j \sigma_2}, \text{ which is } \geq 0.$$

This implies that the longitudinal surface impedance has to be inductive for E-type surface waves to propagate along a coated PEC.

Expression (14) can be rewritten, by making use of equation (12), in a form comparable with the input impedance of a shorted transmission line [6, p. 503]

$$Z_{s\ell} = - \frac{s_{z1}}{\sigma_1 + j \omega \epsilon_1} \tan(s_{z1} h) = j \frac{s_{z1}}{\omega \epsilon_1 - j \sigma_1} \tan(s_{z1} h). \quad (33)$$

Therefore, in order to obtain an inductive surface impedance, the electrical height of the coating must be such that

$$n\pi \leq s_{z1} h < (2n + 1) \frac{\pi}{2} \quad (34)$$

where n is a positive integer and $s_{z1} = \frac{2\pi}{\lambda_{z1}}$.

$n+1$ is also the total number of modes that may exist along a PEC with a given coating of height h . Note that only the fundamental E-type mode has no low-frequency cutoff. It is worth pointing out that below the cutoff frequency a surface wave does not become evanescent but ceases to exist altogether [7, p. 12-7].

The only wave able to propagate along the coated structure is a vertically polarized TEM-wave when $s_{z1} h = n\pi$. This wave can be seen as a degenerate form of an E-type surface wave. The phase constant β_x will equal k_2 in this case and $j s_{z2} \rightarrow 0$.

Likewise, the expression for the transversal surface impedance associated with H-type surface waves is (25)

$$Z_{st} = -j \frac{\omega \mu_2}{j s_{z2}}, \text{ which is } < 0.$$

This means that the transversal surface impedance has to be capacitive in order to have H-type surface wave propagation.

By virtue of (23), (25) becomes

$$Z_{st} = j \frac{\omega \mu_1}{s_{z1}} \tan(s_{z1} h). \quad (35)$$

Hence, the constraints for the height h of the coating are

$$(2n+1) \frac{\pi}{2} \leq s_{z1} h < (n+1)\pi \quad (36)$$

where n is a positive integer and $s_{z1} = \frac{2\pi}{\lambda_{z1}}$.

$n+1$ is also the total number of modes that may exist along a PEC with a given coating of height h . Note that all H-type modes, even the lowest order mode, have low-frequency cutoff. This is why one should refrain from calling the lowest H-type mode the fundamental H-type mode. However, the lowest order E-type surface wave mode *is* the fundamental mode. All this can be explained by the fact that this study deals with surface waves along a coated, electric perfectly conducting plane and not a coated, magnetic perfectly conducting plane.

The only wave able to propagate along the coated structure is a horizontally polarized TEM-wave when $s_{z1} h = (2n+1) \frac{\pi}{2}$.

This wave can be seen as a degenerate form of an H-type surface wave. The phase constant β_x will equal k_2 in this case and $j s_{z2} \rightarrow 0$.

In the case of a coated plane PEC, the fundamental E-type mode is usually called the TM_0 mode. Whereas the lowest H-type is labelled as the TE_1 mode. This somewhat peculiar numbering system originates from the mode numbering in plane dielectric slab waveguides [3, pp. 712-716].

In contrast to ordinary metallic waveguides, only a finite number of discrete surface wave modes (i.e. $n+1$ modes) may exist at any given frequency. As shown in the preceding sections it is necessary that $k_1 > k_2$ for surface wave propagation to occur.

Both E-type and H-type surface waves can also be supported by a corrugated surface with thin metal walls and a suitable artificial surface impedance [3, pp. 708-712]. Corrugated surfaces with thick metal walls will briefly be discussed in Chapter 5.

3.4.7 The Continuous Eigenvalue Spectrum and Improper Solutions

Guiding structures may be classified into closed and open types. A *closed guiding structure* possesses a finite cross section which is bounded by walls that are impermeable to radiation and confine the electromagnetic field to the interior of the waveguide. The field inside a closed guiding structure may be decomposed into a *complete set of discrete normal modes* each of which individually satisfies the relevant boundary conditions [8, p.155].

In contrast to closed waveguides, *open guiding structures* do not possess walls completely impermeable to radiation and, therefore, power flow and stored energy are not confined to the inside of the guiding structure. *The radiated field is represented by a continuous spectrum of modes* which on open structures appears in addition to the discrete mode spectrum. *The continuous eigenvalue spectrum* of planar structures consist of all homogeneous and inhomogeneous standing plane waves that individually satisfy the boundary conditions with a continuous range of phase constants such that $-\infty < \beta_x^2 \leq k_2^2$ [8, p. 156]. On the other hand, the discrete spectrum (also termed proper) contains only a finite number of modes that decay at infinity. *The proper discrete eigenvalue spectrum* corresponds to the various surface waves supported by the structure and which are solutions of the dispersion equations (12) and (23). In contrast to a closed guiding structure, the dispersion equations of an open structure may possess, in addition to the proper solutions, other discrete solutions, termed improper, that correspond to fields which grow away from the structure and violate the radiation condition. *The improper discrete eigenvalue spectrum* represents the various leaky waves which are, as was mentioned before, improper solutions to the dispersion equations. The totality of the proper discrete eigenvalue spectrum and the continuous eigenvalue spectrum corresponds to a complete set of eigenfunctions along which the physical field along an open structure may be expanded.

Note that in the previous discussion the more general term “eigenvalue” is used instead of the word “root”. Here is explained why. Roots are solutions to a dispersion equation, whereas eigenvalues are solutions to Hertz’s vector wave equation (2.1), which is in fact an eigenvalue equation. All roots of a dispersion equation are eigenvalues of (2.1), but not all eigenvalues of (2.1) are roots of a dispersion equation.

To find the complete set of eigenvalues in which the field of an arbitrary source may be expanded, consider a plane wave, not necessary homogeneous, incident at an angle θ_{2i} on a coated PEC, as shown in Figure 3.6 for a parallel polarized plane wave. Remember that an inhomogeneous plane wave is represented by an imaginary angle of incidence.

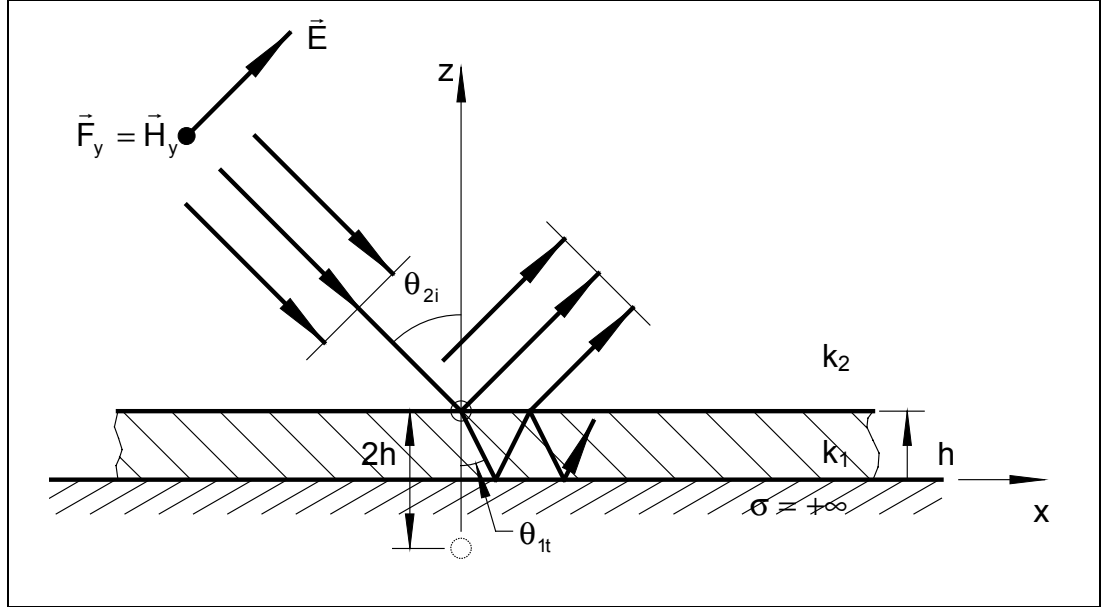


Figure 3.6: A parallel polarized plane wave incident at an angle θ_i on a coated PEC

In the coating, a standing wave may exist due to the reflections at the electric perfectly conducting plane and the material interface. There may also be a reflected wave above the coating. If this is the case, the resulting field above the interface will be that of a standing wave. Note that in these statements no restrictions are put on the value of the wave numbers k_1 and k_2 . This means that even if $k_2 > k_1$, the resulting field in medium 2 will still be a standing wave, not a leaky wave. At this point, it is interesting to compare the situation in Figure 3.6 with that of Figure 3.2 where in medium 2 a leaky wave will exist when $k_2 > k_1$. The big difference between Figure 3.6 and Figure 3.2 is that in Figure 3.6 the incident wave comes from medium 2 while in Figure 3.2 the wave is incident from medium 1. This explains the absence of leaky wave modes in Figure 3.6, even if $k_2 > k_1$.

The transverse field F_y in the two regions may be represented as follows

$$F_{y2} = A_2 \exp[-jk_2[-z \cdot \cos(\theta_{2i}) + x \cdot \sin(\theta_{2i})]] + RA_2 \exp[-jk_2[(z - 2h) \cos(\theta_{2i}) + x \cdot \sin(\theta_{2i})]], \quad (37a)$$

$$F_{y1} = A_1 \cos[k_1 z \cdot \cos(\theta_{1t}) \cdot \exp(-jk_1 x \cdot \sin(\theta_{1t}))] \quad (37b)$$

where

$F_y = E_y$ for perpendicular polarized waves and

$F_y = H_y$ for parallel polarized waves.

It may be necessary to shed some light on the origin of these expressions. The field in medium 2 is written explicitly as the combination of an incident

wave and a reflected wave. The complex amplitude ratio between the reflected and the incident wave is given by *the reflection coefficient* R . The field in medium 1 is a standing wave. In both media the wave vector \vec{k} is decomposed into its components along the x- and z-axis

$$\vec{k}_x = \vec{k} \sin(\theta); \quad \vec{k}_z = \vec{k} \cos(\theta).$$

Note that in (37) the phase is referenced to the phase at the point (0,0,h). Hence, the phase of the reflected wave equals zero in the image point (0,0,-h).

The boundary conditions require the tangential field intensities to be continuous across the material interface. They can easily be imposed by making use of a *transverse equivalent network* (Fig. 3.7) [8, pp. 156-162]. This eliminates the need to deal with the field expressions (37) directly. The dispersion equations and hence the discrete eigenvalue spectrum can be obtained by applying the transverse resonance. *The transverse resonance condition* requires that at any point along the equivalent transmission line, the sum of the impedance looking in one direction and the impedance looking into the other direction equals zero or

$$Z_{\uparrow} + Z_{\downarrow} = 0 \text{ which is equivalent to } Y_{\uparrow} + Y_{\downarrow} = 0 \text{ [8, p. 158].} \quad (38)$$

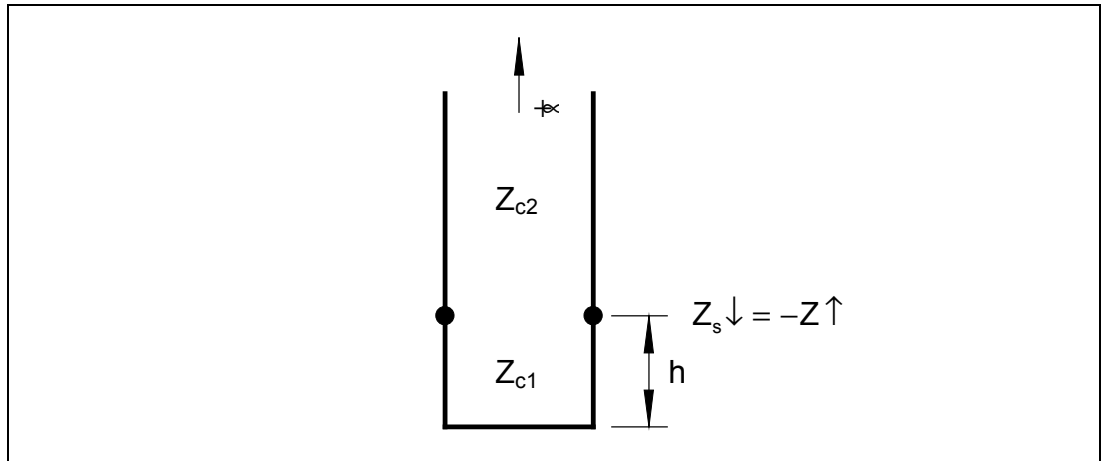


Figure 3.7: Transmission-line equivalent of a coated PEC

In Figure 3.7, Z_{c1} is the characteristic wave impedance of the coating and Z_{c2} the characteristic wave impedance of medium 2. For parallel polarized incident waves these characteristic impedances are

$$Z_{c1//} = \frac{E_{x1}}{H_{y1}} = \eta_1 \cos(\theta_{1t}) \text{ and } Z_{c2//} = \frac{E_{x2}}{H_{y2}} = \eta_2 \cos(\theta_{2i}), \quad (39)$$

whereas for perpendicular polarized incident waves

$$Z_{c1\perp} = \frac{E_{y1}}{H_{x1}} = \frac{\eta_1}{\cos(\theta_{1t})} \text{ and } Z_{c2\perp} = \frac{E_{y2}}{H_{x2}} = \frac{\eta_2}{\cos(\theta_{2i})}. \quad (40)$$

The coating acts like a length of transmission line terminated by a short circuit (Fig. 3.7). Hence, for parallel polarized waves the surface impedance at height $z = h$ is

$$Z_{s\parallel} = \frac{E_x(z=h)}{H_y(z=h)} = jZ_{c\parallel} \tan[hk_1 \cos(\theta_{1t})] = j\eta_1 \cos(\theta_{1t}) \tan[hk_1 \cos(\theta_{1t})], \quad (41)$$

whereas for perpendicular polarized waves

$$Z_{s\perp} = \frac{E_y(z=h)}{H_x(z=h)} = jZ_{c\perp} \tan[hk_1 \cos(\theta_{1t})] = j \frac{\eta_1}{\cos(\theta_{1t})} \tan[hk_1 \cos(\theta_{1t})]. \quad (42)$$

Note that the surface impedance is a longitudinal impedance for parallel polarized waves and a transversal impedance for perpendicular polarized waves.

Applying the transverse resonance condition to (39) and (41), respectively (40) and (42), results in the dispersion equations for E-type and H-type surface waves, respectively. Moreover, the proper solutions to these dispersion equations are poles of the reflection coefficient R , as will be shown now.

For parallel polarized waves, R_{\parallel} equals the current reflection coefficient Γ_i because $F_y = H_y$ in (37a), thus

$$R_{\parallel} = \Gamma_{i\parallel} = \frac{Z_{c2\parallel} - Z_{s\parallel}}{Z_{c2\parallel} + Z_{s\parallel}} = \frac{\eta_2 \cos(\theta_{2i}) - j\eta_1 \cos(\theta_{1t}) \tan[hk_1 \cos(\theta_{1t})]}{\eta_2 \cos(\theta_{2i}) + j\eta_1 \cos(\theta_{1t}) \tan[hk_1 \cos(\theta_{1t})]}. \quad (43)$$

For perpendicular polarized waves, $F_y = E_y$ and hence R_{\perp} must equal the voltage reflection coefficient Γ_v

$$R_{\perp} = \Gamma_{v\perp} = \frac{Z_{s\perp} - Z_{c2\perp}}{Z_{s\perp} + Z_{c2\perp}} = \frac{j \frac{\eta_1}{\cos(\theta_{1t})} \tan[hk_1 \cos(\theta_{1t})] - \frac{\eta_2}{\cos(\theta_{2i})}}{j \frac{\eta_1}{\cos(\theta_{1t})} \tan[hk_1 \cos(\theta_{1t})] + \frac{\eta_2}{\cos(\theta_{2i})}}. \quad (44)$$

A first group of solutions to (37a) and (37b) are the E-type surface wave modes which are poles for the reflection coefficient $R_{//}$. To see this, apply the transverse resonance condition to (43)

$$R_{//} \rightarrow \infty \Leftrightarrow Z_{c2//} + Z_{s\ell//} = 0 \Leftrightarrow \eta_2 \cos(\theta_{2i}) + j\eta_1 \cos(\theta_{1t}) \tan[hk_1 \cos(\theta_{1t})] = 0. \quad (45)$$

In (45), let

$$s_{z1} = k_1 \cos(\theta_{1t}) \quad (46)$$

$$\Rightarrow j\eta_1 \cos(\theta_{1t}) = j \frac{\eta_1}{k_1} s_{z1} = \frac{j \sqrt{\frac{\mu_1}{\epsilon_1 - j \frac{\sigma_1}{\omega}}}}{\omega \sqrt{\mu_1 \left(\epsilon_1 - j \frac{\sigma_1}{\omega} \right)}} s_{z1} = - \frac{s_{z1}}{\sigma_1 + j\omega\epsilon_1} \quad (47)$$

$$\text{and } s_{z2} = k_2 \cos(\theta_{2i}) \Rightarrow \eta_2 \cos(\theta_{2i}) = \frac{j s_{z2}}{\sigma_2 + j\omega\epsilon_2}. \quad (48)$$

Substituting (46), (47) and (48) into (45) results in

$$\frac{s_{z1}}{\sigma_1 + j\omega\epsilon_1} \tan(s_{z1}h) = \frac{j s_{z2}}{\sigma_2 + j\omega\epsilon_2}.$$

This is the dispersion equation for E-type surface wave modes (12) which was derived earlier in Section 3.4.2. The here presented alternative method for finding a dispersion equation might be somewhat quicker, it does not provide the insight into the actual field distributions of the propagating wave.

H-type surface wave modes are also solutions to (37a) and (37b) and at the same time poles for the reflection coefficient R_{\perp} . To see this, apply the transverse resonance condition to (44)

$$R_{\perp} \rightarrow \infty \Leftrightarrow Z_{st\perp} + Z_{c2\perp} = 0 \Leftrightarrow j \frac{\eta_1}{\cos(\theta_{1t})} \tan[hk_1 \cos(\theta_{1t})] + \frac{\eta_2}{\cos(\theta_{2i})} = 0. \quad (49)$$

In (49), let

$$s_{z1} = k_1 \cos(\theta_{1t}) \quad (50)$$

$$\Rightarrow j \frac{\eta_1}{\cos(\theta_{1t})} = j \frac{k_1 \eta_1}{s_{z1}} = j \omega \sqrt{\mu_1 \left(\epsilon_1 - j \frac{\sigma_1}{\omega} \right)} \sqrt{\frac{\mu_1}{\epsilon_1 - j \frac{\sigma_1}{\omega}} \frac{1}{s_{z1}}} = \frac{j \omega \mu_1}{s_{z1}} \quad (51)$$

$$\text{and } s_{z2} = k_2 \cos(\theta_{2i}) \Rightarrow \frac{\eta_2}{\cos(\theta_{2i})} = \frac{j \omega \mu_2}{j s_{z2}}. \quad (52)$$

Substituting (50), (51) and (52) into (49) results in

$$\frac{j \omega \mu_1}{s_{z1}} \tan(s_{z1} h) = - \frac{j \omega \mu_2}{j s_{z2}}.$$

This is the dispersion equation for H-type surface wave modes (23) which was derived earlier in Section 3.4.3.

Although up to now surface waves have been considered to be produced by the pole in the expression for the reflection coefficient, they may equally be seen as being produced by a zero of the reflection coefficient. Whether a surface wave mode should be associated with a zero or a pole of the reflection coefficient depends on the fact whether the field above the dielectric is considered to be a reflected wave or an incident wave, because in case of the latter, (48) and (52) change to

$$s_{z2} = -k_2 \cos(\theta_{2i}) \Rightarrow \eta_2 \cos(\theta_{2i}) = - \frac{j s_{z2}}{\sigma_2 + j \omega \epsilon_2}$$

$$\text{and } s_{z2} = -k_2 \cos(\theta_{2i}) \Rightarrow \frac{\eta_2}{\cos(\theta_{2i})} = - \frac{j \omega \mu_2}{j s_{z2}}, \text{ respectively.}$$

The characteristic wave impedances $Z_{c2//}$ and $Z_{c2\perp}$ change accordingly, but the dispersion equation remains the same.

To summarize, if the field in medium 2 is considered as an incident wave, the solution corresponds to a zero of the reflection coefficient and not a pole, as is the case if the field is considered as a reflected wave [3, p.718].

The system of equations (37a) and (37b) has also other solution types in addition to the previously found surface wave solutions. Standing waves along the z-axis exists for all real angles of incidence $0 \leq \theta_{2i} \leq 90^\circ$

$$\begin{aligned} \Rightarrow 0 \leq s_{z2}^2 &= k_2^2 \cos^2(\theta_{2i}) \leq k_2^2 \\ \Rightarrow 0 \leq \beta_x^2 &= k_2^2 - s_{z2}^2 \leq k_2^2 \\ \Rightarrow 0 \leq \beta_x &\leq k_2. \end{aligned} \tag{53}$$

A standing wave solution along the z-axis will also exist for imaginary angles of incidence

$$\left. \begin{aligned} s_{z2}^2 &= k_2^2 \cos^2(\theta_{2i}) > k_2^2 \\ \beta_x^2 &= k_2^2 - s_{z2}^2 \end{aligned} \right\} \Rightarrow -j\infty < \beta_x < j0. \tag{54}$$

The homogeneous and inhomogeneous standing wave solutions given in (53) and (54), respectively, form the continuous eigenvalue spectrum.

3.4.8 Traveling Waves Categorized by Surface Impedance

Both the proper and the improper discrete eigenvalue spectra represent guided wave modes, which are often called traveling waves. These plane waves are characterized by the orientation of $\vec{\alpha}_2$ and $\vec{\beta}_2$ in medium 2, which in turn depends on the sign of the real and imaginary parts of the surface impedance [8, pp. 164-167]¹. This relation will be explored in more detail now.

The complex wave vector \vec{k}_2 in medium 2 can be decomposed into its components along the x- and the z-axis

$$\vec{k}_{x2} = \vec{k}_2 \sin(\theta_{2i}); \quad \vec{k}_{z2} = \vec{k}_2 \cos(\theta_{2i})$$

$$\text{where } k_{z2} = \beta_{z2} - j\alpha_{z2} = s_{z2}. \quad (55)$$

Substituting (55) into the expression for the surface impedance previously obtained for E-type plane surface waves (14), gives

$$Z_{sl} = R_{sl} + jX_{sl} = -\frac{jS_{z2}}{\sigma_2 + j\omega\epsilon_2} = -\frac{s_{z2}}{\omega\epsilon_2 - j\sigma_2} = \frac{-\beta_{z2} + j\alpha_{z2}}{\omega\epsilon_2 - j\sigma_2}. \quad (56)$$

This results in the following set of rules for parallel (TM) polarized (E-type) traveling waves

$$\text{sign}(\beta_{z2}) = -\text{sign}(R_{sl}), \quad (57a)$$

$$\text{sign}(\alpha_{z2}) = \text{sign}(X_{sl}). \quad (57b)$$

Rewriting the surface impedance expression for H-type plane surface waves (25) as a surface admittance and substituting (55) yields

$$Y_{st} = G_{st} + jB_{st} = -\frac{s_{z2}}{\omega\mu_2} = \frac{-\beta_{z2} + j\alpha_{z2}}{\omega\mu_2}. \quad (58)$$

Hence, for perpendicular (TE) polarized (H-type) traveling waves

$$\text{sign}(\beta_{z2}) = -\text{sign}(G_{st}) \quad \text{and} \quad (59a)$$

$$\text{sign}(\alpha_{z2}) = \text{sign}(B_{st}). \quad (59b)$$

¹ In reference [8], a rather unusual sign convention is used in which -j is replaced by +i.

The classification of traveling wave types according to the surface impedance is shown in Figure 3.8 and Figure 3.9. (For more information, see [8, pp. 166-167].)

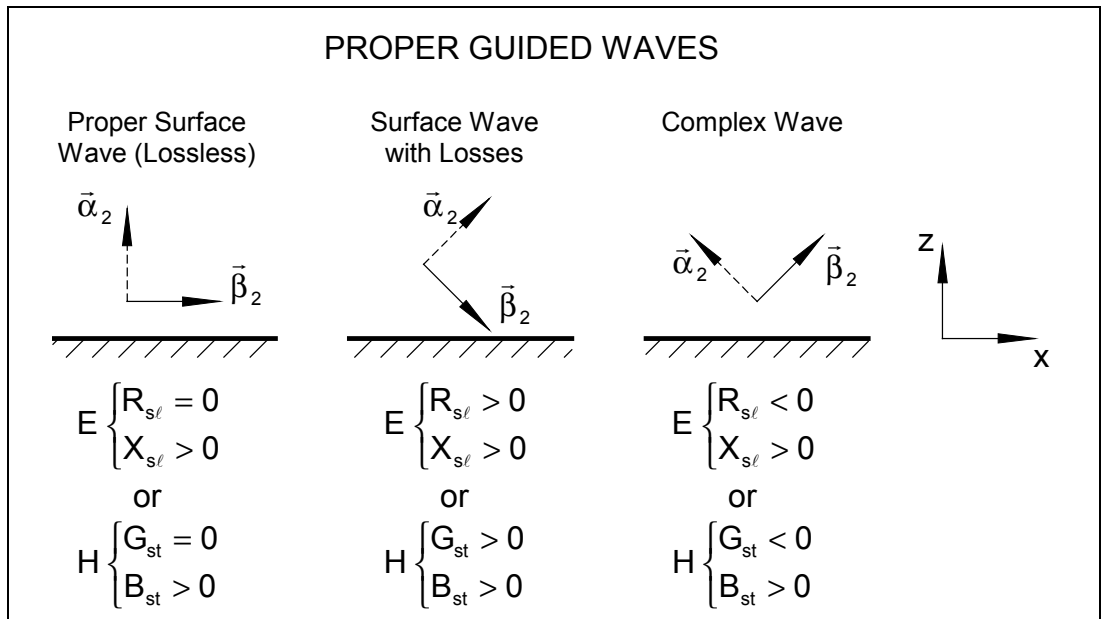


Figure 3.8: Classification of the proper guided waves along a coated plane PEC ($\text{Im}(k_2) = 0$)

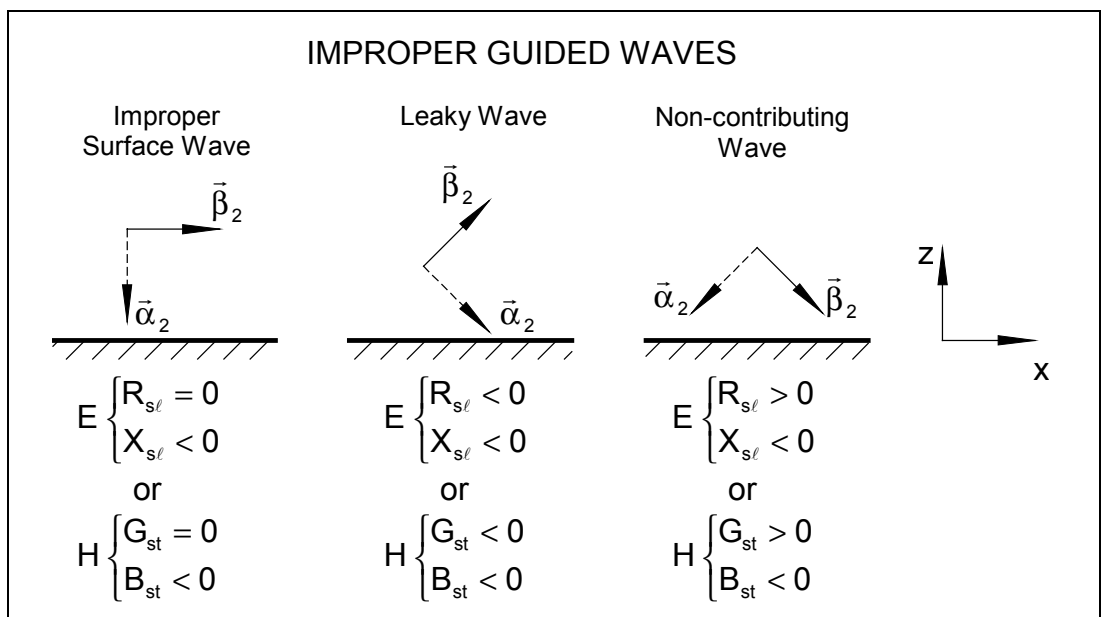


Figure 3.9: Classification of the improper guided waves along a coated plane PEC ($\text{Im}(k_2) = 0$)

3.4.9 The Mapping of Fast and Slow Traveling Waves onto the w-Plane

Up to now, little has been said about the requirements for fast and slow traveling wave propagation. This is mainly due to the fact that s_{z2} has thus far always been expressed as a dual-valued function of β_x . This section explains how s_{z2} can be transformed into a single-valued function of a new complex variable w .

Fast electromagnetic waves are waves with a phase velocity v_p greater than c_0 , whereas *slow electromagnetic waves* are waves with v_p smaller than c_0 . c_0 is the velocity of light in a vacuum, i.e. 299792458m/s.

The phase velocity of a wave is

$$v_p = \frac{\text{Re}(\beta)}{\omega}. \quad (60)$$

In view of (60), alternative definitions for fast and slow waves are $\beta < k_0$ and $\beta > k_0$, respectively.

Note that it is only useful to talk about fast and slow waves when $k_2 = k_0$.

Introducing the trigonometric transformation (Fig. 3.10) [8, pp. 171 & 241]

$$\beta_x = k_0 \sin(w) \quad \text{where } w = \xi + j\eta, \quad (61)$$

results in a single-valued expression for s_{z0}

$$\left. \begin{array}{l} \beta_x = k_0 \sin(w) \quad (61) \\ k_0^2 = \beta_x^2 + s_{z0}^2 \quad (2.13) \end{array} \right\} \Rightarrow s_{z0} = k_0 \cos(w). \quad (62)$$

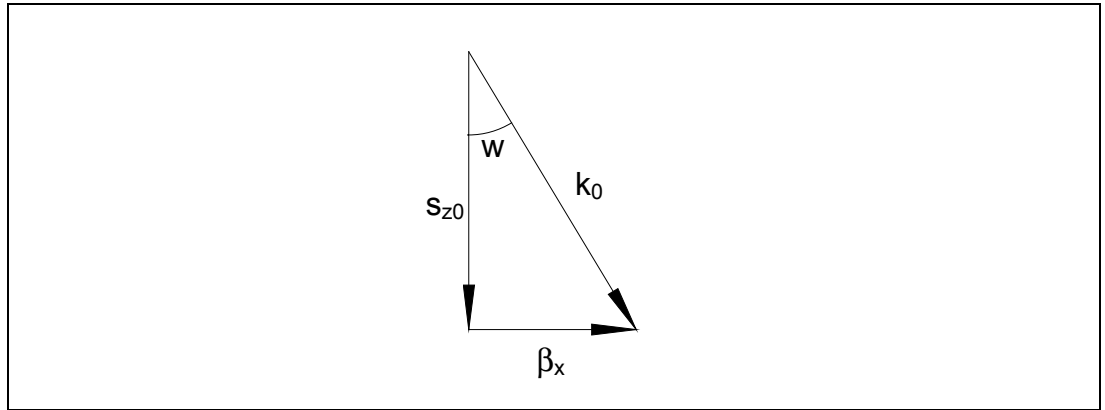


Figure 3.10: Graphical representation of the trigonometric transformation

The real part and imaginary part of the complex phase constant β_x can be written in terms of ξ and η

$$\begin{aligned} \beta_x &= k_0 \sin(w) = k_0 \sin(\xi + j\eta) \\ &= k_0 [\sin(\xi) \cos(j\eta) + \cos(\xi) \sin(j\eta)] \quad [9, \text{p. 15}] \\ &= k_0 [\sin(\xi) \cosh(\eta) + j \cos(\xi) \sinh(\eta)] \quad [9, \text{p. 31}] \\ & (= \beta'_x - j\beta''_x = \beta'_x - j\alpha_x). \end{aligned} \quad (63)$$

Likewise,

$$\begin{aligned}
s_{z0} &= k_0 \cos(w) = k_0 \cos(\xi + j\eta) \\
&= k_0 [\cos(\xi) \cos(j\eta) - \sin(\xi) \sin(j\eta)] \quad [9, \text{p. 15}] \\
&= k_0 [\cos(\xi) \cosh(\eta) - j \sin(\xi) \sinh(\eta)] \quad [9, \text{p. 31}] \\
&= (\beta_{z0} - j\alpha_{z0}).
\end{aligned} \tag{64}$$

All possible traveling wave types (backward and forward propagating) can now be mapped into a strip $-\pi \leq \xi < \pi$ of the w -plane (Fig. 3.11) [8, p. 174].

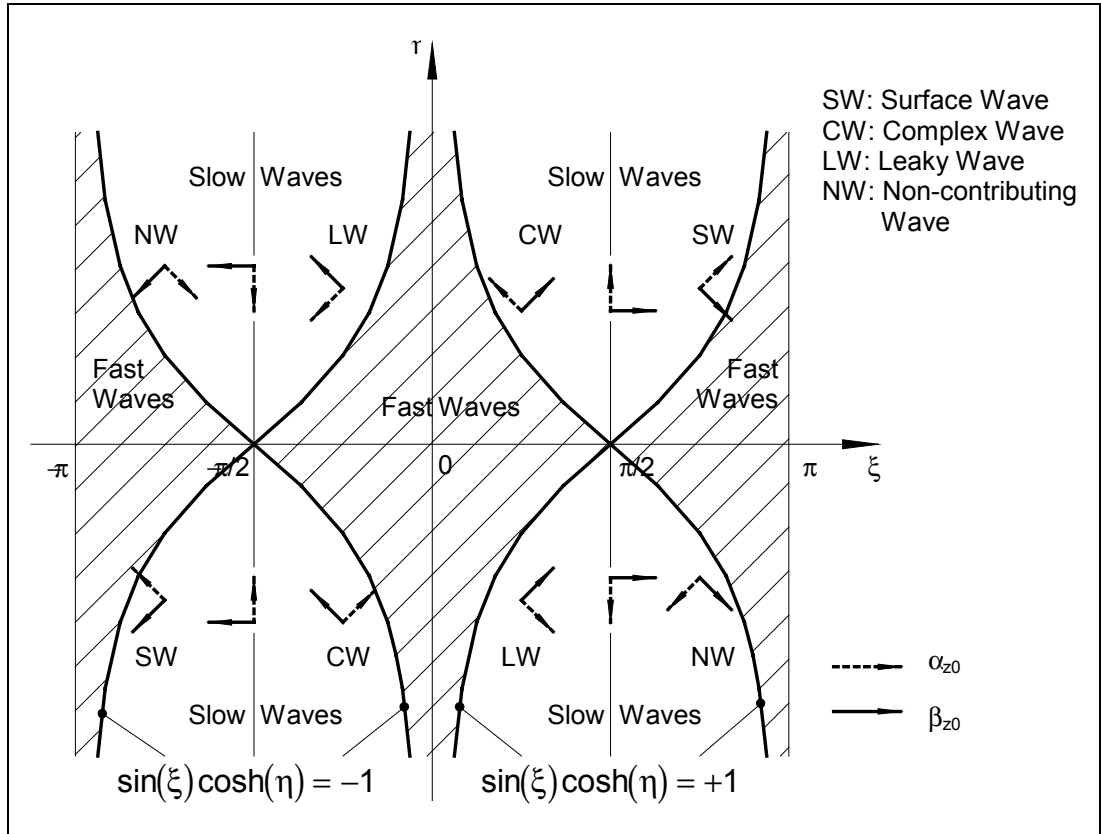


Figure 3.11: Traveling wave types as a function of eigenvalue location in the w -plane

Note that if in (64): $\eta = 0 \Rightarrow \text{Im}(s_{z0}) = 0$, which corresponds to a homogeneous wave. This confirms that a complex angle of incidence implies an inhomogeneous incident wave (in fact, w could be replaced by θ).

Finally, the boundary between fast and slow waves is given by

$$v_p = \frac{\text{Re}(\beta_x)}{k_0} = \sin(\xi) \cosh(\eta) = \pm 1.$$

3.4.10 Numerical Examples

Now will be shown how the discrete eigenvalue spectrum can be found graphically using Mathcad™ Plus 6.0 Professional (©1986-1995 MathSoft, Inc.). Only E-type waves are investigated. The dispersion equation of the proper E-type traveling waves (surface waves and complex waves) (13) is rewritten in a form more suitable for numerical analysis

$$F_{EP}(\beta_x) = \frac{\sqrt{k_1^2 - \beta_x^2}}{\sigma_1 + j\omega\epsilon_1} \tan(h\sqrt{k_1^2 - \beta_x^2}) - \frac{\operatorname{Re}(\sqrt{\beta_x^2 - k_2^2})}{\left| \operatorname{Re}(\sqrt{\beta_x^2 - k_2^2}) \right|} \cdot \frac{\sqrt{\beta_x^2 - k_2^2}}{\sigma_2 + j\omega\epsilon_2} = 0. \quad (65)$$

Similarly, for the improper traveling waves (leaky waves and non-contributing waves)

$$F_{EI}(\beta_x) = \frac{\sqrt{k_1^2 - \beta_x^2}}{\sigma_1 + j\omega\epsilon_1} \tan(h\sqrt{k_1^2 - \beta_x^2}) + \frac{\operatorname{Re}(\sqrt{\beta_x^2 - k_2^2})}{\left| \operatorname{Re}(\sqrt{\beta_x^2 - k_2^2}) \right|} \cdot \frac{\sqrt{\beta_x^2 - k_2^2}}{\sigma_2 + j\omega\epsilon_2} = 0. \quad (66)$$

The eigenvalues of the forward propagating E-type traveling wave modes can be found graphically by plotting equations (65) and (66) respectively in function of the complex phase constant β_x (see Fig. 3.12). An eigenvalue on this plot is characterized by a null (black dot). It turns out that the nulls are often accompanied by sharp peaks in their immediate neighbourhood. Nulls are very localized features and can therefore easily be overlooked because computers can plot the value of a function only in a finite number of points. One way to prevent eigenvalues from being overlooked, is to zoom in on those regions of the plot where eigenvalues may be expected.

Another option is to use a numerical root finder to locate the eigenvalues. Each root finding algorithm requires one or more start values. However, when there is more than one mode propagating, it is often difficult to direct the root finder towards one particular eigenvalue. The Newton-Raphson algorithm, as implemented in the root finder of Mathcad™ is more prone to this defect than the secant algorithm for example. With the secant root finding method, an eigenvalue can be bracketed by appropriately specifying the two start values of the algorithm. Reference [10] describes this method in detail.

Another very elegant graphical solution method has been described in [3, pp. 712-716]. Unfortunately, this method is not applicable for lossy media.

The inability to annotate graphs in Mathcad™, made it necessary to provide additional information on these plots in the form of Figure 3.12.

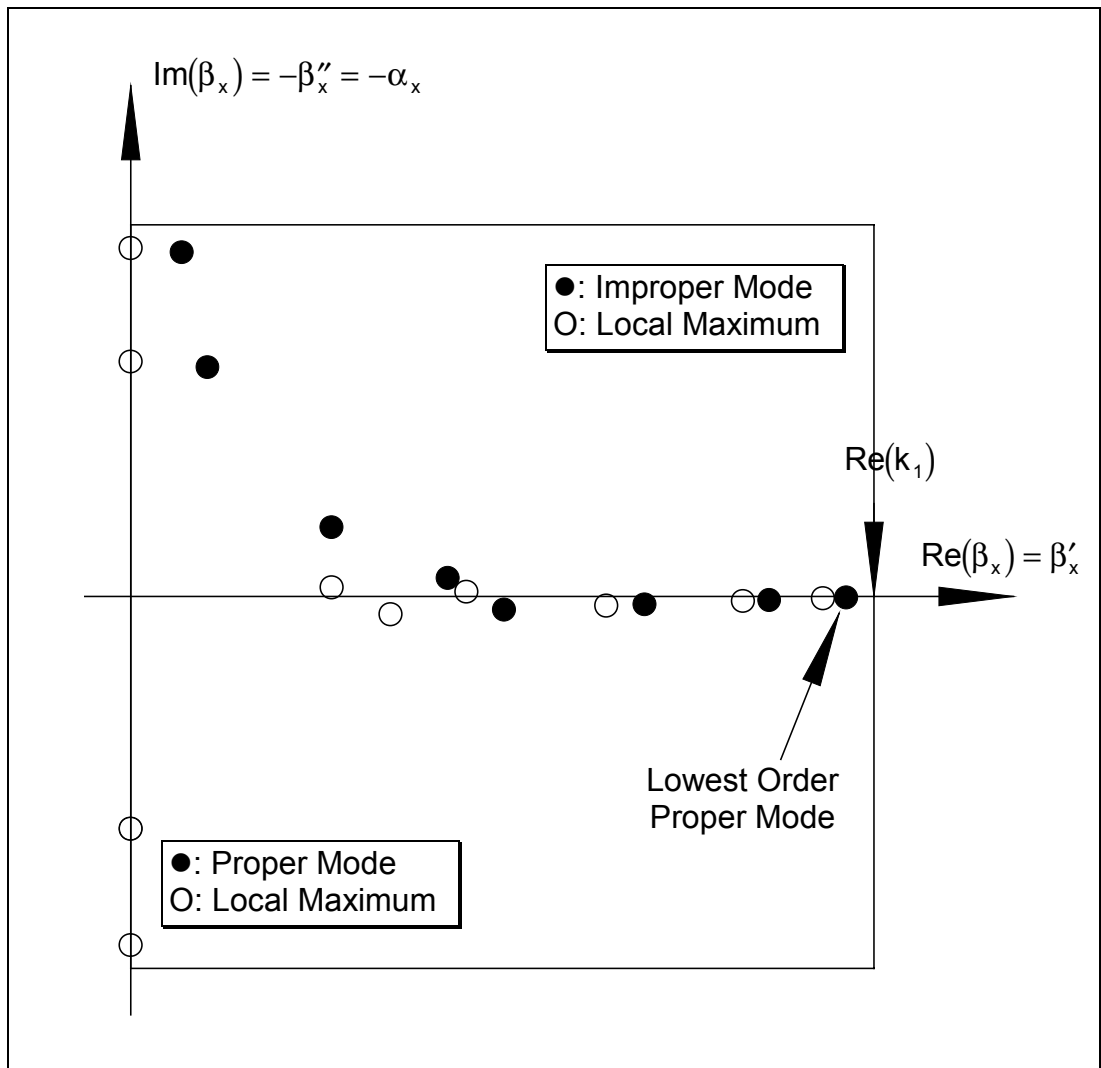


Figure 3.12: Interpretation of the complex β_x -plane plots generated by Mathcad™

Remember that it is not possible to show the eigenvalues of the proper traveling wave modes and those of the improper traveling wave modes simultaneously. Improper wave modes are located in the upper half of the complex β_x -plane and proper wave modes in the lower half of the plane. Thus, for each plot produced by Mathcad™, only one half is relevant, the other half is usually a mirror image and should be ignored.

Also, for all forward propagating *lossless* surface wave modes:

$k_2 < \beta_x \leq k_1$ and the lowest order surface wave mode has the highest $\text{Re}(\beta_x)$ (i.e. the slowest wave).

EXAMPLE 1

This first example shows that only one E-type surface wave mode can propagate in a plane layer of 6mm thick polyethylene (PE) on a PEC. This mode is represented by a black dot (null) on the complex β_x -plane plot. A side view of this plot is also given. (See also Fig. 3.13.)

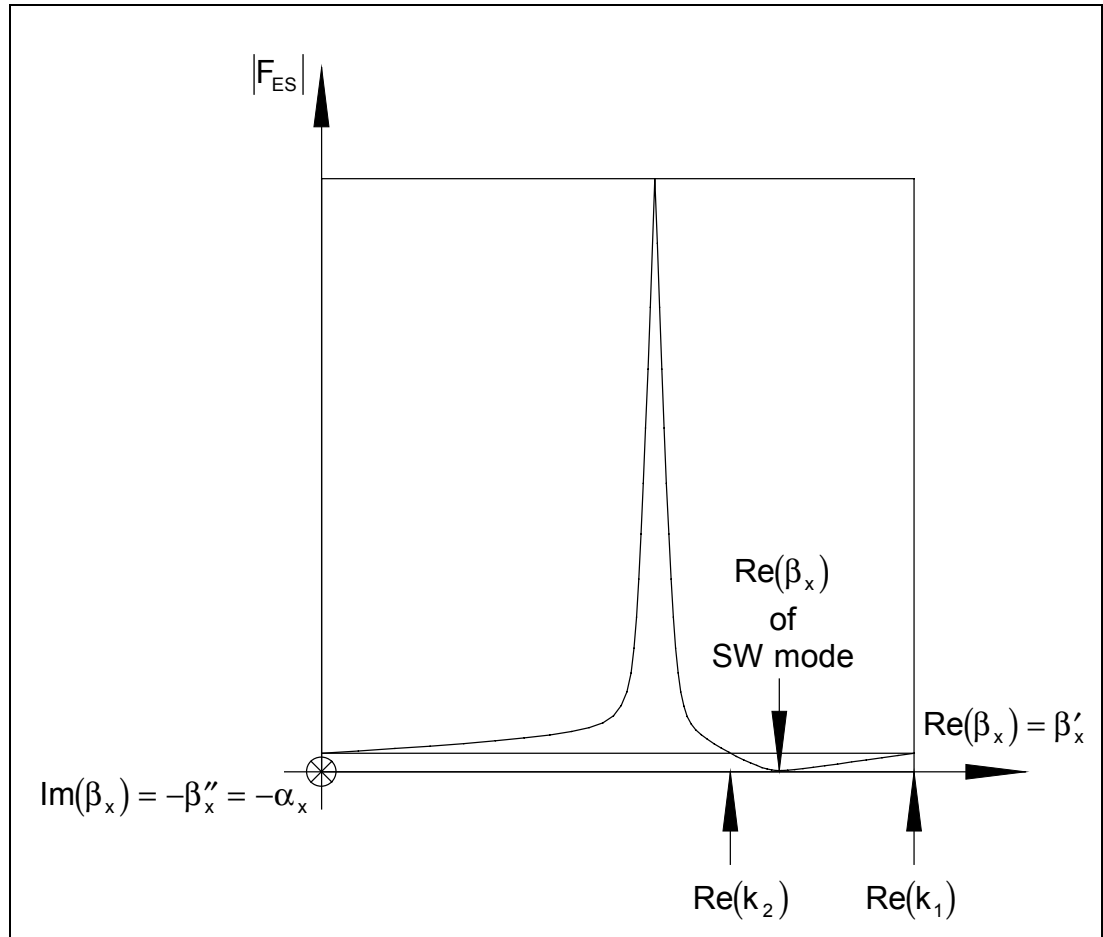


Figure 3.13: Interpretation of the side view of the complex β_x -plane plot with one E-type surface wave mode present

EXAMPLE 2

The complex β_x -plane plot of this example clearly shows that increasing the layer thickness to 15mm results in an additional proper E-type mode.

EXAMPLE 3

Further increasing the thickness to 80mm gives a multitude of proper waves. They are all surface wave modes with $\text{Re}(k_2) < \text{Re}(\beta_x) \leq \text{Re}(k_1)$.

EXAMPLE 4

The same structure of Example 1 is now solved for improper E-type modes. Only one non-contributing wave mode is present in the upper half of the complex β_x -plane. The lower half of the plot is a mirror image and should be ignored.

EXAMPLE 5

With a coating of 15mm PE, one can discern two improper E-type modes. Ignore the lower half of the plot.

EXAMPLE 6

As the thickness of the coating further increases (here to 80mm), more and more improper E-type modes start to appear on the upper half of the plot. The lower half should be ignored.

EXAMPLE 7

This example shows the proper E-type waves along a 0.75mm thick sheet of metal-backed Eccosorb GDS, a surface wave absorbing material available from Emerson & Cuming.

EXAMPLE 8

The same configuration as in Example 7 is now solved for improper E-type modes.

EXAMPLE 9

It is also very instructive to see what happens when more losses are introduced into a relatively thick coating. From the plot can be inferred that the attenuation is higher for the higher order surface wave modes. Some of the higher order modes are fast waves and one null clearly stands out from the rest. This null corresponds to the fast surface wave that will also exist when the metal back plane is removed and the coating made infinitely thick. (See also Section 3.6.)

EXAMPLE 10

The losses in the coating are apparently that high, that no improper wave modes can be found in the upper half of the complex β_x -plane plot.

Example 1: Plane Surface Waves along a Coated PEC

Constants:

$$c_0 := 299792458 \cdot \frac{\text{m}}{\text{sec}} \quad \mu_0 := 4 \cdot \pi \cdot 10^{-7} \cdot \frac{\text{henry}}{\text{m}} \quad \epsilon_0 := \frac{1}{c_0^2 \cdot \mu_0} \quad \epsilon_0 = 8.854 \cdot 10^{-12} \cdot \frac{\text{farad}}{\text{m}}$$

Enter the material parameters:

$$\sigma_1 := 0 \cdot \frac{\text{siemens}}{\text{m}} \quad \epsilon_{r1} := 2.26 - 0.00091j \quad \mu_{r1} := 1 - 0j$$

$$\sigma_2 := 0 \cdot \frac{\text{siemens}}{\text{m}} \quad \epsilon_{r2} := 1 - 0j \quad \mu_{r2} := 1 - 0j$$

Enter the frequency:

$$f := 10 \cdot 10^9 \cdot \text{Hz} \quad \omega := 2 \cdot \pi \cdot f \quad \omega = 6.283 \cdot 10^{10} \cdot \text{Hz} \quad \lambda_0 := \frac{c_0}{f} \quad \lambda_0 = 0.030 \cdot \text{m}$$

Enter the thickness of the coating:

$$h := 0.006 \cdot \text{m}$$

Complex wave numbers:

$$\epsilon_1 := \epsilon_{r1} \cdot \epsilon_0 \quad \epsilon_2 := \epsilon_{r2} \cdot \epsilon_0$$

$$\mu_1 := \mu_{r1} \cdot \mu_0 \quad \mu_2 := \mu_{r2} \cdot \mu_0$$

$$k_0 := \omega \sqrt{\epsilon_0 \cdot \mu_0} \quad k_0 = 209.585 \cdot \frac{\text{rad}}{\text{m}}$$

$$k_1 := \sqrt{-j \cdot \omega \mu_1 \cdot (\sigma_1 + j \cdot \omega \epsilon_1)} \quad k_1 = 315.075 - 0.063j \cdot \frac{\text{rad}}{\text{m}}$$

$$k_2 := \sqrt{-j \cdot \omega \mu_2 \cdot (\sigma_2 + j \cdot \omega \epsilon_2)} \quad k_2 = 209.585 \cdot \frac{\text{rad}}{\text{m}}$$

(k_2 must be smaller than k_1 !)

E-type proper wave modes:

$$F_{EP}(\beta_x) := \frac{\sqrt{k_1^2 - \beta_x^2}}{\sigma_1 + j \cdot \omega \varepsilon_1} \cdot \tan\left(h \cdot \sqrt{k_1^2 - \beta_x^2}\right) - \frac{\operatorname{Re}\left(\sqrt{\beta_x^2 - k_2^2}\right)}{\left|\operatorname{Re}\left(\sqrt{\beta_x^2 - k_2^2}\right)\right|} \cdot \frac{\sqrt{\beta_x^2 - k_2^2}}{\sigma_2 + j \cdot \omega \varepsilon_2}$$

$$\beta_x := \frac{k_1 + k_2}{2} \quad \beta_x := \operatorname{root}\left(F_{EP}(\beta_x), \beta_x\right) \quad \beta_x = 258.189 - 0.045j \cdot \frac{\operatorname{rad}}{\operatorname{m}}$$

$$F_{EP}(\beta_x) = -1.392 \cdot 10^{-6} + 1.134 \cdot 10^{-4} j \cdot \operatorname{kg} \cdot \operatorname{m}^2 \cdot \operatorname{sec}^{-1} \cdot \operatorname{coul}^{-2}$$

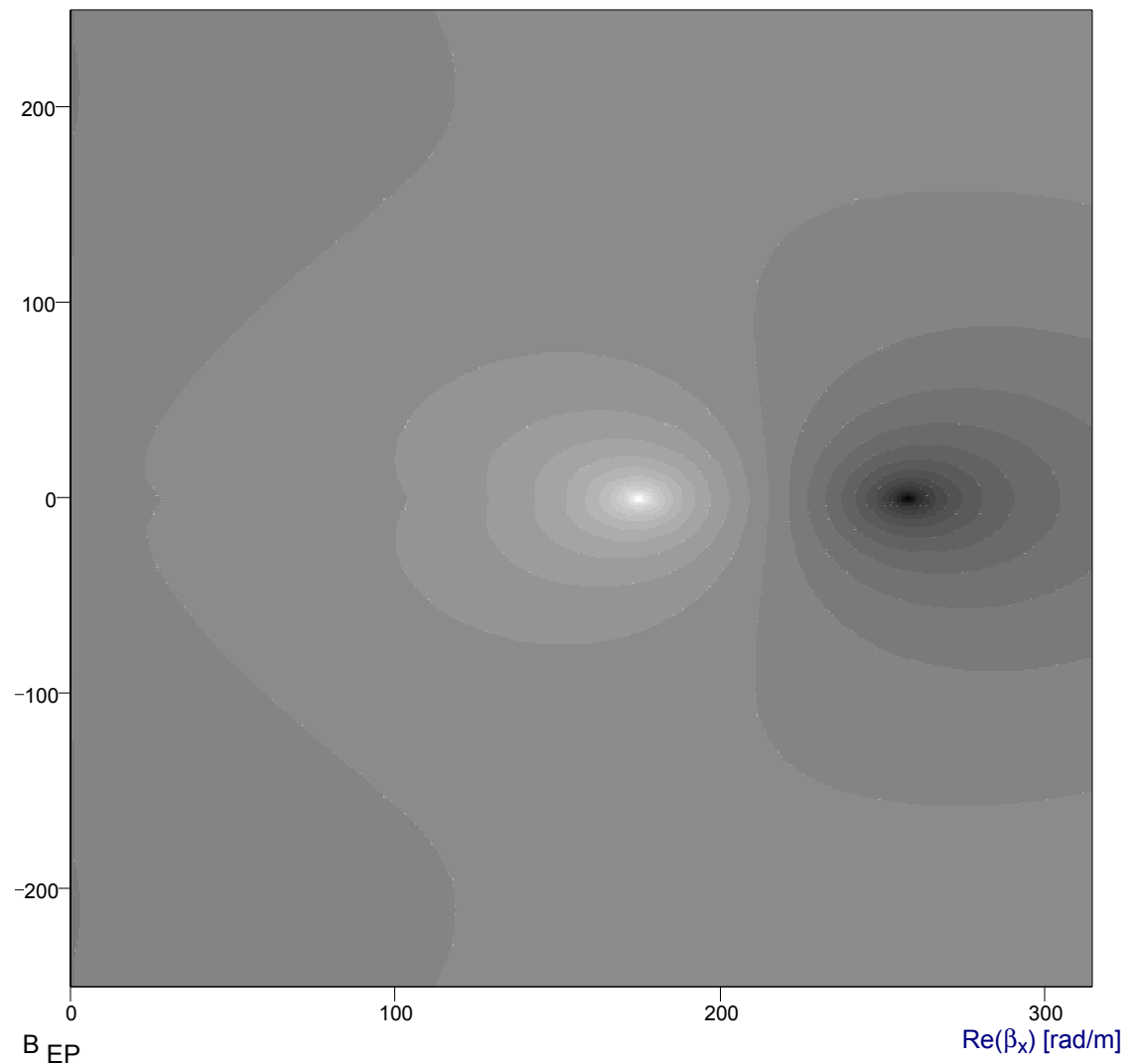
$$s_{z2} := -j \cdot \frac{\operatorname{Re}\left(\sqrt{\beta_x^2 - k_2^2}\right)}{\left|\operatorname{Re}\left(\sqrt{\beta_x^2 - k_2^2}\right)\right|} \cdot \sqrt{\beta_x^2 - k_2^2} \quad s_{z2} = -0.078 - 150.785j \cdot \frac{\operatorname{rad}}{\operatorname{m}}$$

$$N := 301 \quad \operatorname{Start}_x := 0 \cdot \frac{\operatorname{rad}}{\operatorname{m}} \quad \operatorname{End}_x := \operatorname{Re}(k_1) \quad \operatorname{Start}_y := -250 \cdot \frac{\operatorname{rad}}{\operatorname{m}} \quad \operatorname{End}_y := 250 \cdot \frac{\operatorname{rad}}{\operatorname{m}}$$

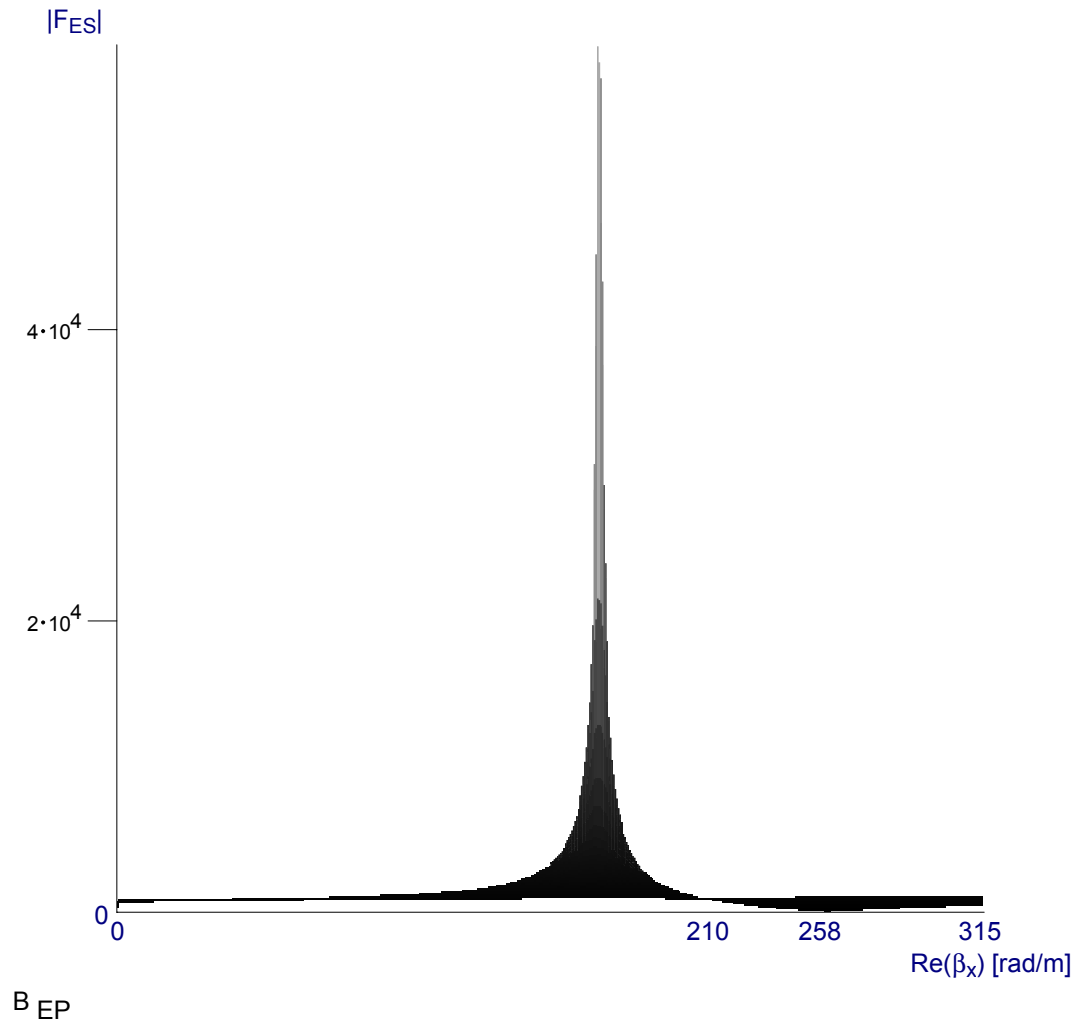
$$x := 0, 1 \dots N \quad y := 0, 1 \dots N \quad \Delta x := \frac{\operatorname{End}_x - \operatorname{Start}_x}{N} \quad \Delta y := \frac{\operatorname{End}_y - \operatorname{Start}_y}{N}$$

$$B_{EP_{x,y}} := \log\left[\left|F_{EP}\left(\left(\operatorname{Start}_x + x \cdot \Delta x\right) + \left[j \cdot \left(\operatorname{Start}_y + y \cdot \Delta y\right)\right]\right)\right| \cdot \frac{\operatorname{siemens} \cdot \operatorname{m}}{\operatorname{m} \cdot \operatorname{rad}}\right]$$

$\operatorname{Im}(\beta_x)$ [rad/m]



$$B_{EP_{x,y}} := \left| F_{EP} \left[\left(\text{Start}_x + x \cdot \Delta x \right) + \left[j \cdot \left(\text{Start}_y + y \cdot \Delta y \right) \right] \right] \right| \cdot \frac{\text{siemens}}{\text{m}} \cdot \frac{\text{m}}{\text{rad}}$$



Example 2: Plane Surface Waves along a Coated PEC

Constants:

$$c_0 := 299792458 \cdot \frac{\text{m}}{\text{sec}} \quad \mu_0 := 4 \cdot \pi \cdot 10^{-7} \cdot \frac{\text{henry}}{\text{m}} \quad \epsilon_0 := \frac{1}{c_0^2 \cdot \mu_0} \quad \epsilon_0 = 8.854 \cdot 10^{-12} \cdot \frac{\text{farad}}{\text{m}}$$

Enter the material parameters:

$$\sigma_1 := 0 \cdot \frac{\text{siemens}}{\text{m}} \quad \epsilon_{r1} := 2.26 - 0.00091j \quad \mu_{r1} := 1 - 0j$$
$$\sigma_2 := 0 \cdot \frac{\text{siemens}}{\text{m}} \quad \epsilon_{r2} := 1 - 0j \quad \mu_{r2} := 1 - 0j$$

Enter the frequency:

$$f := 10 \cdot 10^9 \cdot \text{Hz} \quad \omega := 2 \cdot \pi \cdot f \quad \omega = 6.283 \cdot 10^{10} \cdot \text{Hz} \quad \lambda_0 := \frac{c_0}{f} \quad \lambda_0 = 0.030 \cdot \text{m}$$

Enter the thickness of the coating:

$$h := 0.015 \cdot \text{m}$$

Complex wave numbers:

$$\epsilon_1 := \epsilon_{r1} \cdot \epsilon_0 \quad \epsilon_2 := \epsilon_{r2} \cdot \epsilon_0$$

$$\mu_1 := \mu_{r1} \cdot \mu_0 \quad \mu_2 := \mu_{r2} \cdot \mu_0$$

$$k_0 := \omega \sqrt{\epsilon_0 \cdot \mu_0} \quad k_0 = 209.585 \cdot \frac{\text{rad}}{\text{m}}$$

$$k_1 := \sqrt{-j \cdot \omega \mu_1 \cdot (\sigma_1 + j \cdot \omega \epsilon_1)} \quad k_1 = 315.075 - 0.063j \cdot \frac{\text{rad}}{\text{m}}$$

$$k_2 := \sqrt{-j \cdot \omega \mu_2 \cdot (\sigma_2 + j \cdot \omega \epsilon_2)} \quad k_2 = 209.585 \cdot \frac{\text{rad}}{\text{m}}$$

(k_2 must be smaller than k_1 !)

E-type proper wave modes:

$$F_{EP}(\beta_x) := \frac{\sqrt{k_1^2 - \beta_x^2}}{\sigma_1 + j \cdot \omega \epsilon_1} \cdot \tan\left(h \cdot \sqrt{k_1^2 - \beta_x^2}\right) - \frac{\operatorname{Re}\left(\sqrt{\beta_x^2 - k_2^2}\right)}{\left|\operatorname{Re}\left(\sqrt{\beta_x^2 - k_2^2}\right)\right|} \cdot \frac{\sqrt{\beta_x^2 - k_2^2}}{\sigma_2 + j \cdot \omega \epsilon_2}$$

$$\beta_x := \frac{k_1 + k_2}{2} \quad \beta_x := \operatorname{root}\left(F_{EP}(\beta_x), \beta_x\right) \quad \beta_x = 212.793 - 0.02j \cdot \frac{\operatorname{rad}}{\operatorname{m}}$$

$$F_{EP}(\beta_x) = -9.521 \cdot 10^{-7} + 3.138 \cdot 10^{-7} j \cdot \operatorname{kg} \cdot \operatorname{m}^2 \cdot \operatorname{sec}^{-1} \cdot \operatorname{coul}^{-2}$$

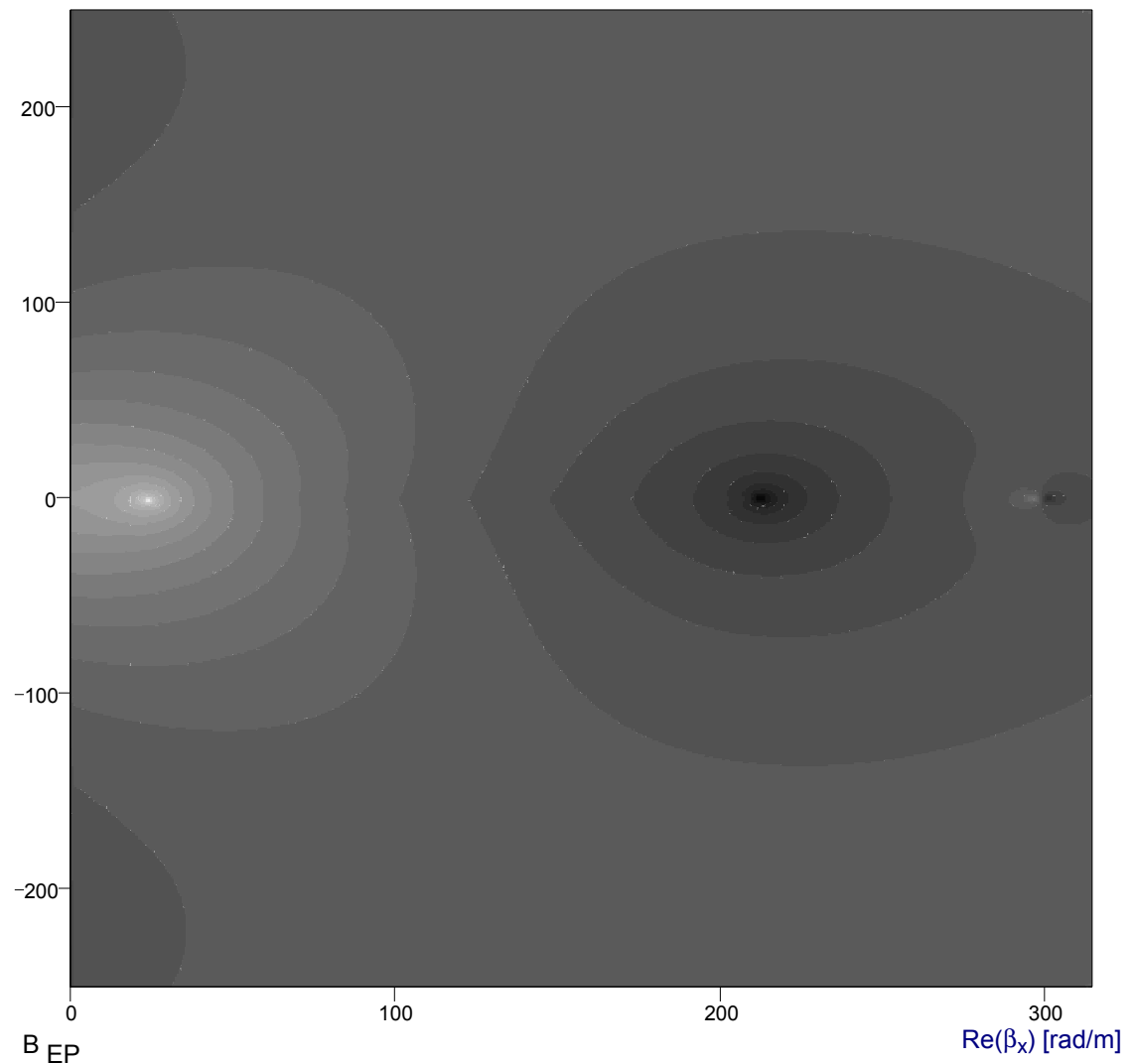
$$s_{z2} := -j \cdot \frac{\operatorname{Re}\left(\sqrt{\beta_x^2 - k_2^2}\right)}{\left|\operatorname{Re}\left(\sqrt{\beta_x^2 - k_2^2}\right)\right|} \cdot \sqrt{\beta_x^2 - k_2^2} \quad s_{z2} = -0.114 - 36.811j \cdot \frac{\operatorname{rad}}{\operatorname{m}}$$

$$N := 301 \quad \operatorname{Start}_x := 0 \cdot \frac{\operatorname{rad}}{\operatorname{m}} \quad \operatorname{End}_x := \operatorname{Re}(k_1) \quad \operatorname{Start}_y := -250 \cdot \frac{\operatorname{rad}}{\operatorname{m}} \quad \operatorname{End}_y := 250 \cdot \frac{\operatorname{rad}}{\operatorname{m}}$$

$$x := 0, 1 \dots N \quad y := 0, 1 \dots N \quad \Delta x := \frac{\operatorname{End}_x - \operatorname{Start}_x}{N} \quad \Delta y := \frac{\operatorname{End}_y - \operatorname{Start}_y}{N}$$

$$B_{EP_{x,y}} := \log\left[\left|F_{EP}\left(\left(\operatorname{Start}_x + x \cdot \Delta x\right) + \left[j \cdot \left(\operatorname{Start}_y + y \cdot \Delta y\right)\right]\right)\right| \cdot \frac{\operatorname{siemens} \cdot \operatorname{m}}{\operatorname{m} \cdot \operatorname{rad}}\right]$$

$\operatorname{Im}(\beta_x)$ [rad/m]



Example 3: Plane Surface Waves along a Coated PEC

Constants:

$$c_0 := 299792458 \cdot \frac{\text{m}}{\text{sec}} \quad \mu_0 := 4 \cdot \pi \cdot 10^{-7} \cdot \frac{\text{henry}}{\text{m}} \quad \epsilon_0 := \frac{1}{c_0^2 \cdot \mu_0} \quad \epsilon_0 = 8.854 \cdot 10^{-12} \cdot \frac{\text{farad}}{\text{m}}$$

Enter the material parameters:

$$\sigma_1 := 0 \cdot \frac{\text{siemens}}{\text{m}} \quad \epsilon_{r1} := 2.26 - 0.00091j \quad \mu_{r1} := 1 - 0j$$
$$\sigma_2 := 0 \cdot \frac{\text{siemens}}{\text{m}} \quad \epsilon_{r2} := 1 - 0j \quad \mu_{r2} := 1 - 0j$$

Enter the frequency:

$$f := 10 \cdot 10^9 \cdot \text{Hz} \quad \omega := 2 \cdot \pi \cdot f \quad \omega = 6.283 \cdot 10^{10} \cdot \text{Hz} \quad \lambda_0 := \frac{c_0}{f} \quad \lambda_0 = 0.030 \cdot \text{m}$$

Enter the thickness of the coating:

$$h := 0.080 \cdot \text{m}$$

Complex wave numbers:

$$\epsilon_1 := \epsilon_{r1} \cdot \epsilon_0 \quad \epsilon_2 := \epsilon_{r2} \cdot \epsilon_0$$

$$\mu_1 := \mu_{r1} \cdot \mu_0 \quad \mu_2 := \mu_{r2} \cdot \mu_0$$

$$k_0 := \omega \sqrt{\epsilon_0 \cdot \mu_0} \quad k_0 = 209.585 \cdot \frac{\text{rad}}{\text{m}}$$

$$k_1 := \sqrt{-j \cdot \omega \mu_1 \cdot (\sigma_1 + j \cdot \omega \epsilon_1)} \quad k_1 = 315.075 - 0.063j \cdot \frac{\text{rad}}{\text{m}}$$

(k_2 must be smaller than k_1 !)

$$k_2 := \sqrt{-j \cdot \omega \mu_2 \cdot (\sigma_2 + j \cdot \omega \epsilon_2)} \quad k_2 = 209.585 \cdot \frac{\text{rad}}{\text{m}}$$

E-type proper wave modes:

$$F_{EP}(\beta_x) := \frac{\sqrt{k_1^2 - \beta_x^2}}{\sigma_1 + j \cdot \omega \epsilon_1} \cdot \tan\left(h \cdot \sqrt{k_1^2 - \beta_x^2}\right) - \frac{\operatorname{Re}\left(\sqrt{\beta_x^2 - k_2^2}\right)}{\left|\operatorname{Re}\left(\sqrt{\beta_x^2 - k_2^2}\right)\right|} \cdot \frac{\sqrt{\beta_x^2 - k_2^2}}{\sigma_2 + j \cdot \omega \epsilon_2}$$

$$\beta_x := \frac{k_1 + k_2}{2} \quad \beta_x := \operatorname{root}\left(F_{EP}(\beta_x), \beta_x\right) \quad \beta_x = 264.487 - 0.072j \cdot \frac{\operatorname{rad}}{\operatorname{m}}$$

$$F_{EP}(\beta_x) = -2.415 \cdot 10^{-4} - 4.666 \cdot 10^{-4}j \cdot \operatorname{kg} \cdot \operatorname{m}^2 \cdot \operatorname{sec}^{-1} \cdot \operatorname{coul}^{-2}$$

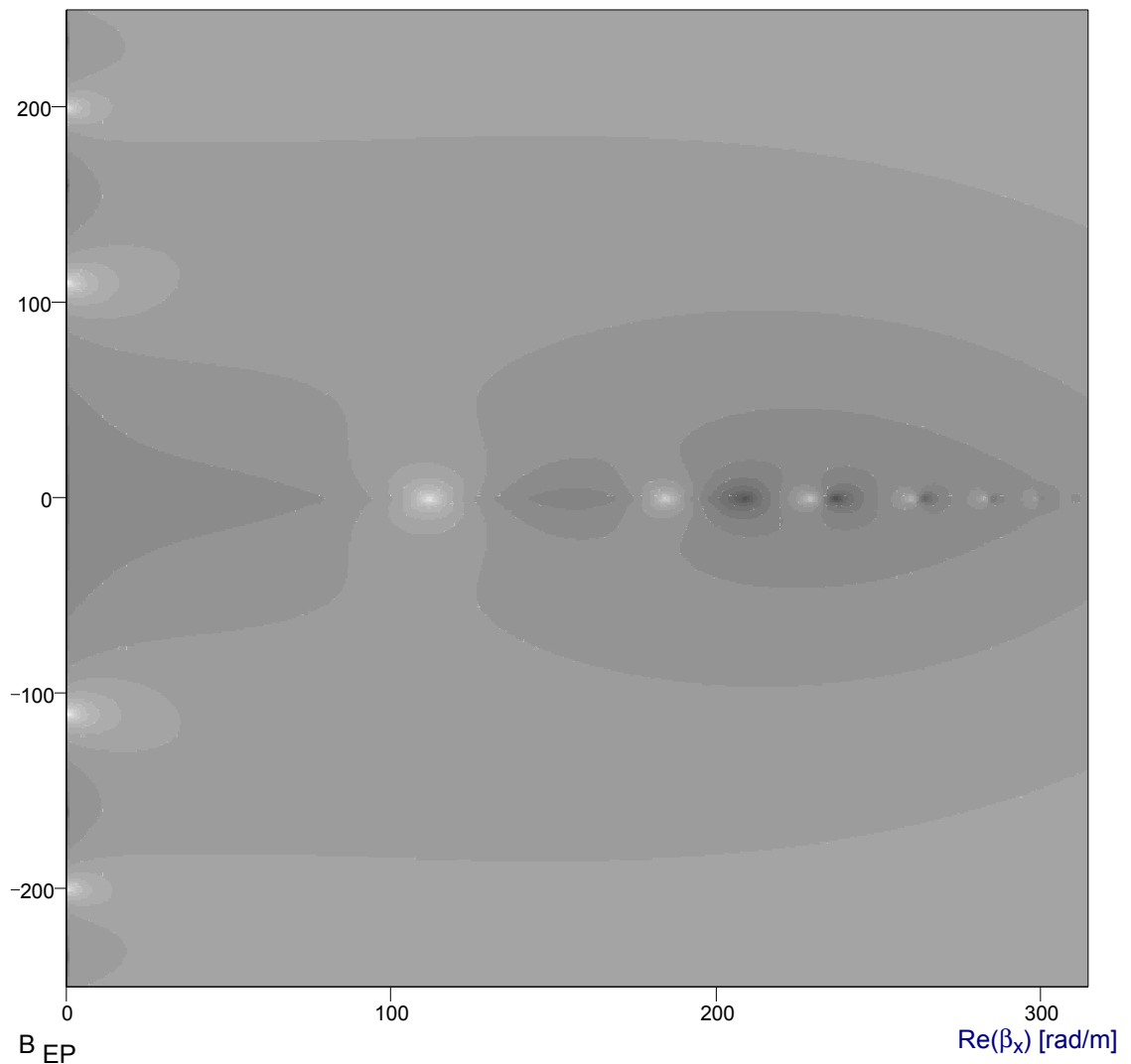
$$s_{z2} := -j \cdot \frac{\operatorname{Re}\left(\sqrt{\beta_x^2 - k_2^2}\right)}{\left|\operatorname{Re}\left(\sqrt{\beta_x^2 - k_2^2}\right)\right|} \cdot \sqrt{\beta_x^2 - k_2^2} \quad s_{z2} = -0.118 - 161.331j \cdot \frac{\operatorname{rad}}{\operatorname{m}}$$

$$N := 301 \quad \operatorname{Start}_x := 0 \cdot \frac{\operatorname{rad}}{\operatorname{m}} \quad \operatorname{End}_x := \operatorname{Re}(k_1) \quad \operatorname{Start}_y := -250 \cdot \frac{\operatorname{rad}}{\operatorname{m}} \quad \operatorname{End}_y := 250 \cdot \frac{\operatorname{rad}}{\operatorname{m}}$$

$$x := 0, 1 \dots N \quad y := 0, 1 \dots N \quad \Delta x := \frac{\operatorname{End}_x - \operatorname{Start}_x}{N} \quad \Delta y := \frac{\operatorname{End}_y - \operatorname{Start}_y}{N}$$

$$B_{EP_{x,y}} := \log\left[\left|F_{EP}\left(\left(\operatorname{Start}_x + x \cdot \Delta x\right) + \left[j \cdot \left(\operatorname{Start}_y + y \cdot \Delta y\right)\right]\right)\right| \cdot \frac{\operatorname{siemens} \cdot \operatorname{m}}{\operatorname{m} \cdot \operatorname{rad}}\right]$$

$\operatorname{Im}(\beta_x)$ [rad/m]



Example 4: Plane Improper Waves along a Coated PEC

Constants:

$$c_0 := 299792458 \cdot \frac{\text{m}}{\text{sec}} \quad \mu_0 := 4 \cdot \pi \cdot 10^{-7} \cdot \frac{\text{henry}}{\text{m}} \quad \varepsilon_0 := \frac{1}{c_0^2 \cdot \mu_0} \quad \varepsilon_0 = 8.854 \cdot 10^{-12} \cdot \frac{\text{farad}}{\text{m}}$$

Enter the material parameters:

$$\sigma_1 := 0 \cdot \frac{\text{siemens}}{\text{m}} \quad \varepsilon_{r1} := 2.26 - 0.00091j \quad \mu_{r1} := 1 - 0j$$
$$\sigma_2 := 0 \cdot \frac{\text{siemens}}{\text{m}} \quad \varepsilon_{r2} := 1 - 0j \quad \mu_{r2} := 1 - 0j$$

Enter the frequency:

$$f := 10 \cdot 10^9 \cdot \text{Hz} \quad \omega := 2 \cdot \pi \cdot f \quad \omega = 6.283 \cdot 10^{10} \cdot \text{Hz} \quad \lambda_0 := \frac{c_0}{f} \quad \lambda_0 = 0.030 \cdot \text{m}$$

Enter the thickness of the coating:

$$h := 0.006 \cdot \text{m}$$

Complex wave numbers:

$$\varepsilon_1 := \varepsilon_{r1} \cdot \varepsilon_0 \quad \varepsilon_2 := \varepsilon_{r2} \cdot \varepsilon_0$$

$$\mu_1 := \mu_{r1} \cdot \mu_0 \quad \mu_2 := \mu_{r2} \cdot \mu_0$$

$$k_0 := \omega \sqrt{\varepsilon_0 \cdot \mu_0} \quad k_0 = 209.585 \cdot \frac{\text{rad}}{\text{m}}$$

$$k_1 := \sqrt{-j \cdot \omega \mu_1 \cdot (\sigma_1 + j \cdot \omega \varepsilon_1)} \quad k_1 = 315.075 - 0.063j \cdot \frac{\text{rad}}{\text{m}}$$

$$k_2 := \sqrt{-j \cdot \omega \mu_2 \cdot (\sigma_2 + j \cdot \omega \varepsilon_2)} \quad k_2 = 209.585 \cdot \frac{\text{rad}}{\text{m}}$$

(k_2 must be smaller than k_1 !)

E-type improper wave modes:

$$F_{EI}(\beta_x) := \frac{\sqrt{k_1^2 - \beta_x^2}}{\sigma_1 + j \cdot \omega \epsilon_1} \cdot \tan\left(h \cdot \sqrt{k_1^2 - \beta_x^2}\right) + \frac{\operatorname{Re}\left(\sqrt{\beta_x^2 - k_2^2}\right)}{\left|\operatorname{Re}\left(\sqrt{\beta_x^2 - k_2^2}\right)\right|} \cdot \frac{\sqrt{\beta_x^2 - k_2^2}}{\sigma_2 + j \cdot \omega \epsilon_2}$$

$$\beta_x := \frac{k_1 + k_2}{2} \quad \beta_x := \operatorname{root}\left(F_{EI}(\beta_x), \beta_x\right) \quad \beta_x = 201.038 + 141.062j \cdot \frac{\operatorname{rad}}{\operatorname{m}}$$

$$F_{EI}(\beta_x) = 3.234 \cdot 10^{-4} + 1.567 \cdot 10^{-4} j \cdot \operatorname{kg} \cdot \operatorname{m}^2 \cdot \operatorname{sec}^{-1} \cdot \operatorname{coul}^{-2}$$

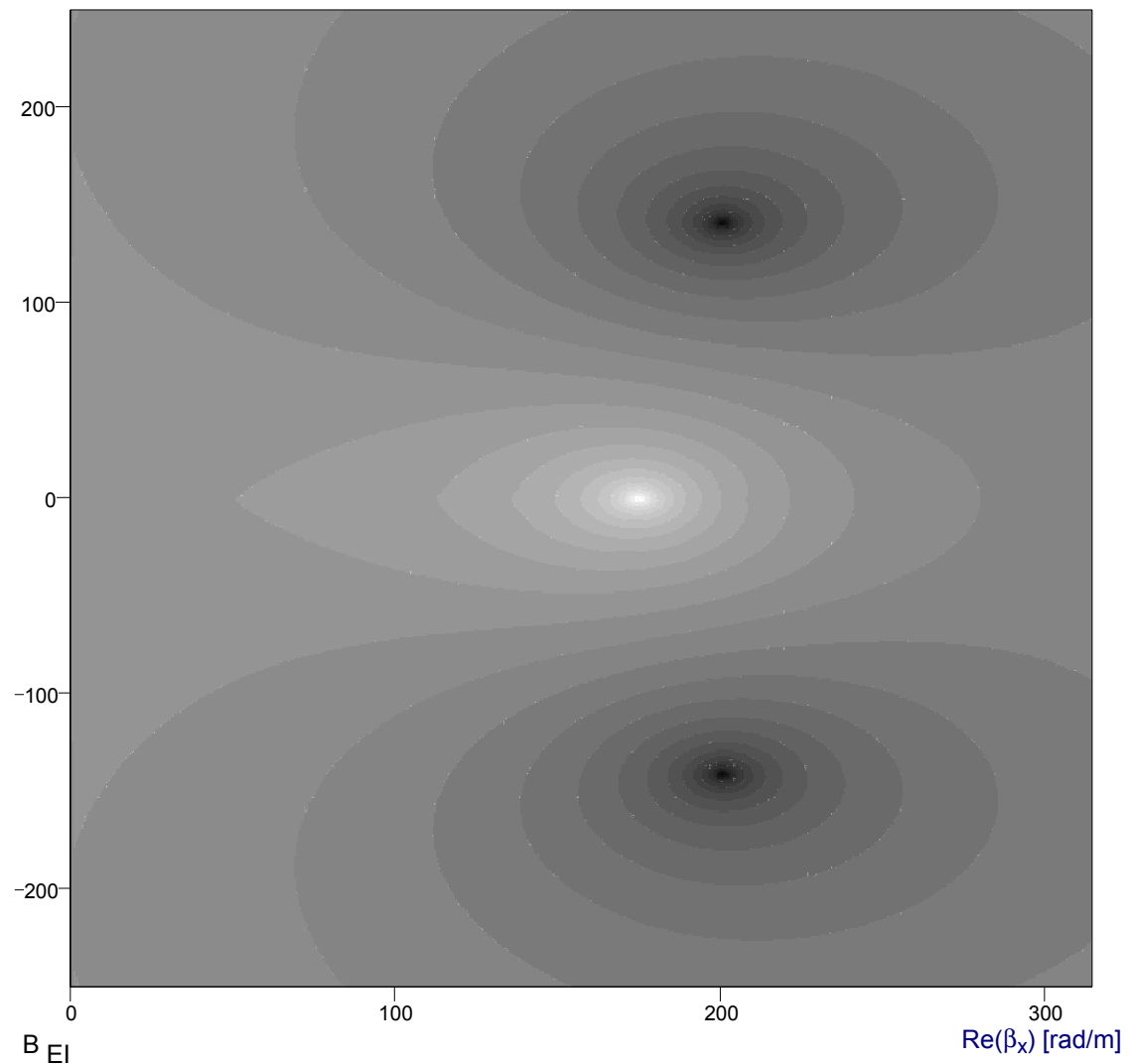
$$s_{z2} := j \cdot \frac{\operatorname{Re}\left(\sqrt{\beta_x^2 - k_2^2}\right)}{\left|\operatorname{Re}\left(\sqrt{\beta_x^2 - k_2^2}\right)\right|} \cdot \sqrt{\beta_x^2 - k_2^2} \quad s_{z2} = -205.872 + 137.75j \cdot \frac{\operatorname{rad}}{\operatorname{m}}$$

$$N := 301 \quad \operatorname{Start}_x := 0 \cdot \frac{\operatorname{rad}}{\operatorname{m}} \quad \operatorname{End}_x := \operatorname{Re}(k_1) \quad \operatorname{Start}_y := -250 \cdot \frac{\operatorname{rad}}{\operatorname{m}} \quad \operatorname{End}_y := 250 \cdot \frac{\operatorname{rad}}{\operatorname{m}}$$

$$x := 0, 1 \dots N \quad y := 0, 1 \dots N \quad \Delta x := \frac{\operatorname{End}_x - \operatorname{Start}_x}{N} \quad \Delta y := \frac{\operatorname{End}_y - \operatorname{Start}_y}{N}$$

$$B_{EI,x,y} := \log\left[\left|F_{EI}\left[\left(\operatorname{Start}_x + x \cdot \Delta x\right) + \left[j \cdot \left(\operatorname{Start}_y + y \cdot \Delta y\right)\right]\right]\right| \cdot \frac{\operatorname{siemens} \cdot \operatorname{m}}{\operatorname{m} \cdot \operatorname{rad}}\right]$$

$\operatorname{Im}(\beta_x)$ [rad/m]



Example 5: Plane Improper Waves along a Coated PEC

Constants:

$$c_0 := 299792458 \cdot \frac{\text{m}}{\text{sec}} \quad \mu_0 := 4 \cdot \pi \cdot 10^{-7} \cdot \frac{\text{henry}}{\text{m}} \quad \epsilon_0 := \frac{1}{c_0^2 \cdot \mu_0} \quad \epsilon_0 = 8.854 \cdot 10^{-12} \cdot \frac{\text{farad}}{\text{m}}$$

Enter the material parameters:

$$\sigma_1 := 0 \cdot \frac{\text{siemens}}{\text{m}} \quad \epsilon_{r1} := 2.26 - 0.00091j \quad \mu_{r1} := 1 - 0j$$
$$\sigma_2 := 0 \cdot \frac{\text{siemens}}{\text{m}} \quad \epsilon_{r2} := 1 - 0j \quad \mu_{r2} := 1 - 0j$$

Enter the frequency:

$$f := 10 \cdot 10^9 \cdot \text{Hz} \quad \omega := 2 \cdot \pi \cdot f \quad \omega = 6.283 \cdot 10^{10} \cdot \text{Hz} \quad \lambda_0 := \frac{c_0}{f} \quad \lambda_0 = 0.030 \cdot \text{m}$$

Enter the thickness of the coating:

$$h := 0.015 \cdot \text{m}$$

Complex wave numbers:

$$\epsilon_1 := \epsilon_{r1} \cdot \epsilon_0 \quad \epsilon_2 := \epsilon_{r2} \cdot \epsilon_0$$

$$\mu_1 := \mu_{r1} \cdot \mu_0 \quad \mu_2 := \mu_{r2} \cdot \mu_0$$

$$k_0 := \omega \sqrt{\epsilon_0 \cdot \mu_0} \quad k_0 = 209.585 \cdot \frac{\text{rad}}{\text{m}}$$

$$k_1 := \sqrt{-j \cdot \omega \mu_1 \cdot (\sigma_1 + j \cdot \omega \epsilon_1)} \quad k_1 = 315.075 - 0.063j \cdot \frac{\text{rad}}{\text{m}}$$

(k_2 must be smaller than k_1 !)

$$k_2 := \sqrt{-j \cdot \omega \mu_2 \cdot (\sigma_2 + j \cdot \omega \epsilon_2)} \quad k_2 = 209.585 \cdot \frac{\text{rad}}{\text{m}}$$

E-type improper wave modes:

$$F_{EI}(\beta_x) := \frac{\sqrt{k_1^2 - \beta_x^2}}{\sigma_1 + j \cdot \omega \epsilon_1} \cdot \tan\left(h \cdot \sqrt{k_1^2 - \beta_x^2}\right) + \frac{\operatorname{Re}\left(\sqrt{\beta_x^2 - k_2^2}\right)}{\left|\operatorname{Re}\left(\sqrt{\beta_x^2 - k_2^2}\right)\right|} \cdot \frac{\sqrt{\beta_x^2 - k_2^2}}{\sigma_2 + j \cdot \omega \epsilon_2}$$

$$\beta_x := \frac{k_1 + k_2}{2} \quad \beta_x := \operatorname{root}\left(F_{EI}(\beta_x), \beta_x\right) \quad \beta_x = 262.33 - 0.032j \cdot \frac{\text{rad}}{\text{m}}$$

$$F_{EI}(\beta_x) = -0.282 - 203.403j \cdot \text{kg} \cdot \text{m}^{-2} \cdot \text{sec}^{-1} \cdot \text{coul}^{-2}$$

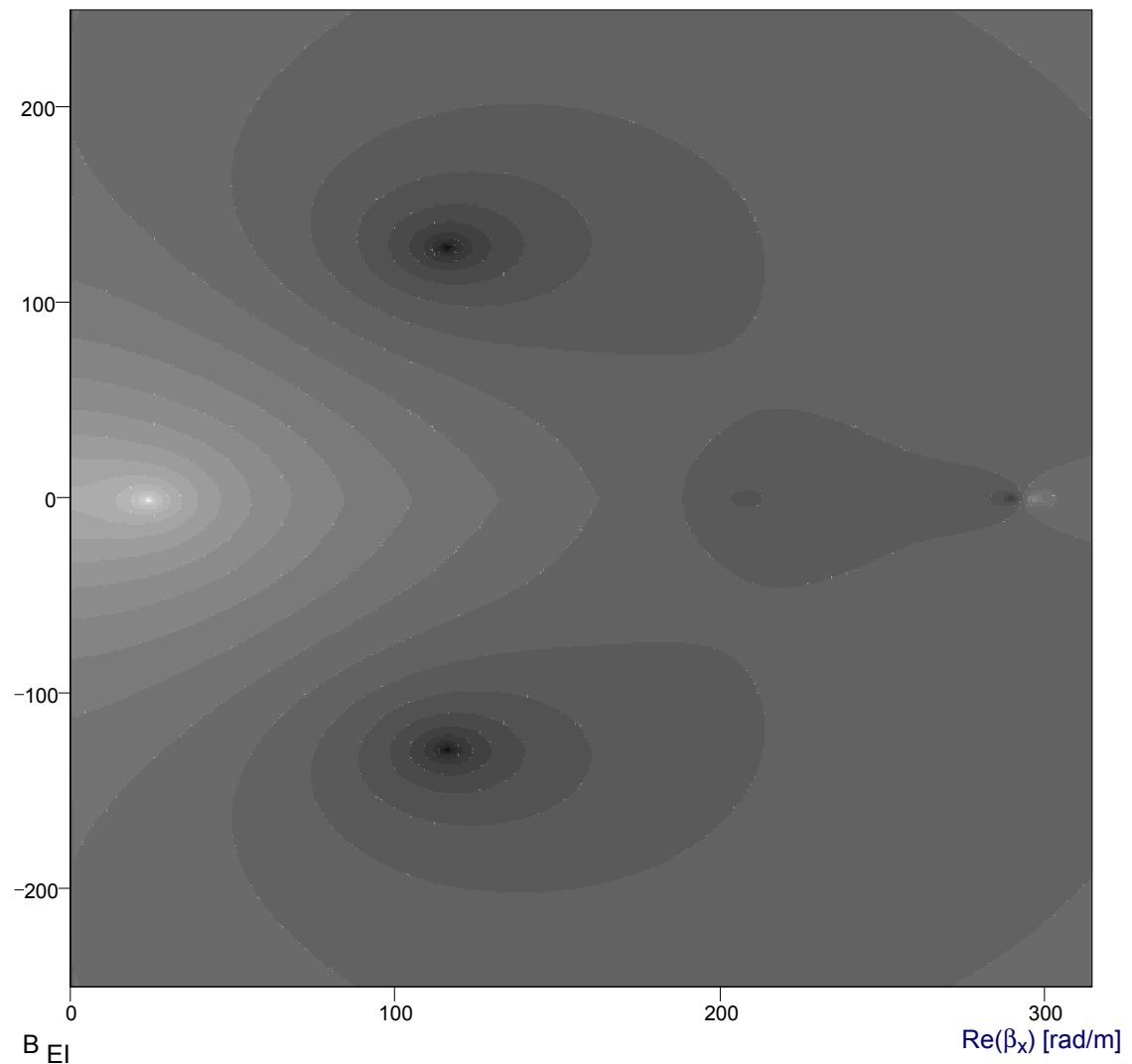
$$s_{z2} := j \cdot \frac{\operatorname{Re}\left(\sqrt{\beta_x^2 - k_2^2}\right)}{\left|\operatorname{Re}\left(\sqrt{\beta_x^2 - k_2^2}\right)\right|} \cdot \sqrt{\beta_x^2 - k_2^2} \quad s_{z2} = 0.053 + 157.769j \cdot \frac{\text{rad}}{\text{m}}$$

$$N := 301 \quad \text{Start}_x := 0 \cdot \frac{\text{rad}}{\text{m}} \quad \text{End}_x := \operatorname{Re}(k_1) \quad \text{Start}_y := -250 \cdot \frac{\text{rad}}{\text{m}} \quad \text{End}_y := 250 \cdot \frac{\text{rad}}{\text{m}}$$

$$x := 0, 1 \dots N \quad y := 0, 1 \dots N \quad \Delta x := \frac{\text{End}_x - \text{Start}_x}{N} \quad \Delta y := \frac{\text{End}_y - \text{Start}_y}{N}$$

$$B_{EI,x,y} := \log\left[\left|F_{EI}\left[\left(\text{Start}_x + x \cdot \Delta x\right) + \left[j \cdot \left(\text{Start}_y + y \cdot \Delta y\right)\right]\right]\right| \cdot \frac{\text{siemens} \cdot \text{m}}{\text{m} \cdot \text{rad}}\right]$$

$\operatorname{Im}(\beta_x)$ [rad/m]



Example 6: Plane Improper Waves along a Coated PEC

Constants:

$$c_0 := 299792458 \cdot \frac{\text{m}}{\text{sec}} \quad \mu_0 := 4 \cdot \pi \cdot 10^{-7} \cdot \frac{\text{henry}}{\text{m}} \quad \epsilon_0 := \frac{1}{c_0^2 \cdot \mu_0} \quad \epsilon_0 = 8.854 \cdot 10^{-12} \cdot \frac{\text{farad}}{\text{m}}$$

Enter the material parameters:

$$\sigma_1 := 0 \cdot \frac{\text{siemens}}{\text{m}} \quad \epsilon_{r1} := 2.26 - 0.00091j \quad \mu_{r1} := 1 - 0j$$
$$\sigma_2 := 0 \cdot \frac{\text{siemens}}{\text{m}} \quad \epsilon_{r2} := 1 - 0j \quad \mu_{r2} := 1 - 0j$$

Enter the frequency:

$$f := 10 \cdot 10^9 \cdot \text{Hz} \quad \omega := 2 \cdot \pi \cdot f \quad \omega = 6.283 \cdot 10^{10} \cdot \text{Hz} \quad \lambda_0 := \frac{c_0}{f} \quad \lambda_0 = 0.030 \cdot \text{m}$$

Enter the thickness of the coating:

$$h := 0.080 \cdot \text{m}$$

Complex wave numbers:

$$\epsilon_1 := \epsilon_{r1} \cdot \epsilon_0 \quad \epsilon_2 := \epsilon_{r2} \cdot \epsilon_0$$

$$\mu_1 := \mu_{r1} \cdot \mu_0 \quad \mu_2 := \mu_{r2} \cdot \mu_0$$

$$k_0 := \omega \sqrt{\epsilon_0 \cdot \mu_0} \quad k_0 = 209.585 \cdot \frac{\text{rad}}{\text{m}}$$

$$k_1 := \sqrt{-j \cdot \omega \mu_1 \cdot (\sigma_1 + j \cdot \omega \epsilon_1)} \quad k_1 = 315.075 - 0.063j \cdot \frac{\text{rad}}{\text{m}}$$

$$k_2 := \sqrt{-j \cdot \omega \mu_2 \cdot (\sigma_2 + j \cdot \omega \epsilon_2)} \quad k_2 = 209.585 \cdot \frac{\text{rad}}{\text{m}}$$

(k_2 must be smaller than k_1 !)

E-type improper wave modes:

$$F_{EI}(\beta_x) := \frac{\sqrt{k_1^2 - \beta_x^2}}{\sigma_1 + j \cdot \omega \varepsilon_1} \cdot \tan\left(h \cdot \sqrt{k_1^2 - \beta_x^2}\right) + \frac{\operatorname{Re}\left(\sqrt{\beta_x^2 - k_2^2}\right)}{\left|\operatorname{Re}\left(\sqrt{\beta_x^2 - k_2^2}\right)\right|} \cdot \frac{\sqrt{\beta_x^2 - k_2^2}}{\sigma_2 + j \cdot \omega \varepsilon_2}$$

$$\beta_x := \frac{k_1 + k_2}{2} \quad \beta_x := \operatorname{root}\left(F_{EI}(\beta_x), \beta_x\right) \quad \beta_x = 113.224 - 29.77j \cdot \frac{\operatorname{rad}}{\operatorname{m}}$$

$$F_{EI}(\beta_x) = -7.483 \cdot 10^{-7} - 2.621 \cdot 10^{-6}j \cdot \operatorname{kg} \cdot \operatorname{m}^2 \cdot \operatorname{sec}^{-1} \cdot \operatorname{coul}^{-2}$$

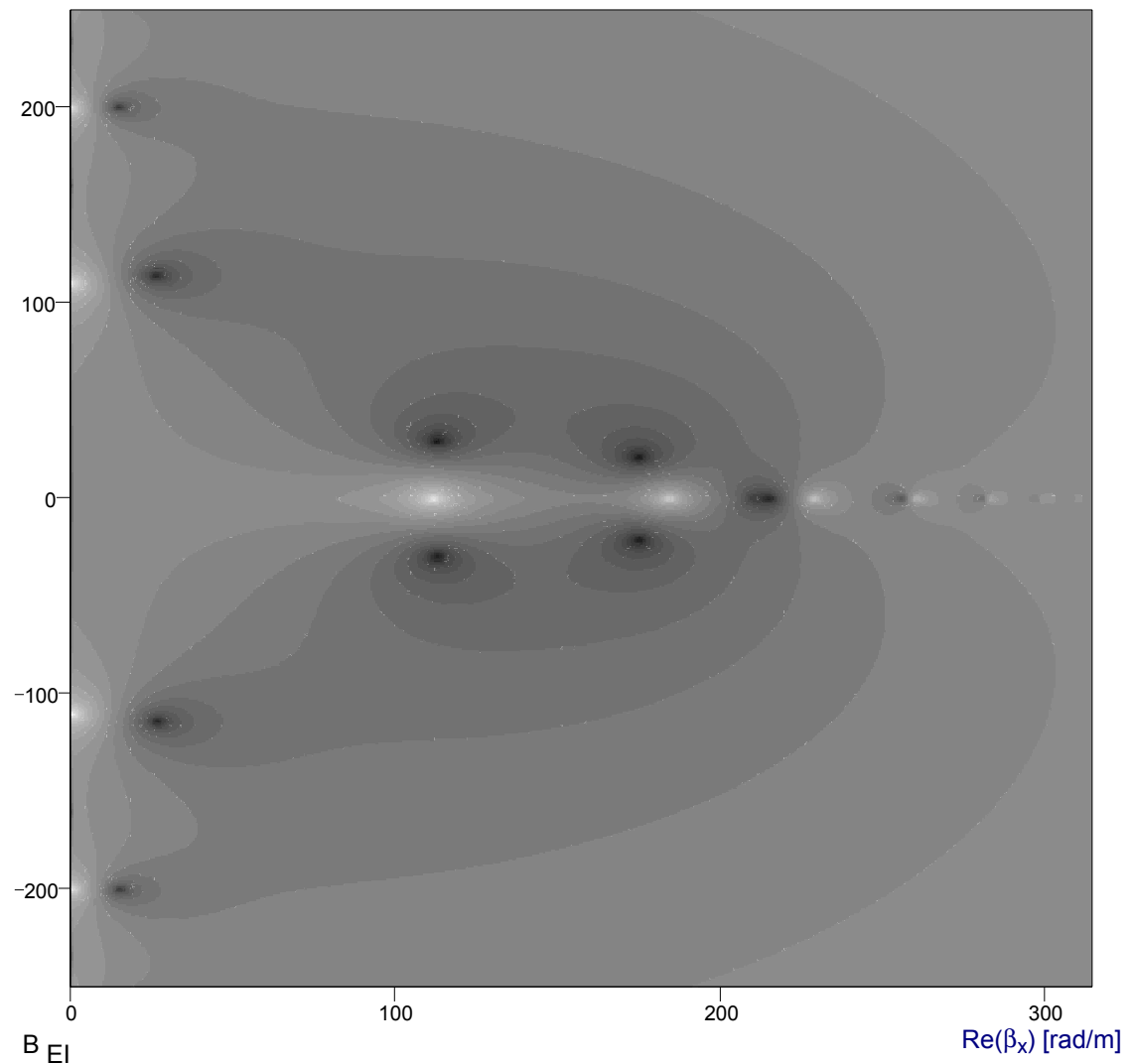
$$s_{z2} := j \cdot \frac{\operatorname{Re}\left(\sqrt{\beta_x^2 - k_2^2}\right)}{\left|\operatorname{Re}\left(\sqrt{\beta_x^2 - k_2^2}\right)\right|} \cdot \sqrt{\beta_x^2 - k_2^2} \quad s_{z2} = 179.843 + 18.743j \cdot \frac{\operatorname{rad}}{\operatorname{m}}$$

$$N := 301 \quad \operatorname{Start}_x := 0 \cdot \frac{\operatorname{rad}}{\operatorname{m}} \quad \operatorname{End}_x := \operatorname{Re}(k_1) \quad \operatorname{Start}_y := -250 \cdot \frac{\operatorname{rad}}{\operatorname{m}} \quad \operatorname{End}_y := 250 \cdot \frac{\operatorname{rad}}{\operatorname{m}}$$

$$x := 0, 1 \dots N \quad y := 0, 1 \dots N \quad \Delta x := \frac{\operatorname{End}_x - \operatorname{Start}_x}{N} \quad \Delta y := \frac{\operatorname{End}_y - \operatorname{Start}_y}{N}$$

$$B_{EI,x,y} := \log\left[\left|F_{EI}\left[\left(\operatorname{Start}_x + x \cdot \Delta x\right) + \left[j \cdot \left(\operatorname{Start}_y + y \cdot \Delta y\right)\right]\right]\right| \cdot \frac{\operatorname{siemens} \cdot \operatorname{m}}{\operatorname{m} \cdot \operatorname{rad}}\right]$$

$\operatorname{Im}(\beta_x)$ [rad/m]



Example 7: Proper Waves along Metal-Coated Eccosorb GDS

Constants:

$$c_0 := 299792458 \cdot \frac{\text{m}}{\text{sec}} \quad \mu_0 := 4 \cdot \pi \cdot 10^{-7} \cdot \frac{\text{henry}}{\text{m}} \quad \varepsilon_0 := \frac{1}{c_0^2 \cdot \mu_0} \quad \varepsilon_0 = 8.854 \cdot 10^{-12} \cdot \frac{\text{farad}}{\text{m}}$$

Enter the material parameters:

$$\sigma_1 := 0 \cdot \frac{\text{siemens}}{\text{m}} \quad \varepsilon_{r1} := 7.4 - 0.15j \quad \mu_{r1} := 1.4 - 0.48j$$
$$\sigma_2 := 0 \cdot \frac{\text{siemens}}{\text{m}} \quad \varepsilon_{r2} := 1 - 0j \quad \mu_{r2} := 1 - 0j$$

Enter the frequency:

$$f := 8.6 \cdot 10^9 \cdot \text{Hz} \quad \omega := 2 \cdot \pi \cdot f \quad \omega = 5.404 \cdot 10^{10} \cdot \text{Hz} \quad \lambda_0 := \frac{c_0}{f} \quad \lambda_0 = 0.035 \cdot \text{m}$$

Enter the thickness of the coating:

$$h := 0.00075 \cdot \text{m}$$

Complex wave numbers:

$$\varepsilon_1 := \varepsilon_{r1} \cdot \varepsilon_0 \quad \varepsilon_2 := \varepsilon_{r2} \cdot \varepsilon_0$$

$$\mu_1 := \mu_{r1} \cdot \mu_0 \quad \mu_2 := \mu_{r2} \cdot \mu_0$$

$$k_0 := \omega \sqrt{\varepsilon_0 \cdot \mu_0} \quad k_0 = 180.243 \cdot \frac{\text{rad}}{\text{m}}$$

$$k_1 := \sqrt{-j \cdot \omega \mu_1 \cdot (\sigma_1 + j \cdot \omega \varepsilon_1)} \quad k_1 = 587.412 - 104.031j \cdot \frac{\text{rad}}{\text{m}}$$

(k_2 must be smaller than k_1 !)

$$k_2 := \sqrt{-j \cdot \omega \mu_2 \cdot (\sigma_2 + j \cdot \omega \varepsilon_2)} \quad k_2 = 180.243 \cdot \frac{\text{rad}}{\text{m}}$$

E-type proper wave modes:

$$F_{EP}(\beta_x) := \frac{\sqrt{k_1^2 - \beta_x^2}}{\sigma_1 + j \cdot \omega \epsilon_1} \cdot \tan\left(h \cdot \sqrt{k_1^2 - \beta_x^2}\right) - \frac{\operatorname{Re}\left(\sqrt{\beta_x^2 - k_2^2}\right)}{\left|\operatorname{Re}\left(\sqrt{\beta_x^2 - k_2^2}\right)\right|} \cdot \frac{\sqrt{\beta_x^2 - k_2^2}}{\sigma_2 + j \cdot \omega \epsilon_2}$$

$$\beta_x := \frac{k_1 + k_2}{2} \quad \beta_x := \operatorname{root}\left(F_{EP}(\beta_x), \beta_x\right) \quad \beta_x = 182.647 - 2.328j \cdot \frac{\operatorname{rad}}{\operatorname{m}}$$

$$F_{EP}(\beta_x) = -2.203 \cdot 10^{-4} + 6.845 \cdot 10^{-4} j \cdot \operatorname{kg} \cdot \operatorname{m}^2 \cdot \operatorname{sec}^{-1} \cdot \operatorname{coul}^{-2}$$

$$s_{z2} := -j \cdot \frac{\operatorname{Re}\left(\sqrt{\beta_x^2 - k_2^2}\right)}{\left|\operatorname{Re}\left(\sqrt{\beta_x^2 - k_2^2}\right)\right|} \cdot \sqrt{\beta_x^2 - k_2^2} \quad s_{z2} = -13.179 - 32.262j \cdot \frac{\operatorname{rad}}{\operatorname{m}}$$

$$N := 301 \quad \operatorname{Start}_x := 0 \cdot \frac{\operatorname{rad}}{\operatorname{m}} \quad \operatorname{End}_x := \operatorname{Re}(k_1) \quad \operatorname{Start}_y := -250 \cdot \frac{\operatorname{rad}}{\operatorname{m}} \quad \operatorname{End}_y := 250 \cdot \frac{\operatorname{rad}}{\operatorname{m}}$$

$$x := 0, 1 \dots N \quad y := 0, 1 \dots N \quad \Delta x := \frac{\operatorname{End}_x - \operatorname{Start}_x}{N} \quad \Delta y := \frac{\operatorname{End}_y - \operatorname{Start}_y}{N}$$

$$B_{EP_{x,y}} := \log\left[\left|F_{EP}\left(\left(\operatorname{Start}_x + x \cdot \Delta x\right) + \left[j \cdot \left(\operatorname{Start}_y + y \cdot \Delta y\right)\right]\right)\right| \cdot \frac{\operatorname{siemens} \cdot \operatorname{m}}{\operatorname{m} \cdot \operatorname{rad}}\right]$$

$\operatorname{Im}(\beta_x)$ [rad/m]



Example 8: Plane Improper Waves along Metal-Backed Eccosorb GDS

Constants:

$$c_0 := 299792458 \cdot \frac{\text{m}}{\text{sec}} \quad \mu_0 := 4 \cdot \pi \cdot 10^{-7} \cdot \frac{\text{henry}}{\text{m}} \quad \varepsilon_0 := \frac{1}{c_0^2 \cdot \mu_0} \quad \varepsilon_0 = 8.854 \cdot 10^{-12} \cdot \frac{\text{farad}}{\text{m}}$$

Enter the material parameters:

$$\sigma_1 := 0 \cdot \frac{\text{siemens}}{\text{m}} \quad \varepsilon_{r1} := 7.4 - 0.15j \quad \mu_{r1} := 1.4 - 0.48j$$

$$\sigma_2 := 0 \cdot \frac{\text{siemens}}{\text{m}} \quad \varepsilon_{r2} := 1 - 0j \quad \mu_{r2} := 1 - 0j$$

Enter the frequency:

$$f := 8.6 \cdot 10^9 \cdot \text{Hz} \quad \omega := 2 \cdot \pi \cdot f \quad \omega = 5.404 \cdot 10^{10} \cdot \text{Hz} \quad \lambda_0 := \frac{c_0}{f} \quad \lambda_0 = 0.035 \cdot \text{m}$$

Enter the thickness of the coating:

$$h := 0.00075 \cdot \text{m}$$

Complex wave numbers:

$$\varepsilon_1 := \varepsilon_{r1} \cdot \varepsilon_0 \quad \varepsilon_2 := \varepsilon_{r2} \cdot \varepsilon_0$$

$$\mu_1 := \mu_{r1} \cdot \mu_0 \quad \mu_2 := \mu_{r2} \cdot \mu_0$$

$$k_0 := \omega \sqrt{\varepsilon_0 \cdot \mu_0} \quad k_0 = 180.243 \cdot \frac{\text{rad}}{\text{m}}$$

$$k_1 := \sqrt{-j \cdot \omega \mu_1 \cdot (\sigma_1 + j \cdot \omega \varepsilon_1)} \quad k_1 = 587.412 - 104.031j \cdot \frac{\text{rad}}{\text{m}}$$

$$k_2 := \sqrt{-j \cdot \omega \mu_2 \cdot (\sigma_2 + j \cdot \omega \varepsilon_2)} \quad k_2 = 180.243 \cdot \frac{\text{rad}}{\text{m}}$$

(k_2 must be smaller than k_1 !)

E-type improper wave modes:

$$F_{EI}(\beta_x) := \frac{\sqrt{k_1^2 - \beta_x^2}}{\sigma_1 + j \cdot \omega \epsilon_1} \cdot \tan\left(h \cdot \sqrt{k_1^2 - \beta_x^2}\right) + \frac{\operatorname{Re}\left(\sqrt{\beta_x^2 - k_2^2}\right)}{\left|\operatorname{Re}\left(\sqrt{\beta_x^2 - k_2^2}\right)\right|} \cdot \frac{\sqrt{\beta_x^2 - k_2^2}}{\sigma_2 + j \cdot \omega \epsilon_2}$$

$$\beta_x := \frac{k_1 + k_2}{2} \quad \beta_x := \operatorname{root}\left(F_{EI}(\beta_x), \beta_x\right) \quad \beta_x = 383.827 - 52.015j \cdot \frac{\operatorname{rad}}{\operatorname{m}}$$

$$F_{EI}(\beta_x) = -140.648 \overset{\text{not converging}}{-752.295j} \operatorname{kg} \cdot \operatorname{m}^2 \cdot \operatorname{sec}^{-1} \cdot \operatorname{coul}^{-2}$$

$$s_{z2} := j \cdot \frac{\operatorname{Re}\left(\sqrt{\beta_x^2 - k_2^2}\right)}{\left|\operatorname{Re}\left(\sqrt{\beta_x^2 - k_2^2}\right)\right|} \cdot \sqrt{\beta_x^2 - k_2^2} \quad s_{z2} = 58.726 + 339.969j \cdot \frac{\operatorname{rad}}{\operatorname{m}}$$

$$N := 301 \quad \operatorname{Start}_x := 0 \cdot \frac{\operatorname{rad}}{\operatorname{m}} \quad \operatorname{End}_x := \operatorname{Re}(k_1) \quad \operatorname{Start}_y := -250 \cdot \frac{\operatorname{rad}}{\operatorname{m}} \quad \operatorname{End}_y := 250 \cdot \frac{\operatorname{rad}}{\operatorname{m}}$$

$$x := 0, 1 \dots N \quad y := 0, 1 \dots N \quad \Delta x := \frac{\operatorname{End}_x - \operatorname{Start}_x}{N} \quad \Delta y := \frac{\operatorname{End}_y - \operatorname{Start}_y}{N}$$

$$B_{EI,x,y} := \log\left[\left|F_{EI}\left[\left(\operatorname{Start}_x + x \cdot \Delta x\right) + \left[j \cdot \left(\operatorname{Start}_y + y \cdot \Delta y\right)\right]\right]\right| \cdot \frac{\operatorname{siemens} \cdot \operatorname{m}}{\operatorname{m} \cdot \operatorname{rad}}\right]$$

$\operatorname{Im}(\beta_x)$ [rad/m]



Example 9: Plane Proper Waves along Thick Lossy Materials

Constants:

$$c_0 := 299792458 \cdot \frac{\text{m}}{\text{sec}} \quad \mu_0 := 4 \cdot \pi \cdot 10^{-7} \cdot \frac{\text{henry}}{\text{m}} \quad \epsilon_0 := \frac{1}{c_0^2 \cdot \mu_0} \quad \epsilon_0 = 8.854 \cdot 10^{-12} \cdot \frac{\text{farad}}{\text{m}}$$

Enter the material parameters:

$$\sigma_1 := 0 \cdot \frac{\text{siemens}}{\text{m}} \quad \epsilon_{r1} := 2.26 - 0.5j \quad \mu_{r1} := 1 - 0j$$
$$\sigma_2 := 0 \cdot \frac{\text{siemens}}{\text{m}} \quad \epsilon_{r2} := 1 - 0j \quad \mu_{r2} := 1 - 0j$$

Enter the frequency:

$$f := 10 \cdot 10^9 \cdot \text{Hz} \quad \omega := 2 \cdot \pi \cdot f \quad \omega = 6.283 \cdot 10^{10} \cdot \text{Hz} \quad \lambda_0 := \frac{c_0}{f} \quad \lambda_0 = 0.030 \cdot \text{m}$$

Enter the thickness of the coating:

$$h := 0.080 \cdot \text{m}$$

Complex wave numbers:

$$\epsilon_1 := \epsilon_{r1} \cdot \epsilon_0 \quad \epsilon_2 := \epsilon_{r2} \cdot \epsilon_0$$

$$\mu_1 := \mu_{r1} \cdot \mu_0 \quad \mu_2 := \mu_{r2} \cdot \mu_0$$

$$k_0 := \omega \sqrt{\epsilon_0 \cdot \mu_0} \quad k_0 = 209.585 \cdot \frac{\text{rad}}{\text{m}}$$

$$k_1 := \sqrt{-j \cdot \omega \mu_1 \cdot (\sigma_1 + j \cdot \omega \epsilon_1)} \quad k_1 = 316.974 - 34.645j \cdot \frac{\text{rad}}{\text{m}}$$

(k_2 must be smaller than k_1 !)

$$k_2 := \sqrt{-j \cdot \omega \mu_2 \cdot (\sigma_2 + j \cdot \omega \epsilon_2)} \quad k_2 = 209.585 \cdot \frac{\text{rad}}{\text{m}}$$

E-type proper wave modes:

$$F_{EP}(\beta_x) := \frac{\sqrt{k_1^2 - \beta_x^2}}{\sigma_1 + j \cdot \omega \epsilon_1} \cdot \tan\left(h \cdot \sqrt{k_1^2 - \beta_x^2}\right) - \frac{\operatorname{Re}\left(\sqrt{\beta_x^2 - k_2^2}\right)}{\left|\operatorname{Re}\left(\sqrt{\beta_x^2 - k_2^2}\right)\right|} \cdot \frac{\sqrt{\beta_x^2 - k_2^2}}{\sigma_2 + j \cdot \omega \epsilon_2}$$

$$\beta_x := \frac{k_1 + k_2}{2} \quad \beta_x := \operatorname{root}\left(F_{EP}(\beta_x), \beta_x\right) \quad \beta_x = 175.338 - 5.359j \cdot \frac{\operatorname{rad}}{\operatorname{m}}$$

$$F_{EP}(\beta_x) = -7.218 \cdot 10^{-7} + 3.616 \cdot 10^{-6}j \cdot \operatorname{kg} \cdot \operatorname{m}^2 \cdot \operatorname{sec}^{-1} \cdot \operatorname{coul}^{-2}$$

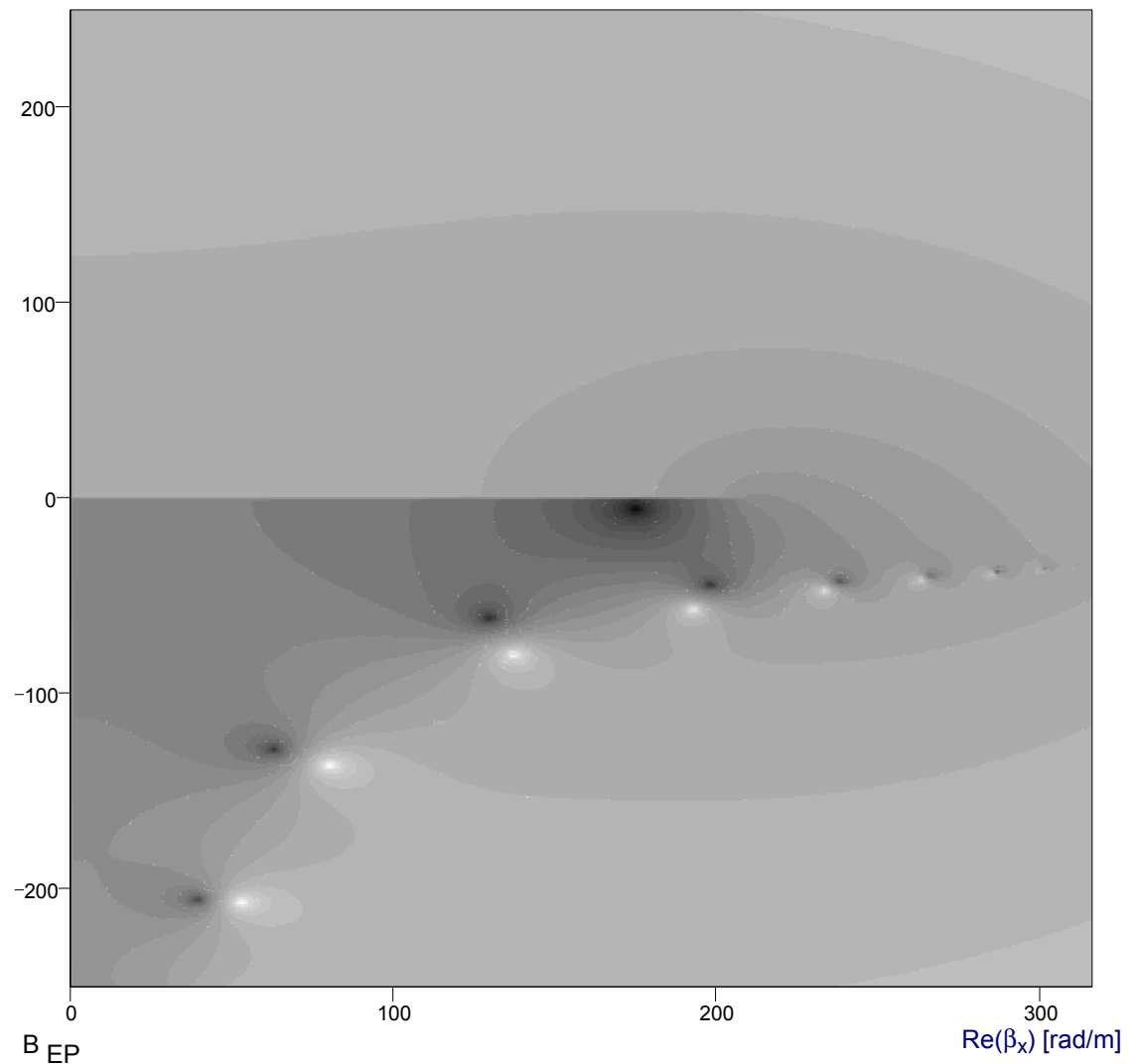
$$s_{z2} := -j \cdot \frac{\operatorname{Re}\left(\sqrt{\beta_x^2 - k_2^2}\right)}{\left|\operatorname{Re}\left(\sqrt{\beta_x^2 - k_2^2}\right)\right|} \cdot \sqrt{\beta_x^2 - k_2^2} \quad s_{z2} = -115.228 - 8.154j \cdot \frac{\operatorname{rad}}{\operatorname{m}}$$

$$N := 301 \quad \operatorname{Start}_x := 0 \cdot \frac{\operatorname{rad}}{\operatorname{m}} \quad \operatorname{End}_x := \operatorname{Re}(k_1) \quad \operatorname{Start}_y := -250 \cdot \frac{\operatorname{rad}}{\operatorname{m}} \quad \operatorname{End}_y := 250 \cdot \frac{\operatorname{rad}}{\operatorname{m}}$$

$$x := 0, 1 \dots N \quad y := 0, 1 \dots N \quad \Delta x := \frac{\operatorname{End}_x - \operatorname{Start}_x}{N} \quad \Delta y := \frac{\operatorname{End}_y - \operatorname{Start}_y}{N}$$

$$B_{EP_{x,y}} := \log\left[\left|F_{EP}\left(\left(\operatorname{Start}_x + x \cdot \Delta x\right) + \left[j \cdot \left(\operatorname{Start}_y + y \cdot \Delta y\right)\right]\right)\right| \cdot \frac{\operatorname{siemens} \cdot \operatorname{m}}{\operatorname{m} \cdot \operatorname{rad}}\right]$$

$\operatorname{Im}(\beta_x)$ [rad/m]



Example 10: Improper Waves along Thick Lossy Materials

Constants:

$$c_0 := 299792458 \cdot \frac{\text{m}}{\text{sec}} \quad \mu_0 := 4 \cdot \pi \cdot 10^{-7} \cdot \frac{\text{henry}}{\text{m}} \quad \epsilon_0 := \frac{1}{c_0^2 \cdot \mu_0} \quad \epsilon_0 = 8.854 \cdot 10^{-12} \cdot \frac{\text{farad}}{\text{m}}$$

Enter the material parameters:

$$\begin{aligned} \sigma_1 &:= 0 \cdot \frac{\text{siemens}}{\text{m}} & \epsilon_{r1} &:= 2.26 - 0.5j & \mu_{r1} &:= 1 - 0j \\ \sigma_2 &:= 0 \cdot \frac{\text{siemens}}{\text{m}} & \epsilon_{r2} &:= 1 - 0j & \mu_{r2} &:= 1 - 0j \end{aligned}$$

Enter the frequency:

$$f := 10 \cdot 10^9 \cdot \text{Hz} \quad \omega := 2 \cdot \pi \cdot f \quad \omega = 6.283 \cdot 10^{10} \cdot \text{Hz} \quad \lambda_0 := \frac{c_0}{f} \quad \lambda_0 = 0.030 \cdot \text{m}$$

Enter the thickness of the coating:

$$h := 0.080 \cdot \text{m}$$

Complex wave numbers:

$$\epsilon_1 := \epsilon_{r1} \cdot \epsilon_0 \quad \epsilon_2 := \epsilon_{r2} \cdot \epsilon_0$$

$$\mu_1 := \mu_{r1} \cdot \mu_0 \quad \mu_2 := \mu_{r2} \cdot \mu_0$$

$$k_0 := \omega \sqrt{\epsilon_0 \cdot \mu_0} \quad k_0 = 209.585 \cdot \frac{\text{rad}}{\text{m}}$$

$$k_1 := \sqrt{-j \cdot \omega \mu_1 \cdot (\sigma_1 + j \cdot \omega \epsilon_1)} \quad k_1 = 316.974 - 34.645j \cdot \frac{\text{rad}}{\text{m}}$$

(k_2 must be smaller than k_1 !)

$$k_2 := \sqrt{-j \cdot \omega \mu_2 \cdot (\sigma_2 + j \cdot \omega \epsilon_2)} \quad k_2 = 209.585 \cdot \frac{\text{rad}}{\text{m}}$$

E-type improper wave modes:

$$F_{EI}(\beta_x) := \frac{\sqrt{k_1^2 - \beta_x^2}}{\sigma_1 + j \cdot \omega \epsilon_1} \cdot \tan\left(h \cdot \sqrt{k_1^2 - \beta_x^2}\right) + \frac{\operatorname{Re}\left(\sqrt{\beta_x^2 - k_2^2}\right)}{\left|\operatorname{Re}\left(\sqrt{\beta_x^2 - k_2^2}\right)\right|} \cdot \frac{\sqrt{\beta_x^2 - k_2^2}}{\sigma_2 + j \cdot \omega \epsilon_2}$$

$$\beta_x := \frac{k_1 + k_2}{2} \quad \beta_x := \operatorname{root}\left(F_{EI}(\beta_x), \beta_x\right) \quad \beta_x = 263.279 - 17.322j \cdot \frac{\operatorname{rad}}{\operatorname{m}}$$

$$F_{EI}(\beta_x) = -192.578 - 291.527j \cdot \operatorname{kg} \cdot \operatorname{m}^2 \cdot \operatorname{sec}^{-1} \cdot \operatorname{coul}^{-2}$$

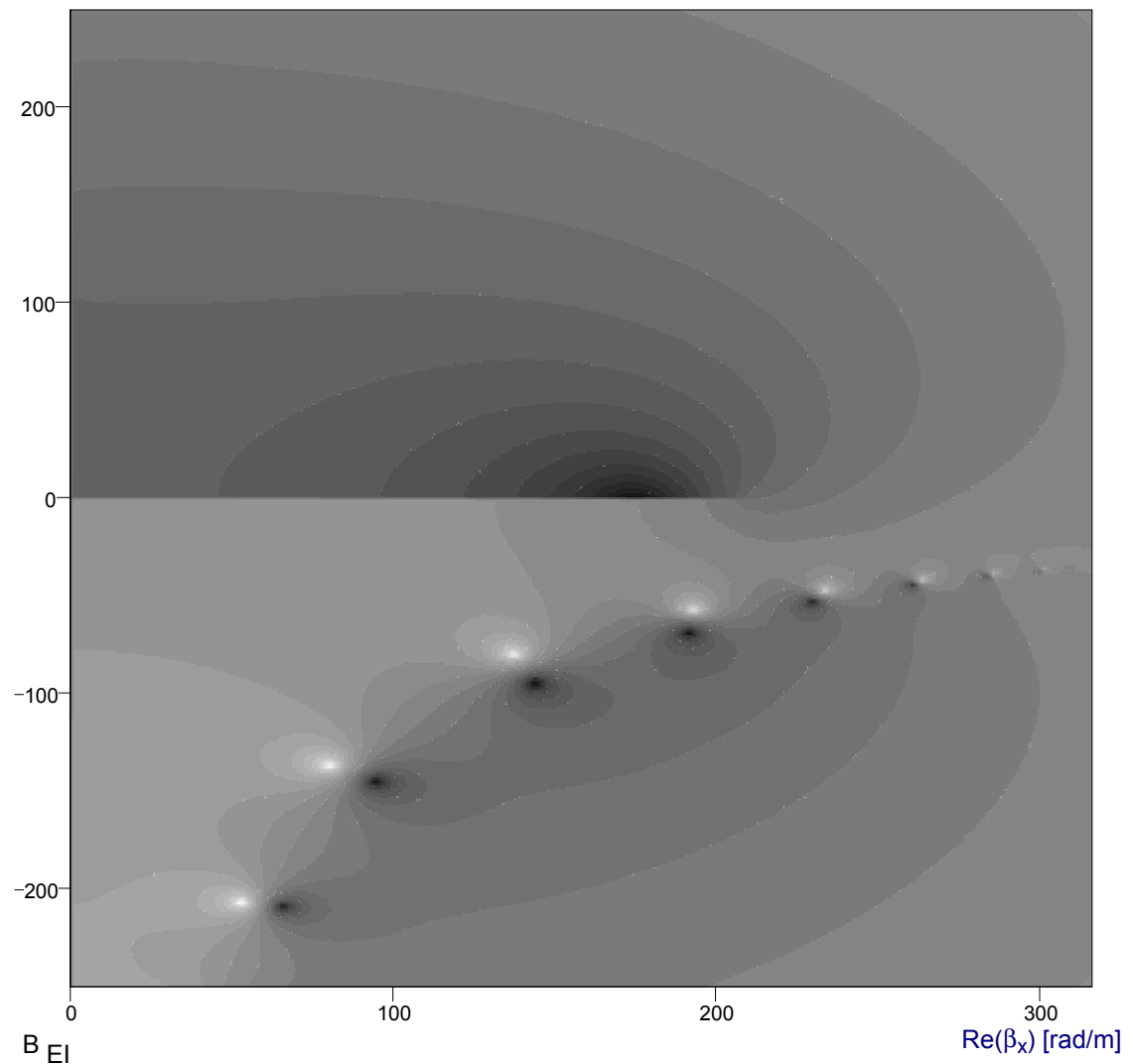
$$s_{z2} := j \cdot \frac{\operatorname{Re}\left(\sqrt{\beta_x^2 - k_2^2}\right)}{\left|\operatorname{Re}\left(\sqrt{\beta_x^2 - k_2^2}\right)\right|} \cdot \sqrt{\beta_x^2 - k_2^2} \quad s_{z2} = 28.342 + 160.914j \cdot \frac{\operatorname{rad}}{\operatorname{m}}$$

$$N := 301 \quad \operatorname{Start}_x := 0 \cdot \frac{\operatorname{rad}}{\operatorname{m}} \quad \operatorname{End}_x := \operatorname{Re}(k_1) \quad \operatorname{Start}_y := -250 \cdot \frac{\operatorname{rad}}{\operatorname{m}} \quad \operatorname{End}_y := 250 \cdot \frac{\operatorname{rad}}{\operatorname{m}}$$

$$x := 0, 1 \dots N \quad y := 0, 1 \dots N \quad \Delta x := \frac{\operatorname{End}_x - \operatorname{Start}_x}{N} \quad \Delta y := \frac{\operatorname{End}_y - \operatorname{Start}_y}{N}$$

$$B_{EI,x,y} := \log\left[\left|F_{EI}\left[\left(\operatorname{Start}_x + x \cdot \Delta x\right) + \left[j \cdot \left(\operatorname{Start}_y + y \cdot \Delta y\right)\right]\right]\right| \cdot \frac{\operatorname{siemens} \cdot \operatorname{m}}{\operatorname{m} \cdot \operatorname{rad}}\right]$$

$\operatorname{Im}(\beta_x)$ [rad/m]



3.5 Plane Surface Waves along a Planar Three-Layer Structure

3.5.1 Introduction

The propagation of plane surface waves along the general planar three-layer topology of Figure 3.14 will be examined now. The structure consists of two half spaces with in between a plane layer of finite height h . All three media are assumed to be homogeneous, linear and isotropic.

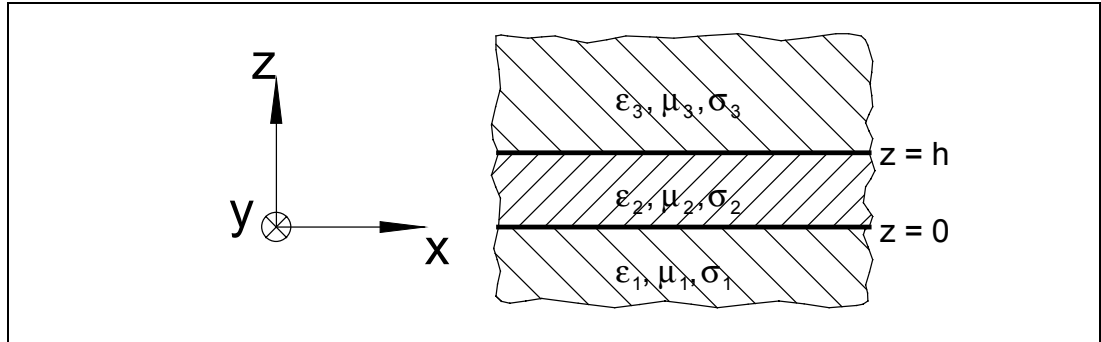


Figure 3.14: The planar three-layer structure; all three media are assumed to be homogeneous, linear and isotropic

For surface propagation it is necessary that both k_1 and k_3 are greater than k_2 . These are the very same requirements to obtain a dielectric waveguide. In fact, the waves propagating in dielectric waveguides (e.g. optical fibres) are surface waves. The structure of Figure 3.14 can also be used to model VLF-propagation or VHF-ducts.

3.5.2 E-Type Plane Surface Waves along a Three-Layer Structure

A suitable Hertz function for medium 1 that satisfies the boundary condition $\vec{E} = \vec{H} = \vec{0}$ when $z \rightarrow -\infty$

$$\text{is } \Pi_1 = A_1 e^{+js_{z1}z} e^{-j\beta_x x}. \quad (67)$$

The factor $e^{+js_{z1}z}$ may be interpreted as a wave propagating in the negative z-direction with phase constant $s_{z1} = s'_{z1} - js''_{z1}$. The traveling wave field will show attenuation in the negative z-direction (i.e. be proper) when $s''_{z1} > 0 \Rightarrow \text{Im}(s_{z1}) < 0$. If on the other hand $\text{Im}(s_{z1}) > 0$, the wave will be an improper traveling wave and the radiation condition violated.

Hence, proper wave solutions are only obtained by letting

$$js_{z1} = \text{sign}\left[\text{Re}\left(\sqrt{\beta_x^2 - k_1^2}\right)\right] \sqrt{\beta_x^2 - k_1^2}. \quad (68a)$$

To obtain improper wave solutions, let

$$js_{z1} = -\text{sign}\left[\text{Re}\left(\sqrt{\beta_x^2 - k_1^2}\right)\right] \sqrt{\beta_x^2 - k_1^2}. \quad (68b)$$

Introducing (67) into (2) leads to

$$E_{z1} = A_1 (k_1^2 - s_{z1}^2) e^{+js_{z1}z} e^{-j\beta_x x}, \quad (69a)$$

$$E_{x1} = \beta_x A_1 s_{z1} e^{+js_{z1}z} e^{-j\beta_x x}, \quad (69b)$$

$$E_{y1} = 0, \quad (69c)$$

$$H_{z1} = 0, \quad (69d)$$

$$H_{x1} = 0, \quad (69e)$$

$$H_{y1} = j\beta_x (\sigma_1 + j\omega\epsilon_1) A_1 e^{+js_{z1}z} e^{-j\beta_x x}. \quad (69f)$$

A suitable Hertz function for medium 2 that can satisfy any boundary condition is

$$\Pi_2 = [A_{2a} \cos(s_{z2}z) + A_{2b} \sin(s_{z2}z)] e^{-j\beta_x x}. \quad (70)$$

In general, this corresponds to a standing wave.

Recalling (2.13)

$$s_{z2}^2 = k_2^2 - \beta_x^2 \Rightarrow s_{z2} = +\sqrt{k_2^2 - \beta_x^2}. \quad (71)$$

It is only for a matter of convenience that s_{z2} is chosen to equal the positive square root. Choosing the negative square root would have no effect on the results.

Introducing (70) into (2) results in

$$E_{z2} = (k_2^2 - s_{z2}^2) [A_{2a} \cos(s_{z2}z) + A_{2b} \sin(s_{z2}z)] e^{-j\beta_x x}, \quad (72a)$$

$$E_{x2} = j\beta_x s_{z2} [A_{2a} \sin(s_{z2}z) - A_{2b} \cos(s_{z2}z)] e^{-j\beta_x x}, \quad (72b)$$

$$E_{y2} = 0, \quad (72c)$$

$$H_{z2} = 0, \quad (72d)$$

$$H_{x2} = 0, \quad (72e)$$

$$H_{y2} = j\beta_x (\sigma_2 + j\omega\epsilon_2) [A_{2a} \cos(s_{z2}z) + A_{2b} \sin(s_{z2}z)] e^{-j\beta_x x}. \quad (72f)$$

A suitable Hertz function for medium 3 that satisfies the boundary condition $\vec{E} = \vec{H} = \vec{0}$ when $z \rightarrow +\infty$

$$\text{is } \Pi_3 = A_3 e^{-js_{z3}(z-h)} e^{-j\beta_x x}. \quad (73)$$

The factor $e^{-js_{z3}(z-h)}$ may be interpreted as a wave propagating in the positive z-direction with phase constant $s_{z3} = s'_{z3} - js''_{z3}$. The traveling wave field will show attenuation in the positive z-direction (i.e. be proper) when $s''_{z3} > 0 \Rightarrow \text{Im}(s_{z3}) < 0$. If on the other hand $\text{Im}(s_{z3}) > 0$, the wave will be an improper traveling wave and the radiation condition violated.

Hence, proper wave solutions are only obtained by letting

$$js_{z3} = \text{sign}\left[\text{Re}\left(\sqrt{\beta_x^2 - k_3^2}\right)\right] \sqrt{\beta_x^2 - k_3^2}. \quad (74a)$$

To obtain improper wave solutions, let

$$js_{z3} = -\text{sign}\left[\text{Re}\left(\sqrt{\beta_x^2 - k_3^2}\right)\right] \sqrt{\beta_x^2 - k_3^2}. \quad (74b)$$

Introducing (73) into (2) leads to

$$E_{z3} = A_3 (k_3^2 - s_{z3}^2) e^{-js_{z3}(z-h)} e^{-j\beta_x x}, \quad (75a)$$

$$E_{x3} = -\beta_x A_3 s_{z3} e^{-js_{z3}(z-h)} e^{-j\beta_x x}, \quad (75b)$$

$$E_{y3} = 0, \quad (75c)$$

$$H_{z3} = 0, \quad (75d)$$

$$H_{x3} = 0, \quad (75e)$$

$$H_{y3} = j\beta_x (\sigma_3 + j\omega\epsilon_3) A_3 e^{-js_{z3}(z-h)} e^{-j\beta_x x}. \quad (75f)$$

The tangential components of both \vec{E} and \vec{H} are continuous across the interface of two media and therefore

$$\begin{aligned} E_{x1} &= E_{x2} \text{ at } z = 0 \\ \Rightarrow A_1 s_{z1} &= -jA_{2b} s_{z2}, \end{aligned} \quad (76)$$

as well as $H_{y1} = H_{y2}$ at $z = 0$

$$\Rightarrow (\sigma_1 + j\omega\epsilon_1) A_1 = (\sigma_2 + j\omega\epsilon_2) A_{2a}. \quad (77)$$

$E_{x2} = E_{x3}$ at $z = h$

$$\Rightarrow js_{z2} [A_{2b} \cos(s_{z2} h) - A_{2a} \sin(s_{z2} h)] = A_3 s_{z3}, \quad (78)$$

as well as $H_{y2} = H_{y3}$ at $z = h$

$$\Rightarrow (\sigma_2 + j\omega\epsilon_2) [A_{2a} \cos(s_{z2} h) + A_{2b} \sin(s_{z2} h)] = (\sigma_3 + j\omega\epsilon_3) A_3. \quad (79)$$

Rewriting (77)

$$A_1 = \frac{\sigma_2 + j\omega\epsilon_2}{\sigma_1 + j\omega\epsilon_1} A_{2a}$$

and substituting the result into (76) gives

$$\frac{\sigma_2 + j\omega\epsilon_2}{\sigma_1 + j\omega\epsilon_1} s_{z1} A_{2a} + js_{z2} A_{2b} = 0. \quad (80)$$

Rewriting (79)

$$A_3 = \frac{\sigma_2 + j\omega\epsilon_2}{\sigma_3 + j\omega\epsilon_3} [A_{2a} \cos(s_{z2}h) + A_{2b} \sin(s_{z2}h)]$$

and substituting the result into (78) leads to

$$\begin{aligned} & - \left[js_{z2} \sin(s_{z2}h) + \frac{\sigma_2 + j\omega\epsilon_2}{\sigma_3 + j\omega\epsilon_3} s_{z3} \cos(s_{z2}h) \right] A_{2a} \\ & + \left[js_{z2} \cos(s_{z2}h) - \frac{\sigma_2 + j\omega\epsilon_2}{\sigma_3 + j\omega\epsilon_3} s_{z3} \sin(s_{z2}h) \right] A_{2b} = 0. \end{aligned} \quad (81)$$

Equations (80) and (81) form a system of linear equations for the two unknown factors A_{2a} and A_{2b} . The system is homogeneous, hence for non-trivial solutions to exist, the coefficient determinant must be zero, that is

$$\begin{aligned} & \frac{\sigma_2 + j\omega\epsilon_2}{\sigma_1 + j\omega\epsilon_1} s_{z1} \left[js_{z2} \cos(s_{z2}h) - \frac{\sigma_2 + j\omega\epsilon_2}{\sigma_3 + j\omega\epsilon_3} s_{z3} \sin(s_{z2}h) \right] \\ & + js_{z2} \left[js_{z2} \sin(s_{z2}h) + \frac{\sigma_2 + j\omega\epsilon_2}{\sigma_3 + j\omega\epsilon_3} s_{z3} \cos(s_{z2}h) \right] = 0 \\ \Rightarrow & \frac{\sigma_2 + j\omega\epsilon_2}{\sigma_1 + j\omega\epsilon_1} s_{z1} \left[js_{z2} - \frac{\sigma_2 + j\omega\epsilon_2}{\sigma_3 + j\omega\epsilon_3} s_{z3} \tan(s_{z2}h) \right] \\ & + js_{z2} \left[js_{z2} \tan(s_{z2}h) + \frac{\sigma_2 + j\omega\epsilon_2}{\sigma_3 + j\omega\epsilon_3} s_{z3} \right] = 0 \\ \Rightarrow & \left(\frac{\sigma_2 + j\omega\epsilon_2}{\sigma_1 + j\omega\epsilon_1} \cdot \frac{\sigma_2 + j\omega\epsilon_2}{\sigma_3 + j\omega\epsilon_3} s_{z1} s_{z3} + s_{z2}^2 \right) \tan(s_{z2}h) = js_{z2} \left(\frac{\sigma_2 + j\omega\epsilon_2}{\sigma_1 + j\omega\epsilon_1} s_{z1} + \frac{\sigma_2 + j\omega\epsilon_2}{\sigma_3 + j\omega\epsilon_3} s_{z3} \right). \end{aligned} \quad (82)$$

Substituting (68a), (71) and (74a) into (82) results in the following expression for proper E-type traveling wave modes

$$\begin{aligned} & \left[-\frac{\sigma_2 + j\omega\epsilon_2}{\sigma_1 + j\omega\epsilon_1} \cdot \frac{\sigma_2 + j\omega\epsilon_2}{\sigma_3 + j\omega\epsilon_3} \cdot \text{sign} \left[\text{Re} \left(\sqrt{\beta_x^2 - k_1^2} \right) \right] \cdot \sqrt{\beta_x^2 - k_1^2} \cdot \text{sign} \left[\text{Re} \left(\sqrt{\beta_x^2 - k_3^2} \right) \right] \cdot \sqrt{\beta_x^2 - k_3^2} + k_2^2 - \beta_x^2 \right] \\ & \cdot \tan \left(h \sqrt{k_2^2 - \beta_x^2} \right) = \\ & \sqrt{k_2^2 - \beta_x^2} \left[\frac{\sigma_2 + j\omega\epsilon_2}{\sigma_1 + j\omega\epsilon_1} \cdot \text{sign} \left[\text{Re} \left(\sqrt{\beta_x^2 - k_1^2} \right) \right] \cdot \sqrt{\beta_x^2 - k_1^2} + \frac{\sigma_2 + j\omega\epsilon_2}{\sigma_3 + j\omega\epsilon_3} \cdot \text{sign} \left[\text{Re} \left(\sqrt{\beta_x^2 - k_3^2} \right) \right] \cdot \sqrt{\beta_x^2 - k_3^2} \right]. \end{aligned} \quad (83)$$

The nomenclature of symmetrical E-type modes (i.e. when $k_1 = k_3$) is discussed in [3, pp. 712-716].

3.5.3 H-Type Plane Surface Waves along a Three-Layer Structure

A suitable Hertz function for medium 1 that satisfies the boundary condition $\vec{E} = \vec{H} = \vec{0}$ when $z \rightarrow -\infty$

$$\text{is } \Pi_1 = A_1 e^{+js_{z1}z} e^{-j\beta_x x}. \quad (84)$$

For s_{z1} , the same reasoning applies as in the previous section. Hence, proper wave solutions are obtained by letting $\text{Re}(js_{z1}) \geq 0$ or

$$js_{z1} = \text{sign}\left[\text{Re}\left(\sqrt{\beta_x^2 - k_1^2}\right)\right] \sqrt{\beta_x^2 - k_1^2}. \quad (85a)$$

To obtain improper wave solutions, let

$$js_{z1} = -\text{sign}\left[\text{Re}\left(\sqrt{\beta_x^2 - k_1^2}\right)\right] \sqrt{\beta_x^2 - k_1^2}. \quad (85b)$$

Introducing (84) into (3) leads to

$$H_{z1} = A_1 (k_1^2 - s_{z1}^2) e^{+js_{z1}z} e^{-j\beta_x x}, \quad (86a)$$

$$H_{x1} = \beta_x A_1 s_{z1} e^{+js_{z1}z} e^{-j\beta_x x}, \quad (86b)$$

$$H_{y1} = 0, \quad (86c)$$

$$E_{z1} = 0, \quad (86d)$$

$$E_{x1} = 0, \quad (86e)$$

$$E_{y1} = \beta_x \omega \mu_1 A_1 e^{+js_{z1}z} e^{-j\beta_x x}. \quad (86f)$$

A suitable Hertz function for medium 2 that can satisfy any boundary condition is

$$\Pi_2 = [A_{2a} \cos(s_{z2}z) + A_{2b} \sin(s_{z2}z)] e^{-j\beta_x x}. \quad (87)$$

In general, this corresponds to a standing wave.

Recalling (2.13)

$$s_{z2}^2 = k_2^2 - \beta_x^2 \Rightarrow s_{z2} = +\sqrt{k_2^2 - \beta_x^2}. \quad (88)$$

It is only for a matter of convenience that s_{z2} is chosen to equal the positive square root. Choosing the negative square root would have no effect on the results.

Introducing (87) into (2) results in

$$H_{z2} = (k_2^2 - s_{z2}^2) [A_{2a} \cos(s_{z2}z) + A_{2b} \sin(s_{z2}z)] e^{-j\beta_x x}, \quad (89a)$$

$$H_{x2} = j\beta_x s_{z2} [A_{2a} \sin(s_{z2}z) - A_{2b} \cos(s_{z2}z)] e^{-j\beta_x x}, \quad (89b)$$

$$H_{y2} = 0, \quad (89c)$$

$$E_{z2} = 0, \quad (89d)$$

$$E_{x2} = 0, \quad (89e)$$

$$E_{y2} = \beta_x \omega \mu_2 [A_{2a} \cos(s_{z2}z) + A_{2b} \sin(s_{z2}z)] e^{-j\beta_x x}. \quad (89f)$$

A suitable Hertz function for medium 3 that satisfies the boundary condition $\vec{E} = \vec{H} = \vec{0}$ when $z \rightarrow +\infty$

$$\text{is } \Pi_3 = A_3 e^{-js_{z3}(z-h)} e^{-j\beta_x x}. \quad (90)$$

For s_{z3} , the same reasoning applies as in the previous section. Hence, proper wave solutions are obtained by letting $\text{Re}(js_{z3}) \geq 0$ or

$$js_{z3} = \text{sign} \left[\text{Re} \left(\sqrt{\beta_x^2 - k_3^2} \right) \right] \sqrt{\beta_x^2 - k_3^2}. \quad (91a)$$

To obtain improper wave solutions, let

$$js_{z3} = -\text{sign} \left[\text{Re} \left(\sqrt{\beta_x^2 - k_3^2} \right) \right] \sqrt{\beta_x^2 - k_3^2}. \quad (91b)$$

Introducing (90) into (3) leads to

$$H_{z3} = A_3 (k_3^2 - s_{z3}^2) e^{-js_{z3}(z-h)} e^{-j\beta_x x}, \quad (92a)$$

$$H_{x3} = -\beta_x A_3 s_{z3} e^{-js_{z3}(z-h)} e^{-j\beta_x x}, \quad (92b)$$

$$H_{y3} = 0, \quad (92c)$$

$$E_{z3} = 0, \quad (92d)$$

$$E_{x3} = 0, \quad (92e)$$

$$E_{y3} = \beta_x \omega \mu_3 A_3 e^{-js_{z3}(z-h)} e^{-j\beta_x x}. \quad (92f)$$

The tangential components of both \vec{E} and \vec{H} are continuous across the interface of two media and therefore

$$\begin{aligned} H_{x1} &= H_{x2} \text{ at } z = 0 \\ \Rightarrow A_1 s_{z1} &= -j A_{2b} s_{z2}, \end{aligned} \quad (93)$$

$$\begin{aligned} \text{as well as } E_{y1} &= E_{y2} \text{ at } z = 0 \\ \Rightarrow \mu_1 A_1 &= \mu_2 A_{2a}. \end{aligned} \quad (94)$$

$$\begin{aligned} H_{x2} &= H_{x3} \text{ at } z = h \\ \Rightarrow js_{z2} [A_{2b} \cos(s_{z2}h) - A_{2a} \sin(s_{z2}h)] &= A_3 s_{z3}, \end{aligned} \quad (95)$$

$$\begin{aligned} \text{as well as } E_{y2} &= E_{y3} \text{ at } z = h \\ \Rightarrow \mu_2 [A_{2a} \cos(s_{z2}h) + A_{2b} \sin(s_{z2}h)] &= \mu_3 A_3. \end{aligned} \quad (96)$$

Rewriting (94)

$$A_1 = \frac{\mu_2}{\mu_1} A_{2a}$$

and substituting the result into (93) gives

$$\frac{\mu_2}{\mu_1} s_{z1} A_{2a} + js_{z2} A_{2b} = 0. \quad (97)$$

Rewriting (96)

$$A_3 = \frac{\mu_2}{\mu_3} [A_{2a} \cos(s_{z2}h) + A_{2b} \sin(s_{z2}h)]$$

and substituting the result into (95) leads to

$$\begin{aligned} & - \left[js_{z2} \sin(s_{z2}h) + \frac{\mu_2}{\mu_3} s_{z3} \cos(s_{z2}h) \right] A_{2a} \\ & + \left[js_{z2} \cos(s_{z2}h) - \frac{\mu_2}{\mu_3} s_{z3} \sin(s_{z2}h) \right] A_{2b} = 0. \end{aligned} \quad (98)$$

Equations (97) and (98) form a system of linear equations for the two unknown factors A_{2a} and A_{2b} . The system is homogeneous, hence for non-trivial solutions to exist, the coefficient determinant must be zero, that is

$$\begin{aligned} & \frac{\mu_2}{\mu_1} s_{z1} \left[js_{z2} \cos(s_{z2}h) - \frac{\mu_2}{\mu_3} s_{z3} \sin(s_{z2}h) \right] \\ & + js_{z2} \left[js_{z2} \sin(s_{z2}h) + \frac{\mu_2}{\mu_3} s_{z3} \cos(s_{z2}h) \right] = 0 \\ \Rightarrow & \frac{\mu_2}{\mu_1} s_{z1} \left[js_{z2} - \frac{\mu_2}{\mu_3} s_{z3} \tan(s_{z2}h) \right] + js_{z2} \left[js_{z2} \tan(s_{z2}h) + \frac{\mu_2}{\mu_3} s_{z3} \right] = 0 \\ \Rightarrow & \left(\frac{\mu_2}{\mu_1} \cdot \frac{\mu_2}{\mu_3} s_{z1} s_{z3} + s_{z2}^2 \right) \tan(s_{z2}h) = js_{z2} \left(\frac{\mu_2}{\mu_1} s_{z1} + \frac{\mu_2}{\mu_3} s_{z3} \right), \end{aligned} \quad (99)$$

Substituting (85a), (88) and (91a) into (99) results in the following expression for proper H-type traveling wave modes

$$\begin{aligned} & \left[-\frac{\mu_2}{\mu_1} \cdot \frac{\mu_2}{\mu_3} \cdot \text{sign} \left[\text{Re} \left(\sqrt{\beta_x^2 - k_1^2} \right) \right] \cdot \sqrt{\beta_x^2 - k_1^2} \cdot \text{sign} \left[\text{Re} \left(\sqrt{\beta_x^2 - k_3^2} \right) \right] \cdot \sqrt{\beta_x^2 - k_3^2} + k_2^2 - \beta_x^2 \right] \\ & \cdot \tan \left(h \sqrt{k_2^2 - \beta_x^2} \right) = \\ & \sqrt{k_2^2 - \beta_x^2} \left[\frac{\mu_2}{\mu_1} \cdot \text{sign} \left[\text{Re} \left(\sqrt{\beta_x^2 - k_1^2} \right) \right] \cdot \sqrt{\beta_x^2 - k_1^2} + \frac{\mu_2}{\mu_3} \cdot \text{sign} \left[\text{Re} \left(\sqrt{\beta_x^2 - k_3^2} \right) \right] \cdot \sqrt{\beta_x^2 - k_3^2} \right]. \end{aligned} \quad (100)$$

This equation is transcendental and can therefore only be solved numerically for β_x .

H-type surface wave modes in a three-layer structure can be subdivided into odd and even modes in the special case when k_1 equals k_3 . These symmetrical H-type modes are further discussed in [3, pp. 712-716].

Example: Plane Proper Waves along a Dielectric Waveguide

Constants:

$$c_0 := 299792458 \cdot \frac{\text{m}}{\text{sec}} \quad \mu_0 := 4 \cdot \pi \cdot 10^{-7} \cdot \frac{\text{henry}}{\text{m}} \quad \epsilon_0 := \frac{1}{c_0^2 \cdot \mu_0} \quad \epsilon_0 = 8.854 \cdot 10^{-12} \cdot \frac{\text{farad}}{\text{m}}$$

Enter the material parameters:

$$\sigma_1 := 0 \cdot \frac{\text{siemens}}{\text{m}} \quad \epsilon_{r1} := 1 - 0j \quad \mu_{r1} := 1 - 0j$$

$$\sigma_2 := 0 \cdot \frac{\text{siemens}}{\text{m}} \quad \epsilon_{r2} := 2.26 - 0.00091j \quad \mu_{r2} := 1 - 0j$$

$$\sigma_3 := 0 \cdot \frac{\text{siemens}}{\text{m}} \quad \epsilon_{r3} := 1 - 0j \quad \mu_{r3} := 1 - 0j$$

Enter the frequency:

$$f := 10 \cdot 10^9 \cdot \text{Hz} \quad \omega := 2 \cdot \pi \cdot f \quad \omega = 6.283 \cdot 10^{10} \cdot \text{Hz} \quad \lambda_0 := \frac{c_0}{f} \quad \lambda_0 = 0.030 \cdot \text{m}$$

Enter the thickness of the middle layer:

$$h := 0.006 \cdot \text{m}$$

Complex wave numbers:

$$\epsilon_1 := \epsilon_{r1} \cdot \epsilon_0 \quad \epsilon_2 := \epsilon_{r2} \cdot \epsilon_0 \quad \epsilon_3 := \epsilon_{r3} \cdot \epsilon_0$$

$$\mu_1 := \mu_{r1} \cdot \mu_0 \quad \mu_2 := \mu_{r2} \cdot \mu_0 \quad \mu_3 := \mu_{r3} \cdot \mu_0$$

$$k_0 := \omega \sqrt{\epsilon_0 \cdot \mu_0} \quad k_0 = 209.585 \cdot \frac{\text{rad}}{\text{m}}$$

$$k_1 := \sqrt{-j \cdot \omega \mu_1 \cdot (\sigma_1 + j \cdot \omega \epsilon_1)} \quad k_1 = 209.585 \cdot \frac{\text{rad}}{\text{m}} \quad (\text{k}_1 \text{ must be smaller than } k_2!)$$

$$k_2 := \sqrt{-j \cdot \omega \mu_2 \cdot (\sigma_2 + j \cdot \omega \epsilon_2)} \quad k_2 = 315.075 - 0.063j \cdot \frac{\text{rad}}{\text{m}}$$

$$k_3 := \sqrt{-j \cdot \omega \mu_3 \cdot (\sigma_3 + j \cdot \omega \epsilon_3)} \quad k_3 = 209.585 \cdot \frac{\text{rad}}{\text{m}} \quad (\text{k}_3 \text{ must be smaller than } k_2!)$$

E-type proper wave modes:

$$js_{z1}(\beta_x) := \frac{\operatorname{Re}\left(\sqrt{\beta_x^2 - k_1^2}\right)}{\left|\operatorname{Re}\left(\sqrt{\beta_x^2 - k_1^2}\right)\right|} \cdot \sqrt{\beta_x^2 - k_1^2}$$

$$js_{z3}(\beta_x) := \frac{\operatorname{Re}\left(\sqrt{\beta_x^2 - k_3^2}\right)}{\left|\operatorname{Re}\left(\sqrt{\beta_x^2 - k_3^2}\right)\right|} \cdot \sqrt{\beta_x^2 - k_3^2}$$

$$F_{EP1}(\beta_x) := \left(-\frac{\sigma_2 + j \cdot \omega \varepsilon_2}{\sigma_1 + j \cdot \omega \varepsilon_1} \cdot \frac{\sigma_2 + j \cdot \omega \varepsilon_2}{\sigma_3 + j \cdot \omega \varepsilon_3} \cdot js_{z1}(\beta_x) \cdot js_{z3}(\beta_x) + k_2^2 - \beta_x^2 \right)$$

$$F_{EP2}(\beta_x) := \tan\left(h \cdot \sqrt{k_2^2 - \beta_x^2}\right)$$

$$F_{EP3}(\beta_x) := \sqrt{k_2^2 - \beta_x^2} \cdot \left(\frac{\sigma_2 + j \cdot \omega \varepsilon_2}{\sigma_1 + j \cdot \omega \varepsilon_1} \cdot js_{z1}(\beta_x) + \frac{\sigma_2 + j \cdot \omega \varepsilon_2}{\sigma_3 + j \cdot \omega \varepsilon_3} \cdot js_{z3}(\beta_x) \right)$$

$$F_{EP}(\beta_x) := F_{EP1}(\beta_x) \cdot F_{EP2}(\beta_x) - F_{EP3}(\beta_x)$$

$$\beta_x := k_2 \quad \beta_x := \operatorname{root}(F_{EP}(\beta_x), \beta_x) \quad \beta_x = 315.075 - 0.063j \cdot \frac{\operatorname{rad}}{\operatorname{m}}$$

$$F_{EP}(\beta_x) = 0 \cdot \operatorname{m}^{-2}$$

$$s_{z1} := -j \cdot js_{z1}(\beta_x) \quad s_{z1} = -0.085 - 235.258j \cdot \frac{\operatorname{rad}}{\operatorname{m}}$$

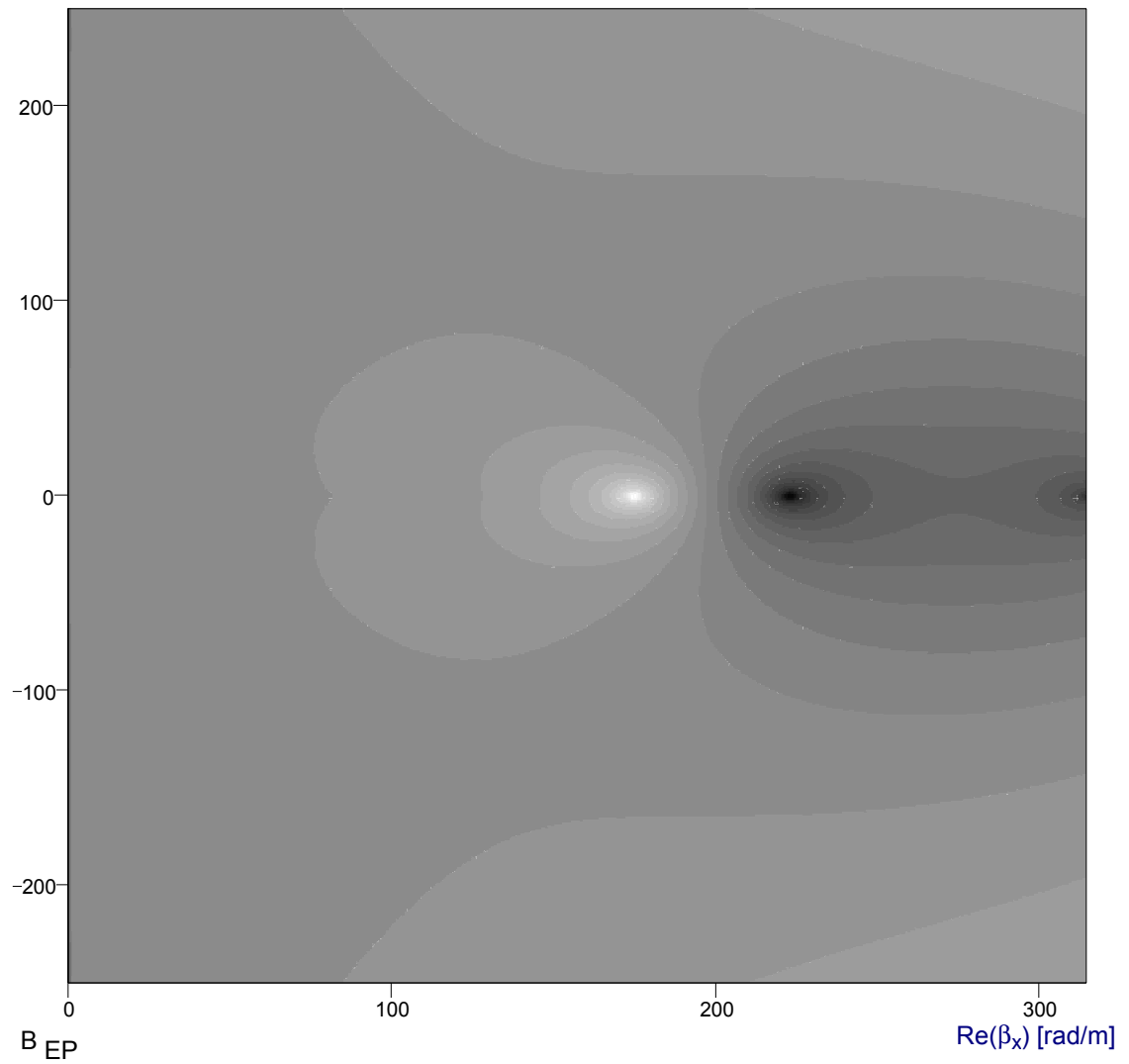
$$s_{z3} := -j \cdot js_{z3}(\beta_x) \quad s_{z3} = -0.085 - 235.258j \cdot \frac{\operatorname{rad}}{\operatorname{m}}$$

$$N := 301 \quad \text{Start}_x := 0 \cdot \frac{\text{rad}}{\text{m}} \quad \text{End}_x := \text{Re}(k_2) \quad \text{Start}_y := -250 \cdot \frac{\text{rad}}{\text{m}} \quad \text{End}_y := 250 \cdot \frac{\text{rad}}{\text{m}}$$

$$x := 0, 1 \dots N \quad y := 0, 1 \dots N \quad \Delta x := \frac{\text{End}_x - \text{Start}_x}{N} \quad \Delta y := \frac{\text{End}_y - \text{Start}_y}{N}$$

$$B_{EP_{x,y}} := \log \left[\left| F_{EP} \left[\left(\text{Start}_x + x \cdot \Delta x \right) + \left[j \cdot \left(\text{Start}_y + y \cdot \Delta y \right) \right] \right] \right| \cdot \text{m}^2 \right]$$

$\text{Im}(\beta_x)$ [rad/m]



H-type proper wave modes:

$$js_{z1}(\beta_x) := \frac{\operatorname{Re}\left(\sqrt{\beta_x^2 - k_1^2}\right)}{\left|\operatorname{Re}\left(\sqrt{\beta_x^2 - k_1^2}\right)\right|} \cdot \sqrt{\beta_x^2 - k_1^2}$$

$$js_{z3}(\beta_x) := \frac{\operatorname{Re}\left(\sqrt{\beta_x^2 - k_3^2}\right)}{\left|\operatorname{Re}\left(\sqrt{\beta_x^2 - k_3^2}\right)\right|} \cdot \sqrt{\beta_x^2 - k_3^2}$$

$$F_{HP1}(\beta_x) := \left(-\frac{\mu_2}{\mu_1} \cdot \frac{\mu_2}{\mu_3} \cdot js_{z1}(\beta_x) \cdot js_{z3}(\beta_x) + k_2^2 - \beta_x^2 \right)$$

$$F_{HP2}(\beta_x) := \tan\left(h \cdot \sqrt{k_2^2 - \beta_x^2}\right)$$

$$F_{HP3}(\beta_x) := \sqrt{k_2^2 - \beta_x^2} \cdot \left(\frac{\mu_2}{\mu_1} \cdot js_{z1}(\beta_x) + \frac{\mu_2}{\mu_3} \cdot js_{z3}(\beta_x) \right)$$

$$F_{HP}(\beta_x) := F_{HP1}(\beta_x) \cdot F_{HP2}(\beta_x) - F_{HP3}(\beta_x)$$

$$\beta_x := k_2 \quad \beta_x := \operatorname{root}(F_{HP}(\beta_x), \beta_x) \quad \beta_x = 315.075 - 0.063j \cdot \frac{\operatorname{rad}}{\operatorname{m}}$$

$$F_{HP}(\beta_x) = 0 \cdot \operatorname{m}^{-2}$$

$$s_{z1} := -j \cdot js_{z1}(\beta_x) \quad s_{z1} = -0.085 - 235.258j \cdot \frac{\operatorname{rad}}{\operatorname{m}}$$

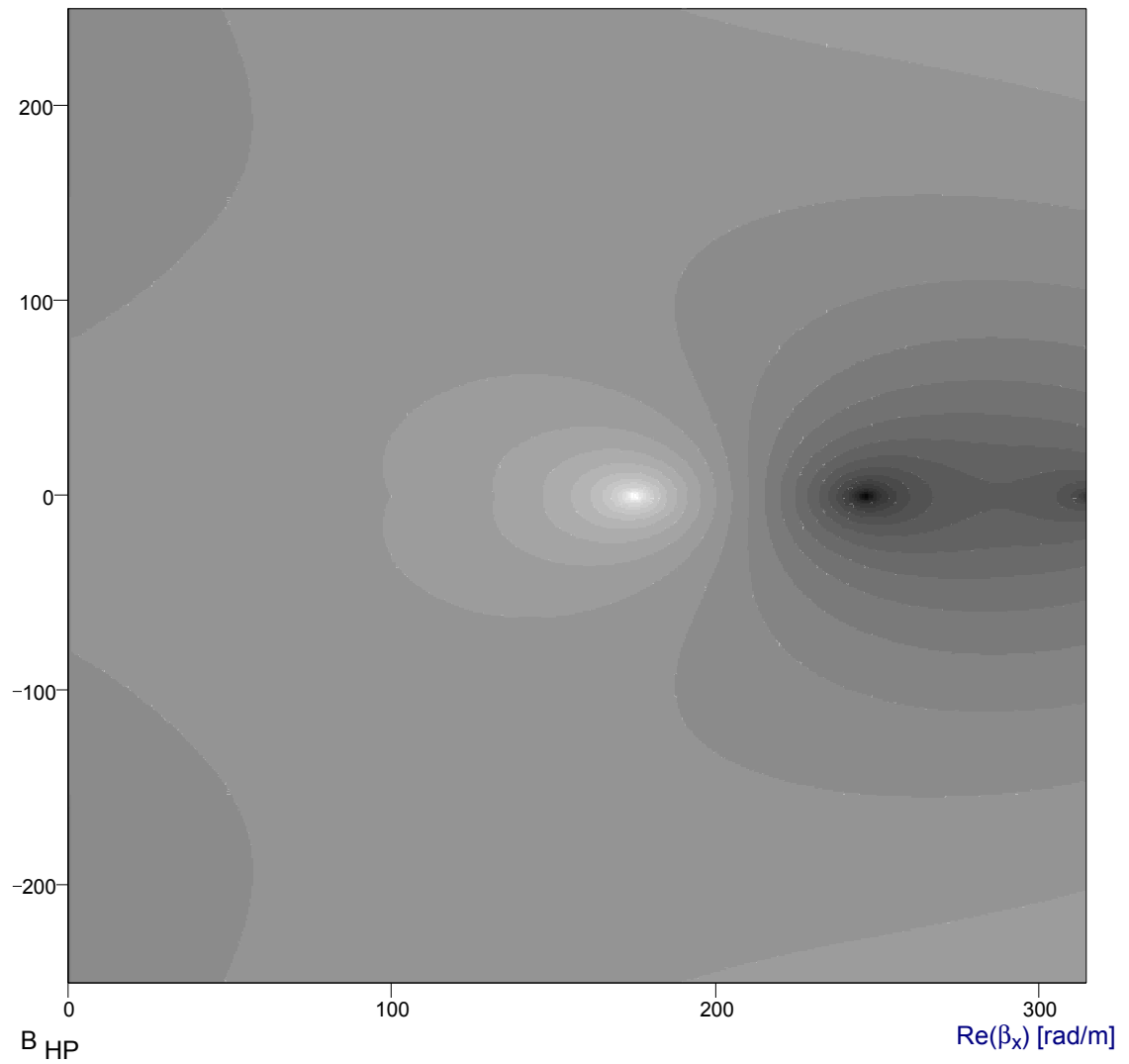
$$s_{z3} := -j \cdot js_{z3}(\beta_x) \quad s_{z3} = -0.085 - 235.258j \cdot \frac{\operatorname{rad}}{\operatorname{m}}$$

$$N := 301 \quad \text{Start}_x := 0 \cdot \frac{\text{rad}}{\text{m}} \quad \text{End}_x := \text{Re}(k_2) \quad \text{Start}_y := -250 \cdot \frac{\text{rad}}{\text{m}} \quad \text{End}_y := 250 \cdot \frac{\text{rad}}{\text{m}}$$

$$x := 0, 1 \dots N \quad y := 0, 1 \dots N \quad \Delta x := \frac{\text{End}_x - \text{Start}_x}{N} \quad \Delta y := \frac{\text{End}_y - \text{Start}_y}{N}$$

$$B_{\text{HP}_{x,y}} := \log \left[\left| F_{\text{HP}} \left[\left(\text{Start}_x + x \cdot \Delta x \right) + \left[j \cdot \left(\text{Start}_y + y \cdot \Delta y \right) \right] \right] \right| \cdot \text{m}^2 \right]$$

$\text{Im}(\beta_x)$ [rad/m]



3.6 Plane Surface Waves along the Plane Interface of Two Half Spaces

Dispersion equations for the proper traveling waves along the plane interface of two half spaces (Fig. 3.1) can be obtained by letting h equal zero in the dispersion equations of the three layer case ((83) and (100)).

For E-type proper waves this results in

$$0 = \text{sign}\left[\text{Re}\left(\sqrt{\beta_x^2 - k_1^2}\right)\right] \cdot \frac{\sqrt{\beta_x^2 - k_1^2}}{\sigma_1 + j\omega\epsilon_1} + \text{sign}\left[\text{Re}\left(\sqrt{\beta_x^2 - k_3^2}\right)\right] \cdot \frac{\sqrt{\beta_x^2 - k_3^2}}{\sigma_3 + j\omega\epsilon_3}. \quad (101)$$

The dispersion for H-type proper waves is

$$0 = \text{sign}\left[\text{Re}\left(\sqrt{\beta_x^2 - k_1^2}\right)\right] \cdot \frac{\sqrt{\beta_x^2 - k_1^2}}{\mu_1} + \text{sign}\left[\text{Re}\left(\sqrt{\beta_x^2 - k_3^2}\right)\right] \cdot \frac{\sqrt{\beta_x^2 - k_3^2}}{\mu_3}. \quad (102)$$

EXAMPLE

The only propagating surface wave mode is a fast wave. Compare also the location of the null in this example with the anomalous null in Example 9 of Section 3.4.10.

Example: Plane Proper Waves along Two Half Spaces

Constants:

$$c_0 := 299792458 \cdot \frac{\text{m}}{\text{sec}} \quad \mu_0 := 4 \cdot \pi \cdot 10^{-7} \cdot \frac{\text{henry}}{\text{m}} \quad \varepsilon_0 := \frac{1}{c_0^2 \cdot \mu_0} \quad \varepsilon_0 = 8.854 \cdot 10^{-12} \cdot \frac{\text{farad}}{\text{m}}$$

Enter the material parameters:

$$\sigma_1 := 0 \cdot \frac{\text{siemens}}{\text{m}} \quad \varepsilon_{r1} := 2.26 - 0.5j \quad \mu_{r1} := 1 - 0j$$

$$\sigma_2 := 0 \cdot \frac{\text{siemens}}{\text{m}} \quad \varepsilon_{r2} := 1 - 0j \quad \mu_{r2} := 1 - 0j$$

Enter the frequency:

$$f := 10 \cdot 10^9 \cdot \text{Hz} \quad \omega := 2 \cdot \pi \cdot f \quad \omega = 6.283 \cdot 10^{10} \cdot \text{Hz} \quad \lambda_0 := \frac{c_0}{f} \quad \lambda_0 = 0.030 \cdot \text{m}$$

Complex wave numbers:

$$\varepsilon_1 := \varepsilon_{r1} \cdot \varepsilon_0 \quad \varepsilon_2 := \varepsilon_{r2} \cdot \varepsilon_0$$

$$\mu_1 := \mu_{r1} \cdot \mu_0 \quad \mu_2 := \mu_{r2} \cdot \mu_0$$

$$k_0 := \omega \sqrt{\varepsilon_0 \cdot \mu_0} \quad k_0 = 209.585 \cdot \frac{\text{rad}}{\text{m}}$$

$$k_1 := \sqrt{-j \cdot \omega \mu_1 \cdot (\sigma_1 + j \cdot \omega \varepsilon_1)} \quad k_1 = 316.974 - 34.645j \cdot \frac{\text{rad}}{\text{m}}$$

$$k_2 := \sqrt{-j \cdot \omega \mu_2 \cdot (\sigma_2 + j \cdot \omega \varepsilon_2)} \quad k_2 = 209.585 \cdot \frac{\text{rad}}{\text{m}}$$

E-type proper wave modes:

$$F_{EP}(\beta_x) := \frac{\operatorname{Re}\left(\sqrt{\beta_x^2 - k_1^2}\right)}{\left|\operatorname{Re}\left(\sqrt{\beta_x^2 - k_1^2}\right)\right|} \cdot \sqrt{\beta_x^2 - k_1^2} + \frac{\operatorname{Re}\left(\sqrt{\beta_x^2 - k_2^2}\right)}{\left|\operatorname{Re}\left(\sqrt{\beta_x^2 - k_2^2}\right)\right|} \cdot \sqrt{\beta_x^2 - k_2^2}$$

$$\beta_x := \frac{k_1 + k_2}{2} \quad \beta_x := \operatorname{root}\left(F_{EP}(\beta_x), \beta_x\right) \quad \beta_x = 175.483 - 5.753j \cdot \frac{\operatorname{rad}}{\operatorname{m}}$$

$$F_{EP}(\beta_x) = -2.349 \cdot 10^{-4} - 2.742 \cdot 10^{-5}j \cdot \operatorname{kg} \cdot \operatorname{m}^2 \cdot \operatorname{sec}^{-1} \cdot \operatorname{coul}^{-2}$$

$$s_{z1} := -j \cdot \frac{\operatorname{Re}\left(\sqrt{\beta_x^2 - k_1^2}\right)}{\left|\operatorname{Re}\left(\sqrt{\beta_x^2 - k_1^2}\right)\right|} \cdot \sqrt{\beta_x^2 - k_1^2} \quad s_{z1} = 264.448 - 37.708j \cdot \frac{\operatorname{rad}}{\operatorname{m}}$$

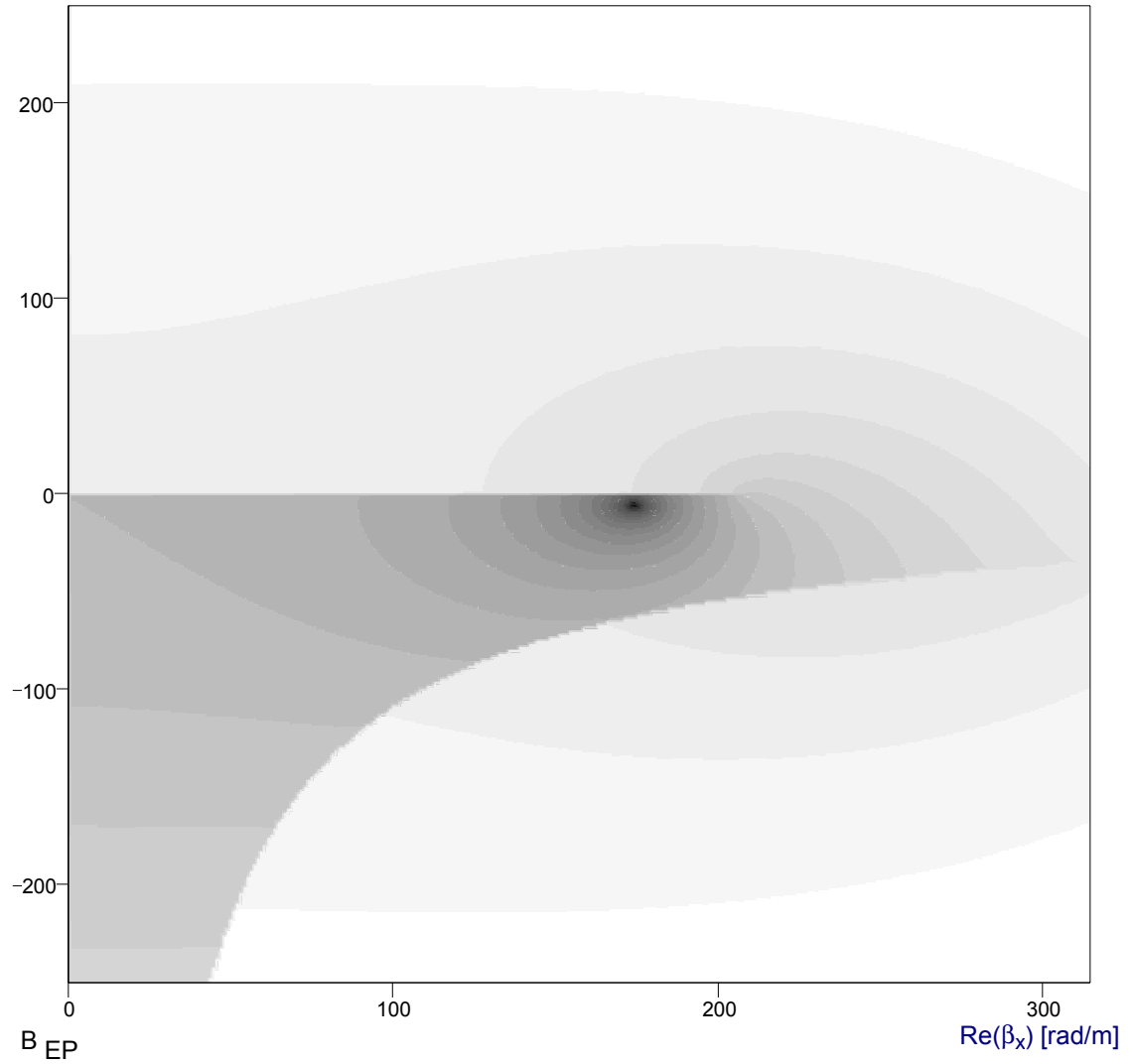
$$s_{z2} := -j \cdot \frac{\operatorname{Re}\left(\sqrt{\beta_x^2 - k_2^2}\right)}{\left|\operatorname{Re}\left(\sqrt{\beta_x^2 - k_2^2}\right)\right|} \cdot \sqrt{\beta_x^2 - k_2^2} \quad s_{z2} = -115.072 - 8.773j \cdot \frac{\operatorname{rad}}{\operatorname{m}}$$

$$N := 301 \quad \text{Start}_x := 0 \cdot \frac{\text{rad}}{\text{m}} \quad \text{End}_x := \text{Re}(k_1) \quad \text{Start}_y := -250 \cdot \frac{\text{rad}}{\text{m}} \quad \text{End}_y := 250 \cdot \frac{\text{rad}}{\text{m}}$$

$$x := 0, 1 \dots N \quad y := 0, 1 \dots N \quad \Delta x := \frac{\text{End}_x - \text{Start}_x}{N} \quad \Delta y := \frac{\text{End}_y - \text{Start}_y}{N}$$

$$B_{EP_{x,y}} := \log \left[\left| F_{EP} \left[(\text{Start}_x + x \cdot \Delta x) + [j \cdot (\text{Start}_y + y \cdot \Delta y)] \right] \right| \cdot \frac{\text{siemens} \cdot \text{m}}{\text{m} \cdot \text{rad}} \right]$$

$\text{Im}(\beta_x)$ [rad/m]



3.7 Appendix A: The Phase Velocity of an Inhomogeneous Wave in a Loss Free Medium

The phase velocity of a wave in its propagation direction is given by

$$v_p = \frac{\omega}{\text{Re}(\beta)}$$

It will be shown now that *every inhomogeneous plane wave in a loss free medium* ($\text{Im}(k)=0$) *is a slow wave* (i.e. $\beta > k_0$) *in its direction of propagation.*

Assume that the inhomogeneous plane wave propagates in the xz-plane. The wave is then characterized by its wave vector

$$\vec{k} = k_x \vec{e}_x + k_z \vec{e}_z \quad (\text{A1})$$

where $k_x = \beta_x - j\alpha_x$ and $k_z = \beta_z - j\alpha_z$.

The direction of \vec{k} corresponds to the propagation direction $\vec{\beta}$.

When the surrounding medium is loss free: $\text{Im}(k) = 0$.

Hence, substituting the definitions of k_x and k_z into (A1) and squaring both sides results in [8, p. 166]

$$k^2 = \beta_x^2 + \beta_z^2 - (\alpha_x^2 + \alpha_z^2) \text{ because } -2j(\alpha_{2x}\beta_{2x} + \alpha_{2z}\beta_{2z}) = 0$$

$$\Rightarrow \vec{k}^2 = \vec{\beta}_2 - \vec{\alpha}_2$$

$$\Rightarrow \beta = \|\vec{\beta}\| = \sqrt{k^2 + \alpha^2} = k \sqrt{1 + \left(\frac{\alpha}{k}\right)^2} \geq k_0. \quad (\text{A2})$$

From this may be concluded that all inhomogeneous plane waves in a loss free medium are slow waves in their direction of propagation.

3.8 Appendix B: Proof of $-j\sqrt{x} = \sqrt{-x}$

Theorem

Let x be a complex number. Then

$$-j\sqrt{x} = \sqrt{-x}. \quad (\text{B1})$$

Proof

The above theorem can easily be proven by applying de Moivre's theorem to each side of (B1).

First, let θ be the argument of x .

Then, for the left hand side

$$\begin{aligned} -j\sqrt{x} &= -j\sqrt{|x|} \left[\cos\left(\frac{\theta + k360^\circ}{2}\right) + j\sin\left(\frac{\theta + k360^\circ}{2}\right) \right] \\ &= \sqrt{|x|} \left[\sin\left(\frac{\theta}{2} + k180^\circ\right) - j\cos\left(\frac{\theta}{2} + k180^\circ\right) \right]. \end{aligned} \quad (\text{B2})$$

The right hand gives

$$\begin{aligned} \sqrt{-x} &= \sqrt{|x|} \left[\cos\left(\frac{\theta + 180^\circ + k360^\circ}{2}\right) + j\sin\left(\frac{\theta + 180^\circ + k360^\circ}{2}\right) \right] \\ &= \sqrt{|x|} \left[\cos\left(\frac{\theta}{2} + 90^\circ + k180^\circ\right) + j\sin\left(\frac{\theta}{2} + 90^\circ + k180^\circ\right) \right] \\ &= \sqrt{|x|} \left[\sin\left(\frac{\theta}{2} + k180^\circ\right) - j\cos\left(\frac{\theta}{2} + k180^\circ\right) \right]. \end{aligned} \quad (\text{B3})$$

(B2) and (B3) are identical, therefore

$$-j\sqrt{x} = \sqrt{-x}.$$

3.9 Conclusions

A plane surface wave is defined as a plane wave that propagates along a plane interface of two different media without radiation.

Dispersion equations are derived for three different kinds of isotropic planar surface wave guiding structures. This is done by treating these structures as boundary-value problems and then solving these using Hertz potentials. The dispersion equations have a discrete number of both proper and improper solutions.

A distinction is made between E-type and H-type surface waves.

The concept of surface impedance has also been introduced. It was shown that E-type surface waves can only propagate along inductive surface impedances. H-type surface waves only propagate when the surface impedance is capacitive. *This is perhaps the important conclusion of this of chapter because it implies that isotropic surface wave absorbers are effective for one polarization only.*

The proper discrete eigenvalue spectrum does not form a complete set of eigenvalues along which the field of an open guiding structure may be expanded. However, the combination of the proper discrete eigenvalue spectrum and the continuous eigenvalue spectrum does.

Surface waves were also compared with other kinds of traveling waves. Some of these other waves are improper waves. By this is meant that they violate the radiation condition.

All traveling wave types can be either fast or slow waves. To prove this, the discrete eigenvalue spectrum is mapped onto the w -plane. This w -plane also proves to be an excellent tool for designing surface wave guiding structures with specific propagation properties.

3.10 References

- [1] H. M. Barlow and J. Brown, *Radio Surface Waves*, Oxford University Press, 1962
- [2] H. M. Barlow and A. L. Cullen, "Surface waves," *Proceedings of the Institution of Electrical Engineers*, Vol. 100, Part III, No. 68, Nov. 1953, pp. 329-347
- [3] R. E. Collin, *Field Theory of Guided Waves*, IEEE Press, 2nd Ed., 1991
- [4] K. Simonyi, *Theoretische Elektrotechnik*, Johann Ambrosius Barth, 10. Auflage, 1993, pp. 753-759, (in German)
- [5] J. A. Stratton, *Electromagnetic Theory*, McGraw-Hill, 1941, pp. 516-520
- [6] J. D. Kraus, *Electromagnetics*, McGraw-Hill, 4th Ed., 1992
- [7] F. J. Zucker, "Surface-Wave Antennas," Chapter 12 in R. C. Johnson, *Antenna Engineering Handbook*, McGraw-Hill, 3rd Ed., 1993
- [8] A. Hessel, "General characteristics of traveling wave antennas," Chapter 19 in R. E. Collin, F. J. Zucker, *Antenna Theory*, Part 2, McGraw-Hill, 1969
- [9] M. R. Spiegel, *Mathematical Handbook of Formulas and Tables*, Schaum's Outline Series, McGraw-Hill, 1968
- [10] W. H. Press et al., *Numerical Recipes: The Art of Scientific Computing*, Cambridge University Press, 1987, pp. 248-251

4 Axial Surface Waves in Isotropic Media

4.1 Definition

An *axial surface wave* is a plane wave that propagates in the axial direction of a cylindrical interface of two different media without radiation.

Axial surface waves are plane waves because the phase remains constant along a plane perpendicular to the cylinder axis. They are also inhomogeneous because the field is not constant along surfaces of constant phase.

A study of axial surface waves has been included in this text because this type of waves may be the cause of some significant contributions to the RCS of an aircraft. Axial surface waves can propagate along the body of a coated missile (13 in Fig. 1.5) and also the waves that propagate along the trailing edge of a coated wing (14 in Fig. 1.5) very much resemble these axial surface waves.

Sommerfeld was first to suggest the existence of axial surface waves in 1899. Goubau subsequently developed the idea in its application to a transmission line consisting of a coated metal wire (Fig. 4.1) [1]. With reference to this early research, the terms *Sommerfeld wave* and *Goubau wave* are sometimes used to denote an axial surface wave along a homogeneous rod and a coated metal wire, respectively. Axial surface waves are perhaps the most important type of surface waves with regard to practical applications [2]. Not only the Goubau line of Figure 4.1, but also the polyrod antenna supports axial surface waves [3].

Formulas for the electromagnetic field components in function of a Hertz potential were found in Section 2.6. Moreover, (2.30) and (2.31) appear to imply that the longitudinal components of \vec{E} and \vec{H} are uncoupled, as was the case with the plane surface waves discussed in Chapter 3. However, in general, coupling of the longitudinal field components E_z and H_z is required by the boundary conditions of the electromagnetic field components [4, p.38]. This is in contrast with plane surface waves where the boundary conditions do not lead to coupling between the field components, resulting in mode solutions for which the longitudinal component of either \vec{E} or \vec{H} is zero. These modes were called H-type (TE) and E-type (TM), respectively. Cylindrical interfaces, however, not only support pure TE and TM axial surface wave modes but also modes for which both E_z and H_z are nonzero. These latter modes are in fact combinations of a TE and TM mode with a same β_z and are therefore called *hybrid modes*. They are designated as EH or HE modes, depending on whether the TM or the TE mode predominates, respectively [5, p. 721]. Representations of the field distributions of these different types of axial surface wave modes can be found at the end of this chapter.

4.2 Axial Surface Waves along a Coated, Electric Perfectly Conducting Cylinder

The propagation of axial surface waves along a uniformly coated PEC cylinder will be analysed in this section. The structure under investigation actually corresponds to the Goubau line (Fig. 4.1).

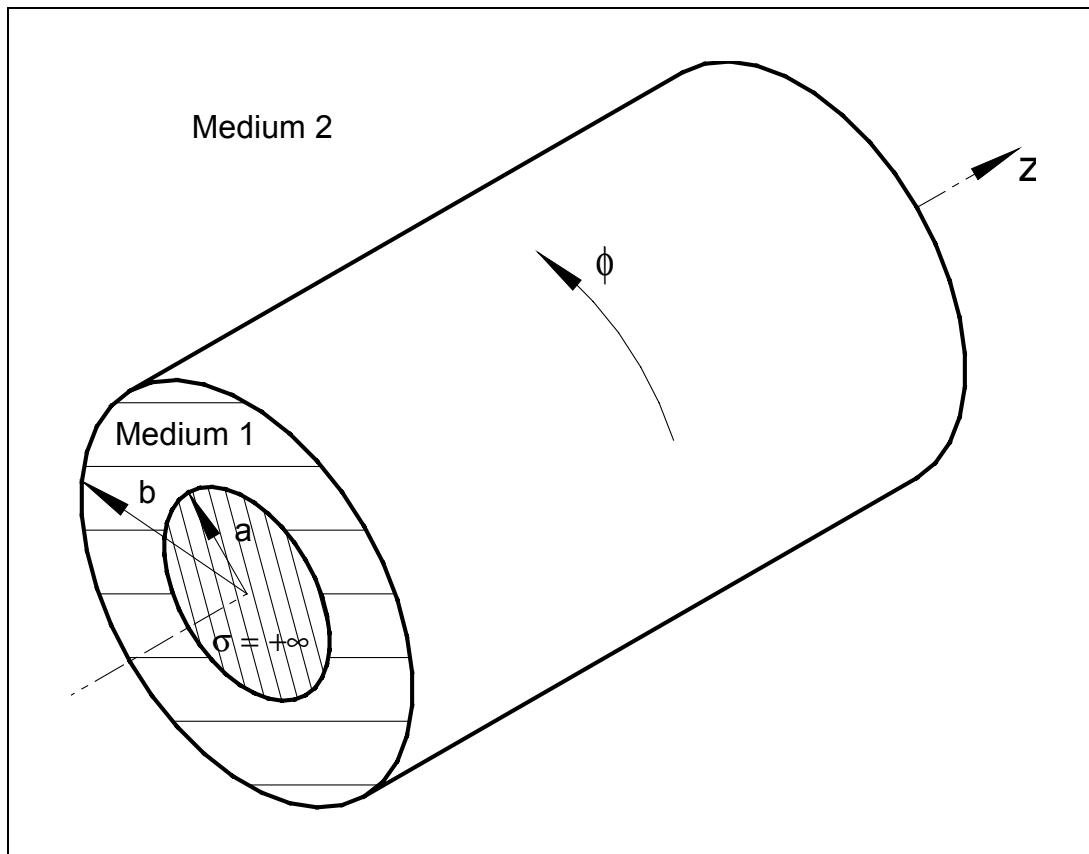


Figure 4.1: A uniformly coated PEC cylinder (Goubau line)

As was pointed out earlier, a cylindrical interface can support hybrid modes in addition to the pure TM and TE modes. In order to obtain hybrid mode solutions, equations (2.30) and (2.31) need to be evaluated simultaneously which makes the analysis more complex than the analysis of plane surface waves.

Suitable Hertz functions for medium 1 that can satisfy the boundary conditions $E_z = 0$ and $E_\phi = 0$ at $r = a$ are

$$\Pi_{1e} = \sum_n [A_{1J_n} J_n(s_{r1}r) + A_{1Y_n} Y_n(s_{r1}r)] e^{-jn\phi} e^{-j\beta_z z} \quad \text{and} \quad (1)$$

$$\Pi_{1m} = \sum_n [B_{1J_n} J_n(s_{r1}r) + B_{1Y_n} Y_n(s_{r1}r)] e^{-jn\phi} e^{-j\beta_z z} \quad (2)$$

where n is a positive integer.

Because of their similarity to harmonic functions and their oscillatory behaviour, the Bessel functions J_n and Y_n may be interpreted here as standing waves in the r -direction.

Substituting (1) and (2) into (2.30) and (2.31), respectively, gives

$$E_{z1} = s_{r1}^2 \sum_n [A_{1J_n} J_n(s_{r1}r) + A_{1Y_n} Y_n(s_{r1}r)] e^{-jn\phi} e^{-j\beta_z z}, \quad (3a)$$

$$E_{r1} = \sum_n \left[-j\beta_z s_{r1} [A_{1J_n} J'_n(s_{r1}r) + A_{1Y_n} Y'_n(s_{r1}r)] - \frac{n\omega\mu_1}{r} [B_{1J_n} J_n(s_{r1}r) + B_{1Y_n} Y_n(s_{r1}r)] \right] e^{-jn\phi} e^{-j\beta_z z}, \quad (3b)$$

$$E_{\phi1} = \sum_n \left[-\frac{n\beta_z}{r} [A_{1J_n} J_n(s_{r1}r) + A_{1Y_n} Y_n(s_{r1}r)] + j\omega\mu_1 s_{r1} [B_{1J_n} J'_n(s_{r1}r) + B_{1Y_n} Y'_n(s_{r1}r)] \right] e^{-jn\phi} e^{-j\beta_z z}, \quad (3c)$$

$$H_{z1} = s_{r1}^2 \sum_n [B_{1J_n} J_n(s_{r1}r) + B_{1Y_n} Y_n(s_{r1}r)] e^{-jn\phi} e^{-j\beta_z z}, \quad (3d)$$

$$H_{r1} = \sum_n \left[-j \frac{n(\sigma_1 + j\omega\epsilon_1)}{r} [A_{1J_n} J_n(s_{r1}r) + A_{1Y_n} Y_n(s_{r1}r)] - j\beta_z s_{r1} [B_{1J_n} J'_n(s_{r1}r) + B_{1Y_n} Y'_n(s_{r1}r)] \right] e^{-jn\phi} e^{-j\beta_z z}, \quad (3e)$$

$$H_{\phi1} = \sum_n \left[-(\sigma_1 + j\omega\epsilon_1) s_{r1} [A_{1J_n} J'_n(s_{r1}r) + A_{1Y_n} Y'_n(s_{r1}r)] - \frac{n\beta_z}{r} [B_{1J_n} J_n(s_{r1}r) + B_{1Y_n} Y_n(s_{r1}r)] \right] e^{-jn\phi} e^{-j\beta_z z}. \quad (3f)$$

Bessel functions of the second kind (Y_n) are not defined for negative real arguments. Hence,

$$s_{r1} = \text{sign} \left[\text{Re} \left(\sqrt{k_1^2 - \beta_z^2} \right) \right] \sqrt{k_1^2 - \beta_z^2}. \quad (4)$$

Large argument approximations for J_n and Y_n are [5, p. 835], [6, p. 228]

$$J_n(x) \approx \sqrt{\frac{2}{\pi x}} \cos \left(x - \frac{\pi}{4} - n \frac{\pi}{2} \right) \quad \text{and} \quad (5)$$

$$Y_n(x) \approx \sqrt{\frac{2}{\pi x}} \sin \left(x - \frac{\pi}{4} - n \frac{\pi}{2} \right), \quad \text{both for } |x| \gg 1. \quad (6)$$

Suitable Hertz functions for medium 2 that satisfy the boundary condition $\vec{E} = \vec{H} = \vec{0}$ when $r \rightarrow +\infty$

are

$$\Pi_{2e} = \sum_n A_2 H_n^{(2)}(s_{r2}r) e^{-jn\phi} e^{-j\beta_z z} \quad \text{and} \quad (7)$$

$$\Pi_{2m} = \sum_n B_2 H_n^{(2)}(s_{r2}r) e^{-jn\phi} e^{-j\beta_z z}. \quad (8)$$

The reason why Hankel functions of the second kind are used instead of those of the first kind, becomes clear by looking at the large argument approximations of both function types. These are [5, p. 835] and [6, p. 228]

$$H_n^{(1)}(x) \approx \sqrt{\frac{2}{\pi x}} e^{j\left(x - \frac{\pi}{4} - n\frac{\pi}{2}\right)} \quad \text{and} \quad (9)$$

$$H_n^{(2)}(x) \approx \sqrt{\frac{2}{\pi x}} e^{-j\left(x - \frac{\pi}{4} - n\frac{\pi}{2}\right)}, \quad \text{both for } |x| \gg 1. \quad (10)$$

Comparing (9) and (10) with the equivalent Hertz potentials for plane surface waves (3.7) and (3.18) and following the same reasoning as in Sections 3.4.2 and 3.4.3 leads to the following conclusions:

- the use of Hankel functions of the second kind in Hertz potentials gives rise to proper axial wave solutions,
- whereas using Hankel functions of the first kind results in improper axial wave solutions.

It is also important to know that Hankel functions are undefined for negative pure real numbers [7]. However, when the imaginary part of the argument is nonzero, the real part can have any value. Hence, for proper axial waves (see also (3.8) and (3.19) and Appendix 3.B)

$$s_{r2} = \text{sign}\left[\text{Re}\left(\sqrt{k_2^2 - \beta_z^2}\right)\right] \sqrt{k_2^2 - \beta_z^2} \Rightarrow js_{r2} = \text{sign}\left[\text{Re}\left(\sqrt{\beta_z^2 - k_2^2}\right)\right] \sqrt{\beta_z^2 - k_2^2}, \quad (11a)$$

whereas for improper axial waves

$$s_{r2} = -\text{sign}\left[\text{Re}\left(\sqrt{k_2^2 - \beta_z^2}\right)\right] \sqrt{k_2^2 - \beta_z^2} \Rightarrow js_{r2} = -\text{sign}\left[\text{Re}\left(\sqrt{\beta_z^2 - k_2^2}\right)\right] \sqrt{\beta_z^2 - k_2^2}. \quad (11b)$$

Substituting (7) and (8) into (2.30) and (2.31), respectively, gives

$$E_{z2} = s_{r2}^2 \sum_n A_2 H_n^{(2)}(s_{r2}r) e^{-jn\phi} e^{-j\beta_z z}, \quad (12a)$$

$$E_{r2} = \sum_n \left[-j\beta_z A_2 s_{r2} H_n^{(2)}(s_{r2}r) - \frac{n\omega\mu_2}{r} B_2 H_n^{(2)}(s_{r2}r) \right] e^{-jn\phi} e^{-j\beta_z z}, \quad (12b)$$

$$E_{\phi 2} = \sum_n \left[-\frac{n\beta_z}{r} A_2 H_n^{(2)}(s_{r2}r) + j\omega\mu_2 B_2 s_{r2} H_n^{(2)}(s_{r2}r) \right] e^{-jn\phi} e^{-j\beta_z z}, \quad (12c)$$

$$H_{z2} = s_{r2}^2 \sum_n B_2 H_n^{(2)}(s_{r2}r) e^{-jn\phi} e^{-j\beta_z z}, \quad (12d)$$

$$H_{r2} = \sum_n \left[-j \frac{n(\sigma_2 + j\omega\epsilon_2)}{r} A_2 H_n^{(2)}(s_{r2}r) - j\beta_z B_2 s_{r2} H_n^{(2)}(s_{r2}r) \right] e^{-jn\phi} e^{-j\beta_z z}, \quad (12e)$$

$$H_{\phi 2} = \sum_n \left[-(\sigma_2 + j\omega\epsilon_2) A_2 s_{r2} H_n^{(2)}(s_{r2}r) - \frac{n\beta_z}{r} B_2 H_n^{(2)}(s_{r2}r) \right] e^{-jn\phi} e^{-j\beta_z z}. \quad (12f)$$

The tangential components of \vec{E} must vanish at the surface of the perfect electric conductor.

$$E_{z1} = 0 \text{ at } r = a$$

$$\Rightarrow A_{1Y_n} = -\frac{J_n(s_{r1}a)}{Y_n(s_{r1}a)} A_{1J_n} \text{ and} \quad (13)$$

$E_{\phi1} = 0$ at $r = a$ gives, by virtue of (3c) and (13),

$$B_{1Y_n} = -\frac{J'_n(s_{r1}a)}{Y'_n(s_{r1}a)} B_{1J_n}. \quad (14)$$

The tangential components of both \vec{E} and \vec{H} are continuous across the interface of two media. This gives, by virtue of (13) and (14)

$$E_{z1} = E_{z2} \text{ at } r = b$$

$$\Rightarrow s_{r1}^2 \left[J_n(s_{r1}b) - \frac{J_n(s_{r1}a)}{Y_n(s_{r1}a)} Y_n(s_{r1}b) \right] A_{1J_n} - s_{r2}^2 H_n^{(2)}(s_{r2}b) A_2 = 0, \quad (15)$$

$$E_{\phi1} = E_{\phi2} \text{ at } r = b$$

$$\begin{aligned} \Rightarrow & -\frac{n\beta_z}{b} \left[J_n(s_{r1}b) - \frac{J_n(s_{r1}a)}{Y_n(s_{r1}a)} Y_n(s_{r1}b) \right] A_{1J_n} \\ & + j\omega\mu_1 s_{r1} \left[J'_n(s_{r1}b) - \frac{J'_n(s_{r1}a)}{Y'_n(s_{r1}a)} Y'_n(s_{r1}b) \right] B_{1J_n} \\ & + \frac{n\beta_z}{b} H_n^{(2)}(s_{r2}b) A_2 - j\omega\mu_2 s_{r2} H_n^{(2)}(s_{r2}b) B_2 = 0, \end{aligned} \quad (16)$$

$$H_{z1} = H_{z2} \text{ at } r = b$$

$$\Rightarrow s_{r1}^2 \left[J_n(s_{r1}b) - \frac{J'_n(s_{r1}a)}{Y'_n(s_{r1}a)} Y_n(s_{r1}b) \right] B_{1J_n} - s_{r2}^2 H_n^{(2)}(s_{r2}b) B_2 = 0 \quad (17)$$

and finally $H_{\phi1} = H_{\phi2}$ at $r = b$

$$\begin{aligned} \Rightarrow & -(\sigma_1 + j\omega\epsilon_1) s_{r1} \left[J'_n(s_{r1}b) - \frac{J_n(s_{r1}a)}{Y_n(s_{r1}a)} Y'_n(s_{r1}b) \right] A_{1J_n} \\ & - \frac{n\beta_z}{b} \left[J_n(s_{r1}b) - \frac{J'_n(s_{r1}a)}{Y'_n(s_{r1}a)} Y_n(s_{r1}b) \right] B_{1J_n} \\ & + (\sigma_2 + j\omega\epsilon_2) s_{r2} H_n^{(2)}(s_{r2}b) A_2 + \frac{n\beta_z}{b} H_n^{(2)}(s_{r2}b) B_2 = 0. \end{aligned} \quad (18)$$

Equations (15), (16), (17) and (18) form a system of linear equations for the four unknown factors A_{1J_n} , B_{1J_n} , A_2 and B_2 . The system is homogeneous, hence for non-trivial solutions to exist, the coefficient determinant must be zero, that is

$$\begin{vmatrix} s_{r1}^2 \left[J_n(s_{r1}, b) - \frac{J_n(s_{r1}, a)}{Y_n(s_{r1}, a)} Y_n(s_{r1}, b) \right] & 0 & -s_{r2}^2 H_n^{(2)}(s_{r2}, b) & 0 \\ -\frac{n\beta_z}{b} \left[J_n(s_{r1}, b) - \frac{J_n(s_{r1}, a)}{Y_n(s_{r1}, a)} Y_n(s_{r1}, b) \right] & j\omega\mu_1 s_{r1} \left[J'_n(s_{r1}, b) - \frac{J'_n(s_{r1}, a)}{Y'_n(s_{r1}, a)} Y'_n(s_{r1}, b) \right] & \frac{n\beta_z}{b} H_n^{(2)}(s_{r2}, b) & -j\omega\mu_2 s_{r2} H_n^{(2)}(s_{r2}, b) \\ 0 & s_{r1}^2 \left[J_n(s_{r1}, b) - \frac{J_n(s_{r1}, a)}{Y_n(s_{r1}, a)} Y_n(s_{r1}, b) \right] & 0 & -s_{r2}^2 H_n^{(2)}(s_{r2}, b) \\ -(\sigma_1 + j\omega\epsilon_1) s_{r1} \left[J'_n(s_{r1}, b) - \frac{J'_n(s_{r1}, a)}{Y'_n(s_{r1}, a)} Y'_n(s_{r1}, b) \right] & -\frac{n\beta_z}{b} \left[J_n(s_{r1}, b) - \frac{J_n(s_{r1}, a)}{Y_n(s_{r1}, a)} Y_n(s_{r1}, b) \right] & (\sigma_2 + j\omega\epsilon_2) s_{r2} H_n^{(2)}(s_{r2}, b) & \frac{n\beta_z}{b} H_n^{(2)}(s_{r2}, b) \end{vmatrix} = 0. \quad (19)$$

Expanding the above determinant does not result in a simplified expression. Equation (19) may therefore be regarded as the dispersion equation of the axial surface waves propagating along a Goubau line.

However, it can be shown that, for $n=0$, (19) reduces to

$$\begin{aligned} & \left[(\sigma_1 + j\omega\epsilon_1) s_{r2} \left[J'_0(s_{r1}, b) - \frac{J'_0(s_{r1}, a)}{Y'_0(s_{r1}, a)} Y'_0(s_{r1}, b) \right] H_0^{(2)}(s_{r2}, b) - (\sigma_2 + j\omega\epsilon_2) s_{r1} \left[J_0(s_{r1}, b) - \frac{J_0(s_{r1}, a)}{Y_0(s_{r1}, a)} Y_0(s_{r1}, b) \right] H_0^{(2)}(s_{r2}, b) \right] \\ & \cdot \left[j\omega\mu_1 s_{r2} \left[J'_0(s_{r1}, b) - \frac{J'_0(s_{r1}, a)}{Y'_0(s_{r1}, a)} Y'_0(s_{r1}, b) \right] H_0^{(2)}(s_{r2}, b) - j\omega\mu_2 s_{r1} \left[J_0(s_{r1}, b) - \frac{J_0(s_{r1}, a)}{Y_0(s_{r1}, a)} Y_0(s_{r1}, b) \right] H_0^{(2)}(s_{r2}, b) \right] = 0. \end{aligned} \quad (20)$$

Also, for $n=0$, two distinct types of uncoupled modes are propagating. This can be seen from (3) and (12):

- H_z , E_r and E_ϕ belong to the field of TM modes,
- whereas E_z , H_r and H_ϕ make up the field of the TE modes.

Finally, comparing the two factors at the left side of (20) with (3.12) and (3.23), shows that these factors correspond to the dispersion equation of the TM and TE modes, respectively. Equations (5), (6), (9) and (10) also show that the field expressions of an axial surface wave tend toward those of a plane surface wave in the limit case of propagation along an electrically extremely thick cylinder.

4.3 Field Distribution of Axial Surface Waves along a Coated, Electric Perfectly Conducting Cylinder

Because of the oscillatory behaviour of the Bessel functions J_n and Y_n , there will be m roots of equation (19) for any given n value. These roots are designated by β_{nm} and the corresponding modes are either TM_{0m} , TE_{0m} , EH_{nm} or HE_{nm} [4, p. 41-42].

As was already suggested towards the end of the previous section, TM and TE modes have no angular dependence, i.e. $n=0$.

The EH_{11} (or HE_{11}) mode is the fundamental mode; it has no low-frequency cutoff [6, p. 769].

Figure 4.2 shows the transverse electric field vectors in medium 1 for the four lowest order modes.

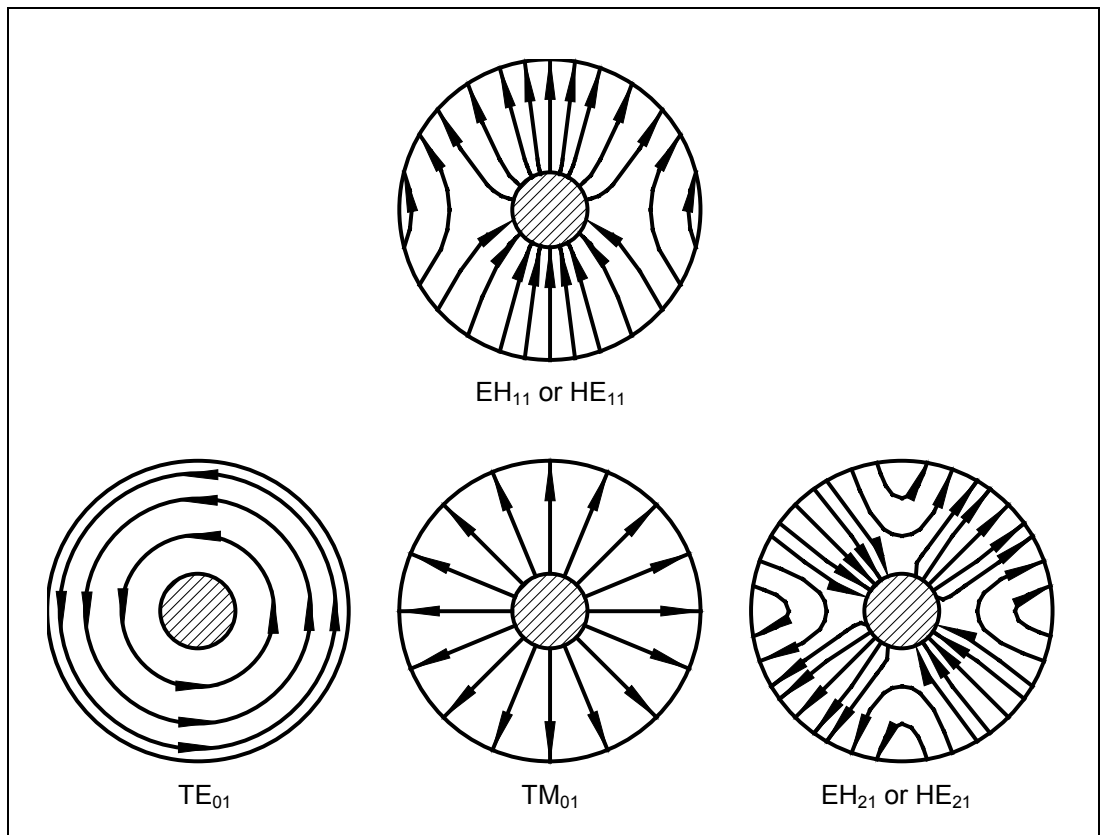


Figure 4.2: The transverse electric field in medium 1 of the four lowest order modes

The external field of a TM axial surface wave is depicted in Figure 4.3. For a TE wave the E- and H-fields are interchanged and one of the fields is reversed in sign.

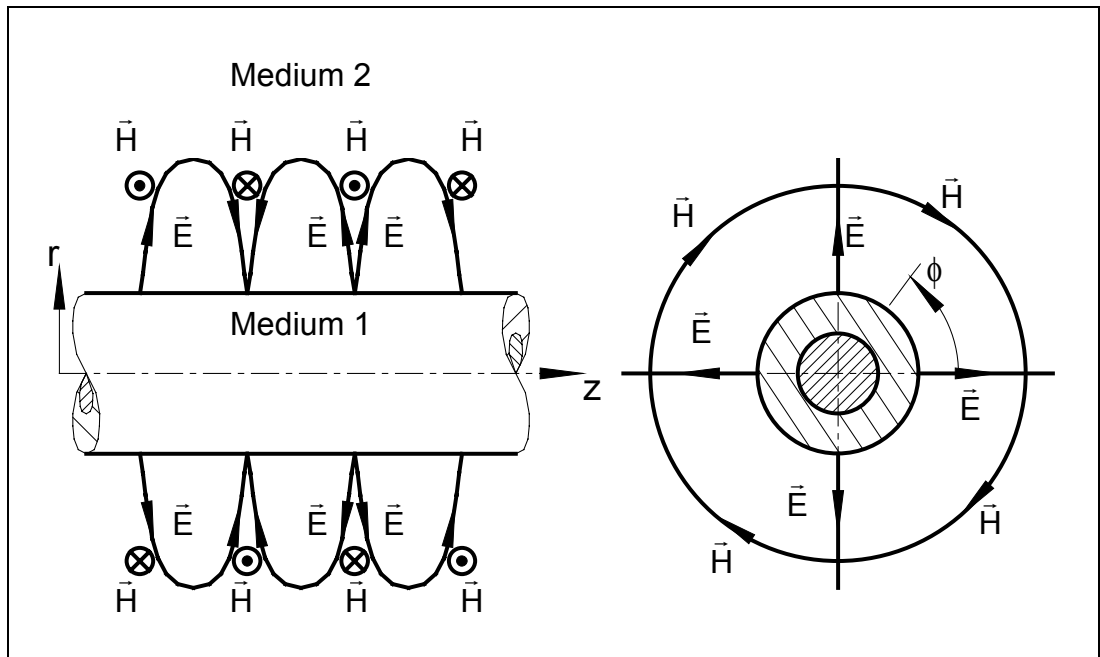


Figure 4.3: The external field of a TM axial surface wave

4.4 Conclusions

Axial surface waves are important because they may be the cause of some significant contributions to the RCS of an aircraft. Axial surface waves can for example propagate along the body of a coated missile.

There are three types of axial wave modes: TM, TE and hybrid. Axial surface waves differ in this respect from plane surface waves that only come in two types: TM (E-type) and TE (H-type).

4.5 References

- [1] H. M. Barlow and A. L. Cullen, "Surface waves," *Proceedings of the Institution of Electrical Engineers*, Vol. 100, Part III, No. 68, Nov. 1953, pp. 329-347
- [2] H. M. Barlow and J. Brown, *Radio Surface Waves*, Oxford University Press, 1962, p. 12
- [3] F. J. Zucker, "Surface-wave antennas," Chapter 12 in R. C. Johnson, *Antenna Engineering Handbook*, McGraw-Hill, 3rd Ed., 1993
- [4] G. Keiser, *Optical Fiber Communications*, McGraw-Hill, 2nd Ed.
- [5] R. E. Collin, *Field Theory of Guided Waves*, IEEE Press, 2nd Ed., 1991
- [6] K. Simonyi, *Theoretische Elektrotechnik*, Johann Ambrosius Barth, 10. Auflage, 1993, (in German)
- [7] M. Abramowitz and I. A. Stegun, *Handbook of Mathematical Functions*, Dover Publications, 1st Ed., 8th Printing, 1972, p. 359

5 RCS Management of Edge Diffracted Waves

5.1 Introduction

Radar absorbing materials (RAM's) applied as a coating on the surface of an object, partially transform the energy of an incident radar beam into heat and reduce the scattered field in some directions. Ordinary RAM's (electric, magnetic or hybrid) can be graded or have multiple layers in order to increase the frequency band. Moreover, they are nearly always homogeneous in directions parallel to the reflecting plate.

However, ordinary RAM's are not effective in absorbing grazing incident waves ($\theta_i \cong 90^\circ$) and are therefore not successful in reducing forward scattering [1]. This fundamental limitation results from the fact that any ordinary RAM, independently of the incident wave polarization, has a reflection coefficient that tends to unity when $\theta_i \rightarrow 90^\circ$. This can be inferred from the reflection coefficient expressions (3.43) and (3.44).

For parallel polarized incident waves

$$\lim_{\theta_{2i} \rightarrow 90^\circ} R_{//} = \lim_{\theta_{2i} \rightarrow 90^\circ} \Gamma_{//} = \lim_{\theta_{2i} \rightarrow 90^\circ} \frac{Z_{c2//} - Z_{s\ell//}}{Z_{c2//} + Z_{s\ell//}} = \lim_{\theta_{2i} \rightarrow 90^\circ} \frac{\eta_2 \cos(\theta_{2i}) - Z_{s\ell//}}{\eta_2 \cos(\theta_{2i}) + Z_{s\ell//}} = -1. \quad (1)$$

Likewise, for perpendicular polarized incident waves

$$\lim_{\theta_{2i} \rightarrow 90^\circ} R_{\perp} = \lim_{\theta_{2i} \rightarrow 90^\circ} \Gamma_{\perp} = \lim_{\theta_{2i} \rightarrow 90^\circ} \frac{Y_{c2\perp} - Y_{st\perp}}{Y_{c2\perp} + Y_{st\perp}} = \lim_{\theta_{2i} \rightarrow 90^\circ} \frac{\frac{\cos(\theta_{2i})}{\eta_2} - Y_{st\perp}}{\frac{\cos(\theta_{2i})}{\eta_2} + Y_{st\perp}} = -1. \quad (2)$$

Ordinary radar absorbing materials are therefore not very useful in reducing the forward scattering of an object.

5.2 Converting the Incident Space Wave into Attenuated Surface Waves

It is conceivable that absorption of grazing incident waves could be realized if some special discontinuity (e.g. an edge, a wire or a grating) were placed along an absorbing layer. Such a discontinuity could partially transform the incident wave into surface wave modes which would propagate and attenuate further along the layer [1]. (See Fig. 5.1.) In fact, gratings are successfully employed in integrated optics as feeding structures for dielectric waveguides where they yield space wave to surface wave power conversion efficiencies of up to 80% [2].

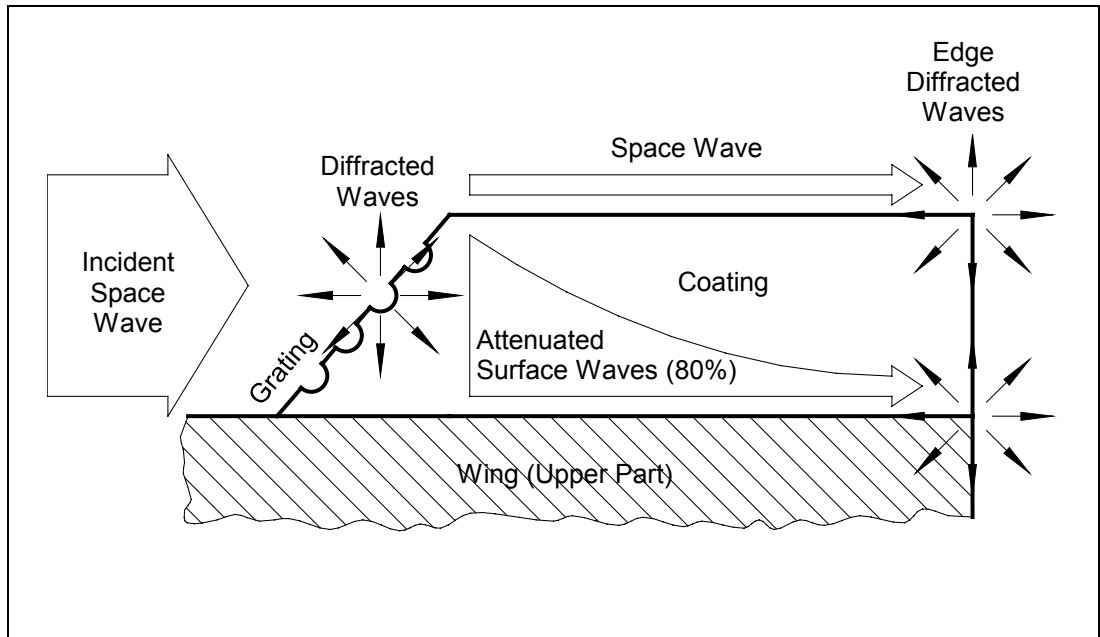


Figure 5.1: Conversion of the incident space wave into attenuated surface wave modes

However, the idea of converting the incident space wave into attenuated surface wave modes has three essential defects for RCS reduction. Firstly, any additional discontinuity creates an additional scattered field. Secondly, the transformation of the incident field into surface wave modes is only partial. Part of the incident field will remain propagating as a space wave to finally interact with the object and reflect. Thirdly, it is extremely difficult, if not impossible, to build an absorbing layer which would allow the propagation of both E-type plane surface waves and H-type plane surface waves. As has been shown in Chapter 3, the longitudinal surface impedance must be inductive to support E-type surface wave modes whereas a capacitive transversal surface impedance is required to support H-type surface wave modes. Thus, the surface impedance needs to be anisotropic to allow propagation of both types of surface waves.

Successfully admitting and then absorbing surface waves in a surface wave absorbing material would therefore require the following actions:

- 1) Convert as much of the incident space wave field into surface wave modes while trying to avoid generating additional forward scattering. This has to be achieved not only for an incident angle of 90° but also for angles close to 90° . Note also that the incident space wave can have any polarization, which complicates matters even more.
- 2) Use a coating with an anisotropic surface impedance to enable the propagation of both surface wave types.
- 3) Moreover, the coating has to have significant losses so that the surface waves are sufficiently attenuated before they hit that part of the structure that causes most of the forward diffracted fields. In the case of an aircraft wing, the problem area which generates most of the edge diffracted waves, is most often either the trailing edge of the wing or the air gap between the flaps or ailerons (See Fig. 1.5 and 1.6). The effect of edge diffraction is at its highest level for edges perpendicular to the radar direction [1]. Step 3 involves maximizing the attenuation constant $\alpha_x = -\text{Im}(\beta_x)$ for all propagating surface wave modes.

Although surface wave absorbers based on the above principles are already commercially available, their successful application under all circumstances has not been reported in literature yet. It is also unclear, if not doubtful, whether these surface wave absorbers are able to support both types of surface waves. As has been pointed out already, the main difficulty of the whole strategy is with the implementation of Step 1 and 2. An edge wave RCS management strategy that does not suffer from these defects will be presented next.

Ordinary surface wave absorbing materials may however still find some useful applications. These are discussed at the beginning of Chapter 6.

5.3 Soft Surfaces

5.3.1 Introduction

The main design goal for the surface wave absorbers discussed in the previous section is to maximize the attenuation constant $\alpha_x = -\text{Im}(\beta_x)$ for all propagating surface wave modes. The strategy presented in this section uses a completely different approach. The intention is to reradiate the incident radar energy in directions away from the radar, rather than to dissipate it.

An important observation is the fact that edge diffraction not only generates surface waves but also space waves. The incident wave can have any polarization depending on the polarization of the radar and the orientation of the target. Therefore, the polarization of the edge diffracted space waves and surface waves is generally unknown.

The effect of edge diffraction is completely absent if no fields are present in the immediate vicinity of an object's surface. First will be examined what is needed to obtain this situation with surface waves. The discussion will be restricted to the case of a coated PEC. However, the same reasoning can be applied to multi-layered structures.

For surface waves to have no field protruding from the coating, it is necessary that $j\mathbf{s}_{z2} \rightarrow +\infty$. In this case, the Hertz function of both the E-type and the H-type surface waves (3.7) and (3.18) will be zero at the interface ($z = h$). Hence, all surface wave field vectors will vanish at the interface. $j\mathbf{s}_{z2} \rightarrow +\infty$, puts the following requirements on the values of the longitudinal (3.14) and the transversal (3.25) surface wave impedance

$$|Z_{s\ell}| = \left| -\frac{j\mathbf{s}_{z2}}{\sigma_2 + j\omega\epsilon_2} \right| \rightarrow +\infty \quad \text{and} \quad (3)$$

$$|Z_{st}| = \left| -\frac{j\omega\mu_2}{j\mathbf{s}_{z2}} \right| \rightarrow 0. \quad (4)$$

These requirements are met by an electromagnetic soft surface, as is explained in the next section.

5.3.2 Definitions

The most general definition for an *electromagnetic soft surface* is a surface along which the power density flux (i.e. the Poynting vector) is zero for any polarization. This means that no electromagnetic wave of any kind (including space waves and surface waves) will propagate along a soft surface. An *electromagnetic hard surface* is a surface along which only a TEM wave (i.e. space wave) can propagate. The density of power flow usually has a maximum at the hard surface. The names soft and hard surface were chosen on the analogy of acoustic soft and hard surface [3].

Although the terms longitudinal surface impedance and transversal surface impedance were used at a number of occasions in this text, they were not defined in their most general sense yet. In order to do so, it is first necessary to define the directions longitudinal, transversal and normal with respect to the propagation direction of a surface wave. *The longitudinal direction of a surface wave*, $\vec{\ell}$, corresponds to the propagation direction of the surface wave and is tangential to surface of the guiding structure. *The transversal direction*, \vec{t} , is orthogonal to $\vec{\ell}$ and also tangential to the surface. Finally, *the normal direction*, \vec{n} , is such that $\vec{n} = \vec{\ell} \times \vec{t}$.

The longitudinal and transversal surface impedances are given by

$$Z_{s\ell} = -\frac{E_\ell}{H_t} \text{ and} \quad (5)$$

$$Z_{st} = \frac{E_t}{H_\ell}, \text{ respectively,} \quad (6)$$

where E_ℓ and E_t are respectively the longitudinal and transversal components of the E-field at the surface, H_ℓ and H_t are the corresponding components of the H-field.

Soft and hard surfaces can be uniquely defined in terms of their longitudinal and transversal surface impedance.

For a soft surface, the Poynting vector needs to be zero at the surface. This is obtained only if both E_t and H_t are zero at the surface, which, in view of (5) and (6), corresponds to: $Z_{s\ell} = \infty$ and $Z_{st} = 0$. (7)

This requirement is identical with (3) and (4).

Only a TEM wave can propagate along a hard surface. Hence, E_ℓ and H_ℓ need to be zero at the surface. This is the same as requiring:

$$Z_{s\ell} = 0 \text{ and } Z_{st} = \infty. \quad (8)$$

Soft and surfaces are sometimes wrongfully defined in terms of grazing reflection coefficients. For example, soft surfaces are said to be a surface for which $R_{//} = R_{\perp} = -1$. However, in the introduction to this chapter was shown that for any material $R_{//} = R_{\perp} = -1$ at grazing angles of incidence (1) and (2). This would lead to the wrong conclusion that all surfaces are soft surfaces, which can not be true of course.

5.4 The Practical Realization of a Soft Surface

5.4.1 Narrow-Band Soft and Hard Surfaces

The classical way to realize a soft surface is to corrugate an ideal conductor with transverse rectangular grooves (Fig. 5.2) [3]. These act as shorted parallel plate waveguides for the longitudinal polarization and transform the short to $Z = \infty$ at the aperture of the corrugations if the slot depth

$$d = \left(\frac{1+2n}{4} \right) \lambda_n \quad (9)$$

where n is positive integer and λ_n the wavelength inside a groove.

Hence, the transversal component H_t will vanish at the aperture of the corrugations. The transversal component E_t is zero at the top face of the perfect electrically conducting walls. At least three corrugations per wavelength are required for the surface to appear as a soft surface [3].

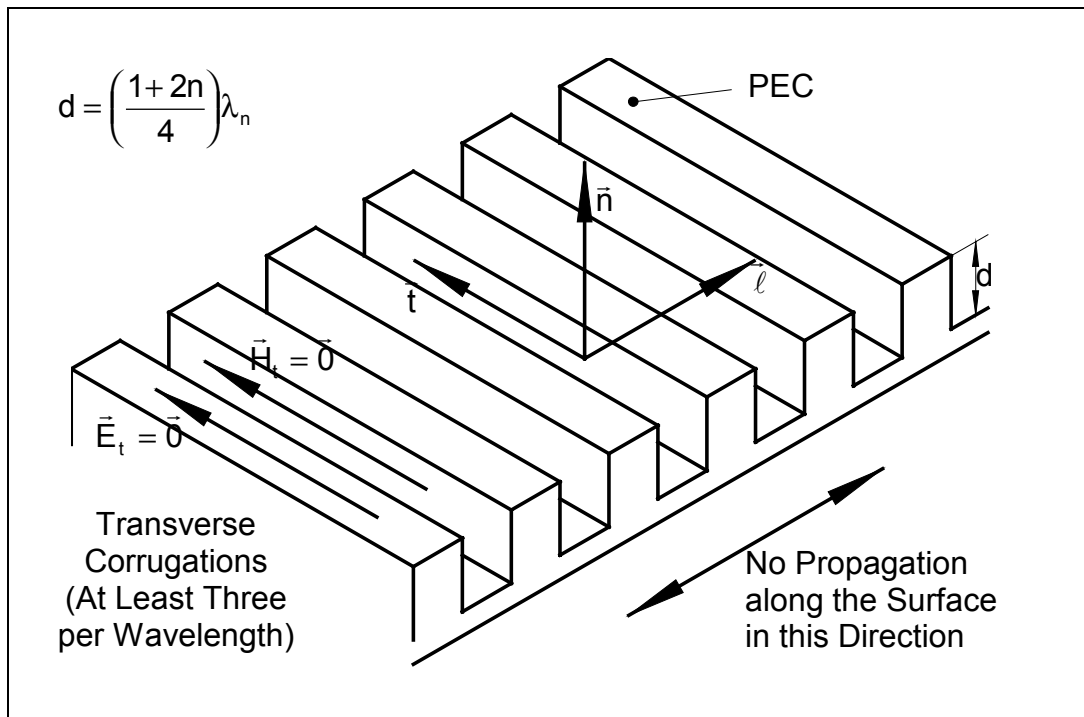


Figure 5.2: A narrow-band soft surface

A narrow band hard surface is obtained by turning the corrugated surface of Figure 5.2 ninety degrees (see Fig. 5.3).

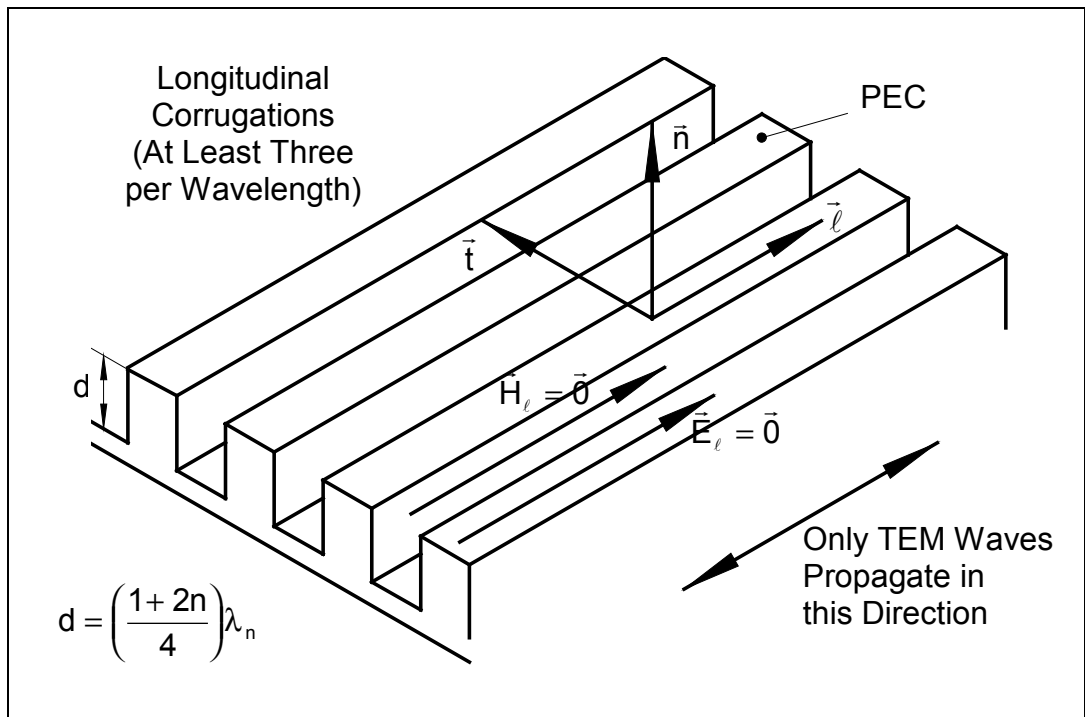


Figure 5.3: A narrow-band hard surface

The grooves of a corrugated surface can be filled with a dielectric in order to maintain the aerodynamic properties of an object. However, corrugated surfaces are still impractical in two ways: they are heavy and they are difficult to manufacture. A much lighter and cheaper alternative is the strip-loaded coating of Figure 5.4 [4].

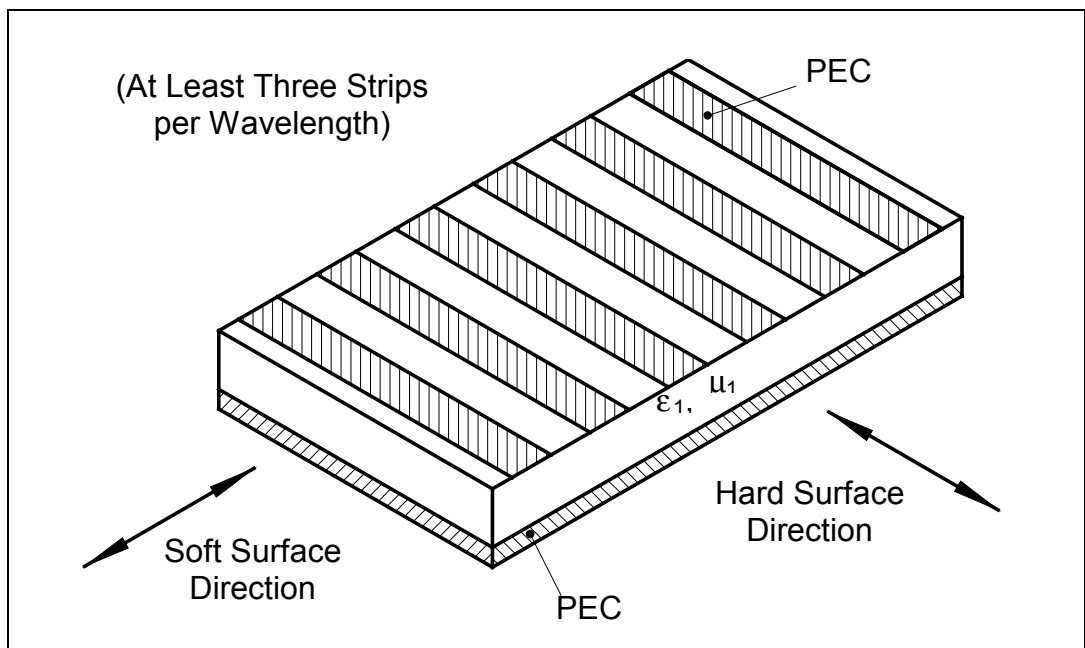


Figure 5.4: A strip-loaded grounded dielectric and/or magnetic slab

5.4.2 A Tuneable Soft Surface

A transversely corrugated surface acts as a soft surface on a discrete set of frequencies only, given by (9). Although dual depth corrugations [4], [5] could double the number of useful frequencies, corrugated surfaces remain impractical because, in general, the operating frequency of a threatening radar is not known in advance. Also the increase in useful bandwidth offered by alternative corrugation techniques [4], [5] is too small to be useful in RCS management.

What is really needed is either a tuneable soft surface, or even better, a broad-band soft surface. A tuneable soft surface could be constructed by replacing the strip-loaded slab of Figure 5.4 with either a strip-loaded electrooptic material or a strip-loaded magnetically biased ferrite slab.

A number of electrooptic materials have the interesting property that their permittivity is light dependent.

The incremental permeability of a ferrite (Fig. 5.5) can be changed by varying the magnetic bias. An electromagnet is used to generate the variable magnetic bias field. A tuneable microstrip antenna on this principle has been reported in literature [6]. However, the relatively high weight of ferrite materials and the energy consumption of an electromagnet make the use of ferrites less favourable than employing electrooptic materials.

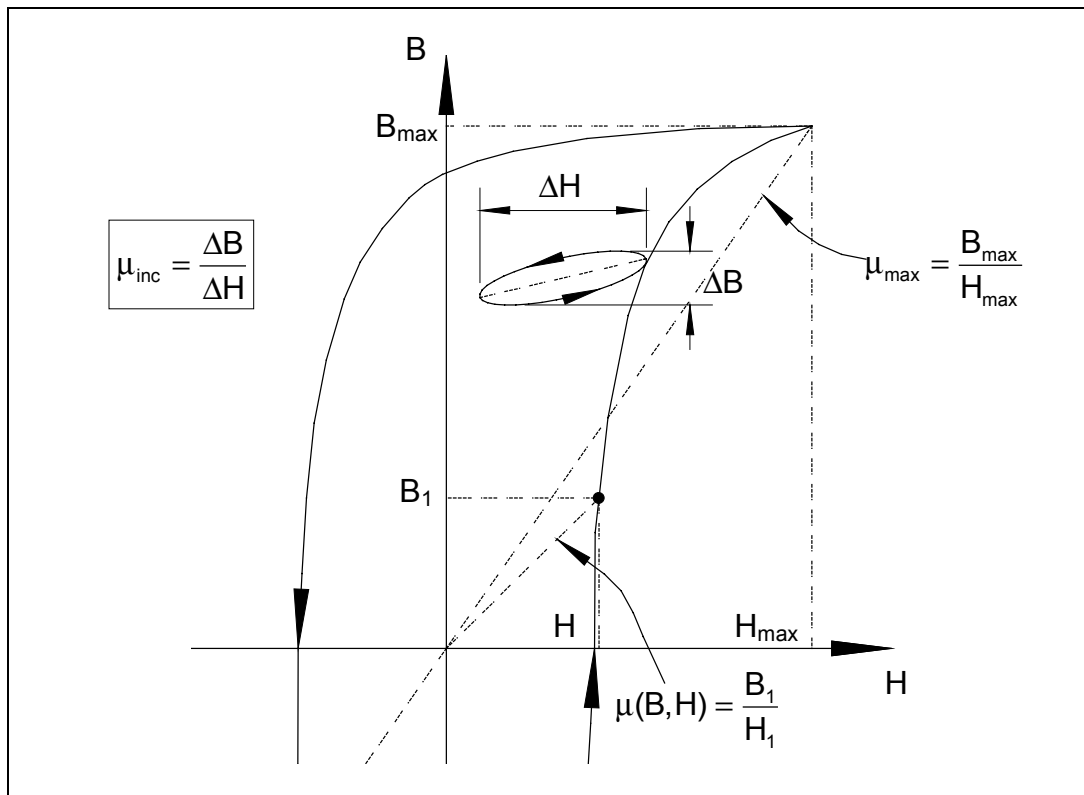


Figure 5.5: Minor hysteresis loop illustrating incremental permeability

5.4.3 What is Needed for a Broad-Band Soft Surface?

A broad-band soft surface would consist of alternate series of good electrically conducting transverse strips and good magnetically conducting strips (see also Fig. 5.4). The tangential components of the electric field vanish at the surface of a *perfect electric conductor (PEC)*. Likewise, the tangential components of the magnetic field are zero at the surface of a *perfect magnetic conductor (PMC)*. A lot of materials are known to be good electric conductors. They are characterized by their high number of free electrically charged particles. On the other hand, magnetic conductors do not exist due to the absence of magnetic charges in nature. However, this is the story for DC. For AC (and hence microwaves) materials that act as good magnetic conductors should, in principle, exist. At least, this is what must be concluded from comparing the definition of complex permittivity with the definition of complex permeability (see also Section 2.2).

$$\text{Permittivity } \varepsilon = \varepsilon' - j\varepsilon'' - j\frac{\sigma}{\omega} \quad (10)$$

where $-j\varepsilon''$ is the loss contribution due to molecular relaxation

and $-j\frac{\sigma}{\omega}$ is the conduction loss contribution.

As was already mentioned in Section 2.2, the distinction between the two loss contributions is rather artificial since it is based on the way these loss contributions are measured.

$$\text{For a PEC: } \sigma = \infty \Rightarrow \text{Im}(\varepsilon) = -\infty. \quad (11)$$

Permeability μ has only one loss contribution due to hysteresis:

$$\mu = \mu' - j\mu'' . \quad (12)$$

By analogy to (11), a perfect magnetic conductor (PMC) is characterized by

$$\text{Im}(\mu) = -\infty . \quad (13)$$

Thus, the magnet equivalent of an electric conductor is, for AC, a material with extremely high magnetic losses. It can be shown that the area enclosed by a hysteresis loop (Fig. 5.5) is a measure for the amount of magnetic loss. Most magnetic materials used at microwave frequencies are so called *soft magnetic materials* with thin hysteresis loops (e.g. ferrites) and hence low losses. However, the exact opposite properties are required for a magnetic conductor at microwave frequencies, namely a wide hysteresis loop and hence high magnetic losses. Magnetic materials with such properties are called *hard magnetic materials*. Permanent magnets are always made of a hard magnetic material. However, the use of hard magnetic materials at microwave frequencies has, to the author's knowledge, not yet been reported in literature.

To summarize, replacing the slab in Figure 5.4 with an extremely lossy magnetic material would, in theory, result in a broad-band soft surface. An experimental proof for this hypothesis is not available, but highly desirable.

5.4.4 Applying Soft Surfaces to an Aircraft Wing

Figure 5.6 shows how an ordinary aircraft wing can be retrofitted for reduced RCS. Specular reflections from the leading wing edge are significantly reduced by applying ordinary RAM. Soft surfaces on both sides of the wing suppresses all edge diffracted waves in the radar direction, independently of the radar polarization. Note however that the wing's RCS will increase for aspects other than head-on. (A soft surface is for example a perfect reflector when viewed from above.) Serrations in the soft surfaces are needed as a gradual impedance match for the incoming radar waves.

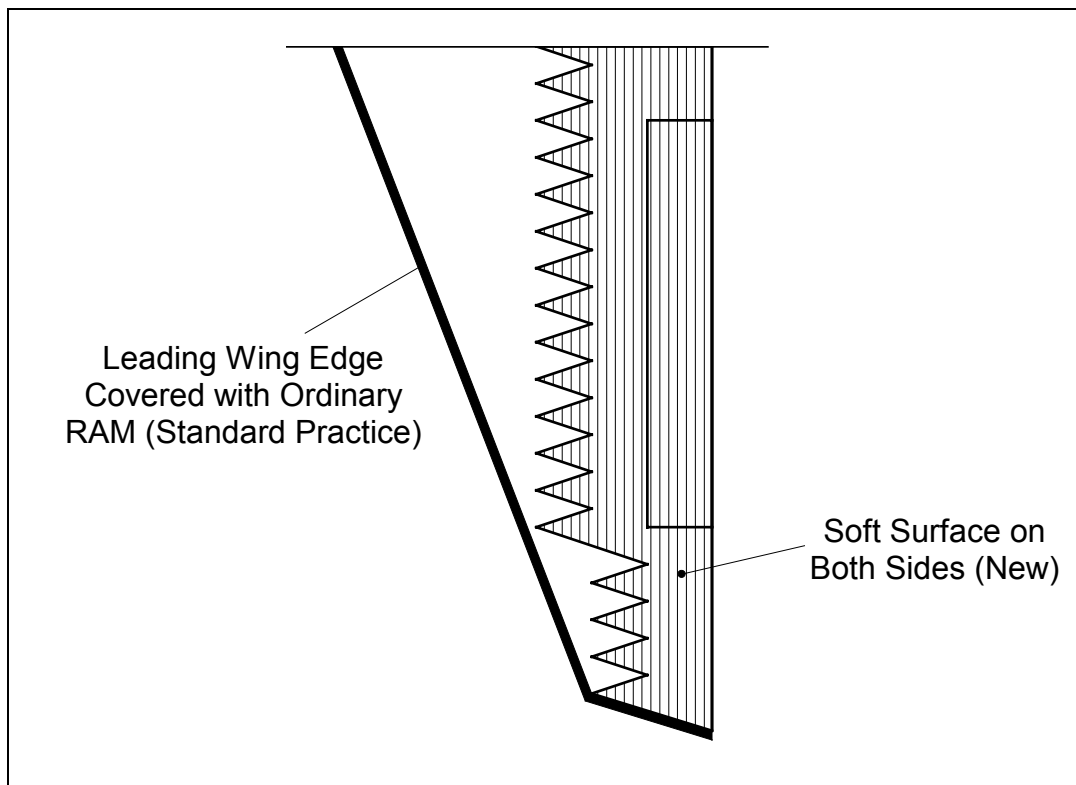


Figure 5.6: Retrofitting an ordinary aircraft wing for reduced RCS

5.4.5 Theoretical Models and Experimental Results Reported in Literature

The corrugated and strip-loaded surfaces are periodic structures. The analysis of periodic structures by means of Floquet's theorem is explained in [7] and [8].

Although no experiments on soft surfaces were conducted by the author, plenty of experimental results are available in literature. In references [5] and [9] a radial surface wave antenna (Fig. 6.2) was employed to measure the efficacy of soft surfaces in suppressing radiation along the surface. A reduction of up to 13dB was measured in comparison with a smooth conducting surface. Numerical simulations using the method of moments gave similar results.

Diffraction coefficients for soft surfaces applied to wedges can be found in [9] and [10].

5.5 Conclusions

Surface wave absorbing materials are not very useful in applications where the radar beam polarization is unknown and/or where the edge diffracted waves come in more than one polarization.

When properly oriented, a soft surface will suppress all radiation (both space wave and surface wave) in the direction of the radar, independently of the radar polarization and the polarization of the edge diffracted waves. In this process, the incident radar energy is not absorbed but reradiated in directions away from the radar.

A narrow-band soft surface can be obtained by corrugating a PEC with transverse grooves of proper slot depth. A much lighter and cheaper alternative is a strip-loaded coating.

Tuneable soft surfaces could be realized by employing electrooptic materials or magnetically biased ferrites.

A broad-band soft surface could in principle be obtained by loading an extremely lossy magnetic material with electrically conducting strips.

Serrations in a soft surface are needed as a gradual impedance match for the incoming radar waves.

5.6 References

- [1] P. Y. Ufimtsev, "Comments on diffraction principles and limitations of RCS reduction techniques," *Proceedings of the IEEE*, Vol. 84, No. 12, December 1996, pp. 1828-1851
- [2] P. Lorrain, D. R. Corson and F. Lorrain, *Electromagnetic Fields and Waves Including Electric Circuits*, W. H. Freeman and Co., 3rd Ed., 1988, p. 654 in German Ed.
- [3] P.-S. Kildal, "Definition of artificially soft and hard surfaces for electromagnetic waves," *Electronic Letters*, Vol. 24, No. 3, February 1988, pp. 168-170
- [4] P.-S. Kildal, *Research 1993-1995 at Antenna Group*, Department of Microwave Technology, Chalmers University of Technology, Gothenburg, Sweden, p. 15
- [5] Z. Ying, P.-S. Kildal and A. A. Kishk, "Study of different realizations and calculation models for soft surfaces by using a vertical monopole on a soft disk as a test bed," *IEEE Transactions on Antennas and Propagation*, Vol. 44, No. 11, November 1996, pp. 1474-1481
- [6] R. K. Mishra, S. S. Pattnaik and N. Das, "Tuning of microstrip antenna on ferrite substrate," *IEEE Transactions on Antennas and Propagation*, Vol. 40, No. 2, February 1993, pp. 230-233
- [7] A. Hessel, "General characteristics of traveling wave antennas," Chapter 19 in R. E. Collin, F. J. Zucker, *Antenna Theory*, Part 2, McGraw-Hill, 1969
- [8] R. E. Collin, *Field Theory of Guided Waves*, IEEE Press, 2nd Ed., 1991, Chapter 9
- [9] S. Marci, R. Tiberio and A. Toccafondi, "Diffraction coefficients at edges in artificially soft and hard surfaces," *Electronic Letters*, Vol. 30, No. 3, November 1993, pp. 203-205
- [10] M. Albani, F. Capolino, S. Maci and R. Tiberio, "Diffraction at a thick screen including corrugations on the top face," *IEEE Transactions on Antennas and Propagation*, Vol. 45, No. 2, February 1997, pp. 277-283

6 Surface Wave Absorber Measurements

6.1 Introduction

Although soft boundaries form an electromagnetic superior solution for reducing the RCS resulting from edge diffracted waves, isotropic surface wave absorbers remain useful in many applications, even for RCS management of edge diffracted waves. For example, surface wave absorbers can be very effective in absorbing creeping waves when applied to the fuselage of a plane. Also, in the case of a surface discontinuity, there may be a problem with edge diffracted waves for one radar polarization only, depending on the nature of the surface discontinuity and its aspect angle. In such a case, an ordinary surface wave absorber (either E-type or H-type, depending on the case) would be a good substitute for a soft boundary. From this perspective it is obvious that there is a lot interest in determining the quality and efficacy of commercially available surface wave absorbers.

In order to fully characterize a surface wave absorber two physical quantities need to be measured: the attenuation constant α and the phase constant β , both in the direction of propagation. However, the two quantities can be combined into one complex phase constant $\beta = \beta' - j\beta'' = \beta' - j\alpha$, as is done in this chapter. (See also Section 2.5.)

Many applications of surface wave absorbing materials are accompanied with propagation of surface waves over planar or near-planar surfaces. A test cell for surface wave absorbing materials should therefore be capable of reproducing the properties of infinite plane surface wave propagation without introducing any other propagation or scattering mechanisms.

6.2 A Historical Overview of Surface Wave Measurement Techniques

6.2.1 The Aperture Method

One of the few ways to generate a plane surface wave is depicted in Figure 6.1. The method was first suggested by Barlow and Cullen [1]¹ in as early as 1951 and is still in use today. The method is based on the theory presented in Section 3.4.7. There, it was shown that a coated PEC will support one or more surface wave modes for certain angles of incidence of an illuminating plane wave (Fig. 3.6). Parallel polarized incident waves will cause E-type surface waves to propagate along the coating, only when they are incident at angles which are solutions of (Snell's law substituted into (3.43))

$$R_{//} = \frac{\eta_2 \cos(\theta_{2i}) - j\eta_1 \sqrt{1 - \left[\frac{k_2}{k_1} \sin(\theta_{2i})\right]^2} \tan \left[hk_1 \sqrt{1 - \left[\frac{k_2}{k_1} \sin(\theta_{2i})\right]^2} \right]}{\eta_2 \cos(\theta_{2i}) + j\eta_1 \sqrt{1 - \left[\frac{k_2}{k_1} \sin(\theta_{2i})\right]^2} \tan \left[hk_1 \sqrt{1 - \left[\frac{k_2}{k_1} \sin(\theta_{2i})\right]^2} \right]} = 0.$$

H-type surface waves will result from perpendicular polarized waves incident at angles which are solutions of (Snell's law substituted into (3.44))

$$R_{\perp} = \frac{\frac{\cos(\theta_{2i})}{\eta_2} + j \frac{\sqrt{1 - \left[\frac{k_2}{k_1} \sin(\theta_{2i})\right]^2}}{\eta_1} \cot \left[hk_1 \sqrt{1 - \left[\frac{k_2}{k_1} \sin(\theta_{2i})\right]^2} \right]}{\frac{\cos(\theta_{2i})}{\eta_2} - j \frac{\sqrt{1 - \left[\frac{k_2}{k_1} \sin(\theta_{2i})\right]^2}}{\eta_1} \cot \left[hk_1 \sqrt{1 - \left[\frac{k_2}{k_1} \sin(\theta_{2i})\right]^2} \right]} = 0.$$

Also, note that the use of the term "Brewster angle" is inappropriate here.

¹ The paper contains some errors which have been corrected in this text.

An experimental set-up as shown in Figure 3.6 is insufficient if the field of the surface wave is to be measured by a probe. Not only the field of the surface wave will be present above the coating, but also the field of the incident wave. (See equation (3.37a).) Therefore, part of the coating needs to be shielded from the incident plane wave, as shown in Figure 6.1.

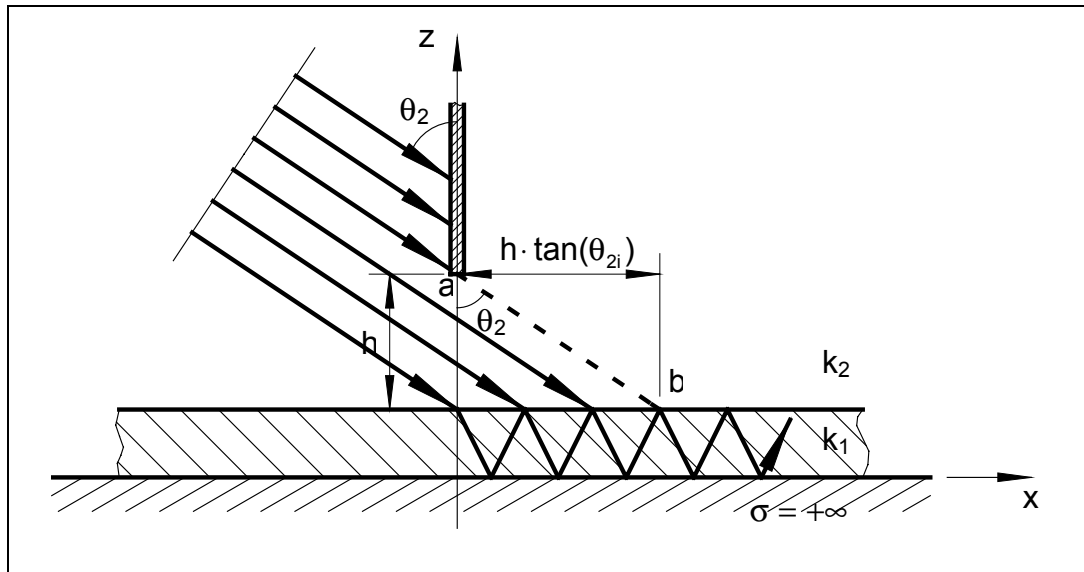


Figure 6.1: A method of generating plane surface waves (See text.)

If the wavelength is small compared with the height h of the aperture, ray-optics theory will give a first approximation to the effect of the screen, namely that below the shadow line ab there will be a plane wave travelling down into the coating, provided that the angle of incidence is chosen well. There will also be some surface wave energy in this region. The region right and above the shadow line ab will contain the field of the surface wave together with a small field contribution of diffracted waves coming from the edge of the aperture. Starting at a distance $b = h \cdot \tan(\theta_{2i})$ away from the aperture, the field distribution near ground level will approximate that of a plane surface wave.

A probe is used to measure the field intensity at different positions of the aperture. From these measurements the surface wave attenuation over a certain length of coating can be calculated. To determine the wavelength of the surface wave, a reflecting wall is placed at the end of the coating and the distance between two consecutive (rectified) maxima of the standing wave pattern is measured. Twice this distance corresponds to the wavelength of the surface wave.

The measurement technique described in this section is not without any defects. Firstly, it is impossible to generate a plane wave; in practice, it can only be approximated. Secondly, it is extremely difficult to determine at what angle unknown coatings under test should be illuminated. Moreover, this angle is often complex, implying that the incident wave should be inhomogeneous. Also, the surface wave field can not be isolated because of diffraction mechanisms. Finally, a probe for measuring the surface wave field will always interfere with the field.

6.2.2 The Broad-Band Radial Surface Wave Antenna

A plane surface wave can also be approximated by a radial surface wave at a large distance from its point of excitation. Radial surface waves can easily be excited using a radial surface wave antenna as in Figure 6.2.

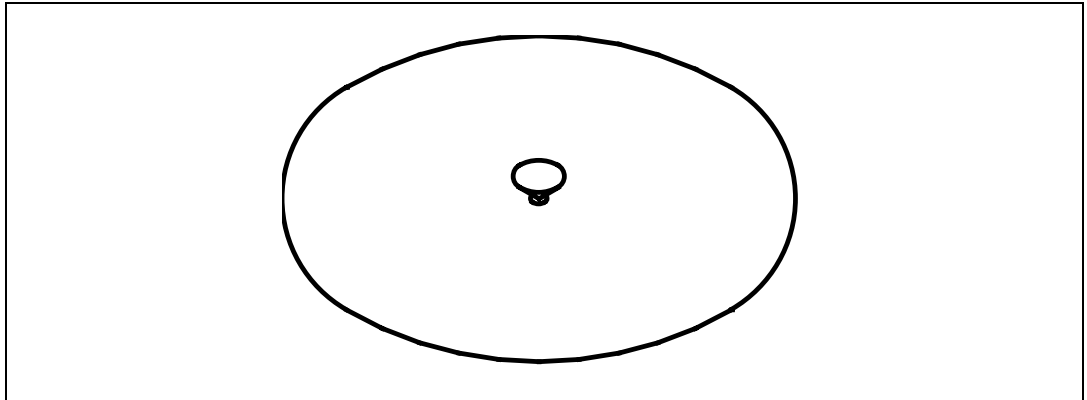


Figure 6.2: A broadband radial surface wave antenna; the groundplane diameter is about 1 meter

A similar set-up was used by Fernando and Barlow to make probe measurements of the surface wave field [2]. However, at The University of Hull this configuration has been used to obtain time domain data from reflection coefficient measurements in the frequency domain over the band 1GHz to 11GHz [3]. For this purpose, the cylindrical antenna described in [2] is replaced by a broad-band conical monopole antenna. The new antenna is optimized for broad-band performance and has a height of 50mm with a flare angle of 90°. (More information on designing conical monopoles can be found in [4].)

Frequency response or tracking error calibration is effected by measuring a coaxial line short circuit at the input to the conical monopole.

After calibration, two measurements can be performed. First, data is taken without coating the groundplane. The second measurement involves covering the groundplane with the material under test. For both measurements a peak in the time domain will occur at approximately $t = \frac{2r}{v}$, where r is the radius of the ground plane and v is the velocity of propagation. This peak in the time domain reflection coefficient data is caused by diffraction at the rim of the groundplane.

Only an average value of the phase constant β can be obtained by this technique because v is a function of frequency for the surface wave. Results are given in [3]. Also, the surface wave launching efficiency of the antenna and the reflection coefficient at the rim are unknown. Therefore, the attenuation data is only of qualitative value.

6.2.3 Loss Measurements of the Goubau-Line

Loss measurements of the Goubau-line are perhaps the most accurate surface wave loss measurements that have ever been made up to now. Clearly, the waves propagating along a Goubau-line are not plane surface waves but axial surface waves, which are easier to measure directly. Nonetheless, a lot can be learned from the techniques employed in these measurements.

Two methods have been reported that both refrain from using a probe to measure the surface wave field. In a first measurement technique [5], a Goubau-line resonator is formed by placing large circular plates at each end of the Goubau-line. The power is fed to and from the resonator by means of small coupling loops, one at each end plate. The attenuation of the Goubau-line is obtained by determining the half power bandwidth of the surface wave resonator. The only thing that is somewhat cumbersome about this method is the fact that the resonator needs to be retuned for each measurement at a different frequency. Also, in order to obtain maximum accuracy, the insertion loss and mutual coupling of the coupling loops should be known.

In the other measurement method [6], an axial surface wave is launched on the Goubau-line at one end by means of a launching horn. At the other end, the Goubau-line is terminated by a movable short. Both the attenuation constant α and the phase constant β can be inferred from two input impedance measurements with different line lengths. A third measurement with a line length shorter than in the previous measurements defines a phase reference plane to which the previous measurements are calibrated for frequency response (tracking error). Unlike the measurement techniques described earlier in this section, this method has no fundamental limitations. A technique very similar to this technique will be employed for measuring plane surface waves. This new technique will be presented in the next section.

6.3 A Plane Surface Wave Simulator Cell Based on a Partially Filled Rectangular Waveguide

6.3.1 Introduction

From the previous it has become clear that the generation of plane surface waves is not evident if also the presence of other propagating waves (e.g. the space wave and diffracted waves) has to be avoided. Moreover, in order to make accurate measurements, at least one surface wave calibration standard should be available.

It is, however, extremely difficult to meet the above-mentioned requirements with plane surface waves. Therefore, the new measurement technique here presented, will be based on the strategy of replacing the plane surface wave by another wave with similar properties but which suits itself better to attenuation and phase constant measurements. The waves propagating in a partially filled waveguide (Fig. 6.3) are proposed here as a replacement for the plane surface waves. A partially filled waveguide has the advantage of being completely shielded, and is hence less susceptible to noise and interference from the lab environment. When taken care for, only one mode will propagate inside the waveguide. Moreover, a short can be reproduced accurately and thus serve as a calibration standard.

Even from an intuitive approach can be seen that the waves propagating inside a partially filled waveguide of sufficient height have a lot in common with plane surface waves. In Chapter 3 was shown that, away from the material interface, the field of a surface wave decays exponentially. Putting a horizontal metallic wall (e.g. the upper wall of a waveguide) sufficiently high above the coated surface will influence the field of a plane surface wave only to a very small extent. Adding vertical metallic walls (e.g. those of a waveguide) will result in a sine or cosine dependence in the transversal direction for all field components. However, these additional sine or cosine factors are fully determined by the distance between the vertical walls (i.e. the width of the waveguide). The presence of vertical walls will also cause the complex phase constant β to be different from that of plane surface wave propagation. Again, this effect can easily be accounted for: the difference between both phase constants only depends upon the distance between the vertical walls. A rigorous proof for all statements made in this paragraph, will be given later in this chapter.

The complex phase constant of the wave in the partially filled waveguide can be inferred from input impedance measurements of the waveguide terminated by a short circuit at different positions.

The proposed measurement method will here only be validated for single layer materials that are linear, homogeneous and isotropic. There is however a high degree of similarity between the surface wave fields over single layer and multi-layer materials. For this reason it may be assumed that the measurement method presented in the section will be equally suited for the characterization of homogeneous linear isotropic multi-layer coatings.

6.3.2 The Partially Filled Rectangular Waveguide

The next two sections deal with the analysis of the waves propagating in a partially filled rectangular waveguide (Fig. 6.3) [7]. In this analysis, it will be assumed that the rectangular waveguide has perfectly conducting walls and that it is filled with two different media as depicted in Figure 6.3. The interface of these media is parallel with upper and lower wall of the rectangular waveguide. Both media are assumed to be homogeneous, linear and isotropic. The x-axis is chosen parallel with the propagation direction.

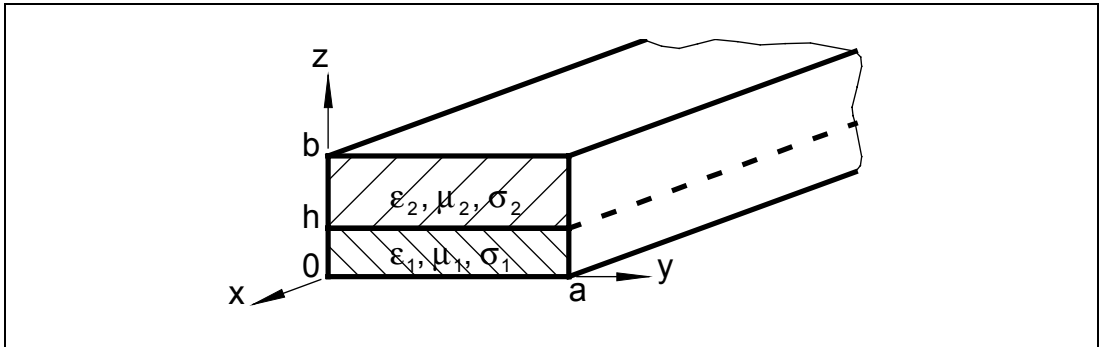


Figure 6.3: A partially filled rectangular waveguide; both media are assumed to be homogenous, linear and isotropic, the walls are perfectly conducting.

The partially filled rectangular waveguide is a 2D-uniform guiding structure. General Hertz potentials for 2D-uniform guiding structures were found in Section 2.5. Contrary to Chapter 3, the Hertz vector potential $\vec{\Pi}$ will here not only depend on the z-coordinate, but the y-coordinate as well.

Therefore,

$$\vec{\Pi} = \Pi(y, z)e^{-j\beta_x x} \vec{e}_z. \quad (1)$$

while

$$u_1 = z; \quad u_2 = x; \quad u_3 = y.$$

Substituting (1) into (2.10) results in general expressions for the field components of E-type waves in one of the media

$$\begin{aligned}
 E_z &= k^2 \Pi_e + \frac{\partial^2 \Pi_e}{\partial z^2}; \quad H_z = 0, \\
 E_x &= -j\beta_x \frac{\partial \Pi_e}{\partial z}; \quad H_x = (\sigma + j\omega\epsilon) \frac{\partial \Pi_e}{\partial y}, \\
 E_y &= \frac{\partial^2 \Pi_e}{\partial z \partial y}; \quad H_y = j\beta_x (\sigma + j\omega\epsilon) \Pi_e.
 \end{aligned} \tag{2}$$

From (2) it can be seen that the E-type waves in a partially filled rectangular waveguide are longitudinal section magnetic (LSM) waves. The magnetic field intensity \vec{H} has no component in the direction normal to the material interface ($H_z = 0$).

Substituting (1) into (2.11) leads general expressions for the field components of H-type waves in one of the media

$$\begin{aligned}
 H_z &= k^2 \Pi_m + \frac{\partial^2 \Pi_m}{\partial z^2}; \quad E_z = 0, \\
 H_x &= -j\beta_x \frac{\partial \Pi_m}{\partial z}; \quad E_x = -j\omega\mu \frac{\partial \Pi_m}{\partial y}, \\
 H_y &= \frac{\partial^2 \Pi_m}{\partial z \partial y}; \quad E_y = \beta_x \omega\mu \Pi_m.
 \end{aligned} \tag{3}$$

From (3) one can conclude that the H-type waves in a partially filled rectangular waveguide are longitudinal section electric (LSE) waves. The electric field intensity \vec{E} has no component in the direction normal to the material interface ($E_z = 0$).

6.3.3 E-Type Waves in a Partially Filled Rectangular Waveguide

A suitable Hertz function for medium 1 that satisfies the boundary conditions

$$E_x = E_z = 0 \text{ at } y = 0 \text{ and } 0 < y < +\infty ,$$

$$E_x = E_y = 0 \text{ at } z = 0$$

$$\text{is } \Pi_1 = A_1 \sin(s_{y1}y) \cos(s_{z1}z) e^{-j\beta_x x} . \quad (4)$$

Introducing (4) into (2)

$$E_{z1} = A_1 (k_1^2 - s_{z1}^2) \sin(s_{y1}y) \cos(s_{z1}z) e^{-j\beta_x x} , \quad (5a)$$

$$E_{x1} = j\beta_x A_1 s_{z1} \sin(s_{y1}y) \sin(s_{z1}z) e^{-j\beta_x x} , \quad (5b)$$

$$E_{y1} = -A_1 s_{y1} s_{z1} \cos(s_{y1}y) \sin(s_{z1}z) e^{-j\beta_x x} , \quad (5c)$$

$$H_{z1} = 0 , \quad (5d)$$

$$H_{x1} = (\sigma_1 + j\omega\epsilon_1) A_1 s_{y1} \cos(s_{y1}y) \cos(s_{z1}z) e^{-j\beta_x x} , \quad (5e)$$

$$H_{y1} = j\beta_x (\sigma_1 + j\omega\epsilon_1) A_1 \sin(s_{y1}y) \cos(s_{z1}z) e^{-j\beta_x x} . \quad (5f)$$

An additional boundary condition is

$$E_x = E_z = 0 \text{ at } y = a .$$

$$\text{Hence, } s_{y1}a = n\pi \Rightarrow s_{y1} = \frac{n\pi}{a} \quad (6)$$

where n is a positive integer different from zero.

n=0 corresponds to the solution for a partially filled parallel plate waveguide.

A suitable Hertz function for medium 2 that satisfies the boundary conditions

$$E_x = E_z = 0 \text{ at } y = 0 \text{ and } 0 < y < +\infty ,$$

$$E_x = E_y = 0 \text{ at } z = b$$

$$\text{is } \Pi_2 = A_2 \sin(s_{y2}y) \cos[s_{z2}(z - b)] e^{-j\beta_x x} . \quad (7)$$

Introducing (7) into (2)

$$E_{z2} = A_2 (k_2^2 - s_{z2}^2) \sin(s_{y2}y) \cos[s_{z2}(z - b)] e^{-j\beta_x x} , \quad (8a)$$

$$E_{x2} = j\beta_x A_2 s_{z2} \sin(s_{y2}y) \sin[s_{z2}(z - b)] e^{-j\beta_x x} , \quad (8b)$$

$$E_{y2} = -A_2 s_{y2} s_{z2} \cos(s_{y2}y) \sin[s_{z2}(z - b)] e^{-j\beta_x x} , \quad (8c)$$

$$H_{z2} = 0 , \quad (8d)$$

$$H_{x2} = (\sigma_2 + j\omega\epsilon_2) A_2 s_{y2} \cos(s_{y2}y) \cos[s_{z2}(z - b)] e^{-j\beta_x x} , \quad (8e)$$

$$H_{y2} = j\beta_x (\sigma_2 + j\omega\epsilon_2) A_2 \sin(s_{y2}y) \cos[s_{z2}(z - b)] e^{-j\beta_x x} . \quad (8f)$$

An additional boundary condition is

$$E_x = E_z = 0 \text{ at } y = a .$$

$$\text{Hence, } s_{y2}a = n\pi \Rightarrow s_{y2} = \frac{n\pi}{a} . \quad (9)$$

By virtue of (2.13), (2.15), (6) and (9)

$$s_{y1}^2 + s_{z1}^2 = \left(\frac{n\pi}{a}\right)^2 + s_{z1}^2 = s_1^2 = k_1^2 - \beta_x^2 \Rightarrow s_{z1} = +\sqrt{k_1^2 - \left(\frac{n\pi}{a}\right)^2 - \beta_x^2}, \quad (10)$$

$$s_{y2}^2 + s_{z2}^2 = \left(\frac{n\pi}{a}\right)^2 + s_{z2}^2 = s_2^2 = k_2^2 - \beta_x^2 \Rightarrow s_{z2} = +\sqrt{k_2^2 - \left(\frac{n\pi}{a}\right)^2 - \beta_x^2}. \quad (11)$$

Choosing the negative square roots would have no effect on the results.

The tangential components of \vec{E} and \vec{H} are continuous across the interface of two media. Furthermore, it was shown that $s_{y1} = s_{y2}$.

Hence,

$$E_{x1} = E_{x2} \text{ and } E_{y1} = E_{y2} \text{ at } z = h$$

$$\Rightarrow A_1 s_{z1} \sin(s_{z1}h) = -A_2 s_{z2} \sin[s_{z2}(b-h)], \quad (12)$$

$$\text{as well as } H_{x1} = H_{x2} \text{ and } H_{y1} = H_{y2} \text{ at } z = h$$

$$\Rightarrow (\sigma_1 + j\omega\epsilon_1)A_1 \cos(s_{z1}h) = (\sigma_2 + j\omega\epsilon_2)A_2 \cos[s_{z2}(b-h)]. \quad (13)$$

Note that (12) and (13) would have resulted in a set of contradictory equations, if $\vec{\Pi}$ were chosen in any direction other than the z-direction.

Dividing (12) by (13) yields

$$\frac{s_{z1}}{\sigma_1 + j\omega\epsilon_1} \tan(s_{z1}h) = -\frac{s_{z2}}{\sigma_2 + j\omega\epsilon_2} \tan[s_{z2}(b-h)] \quad (14)$$

or by virtue of (10) and (11)

$$\begin{aligned} & \frac{\sqrt{k_1^2 - \left(\frac{n\pi}{a}\right)^2 - \beta_x^2}}{\sigma_1 + j\omega\epsilon_1} \tan\left[h\sqrt{k_1^2 - \left(\frac{n\pi}{a}\right)^2 - \beta_x^2}\right] \\ &= -\frac{\sqrt{k_2^2 - \left(\frac{n\pi}{a}\right)^2 - \beta_x^2}}{\sigma_2 + j\omega\epsilon_2} \tan\left[(b-h)\sqrt{k_2^2 - \left(\frac{n\pi}{a}\right)^2 - \beta_x^2}\right] \end{aligned} \quad (15)$$

This dispersion equation is transcendental and can therefore only be solved numerically for β_x .

Letting $h = 0$ in (15), results in

$\beta_x = \sqrt{k_2^2 - \left(\frac{n\pi}{a}\right)^2 - \left(\frac{m\pi}{b}\right)^2}$, the dispersion equation of the TE_{nm} empty waveguide modes.

The dispersion equation for the TE_{nm} modes of the homogeneously filled waveguide is obtained by letting $h=b$ in (15).

6.3.4 H-Type Waves in a Partially Filled Rectangular Waveguide

A suitable Hertz function for medium 1 that satisfies the boundary conditions

$$E_x = E_z = 0 \text{ at } y = 0 \text{ and } 0 < y < +\infty ,$$

$$E_x = E_y = 0 \text{ at } z = 0$$

$$\text{is } \Pi_1 = A_1 \cos(s_{y1}y) \sin(s_{z1}z) e^{-j\beta_x x} . \quad (17)$$

Introducing (17) into (3)

$$H_{z1} = A_1 (k_1^2 - s_{z1}^2) \cos(s_{y1}y) \sin(s_{z1}z) e^{-j\beta_x x} , \quad (18a)$$

$$H_{x1} = -j\beta_x A_1 s_{z1} \cos(s_{y1}y) \cos(s_{z1}z) e^{-j\beta_x x} , \quad (18b)$$

$$H_{y1} = -A_1 s_{y1} s_{z1} \sin(s_{y1}y) \cos(s_{z1}z) e^{-j\beta_x x} , \quad (18c)$$

$$E_{z1} = 0 , \quad (18d)$$

$$E_{x1} = j\omega\mu_1 A_1 s_{y1} \sin(s_{y1}y) \sin(s_{z1}z) e^{-j\beta_x x} , \quad (18e)$$

$$E_{y1} = \beta_x \omega\mu_1 A_1 \cos(s_{y1}y) \sin(s_{z1}z) e^{-j\beta_x x} . \quad (18f)$$

An additional boundary condition is

$$E_x = E_z = 0 \text{ at } y = a .$$

$$\text{Hence, } s_{y1}a = n\pi \Rightarrow s_{y1} = \frac{n\pi}{a} \quad (19)$$

where n is a positive integer different from zero.

A suitable Hertz function for medium 2 that satisfies the boundary conditions

$$E_x = E_z = 0 \text{ at } y = 0 \text{ and } 0 < y < +\infty ,$$

$$E_x = E_y = 0 \text{ at } z = b$$

$$\text{is } \Pi_2 = A_2 \cos(s_{y2}y) \sin[s_{z2}(z - b)] e^{-j\beta_x x} . \quad (20)$$

Introducing (20) into (3)

$$H_{z2} = A_2 (k_2^2 - s_{z2}^2) \cos(s_{y2}y) \sin[s_{z2}(z - b)] e^{-j\beta_x x} , \quad (21a)$$

$$H_{x2} = -j\beta_x A_2 s_{z2} \cos(s_{y2}y) \cos[s_{z2}(z - b)] e^{-j\beta_x x} , \quad (21b)$$

$$H_{y2} = -A_2 s_{y2} s_{z2} \sin(s_{y2}y) \cos[s_{z2}(z - b)] e^{-j\beta_x x} , \quad (21c)$$

$$E_{z1} = 0 , \quad (21d)$$

$$E_{x2} = j\omega\mu_2 A_2 s_{y2} \sin(s_{y2}y) \sin[s_{z2}(z - b)] e^{-j\beta_x x} , \quad (21e)$$

$$E_{y2} = \beta_x \omega\mu_2 A_2 \cos(s_{y2}y) \sin[s_{z2}(z - b)] e^{-j\beta_x x} . \quad (21f)$$

An additional boundary condition is

$$E_x = E_z = 0 \text{ at } y = a .$$

$$\text{Hence, } s_{y2}a = n\pi \Rightarrow s_{y2} = \frac{n\pi}{a} . \quad (22)$$

By virtue of (2.13), (2.15), (19) and (22)

$$s_{y1}^2 + s_{z1}^2 = \left(\frac{n\pi}{a}\right)^2 + s_{z1}^2 = s_1^2 = k_1^2 - \beta_x^2 \Rightarrow s_{z1} = +\sqrt{k_1^2 - \left(\frac{n\pi}{a}\right)^2 - \beta_x^2}, \quad (23)$$

$$s_{y2}^2 + s_{z2}^2 = \left(\frac{n\pi}{a}\right)^2 + s_{z2}^2 = s_2^2 = k_2^2 - \beta_x^2 \Rightarrow s_{z2} = +\sqrt{k_2^2 - \left(\frac{n\pi}{a}\right)^2 - \beta_x^2}. \quad (24)$$

Choosing the negative square roots would have no effect on the results.

The tangential components of \vec{E} and \vec{H} are continuous across the interface of two media. Furthermore, it was shown that $s_{y1} = s_{y2}$.

Hence,

$$H_{x1} = H_{x2} \text{ and } H_{y1} = H_{y2} \text{ at } z = h$$

$$\Rightarrow A_1 s_{z1} \cos(s_{z1}h) = A_2 s_{z2} \cos[s_{z2}(b-h)], \quad (25)$$

$$\text{as well as } E_{x1} = E_{x2} \text{ and } E_{y1} = E_{y2} \text{ at } z = h$$

$$\Rightarrow \mu_1 A_1 \sin(s_{z1}h) = -\mu_2 A_2 \sin[s_{z2}(b-h)]. \quad (26)$$

Note that (26) and (25) would have resulted in a set of contradictory equations, if $\vec{\Pi}$ were chosen in any direction other than the z-direction.

Dividing (26) by (25) and multiplying both sides by $j\omega$ yields

$$\frac{j\omega\mu_1 \tan(s_{z1}h)}{s_{z1}} = -\frac{j\omega\mu_2 \tan[s_{z2}(b-h)]}{s_{z2}} \quad (27)$$

or by virtue of (23) and (24)

$$\begin{aligned} & \frac{j\omega\mu_1}{\sqrt{k_1^2 - \left(\frac{n\pi}{a}\right)^2 - \beta_x^2}} \tan\left[h\sqrt{k_1^2 - \left(\frac{n\pi}{a}\right)^2 - \beta_x^2}\right] \\ &= -\frac{j\omega\mu_2}{\sqrt{k_2^2 - \left(\frac{n\pi}{a}\right)^2 - \beta_x^2}} \tan\left[(b-h)\sqrt{k_2^2 - \left(\frac{n\pi}{a}\right)^2 - \beta_x^2}\right]. \end{aligned} \quad (28)$$

This dispersion equation is transcendental and can therefore only be solved numerically for β_x .

Letting $h = 0$ in (15), results in

$$\beta_x = \sqrt{k_2^2 - \left(\frac{n\pi}{a}\right)^2 - \left(\frac{m\pi}{b}\right)^2}, \text{ the dispersion equation of the } TM_{nm} \text{ empty}$$

waveguide modes.

The dispersion equation for the TM_{nm} modes of the homogeneously filled waveguide is obtained by letting $h=b$ in (28).

6.3.5 On the Relation between Partially Filled Rectangular Waveguide Modes and Plane Surface Waves

Compare the dispersion equations for plane surface waves, both E-type (3.12) and H-type (3.23) with those of the waves in a partially filled waveguide (14) and (27), respectively.

Dispersion equation for E-type plane surface wave modes:

$$\frac{s_{z1}}{\sigma_1 + j\omega\epsilon_1} \tan(s_{z1}h) = \frac{js_{z2}}{\sigma_2 + j\omega\epsilon_2} \quad (3.12)$$

Dispersion equation for E-type partially filled waveguide modes:

$$\frac{s_{z1}}{\sigma_1 + j\omega\epsilon_1} \tan(s_{z1}h) = -\frac{s_{z2}}{\sigma_2 + j\omega\epsilon_2} \tan[s_{z2}(b-h)] \quad (14)$$

Dispersion equation for H-type plane surface wave modes:

$$\frac{j\omega\mu_1}{s_{z1}} \tan(s_{z1}h) = -\frac{j\omega\mu_2}{js_{z2}} \quad (3.23)$$

Dispersion equation for H-type partially filled waveguide modes:

$$\frac{j\omega\mu_1}{s_{z1}} \tan(s_{z1}h) = -\frac{j\omega\mu_2}{s_{z2}} \tan[s_{z2}(b-h)] \quad (27)$$

The only significant difference between them is a factor $\tan[s_{z2}(b-h)]$ on the right hand side of the waveguide equations, which is replaced by $-j$ for plane surface waves.

However, one can show that

$$\lim_{\substack{(b-h)\alpha_{z2} \rightarrow +\infty \\ (b-h)\beta_{z2} \rightarrow 0}} \tan[s_{z2}(b-h)] = -j \quad (29)$$

where $s_{z2} = \beta_{z2} - j\alpha_{z2}$.

The proof is as follows:

$$\begin{aligned} \lim_{\substack{(b-h)\alpha_{z2} \rightarrow +\infty \\ (b-h)\beta_{z2} \rightarrow 0}} \tan[(b-h)s_{z2}] &= \lim_{\substack{(b-h)\alpha_{z2} \rightarrow +\infty \\ (b-h)\beta_{z2} \rightarrow 0}} \tan[(b-h)(\beta_{z2} - j\alpha_{z2})] \\ &= \lim_{\substack{(b-h)\alpha_{z2} \rightarrow +\infty \\ (b-h)\beta_{z2} \rightarrow 0}} \frac{\tan[(b-h)\beta_{z2}] - \tan[j(b-h)\alpha_{z2}]}{1 + \tan[(b-h)\beta_{z2}] \cdot \tan[j(b-h)\alpha_{z2}]} \quad [8, p. 15] \\ &= \lim_{\substack{(b-h)\alpha_{z2} \rightarrow +\infty \\ (b-h)\beta_{z2} \rightarrow 0}} \frac{\tan[(b-h)\beta_{z2}] - j \cdot \tanh[(b-h)\alpha_{z2}]}{1 + j \cdot \tan[(b-h)\beta_{z2}] \cdot \tanh[(b-h)\alpha_{z2}]} \quad [8, p. 31] \\ &= -j \quad [8, p. 29] \end{aligned}$$

It is possible that the requirement $(b-h)\alpha_{z2} \rightarrow +\infty$, is not met by thin samples and/or samples with low values for their permittivity and permeability (see also Section 3.4.5). The requirement $(b-h)\beta_{z2} \rightarrow 0$ may cause problems for sample materials with extremely high losses, because β_{z2} becomes highly negative (see Fig. 3.8). Although the factor $(b-h)$ gives an additional degree of freedom, it should not be chosen too small though. In practice, both requirements are usually met even by surface wave absorbing materials, as is demonstrated by Example 3.

If both requirements are met, the phase constants of the partially filled waveguide modes will differ from those of the plane surface wave modes by a known constant term only.

Namely, in view of (3.8a), (3.19a), (11) and (24)

$$\beta_{xS} \Big|_{\substack{(b-h)\alpha_{z2} \rightarrow +\infty \\ (b-h)\beta_{z2} \rightarrow 0}} = \sqrt{\beta_{xW}^2 \Big|_{\substack{(b-h)\alpha_{z2} \rightarrow +\infty \\ (b-h)\beta_{z2} \rightarrow 0}} + \left(\frac{n\pi}{a}\right)^2} \quad (30)$$

where β_S is the phase constant of a proper surface wave mode and β_W the phase constant of the corresponding partially filled waveguide mode.

The Plane Surface Wave Simulator Cell: Example 1

Constants:

$$c_0 := 299792458 \cdot \frac{\text{m}}{\text{sec}} \quad \mu_0 := 4 \cdot \pi \cdot 10^{-7} \cdot \frac{\text{henry}}{\text{m}} \quad \epsilon_0 := \frac{1}{c_0^2 \cdot \mu_0} \quad \epsilon_0 = 8.854 \cdot 10^{-12} \cdot \frac{\text{farad}}{\text{m}}$$

Enter the material parameters:

$$\sigma_1 := 0 \cdot \frac{\text{siemens}}{\text{m}} \quad \epsilon_{r1} := 2.33 - 0.001j \quad \mu_{r1} := 1 - 0j$$
$$\sigma_2 := 0 \cdot \frac{\text{siemens}}{\text{m}} \quad \epsilon_{r2} := 1 - 0j \quad \mu_{r2} := 1 - 0j$$

Enter the frequency:

$$f := 8.5 \cdot 10^9 \cdot \text{Hz} \quad \omega := 2 \cdot \pi \cdot f \quad \omega = 5.341 \cdot 10^{10} \cdot \text{Hz} \quad \lambda_0 := \frac{c_0}{f} \quad \lambda_0 = 0.035 \cdot \text{m}$$

Enter the thickness of the coating:

$$h := 0.00615 \cdot \text{m}$$

Complex wave numbers:

$$\epsilon_1 := \epsilon_{r1} \cdot \epsilon_0 \quad \epsilon_2 := \epsilon_{r2} \cdot \epsilon_0$$

$$\mu_1 := \mu_{r1} \cdot \mu_0 \quad \mu_2 := \mu_{r2} \cdot \mu_0$$

$$k_0 := \omega \sqrt{\epsilon_0 \cdot \mu_0} \quad k_0 = 178.147 \cdot \frac{\text{rad}}{\text{m}}$$

$$k_1 := \sqrt{-j \cdot \omega \mu_1 \cdot (\sigma_1 + j \cdot \omega \epsilon_1)} \quad k_1 = 271.929 - 0.058j \cdot \frac{\text{rad}}{\text{m}}$$

$$k_2 := \sqrt{-j \cdot \omega \mu_2 \cdot (\sigma_2 + j \cdot \omega \epsilon_2)} \quad k_2 = 178.147 \cdot \frac{\text{rad}}{\text{m}}$$

(k_2 must be smaller than k_1 !)

E-type proper surface wave modes:

$$F_{ES}(\beta_x) := \frac{\sqrt{k_1^2 - \beta_x^2}}{\sigma_1 + j \cdot \omega \varepsilon_1} \cdot \tan\left(h \cdot \sqrt{k_1^2 - \beta_x^2}\right) - \frac{\operatorname{Re}\left(\sqrt{\beta_x^2 - k_2^2}\right)}{\left|\operatorname{Re}\left(\sqrt{\beta_x^2 - k_2^2}\right)\right|} \cdot \frac{\sqrt{\beta_x^2 - k_2^2}}{\sigma_2 + j \cdot \omega \varepsilon_2}$$

$$\beta_x := \frac{k_1 + k_2}{2} \quad \beta_{xES} := \operatorname{root}(F_{ES}(\beta_x), \beta_x) \quad \beta_{xES} = 214.379 - 0.036j \cdot \frac{\text{rad}}{\text{m}}$$

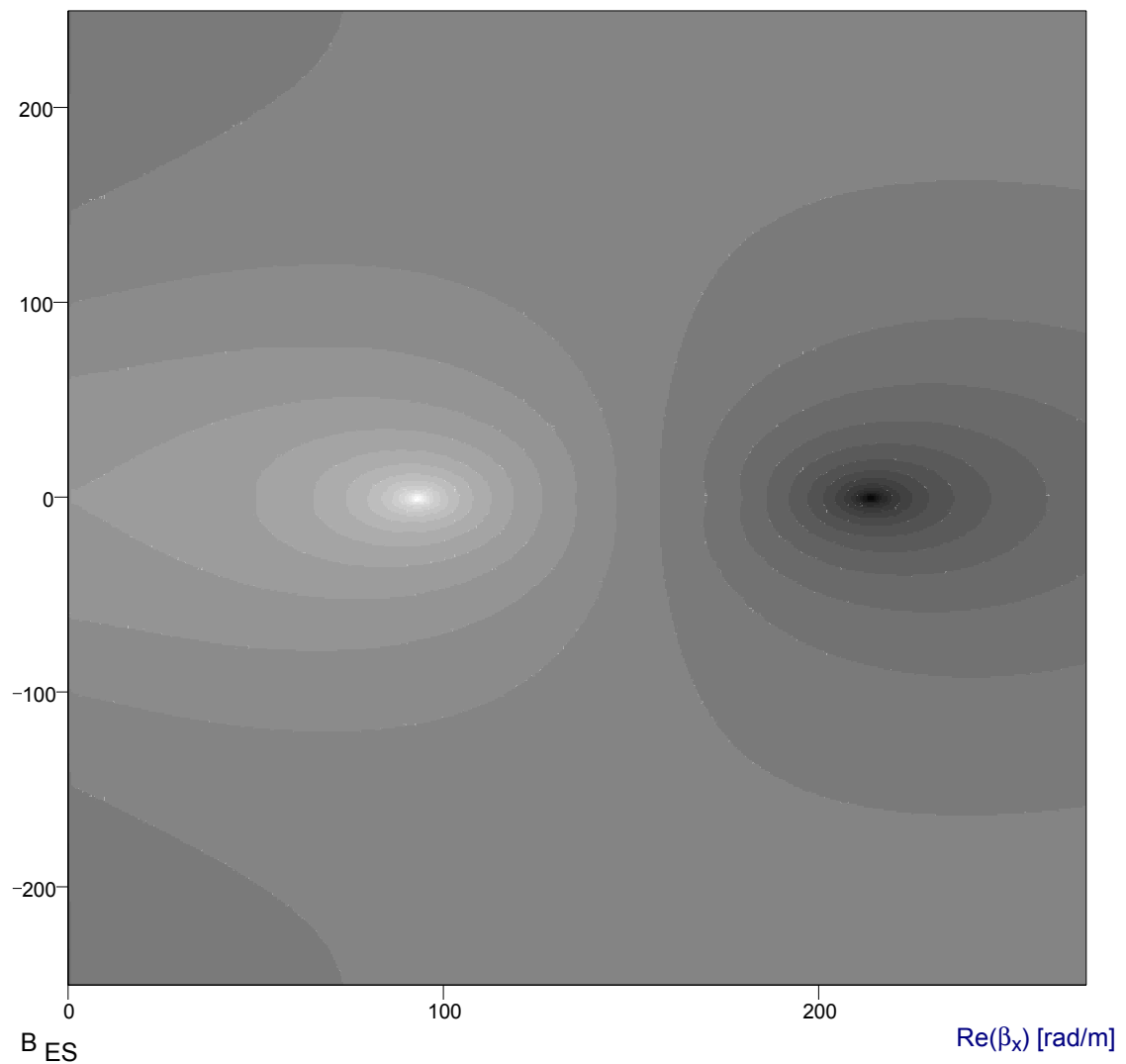
$$F_{ES}(\beta_{xES}) = 2.091 \cdot 10^{-9} - 1.441 \cdot 10^{-6} j \cdot \text{kg} \cdot \text{m}^2 \cdot \text{sec}^{-1} \cdot \text{coul}^{-2}$$

$$N := 301 \quad \text{Start}_x := 0 \cdot \frac{\text{rad}}{\text{m}} \quad \text{End}_x := \operatorname{Re}(k_1) \quad \text{Start}_y := -250 \cdot \frac{\text{rad}}{\text{m}} \quad \text{End}_y := 250 \cdot \frac{\text{rad}}{\text{m}}$$

$$x := 0, 1 \dots N \quad y := 0, 1 \dots N \quad \Delta x := \frac{\text{End}_x - \text{Start}_x}{N} \quad \Delta y := \frac{\text{End}_y - \text{Start}_y}{N}$$

$$B_{ES_{x,y}} := \log \left[\left| F_{ES} \left[\left(\text{Start}_x + x \cdot \Delta x \right) + \left[j \cdot \left(\text{Start}_y + y \cdot \Delta y \right) \right] \right] \right| \cdot \frac{\text{siemens} \cdot \text{m}}{\text{m} \cdot \text{rad}} \right]$$

$\operatorname{Im}(\beta_x)$ [rad/m]



Waveguide dimensions and mode:

$$a := 0.022860 \cdot \text{m} \quad b := 0.034040 \cdot \text{m} \quad n := 1$$

E-type modes in partially filled waveguide:

$$F_{EW1}(\beta_x) := \frac{\sqrt{k_1^2 - \left(\frac{n \cdot \pi}{a}\right)^2 - \beta_x^2}}{\sigma_1 + j \cdot \omega \varepsilon_1} \cdot \tan \left[h \cdot \sqrt{k_1^2 - \left(\frac{n \cdot \pi}{a}\right)^2 - \beta_x^2} \right]$$

$$F_{EW2}(\beta_x) := \frac{\sqrt{k_2^2 - \left(\frac{n \cdot \pi}{a}\right)^2 - \beta_x^2}}{\sigma_2 + j \cdot \omega \varepsilon_2} \cdot \tan \left[(b - h) \cdot \sqrt{k_2^2 - \left(\frac{n \cdot \pi}{a}\right)^2 - \beta_x^2} \right]$$

$$F_{EW}(\beta_x) := F_{EW1}(\beta_x) + F_{EW2}(\beta_x)$$

$$\beta_x := \sqrt{\beta_{xES}^2 - \left(\frac{n \cdot \pi}{a}\right)^2} \quad \beta_{xEW} := \text{root}(F_{EW}(\beta_x), \beta_x) \quad \beta_{xEW} = 164.618 - 0.047j \cdot \frac{\text{rad}}{\text{m}}$$

$$F_{ES}(\beta_{xES}) = 2.091 \cdot 10^{-9} - 1.441 \cdot 10^{-6} j \cdot \text{kg} \cdot \text{m}^2 \cdot \text{sec}^{-1} \cdot \text{coul}^{-2}$$

$$\beta_{xEWc} := \sqrt{\beta_{xEW}^2 + \left(\frac{n \cdot \pi}{a}\right)^2} \quad \beta_{xEWc} = 214.442 - 0.036j \cdot \frac{\text{rad}}{\text{m}} \quad \beta_{xEW} = 164.618 - 0.047j \cdot \frac{\text{rad}}{\text{m}}$$

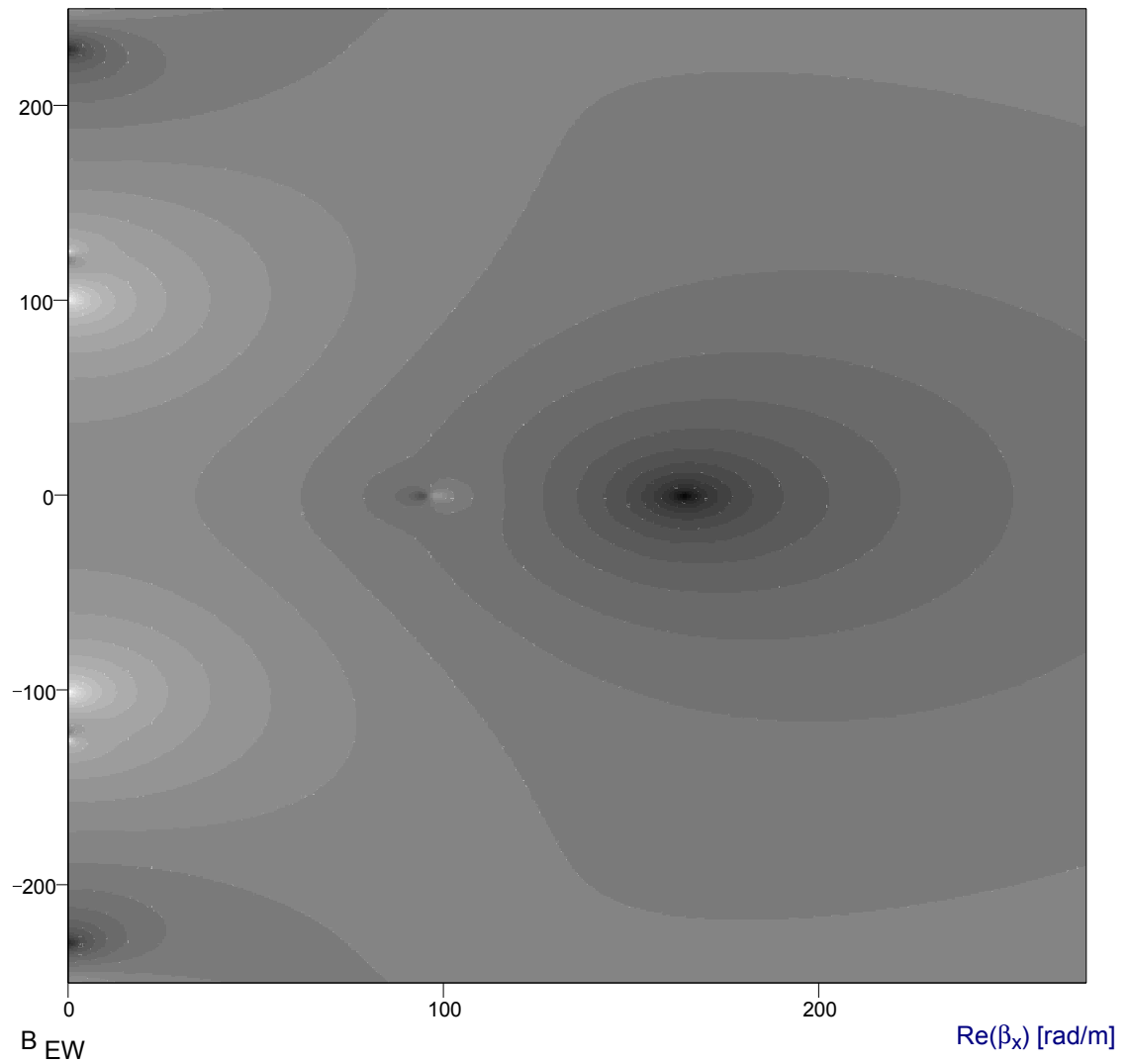
$$\frac{|\beta_{xEWc}| - |\beta_{xES}|}{|\beta_{xES}|} = 0.03 \cdot \% \quad \frac{|\beta_{xEWc}| - |\beta_{xES}|}{|k_1| - |k_2|} = 0.067 \cdot \%$$

$$N := 301 \quad \text{Start}_x := 0 \cdot \frac{\text{rad}}{\text{m}} \quad \text{End}_x := \text{Re}(k_1) \quad \text{Start}_y := -250 \cdot \frac{\text{rad}}{\text{m}} \quad \text{End}_y := 250 \cdot \frac{\text{rad}}{\text{m}}$$

$$x := 0, 1 \dots N \quad y := 0, 1 \dots N \quad \Delta x := \frac{\text{End}_x - \text{Start}_x}{N} \quad \Delta y := \frac{\text{End}_y - \text{Start}_y}{N}$$

$$B_{EW_{x,y}} := \log \left[\left| F_{EW} \left[\left(\text{Start}_x + x \cdot \Delta x \right) + \left[j \cdot \left(\text{Start}_y + y \cdot \Delta y \right) \right] \right] \right| \cdot \frac{\text{siemens}}{\text{m}} \cdot \frac{\text{m}}{\text{rad}} \right]$$

$\text{Im}(\beta_x)$ [rad/m]



The Plane Surface Wave Simulator Cell: Example 2

Constants:

$$c_0 := 299792458 \cdot \frac{\text{m}}{\text{sec}} \quad \mu_0 := 4 \cdot \pi \cdot 10^{-7} \cdot \frac{\text{henry}}{\text{m}} \quad \varepsilon_0 := \frac{1}{c_0^2 \cdot \mu_0} \quad \varepsilon_0 = 8.854 \cdot 10^{-12} \cdot \frac{\text{farad}}{\text{m}}$$

Enter the material parameters:

$$\sigma_1 := 0 \cdot \frac{\text{siemens}}{\text{m}} \quad \varepsilon_{r1} := 2.33 - 0.001j \quad \mu_{r1} := 1 - 0j$$

$$\sigma_2 := 0 \cdot \frac{\text{siemens}}{\text{m}} \quad \varepsilon_{r2} := 1 - 0j \quad \mu_{r2} := 1 - 0j$$

Enter the frequency:

$$f := 8.5 \cdot 10^9 \cdot \text{Hz} \quad \omega := 2 \cdot \pi \cdot f \quad \omega = 5.341 \cdot 10^{10} \cdot \text{Hz} \quad \lambda_0 := \frac{c_0}{f} \quad \lambda_0 = 0.035 \cdot \text{m}$$

Enter the thickness of the coating:

$$h := 0.00325 \cdot \text{m}$$

Complex wave numbers:

$$\varepsilon_1 := \varepsilon_{r1} \cdot \varepsilon_0 \quad \varepsilon_2 := \varepsilon_{r2} \cdot \varepsilon_0$$

$$\mu_1 := \mu_{r1} \cdot \mu_0 \quad \mu_2 := \mu_{r2} \cdot \mu_0$$

$$k_0 := \omega \sqrt{\varepsilon_0 \cdot \mu_0} \quad k_0 = 178.147 \cdot \frac{\text{rad}}{\text{m}}$$

$$k_1 := \sqrt{-j \cdot \omega \mu_1 \cdot (\sigma_1 + j \cdot \omega \varepsilon_1)} \quad k_1 = 271.929 - 0.058j \cdot \frac{\text{rad}}{\text{m}}$$

$$k_2 := \sqrt{-j \cdot \omega \mu_2 \cdot (\sigma_2 + j \cdot \omega \varepsilon_2)} \quad k_2 = 178.147 \cdot \frac{\text{rad}}{\text{m}}$$

(k_2 must be smaller than k_1 !)

E-type proper surface wave modes:

$$F_{ES}(\beta_x) := \frac{\sqrt{k_1^2 - \beta_x^2}}{\sigma_1 + j \cdot \omega \epsilon_1} \cdot \tan\left(h \cdot \sqrt{k_1^2 - \beta_x^2}\right) - \frac{\operatorname{Re}\left(\sqrt{\beta_x^2 - k_2^2}\right)}{\left|\operatorname{Re}\left(\sqrt{\beta_x^2 - k_2^2}\right)\right|} \cdot \frac{\sqrt{\beta_x^2 - k_2^2}}{\sigma_2 + j \cdot \omega \epsilon_2}$$

$$\beta_x := \frac{k_1 + k_2}{2} \quad \beta_{xES} := \operatorname{root}(F_{ES}(\beta_x), \beta_x) \quad \beta_{xES} = 188.666 - 0.009j \cdot \frac{\text{rad}}{\text{m}}$$

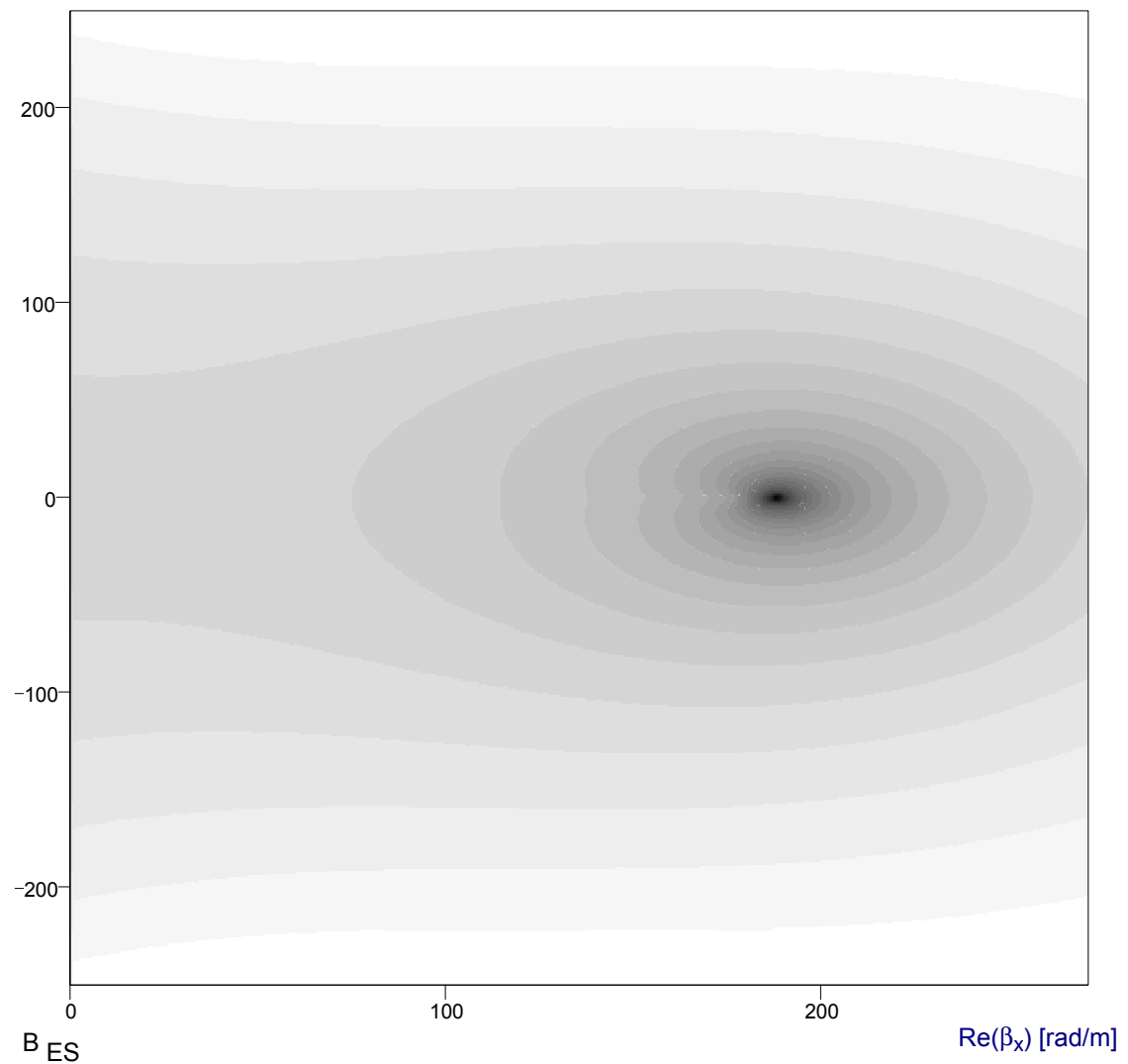
$$F_{ES}(\beta_{xES}) = -4.649 \cdot 10^{-6} + 9.477 \cdot 10^{-4} j \cdot \text{kg} \cdot \text{m}^2 \cdot \text{sec}^{-1} \cdot \text{coul}^{-2}$$

$$N := 301 \quad \text{Start}_x := 0 \cdot \frac{\text{rad}}{\text{m}} \quad \text{End}_x := \operatorname{Re}(k_1) \quad \text{Start}_y := -250 \cdot \frac{\text{rad}}{\text{m}} \quad \text{End}_y := 250 \cdot \frac{\text{rad}}{\text{m}}$$

$$x := 0, 1 \dots N \quad y := 0, 1 \dots N \quad \Delta x := \frac{\text{End}_x - \text{Start}_x}{N} \quad \Delta y := \frac{\text{End}_y - \text{Start}_y}{N}$$

$$B_{ES_{x,y}} := \log\left[\left|F_{ES}\left(\left(\text{Start}_x + x \cdot \Delta x\right) + \left[j \cdot \left(\text{Start}_y + y \cdot \Delta y\right)\right]\right)\right| \cdot \frac{\text{siemens} \cdot \text{m}}{\text{m} \cdot \text{rad}}\right]$$

$\operatorname{Im}(\beta_x)$ [rad/m]



Waveguide dimensions and mode:

$$a := 0.022860 \cdot \text{m} \quad b := 0.034040 \cdot \text{m} \quad n := 1$$

E-type modes in partially filled waveguide:

$$F_{EW1}(\beta_x) := \frac{\sqrt{k_1^2 - \left(\frac{n \cdot \pi}{a}\right)^2 - \beta_x^2}}{\sigma_1 + j \cdot \omega \varepsilon_1} \cdot \tan \left[h \cdot \sqrt{k_1^2 - \left(\frac{n \cdot \pi}{a}\right)^2 - \beta_x^2} \right]$$

$$F_{EW2}(\beta_x) := \frac{\sqrt{k_2^2 - \left(\frac{n \cdot \pi}{a}\right)^2 - \beta_x^2}}{\sigma_2 + j \cdot \omega \varepsilon_2} \cdot \tan \left[(b - h) \cdot \sqrt{k_2^2 - \left(\frac{n \cdot \pi}{a}\right)^2 - \beta_x^2} \right]$$

$$F_{EW}(\beta_x) := F_{EW1}(\beta_x) + F_{EW2}(\beta_x)$$

$$\beta_x := \sqrt{\beta_{xES}^2 - \left(\frac{n \cdot \pi}{a}\right)^2} \quad \beta_{xEW} := \text{root}(F_{EW}(\beta_x), \beta_x) \quad \beta_{xEW} = 130.216 - 0.012j \cdot \frac{\text{rad}}{\text{m}}$$

$$F_{ES}(\beta_{xES}) = -4.649 \cdot 10^{-6} + 9.477 \cdot 10^{-4} j \cdot \text{kg} \cdot \text{m}^2 \cdot \text{sec}^{-1} \cdot \text{coul}^{-2}$$

$$\beta_{xEWc} := \sqrt{\beta_{xEW}^2 + \left(\frac{n \cdot \pi}{a}\right)^2} \quad \beta_{xEWc} = 189.321 - 0.008j \cdot \frac{\text{rad}}{\text{m}} \quad \beta_{xEW} = 130.216 - 0.012j \cdot \frac{\text{rad}}{\text{m}}$$

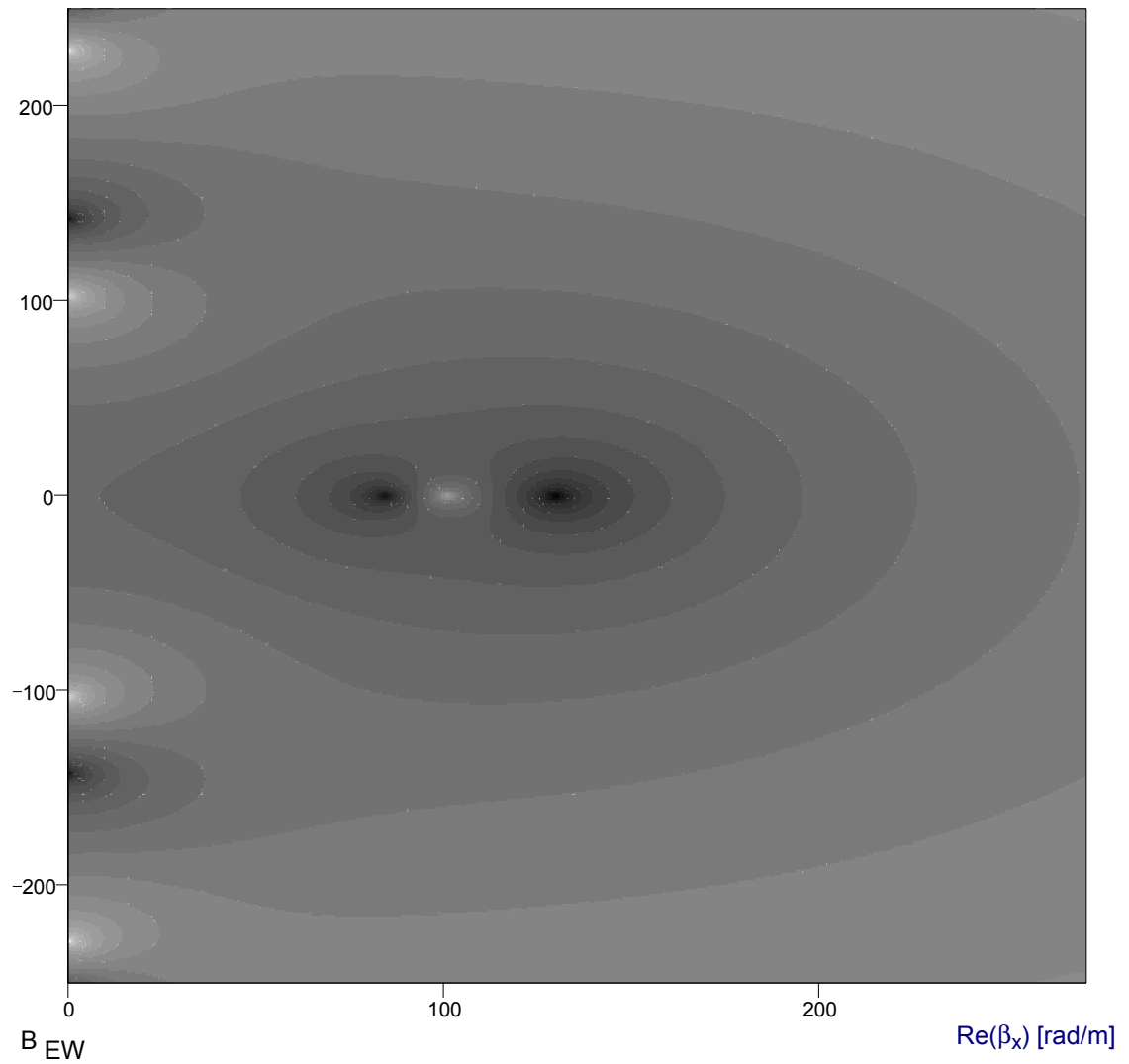
$$\frac{|\beta_{xEWc}| - |\beta_{xES}|}{|\beta_{xES}|} = 0.347 \cdot \% \quad \frac{|\beta_{xEWc}| - |\beta_{xES}|}{|k_1| - |k_2|} = 0.699 \cdot \%$$

$$N := 301 \quad \text{Start}_x := 0 \cdot \frac{\text{rad}}{\text{m}} \quad \text{End}_x := \text{Re}(k_1) \quad \text{Start}_y := -250 \cdot \frac{\text{rad}}{\text{m}} \quad \text{End}_y := 250 \cdot \frac{\text{rad}}{\text{m}}$$

$$x := 0, 1 \dots N \quad y := 0, 1 \dots N \quad \Delta x := \frac{\text{End}_x - \text{Start}_x}{N} \quad \Delta y := \frac{\text{End}_y - \text{Start}_y}{N}$$

$$B_{EW_{x,y}} := \log \left[\left| F_{EW} \left[(\text{Start}_x + x \cdot \Delta x) + [j \cdot (\text{Start}_y + y \cdot \Delta y)] \right] \right| \cdot \frac{\text{siemens} \cdot \text{m}}{\text{m} \cdot \text{rad}} \right]$$

$\text{Im}(\beta_x)$ [rad/m]



The Plane Surface Wave Simulator Cell: Example 3

Constants:

$$c_0 := 299792458 \cdot \frac{\text{m}}{\text{sec}} \quad \mu_0 := 4 \cdot \pi \cdot 10^{-7} \cdot \frac{\text{henry}}{\text{m}} \quad \varepsilon_0 := \frac{1}{c_0^2 \cdot \mu_0} \quad \varepsilon_0 = 8.854 \cdot 10^{-12} \cdot \frac{\text{farad}}{\text{m}}$$

Enter the material parameters:

$$\begin{aligned} \sigma_1 &:= 0 \cdot \frac{\text{siemens}}{\text{m}} & \varepsilon_{r1} &:= 7.4 - 0.15j & \mu_{r1} &:= 1.4 - 0.48j \\ \sigma_2 &:= 0 \cdot \frac{\text{siemens}}{\text{m}} & \varepsilon_{r2} &:= 1 - 0j & \mu_{r2} &:= 1 - 0j \end{aligned}$$

Enter the frequency:

$$f := 8.6 \cdot 10^9 \cdot \text{Hz} \quad \omega := 2 \cdot \pi \cdot f \quad \omega = 5.404 \cdot 10^{10} \cdot \text{Hz} \quad \lambda_0 := \frac{c_0}{f} \quad \lambda_0 = 0.035 \cdot \text{m}$$

Enter the thickness of the coating:

$$h := 0.00075 \cdot \text{m}$$

Complex wave numbers:

$$\varepsilon_1 := \varepsilon_{r1} \cdot \varepsilon_0 \quad \varepsilon_2 := \varepsilon_{r2} \cdot \varepsilon_0$$

$$\mu_1 := \mu_{r1} \cdot \mu_0 \quad \mu_2 := \mu_{r2} \cdot \mu_0$$

$$k_0 := \omega \sqrt{\varepsilon_0 \cdot \mu_0} \quad k_0 = 180.243 \cdot \frac{\text{rad}}{\text{m}}$$

$$k_1 := \sqrt{-j \cdot \omega \mu_1 \cdot (\sigma_1 + j \cdot \omega \varepsilon_1)} \quad k_1 = 587.412 - 104.031j \cdot \frac{\text{rad}}{\text{m}}$$

(k_2 must be smaller than k_1 !)

$$k_2 := \sqrt{-j \cdot \omega \mu_2 \cdot (\sigma_2 + j \cdot \omega \varepsilon_2)} \quad k_2 = 180.243 \cdot \frac{\text{rad}}{\text{m}}$$

E-type proper surface wave modes:

$$F_{ES}(\beta_x) := \frac{\sqrt{k_1^2 - \beta_x^2}}{\sigma_1 + j \cdot \omega \varepsilon_1} \cdot \tan\left(h \cdot \sqrt{k_1^2 - \beta_x^2}\right) - \frac{\operatorname{Re}\left(\sqrt{\beta_x^2 - k_2^2}\right)}{\left|\operatorname{Re}\left(\sqrt{\beta_x^2 - k_2^2}\right)\right|} \cdot \frac{\sqrt{\beta_x^2 - k_2^2}}{\sigma_2 + j \cdot \omega \varepsilon_2}$$

$$\beta_x := \frac{k_1 + k_2}{2} \quad \beta_{xES} := \operatorname{root}(F_{ES}(\beta_x), \beta_x) \quad \beta_{xES} = 182.647 - 2.328j \cdot \frac{\operatorname{rad}}{\operatorname{m}}$$

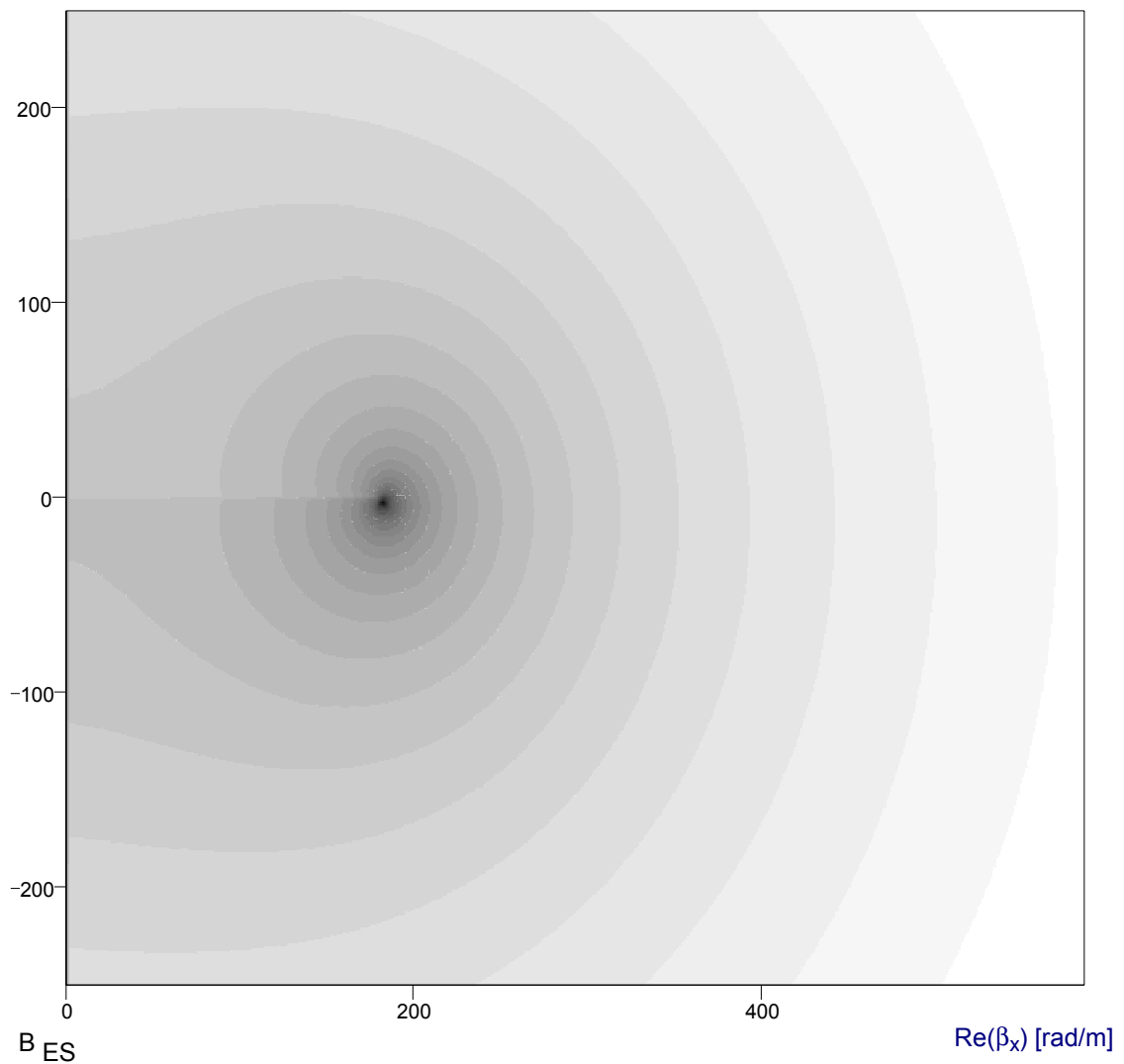
$$F_{ES}(\beta_{xES}) = -2.203 \cdot 10^{-4} + 6.845 \cdot 10^{-4} j \cdot \operatorname{kg} \cdot \operatorname{m}^2 \cdot \operatorname{sec}^{-1} \cdot \operatorname{coul}^{-2}$$

$$N := 301 \quad \operatorname{Start}_x := 0 \cdot \frac{\operatorname{rad}}{\operatorname{m}} \quad \operatorname{End}_x := \operatorname{Re}(k_1) \quad \operatorname{Start}_y := -250 \cdot \frac{\operatorname{rad}}{\operatorname{m}} \quad \operatorname{End}_y := 250 \cdot \frac{\operatorname{rad}}{\operatorname{m}}$$

$$x := 0, 1 \dots N \quad y := 0, 1 \dots N \quad \Delta x := \frac{\operatorname{End}_x - \operatorname{Start}_x}{N} \quad \Delta y := \frac{\operatorname{End}_y - \operatorname{Start}_y}{N}$$

$$B_{ES_{x,y}} := \log \left[\left| F_{ES} \left[\left(\operatorname{Start}_x + x \cdot \Delta x \right) + \left[j \cdot \left(\operatorname{Start}_y + y \cdot \Delta y \right) \right] \right] \right| \cdot \frac{\operatorname{siemens}}{\operatorname{m}} \cdot \frac{\operatorname{m}}{\operatorname{rad}} \right]$$

$\operatorname{Im}(\beta_x)$ [rad/m]



Waveguide dimensions and mode:

$$a := 0.022860 \cdot \text{m} \quad b := 0.034040 \cdot \text{m} \quad n := 1$$

E-type modes in partially filled waveguide:

$$F_{EW1}(\beta_x) := \frac{\sqrt{k_1^2 - \left(\frac{n \cdot \pi}{a}\right)^2 - \beta_x^2}}{\sigma_1 + j \cdot \omega \varepsilon_1} \cdot \tan \left[h \cdot \sqrt{k_1^2 - \left(\frac{n \cdot \pi}{a}\right)^2 - \beta_x^2} \right]$$

$$F_{EW2}(\beta_x) := \frac{\sqrt{k_2^2 - \left(\frac{n \cdot \pi}{a}\right)^2 - \beta_x^2}}{\sigma_2 + j \cdot \omega \varepsilon_2} \cdot \tan \left[(b - h) \cdot \sqrt{k_2^2 - \left(\frac{n \cdot \pi}{a}\right)^2 - \beta_x^2} \right]$$

$$F_{EW}(\beta_x) := F_{EW1}(\beta_x) + F_{EW2}(\beta_x)$$

$$\beta_x := \sqrt{\beta_{xES}^2 - \left(\frac{n \cdot \pi}{a}\right)^2} \quad \beta_{xEW} := \text{root}(F_{EW}(\beta_x), \beta_x) \quad \beta_{xEW} = 122.142 - 3.364j \cdot \frac{\text{rad}}{\text{m}}$$

$$F_{ES}(\beta_{xES}) = -2.203 \cdot 10^{-4} + 6.845 \cdot 10^{-4} j \cdot \text{kg} \cdot \text{m}^2 \cdot \text{sec}^{-1} \cdot \text{coul}^{-2}$$

$$\beta_{xEWc} := \sqrt{\beta_{xEW}^2 + \left(\frac{n \cdot \pi}{a}\right)^2} \quad \beta_{xEWc} = 183.844 - 2.235j \cdot \frac{\text{rad}}{\text{m}} \quad \beta_{xEW} = 122.142 - 3.364j \cdot \frac{\text{rad}}{\text{m}}$$

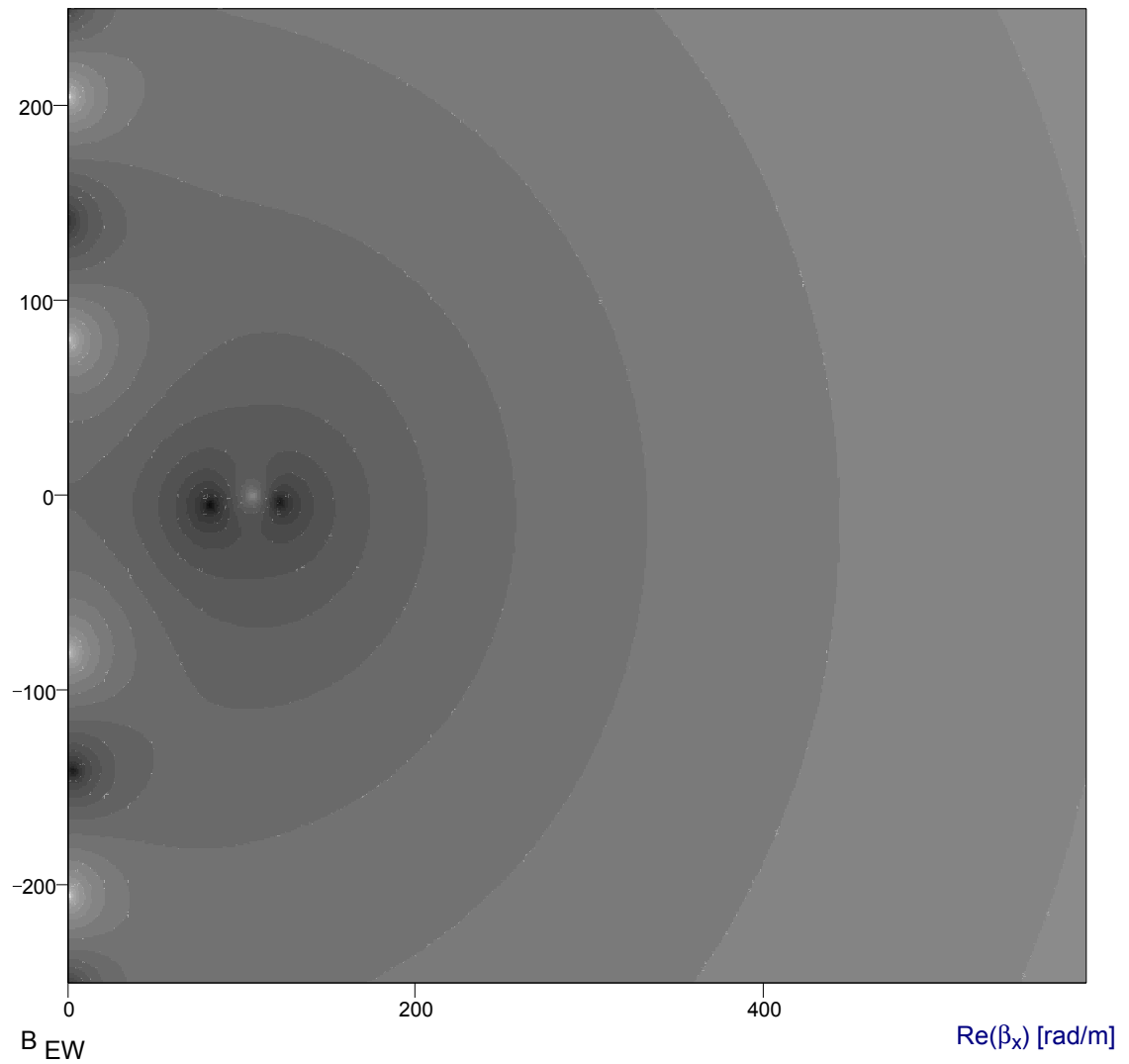
$$\frac{|\beta_{xEWc}| - |\beta_{xES}|}{|\beta_{xES}|} = 0.655 \cdot \% \quad \frac{|\beta_{xEWc}| - |\beta_{xES}|}{|k_1| - |k_2|} = 0.287 \cdot \%$$

$$N := 301 \quad \text{Start}_x := 0 \cdot \frac{\text{rad}}{\text{m}} \quad \text{End}_x := \text{Re}(k_1) \quad \text{Start}_y := -250 \cdot \frac{\text{rad}}{\text{m}} \quad \text{End}_y := 250 \cdot \frac{\text{rad}}{\text{m}}$$

$$x := 0, 1 \dots N \quad y := 0, 1 \dots N \quad \Delta x := \frac{\text{End}_x - \text{Start}_x}{N} \quad \Delta y := \frac{\text{End}_y - \text{Start}_y}{N}$$

$$B_{EW_{x,y}} := \log \left[\left| F_{EW} \left[(\text{Start}_x + x \cdot \Delta x) + [j \cdot (\text{Start}_y + y \cdot \Delta y)] \right] \right| \cdot \frac{\text{siemens} \cdot \text{m}}{\text{rad}} \right]$$

$\text{Im}(\beta_x)$ [rad/m]



6.3.6 The Plane Surface Wave Simulator Cell

A plane surface wave simulator cell (Fig. 6.4) has been designed to measure the complex phase constant of a fundamental E-mode plane surface wave mode at X-band frequencies. The experimental system can be used to measure materials up to approximately 8mm in thickness. A sample of the material under test is placed on the floor of the test cell over its entire length, 800mm for this design. The first section of the test cell, ①, is a section of standard X-band waveguide. A coax to waveguide adaptor fits to the input of the test cell. Along the length of section ①, the sample is tapered in the H-plane to provide a matched transition between the empty and partially filled waveguide sections. The transition converts the fundamental empty waveguide mode TE_{10} into a fundamental ($n=1$) partially filled waveguide mode. After this transition, the waveguide height is increased to 34.04mm via a taper (section ②) on the upper horizontal wall of the waveguide. A taper from 10.16mm to 34.04 mm (the height of a WG10 S-band waveguide) is quite common in industry and will not convert a lot of fundamental mode energy into higher order modes. Section ③ will support the fundamental partially filled waveguide mode that resembles the plane surface wave. At the furthest end, the test cell is terminated with a short circuit ④. The test cell can be opened at the top. This makes fastening the test material a lot easier. However, this also implies that the waveguide has to be cut along its length. The cut is parallel with the H-plane and located in a corner of the waveguide as field intensities are at their lowest there. Also, the wall thickness of the waveguide is an odd multiple of the trapping distance of a standard WG16 X-band waveguide flange. The screws are positioned at an even multiple of this distance. Detailed engineering drawings are included at the end of this section.

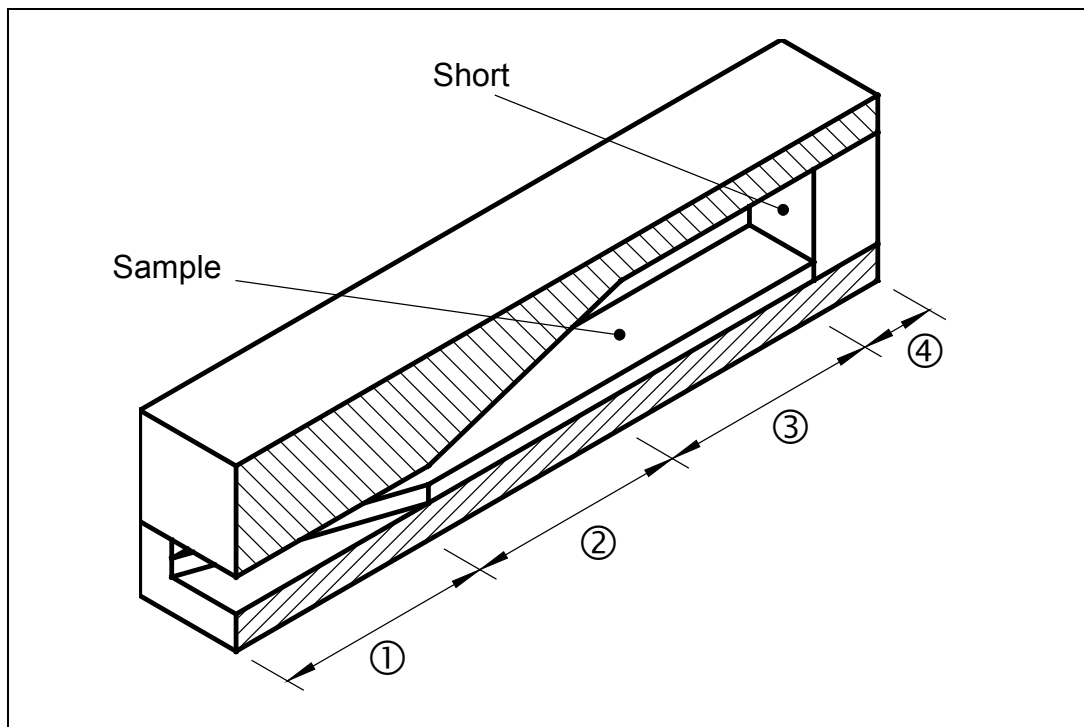


Figure 6.4: Cutaway view of the plane surface wave simulator cell (not to scale)

Two or more measurements of the input impedance Z_{in} are made the plane surface wave simulator cell terminated by a short circuit at different positions. From this, the complex propagation constant of the fundamental partially filled waveguide mode in section ③ can be obtained as follows.

The input impedance Z_{in} of a transmission line of length ℓ and terminated by a short circuit is given by the following expression

$$Z_{in} = jZ_c \tan(\beta\ell) \quad (31)$$

where Z_c is the characteristic impedance of the transmission line.

Rearranging (31) for Z_c gives

$$Z_c = \frac{Z_{in}}{j \cdot \tan(\beta\ell)} = -jZ_{in} \cot(\beta\ell). \quad (32)$$

The wave impedance of a waveguide corresponds to the characteristic impedance of a transmission line. Moreover, the wave impedance is constant over the length of section ③. Hence, for two input impedance measurements made with a short circuit in two different positions:

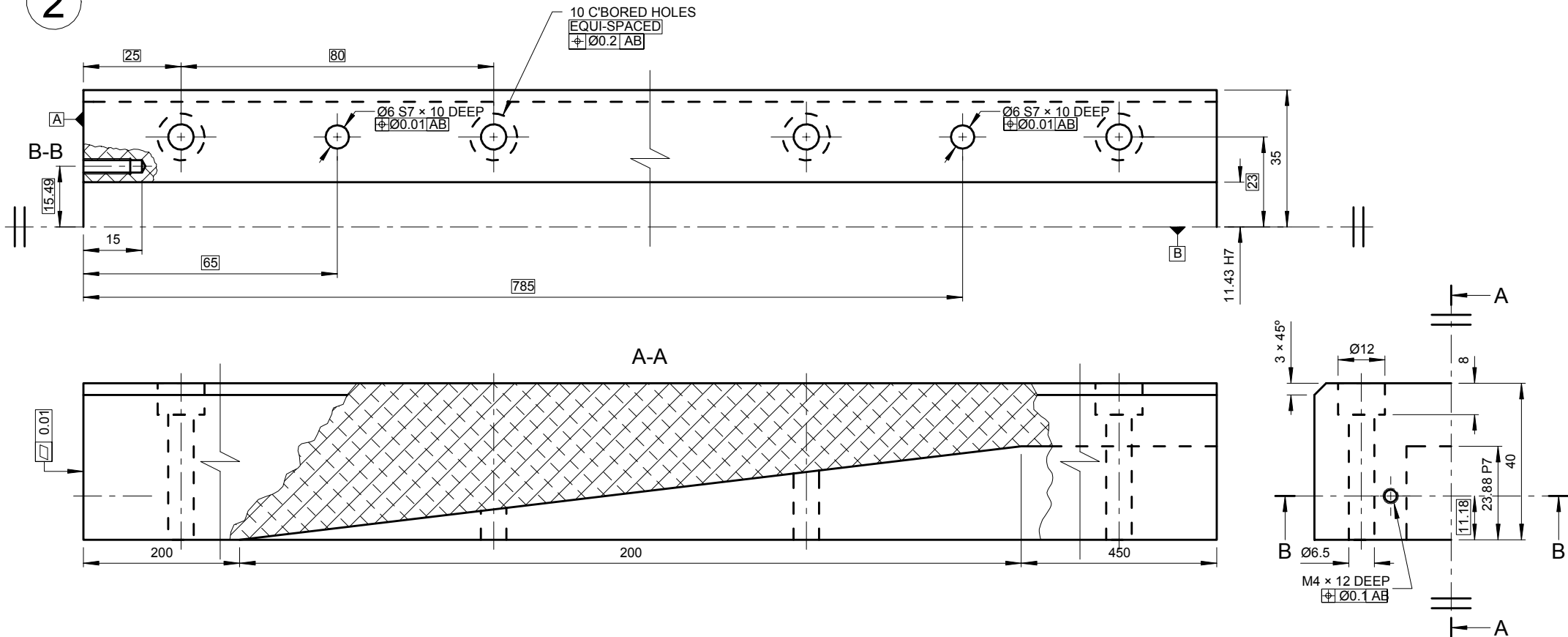
$$\begin{aligned} -jZ_{in1} \cot(\beta_m \ell_1) &= -jZ_{in2} \cot(\beta_m \ell_2) \\ \Rightarrow Z_{in1} \cot(\beta_m \ell_1) &= Z_{in2} \cot(\beta_m \ell_2) \end{aligned} \quad (33)$$

where β_m is the measured complex phase constant of the fundamental partially filled waveguide mode in section ③.

Equation (33) is a transcendental and can therefore only be solved numerically for β_m . In general, equation (33) will have more than one solution. There are two ways of finding the right solution. If the permittivity and permeability of the material under test is known from other measurements, the correct solution will be the solution closest to the theoretical value of β_s . However, in many cases, very little is known on the electromagnetic properties of surface wave absorbing materials. For these materials, more than two input impedance measurements are needed, resulting in additional equations similar to (33). The correct solution in this case is the solution which all equations have in common.

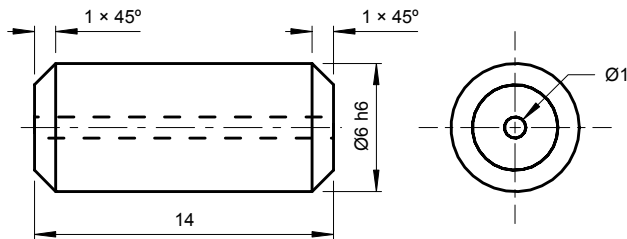
The input impedance data is obtained from reflection measurements made with the aid of a vector network analyser (VNA). Here, the reflection measurements are calibrated for tracking error (variations in magnitude and phase frequency response) using an additional measurement which defines the phase reference plane. The remaining two systematic errors are reduced using time domain filtering. The dimensions of the test cell ensure the time domain response of the sample is isolated from other error responses. Note that the directivity error is not only caused by leakage signals in the separation device of the VNA but is also due to residual reflection effects of test cables, adaptors and waveguide transitions between the signal separation device and the measurement plane. Source match error is particularly a problem when measuring very high or very low impedances (large mismatch at the measurement plane) [9].

2



- MATERIAL: ALUMINIUM
- USE STAINLESS STEEL SOCKET CAP SCREWS

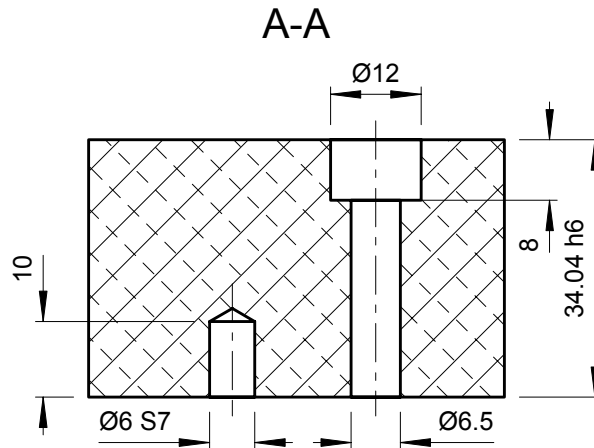
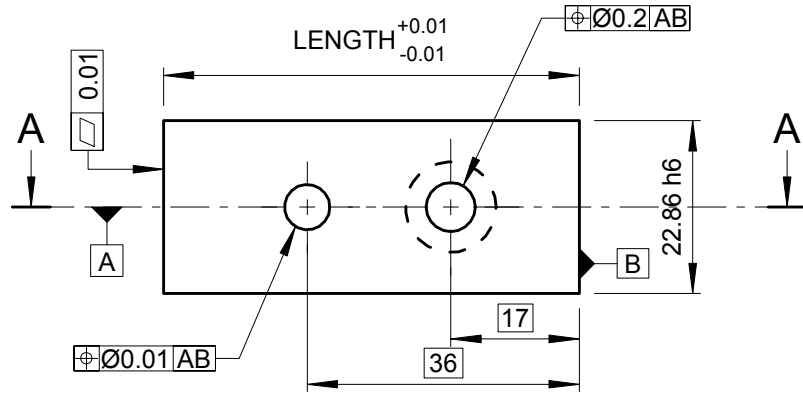
3



- ORIGINAL SCALE: 4:1 ON A3
- MATERIAL: STAINLESS STEEL

TITLE			
MEASUREMENT CELL			
THE UNIVERSITY OF HULL			
	DRAWN BY	S. Y. M. R. STROOBANDT	DRAWING
	APPROVED BY	F. C. SMITH	2 OF 3
	DATE	4 OCTOBER 1996	ORIGINAL SCALE
			DIMENSIONS IN MILLIMETERS

4 5 6



PART	LENGTH
4	250
5	55
6	50

- MATERIAL: ALUMINIUM
- USE A STAINLESS STEEL SOCKET CAP SCREW

TITLE		
MEASUREMENT CELL		
THE UNIVERSITY OF HULL		
	DRAWN BY S. Y. M. R. STROOBANDT	DRAWING 3 OF 3
	APPROVED BY F. C. SMITH	ORIGINAL SCALE 1:1 ON A4
	DATE 8 OCTOBER 1996	DIMENSIONS IN MILLIMETERS

6.3.7 Measurement Results

Measurements have been performed using high molecular weight polyethylene (HMW-PE). Material thicknesses of 6.15mm and 3.25mm have been used. Because polyethylene has very low losses, only results relating to phase constants have been calculated. The measurement of lossy materials is made marginally easier by the reduction in the magnitude of the source match error.

The cell has only been used to interrogate the fundamental E-type plane surface wave mode because only a probe-type coax to waveguide adaptor was available. However, the same test cell could also be used to interrogate the fundamental H-type plane surface wave mode by employing a loop-type coax to waveguide adaptor.

Results for measurements of the fundamental E-type plane surface wave mode are presented on the following pages. The tabulated quantities are:

β_{S_th} is the theoretical predicted value for the phase constant of the proper fundamental E-type plane surface wave; this value is obtained from equation (3.13), using measured data of ϵ_r and μ_r ,

$\beta_{W_th\&c}$ is the theoretical value for the phase constant of the fundamental E-type partially filled waveguide mode (eq. (15)), corrected for horizontal confinement (eq. (30)),

$\beta_{m\&c}$ is the value for the measured phase constant of the fundamental E-type partially filled waveguide mode, obtained from Z_{in1} , Z_{in2} and equation (33), also corrected for horizontal confinement (eq. (30)),

$$\text{relative error} = \frac{|\beta_{m\&c}| - |\beta_{S_th}|}{|\beta_{S_th}|}, \quad (34)$$

$$\text{nominal error} = \frac{|\beta_{m\&c}| - |\beta_{S_th}|}{|k_1| - |k_2|}, \quad (35)$$

and finally, the relative estimated uncertainty in $\beta_{m\&c}$ due to measurement uncertainties in Z_{in1} and Z_{in2} are given by

$$\frac{\partial \beta_{m\&c}}{\partial Z_1} \text{ and } \frac{\partial \beta_{m\&c}}{\partial Z_2}, \text{ respectively.}$$

If the measurement uncertainties ΔZ_{in1} and ΔZ_{in2} were known, then the total estimated uncertainty in $\beta_{m\&c}$ could be calculated as follows

$$\Delta \beta_{m\&c} = \sqrt{\left(\frac{\partial \beta_{m\&c}}{\partial Z_{in1}} \cdot \Delta Z_{in1} \right)^2 + \left(\frac{\partial \beta_{m\&c}}{\partial Z_{in2}} \cdot \Delta Z_{in2} \right)^2}. \quad (36)$$

However, in practice, it is extremely difficult to make reasonable estimations of the measurement uncertainties ΔZ_{in1} and ΔZ_{in2} ; the values specified in the VNA manual are very pessimistic worst-case values and hence not realistic.

The results show good agreement between the measured and predicted values. Due to the higher impedance mismatch between the empty and partially filled sections of waveguide, an increase in ripple is seen in the data corresponding to the 6.15mm sample. However, improved tapering between the empty and partially filled sections would reduce this error. Care should also be taken when fastening the sample in the test cell. Air gaps between the sample and the bottom of the test cell can significantly affect the results.

The Plane Surface Wave Simulator Cell

Measurement Results for a 6.15mm Thick HMW-PE Sample

Physical constants

c_0 (m/s)	299 792 458
μ_0 (H/m)	1.257E-06
ε_0 (F/m)	8.854E-12

Material parameters

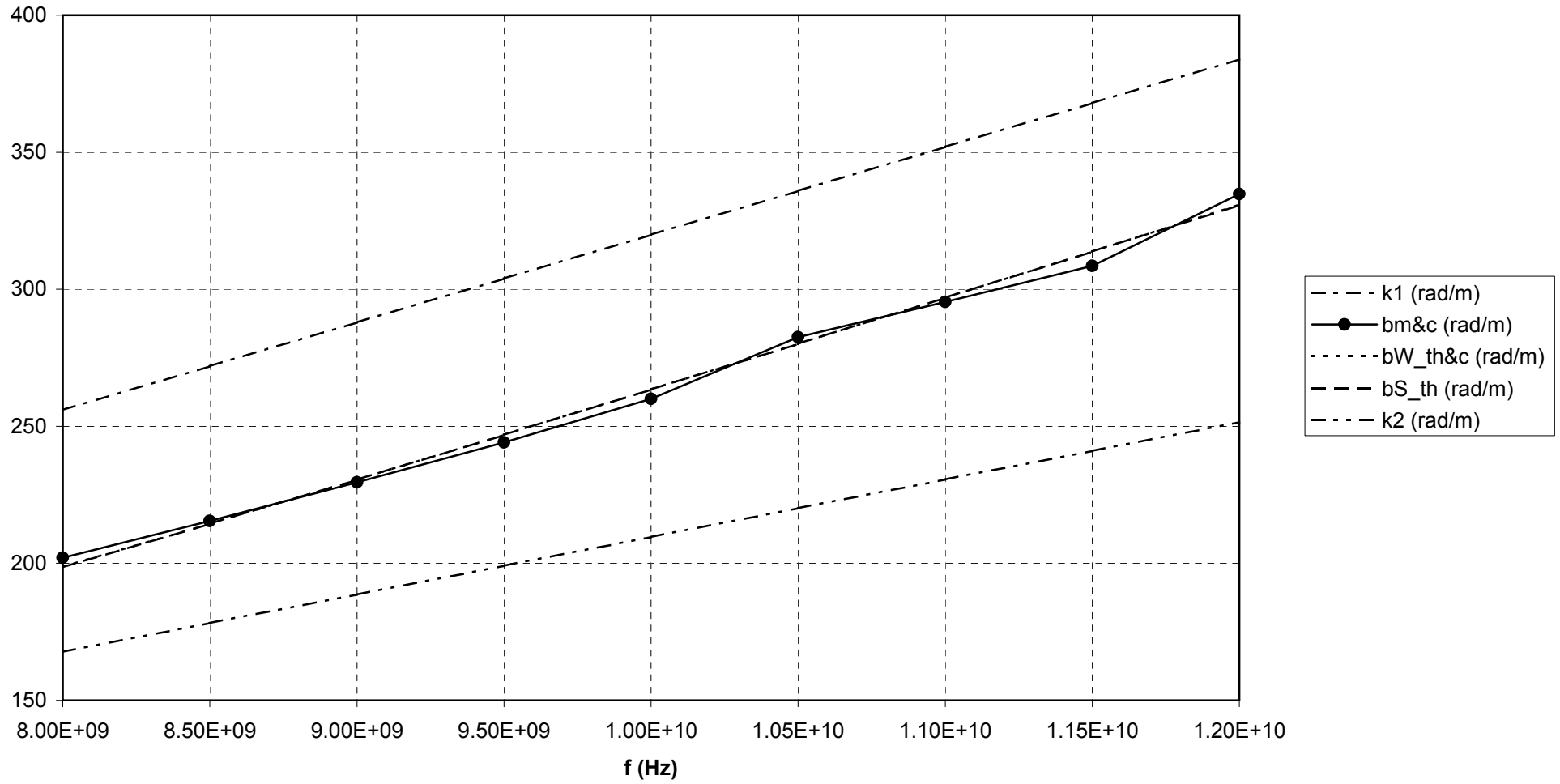
	medium 1	medium 2
ε_r	2.33	1.00
μ_r	1.00	1.00
ε (F/m)	2.063E-11	8.854E-12
μ (H/m)	1.257E-06	1.257E-06
h (m)	6.000E-03	

Results

f (Hz)	β_{S_th} (rad/m)	$\beta_{W_th\&c}$ (rad/m)	X_{in1} (Ω)	X_{in2} (Ω)	$\beta_{m\&c}$ (rad/m)	rel. err.	nom. err.	$\partial\beta_{m\&c}/\partial Z_{in1}$ (rad·m ⁻¹ · Ω^{-1})	$\partial\beta_{m\&c}/\partial Z_{in2}$ (rad·m ⁻¹ · Ω^{-1})
8.00E+09	198.5	198.7	+12.4	+75.8	202.0	+1.7%	+3.9%	NC	NC
8.50E+09	214.4	214.4	+46.1	-168	215.4	+0.5%	+1.1%	3.65E-04	3.18E-03
9.00E+09	230.5	230.5	+122	-46.7	229.5	-0.4%	-1.0%	5.68E-03	1.48E-02
9.50E+09	246.9	246.9	-361	-13.3	244.1	-1.1%	-2.6%	9.61E-04	2.61E-02
1.00E+10	263.4	263.4	-102	+12.5	260.0	-1.3%	-3.1%	5.08E-03	4.12E-02
1.05E+10	280.1	280.1	-59.0	+44.9	282.6	+0.9%	+2.1%	1.75E-02	2.30E-02
1.10E+10	296.9	296.9	-32.4	+74.0	295.4	-0.5%	-1.2%	3.05E-02	1.33E-02
1.15E+10	313.8	313.8	-25.5	+196	308.5	-1.7%	-4.2%	2.71E-02	3.52E-03
1.20E+10	330.7	331.0	-34.0	+865	334.7	+1.2%	+3.0%	1.29E-02	5.06E-04

See text for more information on the tabulated quantities. NC means "Not Converging."

HMW-PE 6.15mm



The Plane Surface Wave Simulator Cell

Measurement Results for a 3.25mm Thick HMW-PE Sample

Physical constants

c_0 (m/s)	299 792 458
μ_0 (H/m)	1.257E-06
ϵ_0 (F/m)	8.854E-12

Material parameters

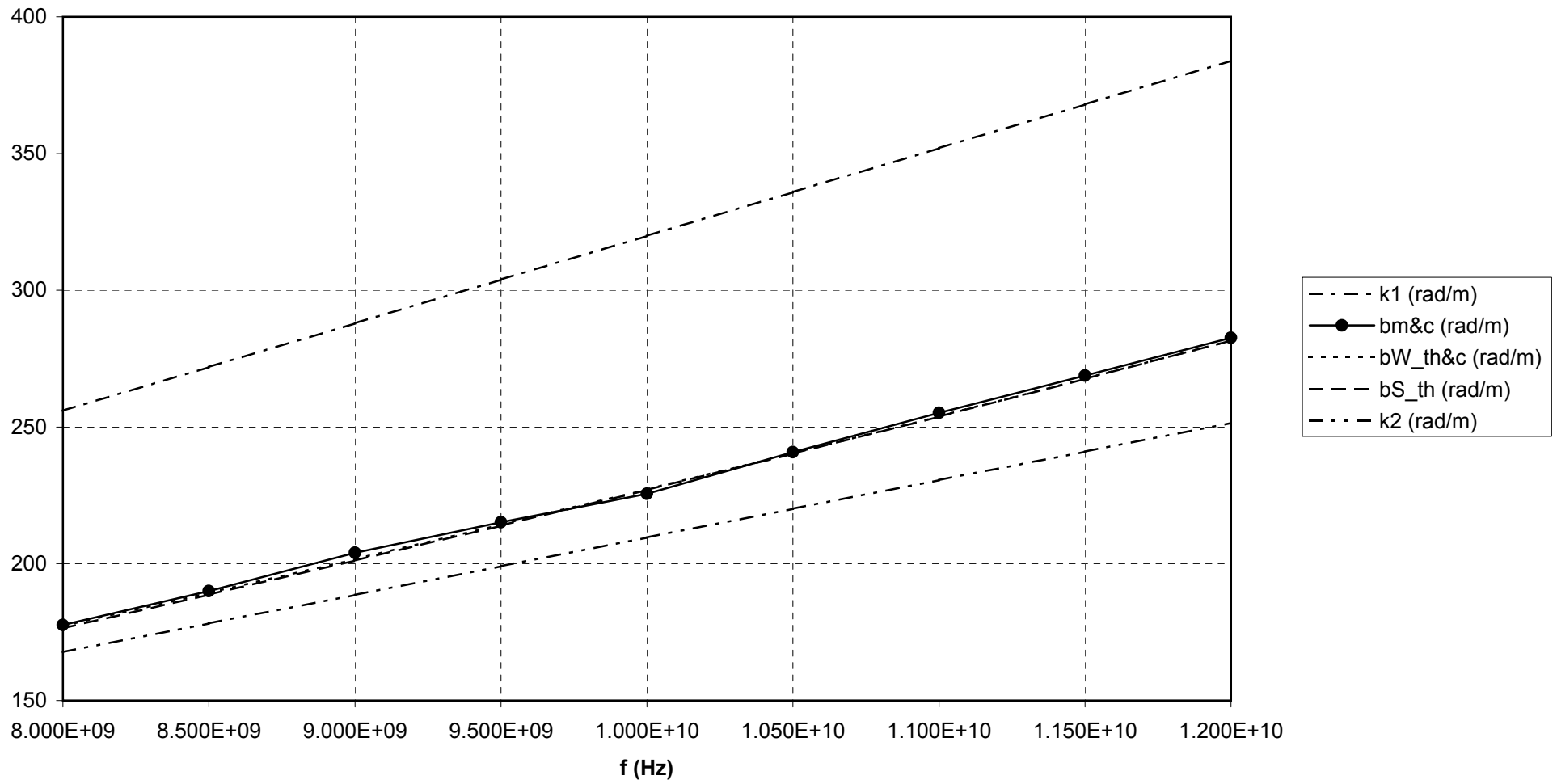
	medium 1	medium 2
ϵ_r	2.33	1.00
μ_r	1.00	1.00
ϵ (F/m)	2.063E-11	8.854E-12
μ (H/m)	1.257E-06	1.257E-06
h (m)	3.250E-03	

Results

f (Hz)	β_{S_th} (rad/m)	$\beta_{W_th\&c}$ (rad/m)	X_{in1} (Ω)	X_{in2} (Ω)	$\beta_{m\&c}$ (rad/m)	rel. err.	nom. err.	$\partial\beta_{m\&c}/\partial Z_{in1}$ (rad·m ⁻¹ · Ω^{-1})	$\partial\beta_{m\&c}/\partial Z_{in2}$ (rad·m ⁻¹ · Ω^{-1})
8.000E+09	176.4	177.2	-2.0	+20.3	177.6	+0.7%	+1.4%	7.84E-04	7.73E-03
8.500E+09	188.7	189.3	+16.5	+44.3	190.0	+0.7%	+1.4%	NC	NC
9.000E+09	201.2	201.7	+29.9	-42.0	204.0	+1.4%	+2.9%	2.09E-02	1.49E-02
9.500E+09	213.9	214.3	+76.9	-530	215.2	+0.6%	+1.2%	4.90E-03	7.11E-04
1.000E+10	227.0	227.2	+36.5	+161	225.6	-0.6%	-1.2%	NC	NC
1.050E+10	240.2	240.4	+41.1	-132	240.8	+0.2%	+0.5%	1.69E-02	5.28E-03
1.100E+10	253.8	253.9	+70.6	-55.8	255.2	+0.5%	+1.1%	1.32E-02	1.67E-02
1.150E+10	267.6	267.6	+83.4	-58.9	268.8	+0.5%	+1.0%	1.18E-02	1.66E-02
1.200E+10	281.7	281.7	+96.7	-67.6	282.6	+0.3%	+0.7%	1.06E-02	1.52E-02

See text for more information on the tabulated quantities. NC means "Not Converging."

HMW-PE 3.25mm



6.4 Conclusions

Although soft boundaries form an electromagnetic superior solution for reducing the RCS resulting from edge diffracted waves, isotropic surface wave absorbers remain useful in many applications, even for RCS management of edge diffracted waves.

A new measuring apparatus based on a partially filled rectangular waveguide has been developed for determining the attenuation constant and phase constant of plane surface waves propagating along metal-backed surface wave absorbing materials. Measurements were performed which validate this new measuring method.

6.5 References

- [1] H. M. Barlow and A. L. Cullen, "Surface waves," *Proceedings of the Institution of Electrical Engineers*, Vol. 100, Part III, No. 68, Nov. 1953, pp. 329-347
- [2] W. M. G. Fernando, H. E. M. Barlow, "An investigation of the properties of radial cylindrical surface waves launched over flat reactive surfaces," *Proceedings of the Institution of Electrical Engineers*, Vol. 103, Part B, May 1956, pp. 307-318
- [3] F. C. Smith and S. Stroobandt, "The measurement of surface wave attenuation," *Progress Report*, The University of Hull (U.K.)
- [4] H. Jasik, *Antenna Engineering Handbook*, McGraw-Hill, 1st Ed., 1961, pp. 3.11-3.12
- [5] E. H. Scheibe, B. G. King and D. L. Van Zeeland, "Loss measurements of surface wave transmission lines," *Journal of Applied Physics*, Vol. 25, No. 6, June 1954, pp. 790-797
- [6] H. M. Barlow and A. E. Karbowski, "An investigation of the characteristics of cylindrical surface waves," *Proceedings of the Institution of Electrical Engineers*, Vol. 100, Part III, No. 68, Nov. 1953, pp. 321-328
- [7] K. Simonyi, *Theoretische Elektrotechnik*, Johann Ambrosius Barth, 10. Auflage, 1993, (in German), pp. 823-825
- [8] M. R. Spiegel, *Mathematical Handbook of Formulas and Tables*, Schaum's Outline Series, McGraw-Hill, 1968
- [9] HP 8510 Network Analyzer, *Operating and Service Manual*, Vol. 1, Operating and Programming, p. 166

7 Conclusions

Edge diffracted waves resulting from surface discontinuities contribute significantly to the radar cross section of an object. Although this problem could be alleviated by altering the shape of the discontinuity, this is not always possible due to other mission requirements.

The use of isotropic surface wave absorbing materials is often advocated to remedy the problem of edge diffracted waves. However, this work has shown that the efficacy of isotropic surface wave absorbing materials is strongly polarization dependent. Hence, isotropic surface wave absorbing materials are only useful in a limited number of applications.

A superior solution consists in replacing the scattering surface by a soft surface. When properly oriented, a soft surface will suppress all radiation (both space wave and surface wave) in the direction of the radar, independently of the radar polarization and the polarization of the edge diffracted waves. In this process, the incident radar energy is not absorbed but reradiated in directions away from the radar.

Notwithstanding the limited applicability of isotropic surface wave absorbers, there is still an enormous amount of interest in characterizing these commercially available materials. A new measuring apparatus based on a partially filled rectangular waveguide has been developed for determining the attenuation constant and phase constant of plane surface waves along metal-backed isotropic surface wave absorbing materials. Measurements have been performed which validate this new measuring method.

Further Work

A better understanding of the mechanisms that lie at the origin of edge diffracted waves is needed. More information could be obtained by developing a computer program that solves the coated wedge problem.

Little is published on the propagation of surface waves along anisotropic and gyrotropic materials. This is important because nearly all of today's new aircraft have a high number of parts or are completely constructed out of carbon fibre, which is an anisotropic material.

The new measuring apparatus for characterizing surface wave absorbers still needs to be tested with multi-layered and lossy materials. Furthermore, the test cell was designed to interrogate the fundamental E-type plane surface wave at X-band frequencies. A similar cell could be built to interrogate the fundamental H-type plane surface wave. It may also be very interesting to have test cells for other radar frequency bands. The stealth design community would welcome a database containing the characteristics of existing surface wave absorbers at different radar frequencies.

Further work should also focus on the new technology of soft surfaces. To the author's knowledge, RCS measurements of objects with soft surfaces have not been reported in literature yet. Finally, efforts should be made to develop a broad-band soft surface.